



ASSESSMENT OF MEMBRANE DISTILLATION MODULES FOR SEAWATER DESALINATION AND OILFIELD-PRODUCED WATER TREATMENT APPLICATIONS

Ph.D. Thesis

By

HUSSAIN ALSAIRFI

A thesis submitted for the degree of
Doctor of Philosophy
Department of Mechanical Engineering
University of Strathclyde, Glasgow
September 13, 2024

This thesis is the result of the author's original research. It has been composed by the author and has not been previously submitted for examination, which has led to the award of a degree.

The copyright of this thesis belongs to the author under the terms of the United Kingdom Copyright Acts as qualified by the University of Strathclyde Regulation 3.50. Due acknowledgement must always be made of the use of any material contained in or derived from this thesis.

Abstract

Membrane distillation (MD) is a technology that is emerging as a viable alternative to traditional desalination techniques such as Reverse Osmosis, Multi-stage flash distillation, Multiple-effect distillation, Vapour-compression evaporation, etc. The advantages of MD over conventional desalination technologies include higher ionic rejection capacity, greater feasibility for high saline brine treatments, ability to operate using low-grade heat energy, a single-stage process and remote operation using renewable energy, among others.

In this dissertation, a parametric study was performed using experiments to assess the feasibility of using direct contact membrane distillation (DCMD) technology to desalinate saline water of different concentrations. The results showed that the permeate flux increased to 37.1 L/m².h from 11.6 L/m².h when the temperature was raised from 45 °C to 75 °C. Additionally, the permeate flux decreased to 13.6 L/m².h from 27.3 L/m².h, and the reduction in flux was around 50% when the concentration of sodium chloride in the feed solution was increased from 0% to 26%.

The experimental results obtained using oilfield-produced water were highly encouraging. The permeate flux was 11.5 L/m².h and 12.5 L/m².h at 80 °C and 85 °C, respectively. The results indicate the enormous potential of DCMD to treat hypersaline oilfield-produced water, with an overall rejection of salts above 99%. The base-line technology is the DCMD technology.

This study also evaluated the viability of air-gap membrane distillation (AGMD) and vacuum membrane distillation (VMD) for treating different types of saline water (3.5%, 7%, 15% and 26% NaCl solutions), including Arabian Gulf Seawater (AGS) and oilfield-produced water. AGMD experiments at different feed temperatures found that increasing the test temperature from 70 °C to 85 °C increased the permeate flux by 56.64%. In contrast, the VMD experiments showed that increasing the feed temperature from 65 °C to 85 °C resulted in a 26.87% increase in permeate flux. The results obtained from the experiments showed that VMD performed better at higher feed concentrations, while AGMD was superior at lower feed concentrations. The flow-rate experimental results showed that increasing the flow rate from 1.3 to 2.0 litres per minute resulted in a 1.2-fold increase in permeate flux for both configurations, with salt rejection close to 99.9% and

unaffected by the feed flow rate. AGMD outperformed VMD at all flow rates, and the increase in permeate flux with flow rate was similar for both configurations.

This study found lower gaps, i.e. air gap and vacuum space, were preferred in AGMD and VMD configurations, respectively, as they showed good flux, potentially due to the reduced effects of heat and mass-transfer mechanisms at smaller gaps. The experimental results showed that AGMD and VMD processes were highly efficient in treating oilfield-produced water and AGS, achieving high salt rejections as high as 99.97%. The results showed that the tested membranes achieved salt rejections as high as 99.97%, and the order of fluxes observed in the VMD configuration was Polyvinylidene fluoride (PVDF) > Polypropylene (PP) > Polytetrafluoroethylene (PTFE). In the AGMD configuration, the order of fluxes observed was Polypropylene (PP) > Polyvinylidene fluoride (PVDF) > Polytetrafluoroethylene (PTFE).

This study's results will provide valuable insights into the potential applications of AGMD and VMD processes in desalination, especially in regions where freshwater resources are scarce or contaminated. The information gained from this study can be used to optimise the performance of these processes, improve their cost-effectiveness and energy efficiency, and enhance their viability as potential solutions for addressing water scarcity and pollution issues. The study discussed in this dissertation is the first to present laboratory-scale results of using AGMD and VMD technologies to treat AGS and oilfield-produced water in Kuwait while considering prevailing conditions. The findings of this study lay the groundwork for conducting pilot-scale studies on Arabian Gulf Seawater and oilfield-produced water utilising DCMD, AGMD and VMD technologies, not only in the Middle East region but globally.

Contents

1 Chapter 1 Introduction	1
1.1 The Clean Water Problem	1
1.2 Membrane Distillation	2
1.3 Aims and Objectives	3
2 Chapter 2 Literature Review	6
2.1 Introduction.....	6
2.2 Types of MD.....	8
2.3 MD Design Techniques	12
2.4 Temperature Polarisation	19
2.5 Membrane Modification	22
2.6 Flow Promoters	24
2.7 Induction Heat	26
2.8 MD Characteristics	30
2.9 Economics and Energy Consumption in MD	36
2.10 MD Modelling Techniques	40
2.11 Mathematical Model Formulation.....	45
2.11.1 Water Mass Flux.....	45
2.11.2 Heat Transfer Coefficient.....	47
2.11.3 Performance Parameters	48
2.12 Conclusion	48
3 Chapter 3 Methodology	50
3.1 Introduction.....	50
3.2 Experimental Procedure.....	50
3.3 Membrane Characterisation	55
3.4 Experimental Technique	58
4 Chapter 4 A Performance Feasibility Study of DCMD Systems for Treating Arabian Gulf Seawater and Oilfield-Produced Brine	60
4.1 Introduction.....	60
4.2 Materials, Experimental Setup and Procedure	62
4.3 Validation of a DCMD System	68
4.3.1 Effect of Feed Temperature	69

4.3.2	Effect of Feed Concentration.....	74
4.3.3	Effect of Flow Rate	80
4.3.4	Effect of Channel Depth on Permeate Flux	85
4.4	An Oilfield-Produced Water Desalination Performance Study Using the DCMD Process	90
4.5	Seawater Desalination Performance of PP and PVDF Membranes at Different Flow Rates and Temperatures Using the DCMD Configuration	93
4.6	Conclusion	94
5	Chapter 5 A Comparative Study of Air-Gap and Vacuum-Driven Membrane Distillation Modules for Seawater Desalination and Oilfield- produced water treatment	98
5.1	Introduction	98
5.2	Materials and Methods	103
5.2.1	Experimental Setup and Procedure.....	103
5.3	Results and Discussions	108
5.3.1	Influence of Feed Temperature.....	108
5.3.2	Influence of Solute Concentration on Feed.....	112
5.3.3	Influence of Feed Flow Rate on Permeate Flux.....	117
5.3.4	Influence of Air Gap Depth and Vacuum Space on Permeate Flux.....	122
5.3.5	Performance of AGMD and VMD Processes for Treating Oilfield-produced Water and AGS.....	128
5.3.6	Performance of PP, PVDF and PTFE Membranes in the AGMD and VMD Process	131
5.4	Conclusion.....	132
	Chapter 6 Conclusion and Future Research.....	138
6.1	Conclusion.....	138
6.2	Future Research	144
	References.....	146

List of Figures

Figure 1.1. Comparative Schematic of Membrane Distillation Configurations: Direct Contact Membrane Distillation (DCMD), Air Gap Membrane Distillation (AGMD), Vacuum Membrane Distillation (VMD), and Sweeping Gas Membrane Distillation (SGMD) [2].....	3
Figure 1.2. Flow Chart for Performing the Proposed Objectives	5
Figure 2.1. Schematic Representation of a Typical MD Process [5].....	7
Figure 2.2. Process Flow Schematic Highlighting Differences in Membrane Distillation Configurations, (a) DCMD, (b) AGMD, (c) VMD and (d) SGMD [4]	8
Figure 2.3. Variation of GOR for Different Membrane Distillation Configurations Under Various Test Conditions [9].....	11
Figure 2.4. Profiles of Distillate Flux and Specific Thermal Energy Consumption in Different MD Configurations [10]	12
Figure 2.5. (a) Flow Diagram of MSVMD System, and (b and c) Effect of Temperature Differences and Brine Salinity on GOR [17]	15
Figure 2.6. Integrated VMD System With the Solar Flat-Plate Collector [20]	16
Figure 2.7. Modified V-MEDM Configurations [21]	18
Figure 2.8. Photo of the V-MEMD System [26]	19
Figure 2.9. Recent Technologies to Overcome Temperature Polarisation in Membrane Distillation [27]	21
Figure 2.10. Solar Energy Systems Integrated with VMD [31]	22
Figure 2.11. Performance of CPC and TPC with Changing Flow Patterns (left) and Feed Inlet Temperature (right) [32].....	22
Figure 2.12. Effect of: (a) Feed Temperature and Velocity, and (b) Membrane Thickness on the TPC Performance [33]	23
Figure 2.13. Comparison Between (a) Typical Membrane and (b) Modified Membrane [36]	24
Figure 2.14. Comparison of (A) Custom-made VMD system and (B) Typical VMD Design [42].....	25
Figure 2.15. Effect of Integrating the Microwave with the VMD System [49].....	27
Figure 2.16. Effect of IH-VMD on the Permeate Flux and Specific Energy Consumption Compared with the VMD System [45]	28

Figure 2.17. Effect of the Induction Heating Methods on the Performance of the MD System [27].....	30
Figure 2.18. Mass Flux Profiles of VMD System Under Different Operating Conditions [65]	32
Figure 2.19. Effect of : a) Flow velocity, b) Vacuum level, c) Nanoparticle Layer Thickness, and d) Salt Concentration on Permeate Flux [45]	34
Figure 2.20. Effect of Hot Water Temperature on the Production Rate and Specific Energy Consumption [69]	35
Figure 2.21. Effect of : a) Feed Temperature, b) Feed Flow Rate, c) Vacuum Pressure, d) Feed Salinity, and e) Number of Stages on the LCOW of Different VMD Configurations [70]	36
Figure 2.22. Influence of Number of Effects and Membrane Frames on Overall Productivity [69].....	38
Figure 2.23. Influence of Number of Effects and Membrane Frames on Specific Energy Consumption [69]	39
Figure 2.24. Influence of Number of Effects and Membrane Frames on Specific Flux [69]	39
Figure 2.25. Pie Chart Cost Breakdown of Different Multistage VMD Configurations Compared With the Single-Stage VMD System [70]	41
Figure 2.26. Comparison Between the Numerical Finite Volume Results (Lines) Against Experimental Data (Symbol) [13]	42
Figure 2.27. Effect of (a) Row Spacing (1.5 D to 3.0 D, M1 to M4) and (b) Intersection Angles (60° to 120°) on Cross-Flow Velocity Magnitude [79]	44
Figure 3.1. Schematic Diagram of the Experimental Rig	52
Figure 3.2. Parts of the MD Membrane Module	53
Figure 3.3. Components of the DCMD Membrane Module Configuration.....	54
Figure 3.4. Components of the AGMD Membrane Module Configuration.....	54
Figure 3.5. Membrane Surface Images Captured by SEM	56
Figure 3.6. AFM Image Showing Surface Roughness.....	57
Figure 4.1. Schematic Diagram of the Bench-Scale MD Unit	63
Figure 4.2. Bench-Scale Direct Contact Membrane Distillation (DCMD) Test Unit ..	63
Figure 4.3. (a) Fully Assembled Membrane Module, (b) Feed Section of the Membrane Module, (c) Permeate Section of the Membrane Module	65

Figure 4.4. DCMD Module Used for Channel Depth Variation Study, (a) and (b) Membrane Cell Plates, (c) Fully Assembled Module, and (d) One mm Thick Plate .	65
Figure 4.5. Effect of Feed Temperature on the Permeate Flux of Polypropylene Membrane in DCMD.....	69
Figure 4.6. Permeate Flux Produced with Time at Different Feed Temperatures	71
Figure 4.7. Effect of Feed Temperature on (a) TPC and (b) the Nusselt Number in DCMD.....	72
Figure 4.8. Effect of Feed Temperature on (a) GOR and (b) STEC in DCMD	74
Figure 4.9. Effect of Feed Concentration on the Permeate Flux of Polypropylene Membrane in DCMD.....	75
Figure 4.10. Permeate Flux at Different Feed Concentrations and Uniformity of Permeate Flux Over Desalination Time	76
Figure 4.11. Effect of Feed Concentration on the Salt Rejection of Polypropylene Membrane in DCMD.....	77
Figure 4.12. Effect of Feed Concentration on (a) TPC and (b) the Nusselt Number in DCMD.....	78
Figure 4.13. Effect of Feed Concentration on (a) GOR and (b) STEC in DCMD.....	80
Figure 4.14. Effect of Feed Flow Rate on the Permeate Flux of Polypropylene Membrane in DCMD.....	81
Figure 4.15. Permeate Flux at Different Feed-Flow Rates and Comparative Consistency Over Desalination Time in DCMD.....	82
Figure 4.16. Effect of Flow Rate on the Salt Rejection of Polypropylene Membrane in DCMD.....	82
Figure 4.17. Effect of Feed Flow Rate on (a) TPC and (b) the Nusselt Number in DCMD.....	83
Figure 4.18. Effect of Feed Flow Rate on (a) GOR and (b) STEC in DCMD.....	84
Figure 4.19. Permeate Flux at Different Flow Channel Depths Showing Improved Flux at Lower Depths.....	86
Figure 4.20. Permeate Flux at Different Flow Rates and Temperatures (Hot-side Depth of 8 mm and Cold-side Depth of 2 mm).....	88
Figure 4.21. Effect of Channel Depths on (a) GOR and (b) STEC in DCMD	89
Figure 4.22. Effect of Channel Depths on (a) TPC and (b) Nusselt Number in DCMD	90

Figure 4.23. Permeate Flux at Different Temperatures Using Oilfield-Produced Water in DCMD	91
Figure 4.24. Salt Rejection Percentage at Different Temperatures Using Oilfield-Produced Water in DCMD	92
Figure 5.1. Schematic Representation and Photos of the VMD Membrane Module (a) Feed Side Shell, (b) Vacuum Side Shell, (c) Assembled VMD Module	103
Figure 5.2. Schematic Representation and Photos of the AGMD Membrane Module, (a) Membrane Module Shell Plate, (b) Plate to Introduce Air Gap, (c) Condensation Plate, (d) Assembled AGMD Module.....	104
Figure 5.3. Schematic Representation of the AGMD Process [135].....	104
Figure 5.4. Schematic Representation of the VMD Process [135]	105
Figure 5.5. Schematic Diagram of AGMD Setup.....	105
Figure 5.6. Schematic Diagram of VMD Setup	106
Figure 5.7. Effect of Feed Temperature on Permeate Flux in AGMD	108
Figure 5.8. Effect of Feed Temperature on Permeate Flux in VMD.....	108
Figure 5.9. Comparison of Permeate Flux at Different Feed Temperatures in AGMD and VMD Configurations.....	110
Figure 5.10. Effect of Feed Temperature on Nusselt Number in AGMD and VMD	110
Figure 5.11. Effect of Feed Temperature on GOR in AGMD and VMD	111
Figure 5.12. Effect of Feed Temperature on STEC in AGMD and VMD	112
Figure 5.13. Permeate Flux Over Time at Different Feed Concentrations in AGMD	113
Figure 5.14. Permeate Flux Over Time at Different Feed Concentrations in VMD .	113
Figure 5.15. Comparison of Permeate Flux at Various Feed Concentrations in AGMD and VMD.....	114
Figure 5.16. Effect of Feed Concentration on Nusselt Number in AGMD and VMD	115
Figure 5.17. Effect of Feed Concentration on GOR in AGMD and VMD.....	116
Figure 5.18. Effect of Feed Concentration on STEC in AGMD and VMD	117
Figure 5.19. Effect of Feed Flow Rate on Permeate Flux in AGMD	118
Figure 5.20. Effect of Feed Flow Rate on Permeate Flux in VMD	118
Figure 5.21. Comparison of Permeate Flux at Various Feed Flow Rates in AGMD and VMD.....	120

Figure 5.22. Effect of Feed Flow Rate on Nusselt Number in AGMD and VMD.....	120
Figure 5.23. Effect of Feed Flow Rate on GOR in AGMD and VMD	121
Figure 5.24. Effect of Feed Flow Rate on STEC in AGMD and VMD	122
Figure 5.25. Effect of Air Gap Depth on Permeate Flux in AGMD Configuration at Constant Hot-Channel Depth	123
Figure 5.26. Effect of Feed-Channel Depth on Permeate Flux in AGMD Configuration at Constant Cold-Channel Depth	123
Figure 5.27. Effect of Vacuum Space Depth on Permeate Flux in VMD Configuration at Constant Feed-Channel Depth.....	124
Figure 5.28. Effect of Feed-Channel Depth on Permeate Flux in VMD Configuration at Constant Vacuum Space	125
Figure 5.29. Effect of Channel Depth on (a) STEC and (b) GOR in AGMD	127
Figure 5.30. Effect of Channel Depth on (a) STEC and (b) GOR in VMD.....	128
Figure 5.31. Permeate Flux in VMD Experimentation Using Oilfield-Produced Water as Feed at 80°C and 85°C	129
Figure 5.32. Permeate Flux from VMD and AGMD Experiments Using AGS from Beach Well as Feed at 85°C.....	130

List of Tables

Table 2-1. Functions and Properties of MD Configurations [5, 6].....	9
Table 2-2. Summary of Induction Heating Methods and Their Key Achievements in Literature.....	29
Table 2-3. Comparison of Permeate Flux for Different Hollow-Fibre Membranes	31
Table 3-1. Characteristics of the Flat-Sheet Membranes.....	56
Table 4-1. Overview of the Logic of the Experimental Envelop.....	62
Table 4-2. Physicochemical Analysis of Arabian Gulf Seawater (AGS)	67
Table 4-3. Effect of Temperature on Permeate Flux and Salt Rejection in DCMD ...	70
Table 4-4. Salinity of Feed at Different Temperatures Over Time During the Experimentation Period	71
Table 4-5. Permeate Flux at Different Feed Concentrations Over Time	76
Table 4-6. Physicochemical Analysis of Oilfield-Produced Water and Permeate Water.....	93
Table 4-7. Water Flux and Salt Rejection Percentages of PP and PVDF Membranes at Different Flow Rates Using AGS Feed	94
Table 5-1. Experimental Framework and Methodology	102
Table 5-2. Chemical Analysis of Arabian Gulf Seawater	107
Table 5-3. Chemical and Physical Analysis of Oilfield-Produced Water and Permeate Water from AGMD and VMD.....	130
Table 5-4. Water Flux and Salt Rejection Performance of PP, PVDF, and PTFE Membranes in VMD.....	131
Table 5-5. Water Flux and Salt Rejection Performance of PP, PVDF, and PTFE Membranes in AGMD	132

List of Publications

- 1- Al-Sairfi, H., Koshuriyan, M., Ahmed, M. "Performance feasibility study of direct contact membrane distillation systems in the treatment of seawater and oilfield-produced brine: the effect of hot- and cold-channel depth". *Journal of Desalination and Water Treatment*. 313 (2023) 26-36.
- 2- Al-Sairfi, H., Koshuriyan, M., Ahmed, M. "Membrane Distillation of Saline Feeds and Produced Water: A Comparative Study of an Air-Gap and Vacuum-Driven Modules". *Journal of Desalination and Water Treatment*. 317 (2024).

Preface/Acknowledgements

I want to thank my supervisors, Dr Zamir Koshuriyan and Dr Edmondo Minisci, for their continued help and assistance, without which this work could not have been completed. You have been exceedingly patient and helpful whenever I encounter obstacles and understand my ambitions to work in the MD field.

I am also grateful to the KISR for providing me with the Ph.D. scholarship.

I am incredibly grateful to my parents, wife, and lovely sons for their significant support and help during the turbulent period of my PhD research. Many thanks also go to my brother and sisters and all the family members of my father-in-law.

Finally, I am grateful to all my friends at the University of Strathclyde, who have witnessed my PhD struggles and supported me in overcoming them.

Nomenclature

MD	Membrane distillation
DCMD	Direct contact membrane distillation
VMD	Vacuum membrane distillation
AGMD	Air-gap membrane distillation
AGS	Arabian Gulf Seawater
PP	Polypropylene
PVDF	Polyvinylidene fluoride
PTFE	Polytetrafluoroethylene
V-MEDM	Vacuum multi-effect membrane distillation
CPC	Concentration polarisation coefficient
TPC	Temperature polarisation coefficient
IH-VMD	Induction heating- vacuum membrane distillation
LCOW	Levelised cost of the water
KISR	Kuwait Institute for Scientific Research
ED	Electrodialysis
RO	Reverse osmosis
SGMD	Sweeping gas membrane distillation
VLE	Vapour–liquid equilibrium
MED	Multi-effect distillation
MSF	Multi-stage flash
GOR	Gained output ratio
PGMD	Permeate gap membrane distillation
CGMD	Conductive gap membrane distillation
MEVMD	Multi-effect vacuum membrane distillation
HRUs	Heat recovery units
DE-MD	Dead-end membrane distillation
LGMD	Liquid-gap membrane distillation
T_f	Bulk hot-feed solution temperature on the feed side
T_{fm}	Membrane surface temperature on the feed side
T_v	Liquid equilibrium temperature on the permeate side
Re_{tp}	Reynolds number represents the flow patterns for the two-phase gas and liquid

CNIM-f	Carbon nano-tubes immobilization
LEP	Liquid entry pressure
TP	Temperature Polarisation
RF-VMD	Ratio frequency vacuum membrane distillation
FEP	Poly(tetrafluoroethylene-co-hexafluoropropylene)
CFD	Computational fluid dynamics
J	Water flux
P_m^F	Membrane surface pressures at the feed side
P_m^V	Membrane surface pressures at the vacuum side
C_V	The membrane surface coefficient
δ	Membrane thickness
τ	Membrane pore tortuosity
ε	Porosity
r	Average pore size
M_w	Water molecular weight
T	The mean vapour temperature in the membrane pores
P	Mean vapour pressure in the membrane pores
T_m^F	The membrane surface temperature at the feed side
T_m^V	The membrane surface temperature at the vacuum side
Kn	Knudsen number
l	The transferred gas molecule mean free path
d	The membrane mean pore diameter.
h_F	Heat transfer coefficient on the feed side
d_h	The hydraulic diameter of the module measured in metre,
k_F	The feed thermal conductivity measured
k_g	The gas thermal conductivity

k_p	Polymer thermal conductivity
Nu	Nusselt number
Re	Reynolds number
Pr	Prandtl number
ρ_F	Feed's density
μ_F	Feed's dynamic viscosity
C_{PF}	Feed's specific heat capacity
V_F	Feed's velocity
Q_F	Heat transferred from the feed side
Q_m	Heat transferred to vacuum side
d_o	The fibre outer diameter.
N	The number of fibres
d_{lm}	The logarithmic mean diameter
L	The fibre effective length
ΔH	The enthalpy of vapourisation
A	Area of membrane
STEC	Specific thermal energy consumption
WCA	Water contact angle
R	Rejected salt percentage
AR	Analytical reagent
DRP	Desalination Research Plant
C_f	Feed concentration
C_p	Permeate concentration
ZTIMD	Zero thermal input membrane distillation

Chapter 1

Introduction

1.1 The Clean Water Problem

One of humanity's most critical issues nowadays is having access to clean water. This fundamental issue reflects various critical drawbacks worldwide. Among these issues, up to 2.5 billion people do not have access to sufficient water for sanitation, and more than 780 million people cannot access clean water [1]. The availability and quality of water are interlinked with human health and economic progress. Ensuring a sustainable supply of clean water is vital for maintaining public health, supporting agricultural and industrial activities, and fostering economic growth and development. Based on the water types employed in the industrial sectors, water quantity and quality differ from one department to another. For example, water is widely used in power plants to produce steam, which is used for power generation and other daily-life applications, such as medicines, soups, beverages, pulp, paper and textiles.

It can be deduced that the water problem is urgent, especially with an increasing human population, which is leading to a significant, growing global rate of clean water demand. For these problems, clean water availability needs an optimum approach and adapted solution that can be satisfactory for current and future populations and other daily-life demands.

Different water treatment techniques on a large scale have been proposed and applied in previous studies to provide sufficient quality and quantity of water for various industrial purposes. Among these treatment methods, membrane distillation (MD) technology is one of the most advanced alternative technologies that can produce an adequate amount of clean water with lower energy impact and higher separation efficiency compared with other water treatment methods, such as electro dialysis (ED) and reverse osmosis (RO), which require large specific electricity requirements. MD technology has become the most commercially developed method for desalinating different fluids. However, the substantial heat requirement is the major drawback of integrated MD technology, which is in line with other parametric

issues, such as permeate flux and salt rejection. Several techniques have been proposed to overcome this issue and improve MD performance.

1.2 Membrane Distillation

Membrane distillation is a process that combines thermal and membrane-based separation principles to desalinate water. This technology can be described as a thermal desalination technique, because like other thermal desalination methods, such as Multi-Stage Flash (MSF) and Multi-Effect Distillation (MED), MD relies on the input of thermal energy to facilitate the separation process. The temperature difference between the feed side and the permeate side drives the evaporation and condensation cycle. The thermal aspect involves heating saline feed stream to create a temperature gradient across a hydrophobic membrane. This heated water causes water vapour to evaporate from the saline feeds stream. The hydrophobic membrane allows water vapour to pass through but blocks the passage of liquid water and dissolved salts. This vapour then condenses on the cooler side of the membrane, resulting in purified water. The MD system has been significantly investigated and received wide attention from academic researchers in the last few years compared to traditional desalination methods, such as RO, MSF, MED, etc., for better performance and higher efficiency. Several structural features and flow characteristics have helped the MD system to be an alternative technology for renewable desalination techniques, such as the ability to use waste heat sources, lower working fluid temperatures, and the complexity of the MD system being more straightforward than other technologies [2].

The MD systems are mainly classified into four different configurations based on the process of water vapour generated and the methods of collecting/condensing on the cold side: vacuum membrane distillation (VMD), sweeping gas membrane distillation (SGMD), direct contact membrane distillation (DCMD) and air gap membrane distillation (AGMD). All these configurations are shown in Figure 1.1.

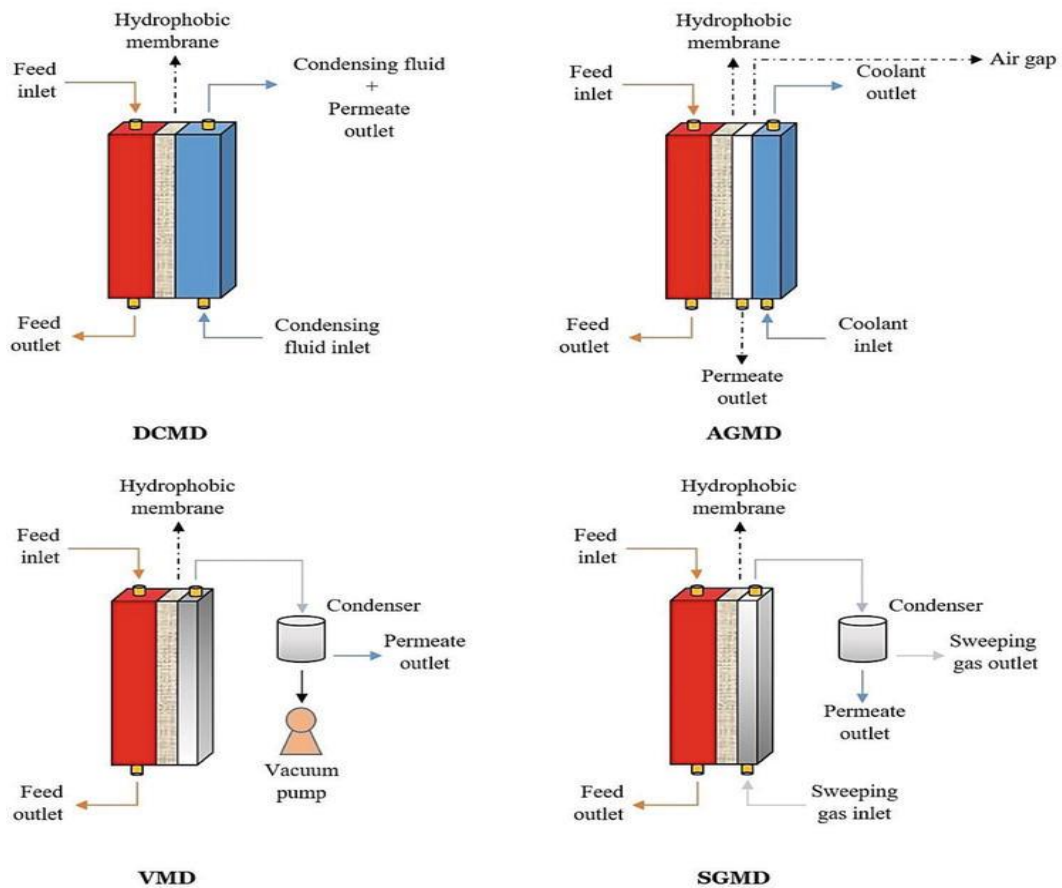


Figure 1.1. Comparative Schematic of Membrane Distillation Configurations: Direct Contact Membrane Distillation (DCMD), Air Gap Membrane Distillation (AGMD), Vacuum Membrane Distillation (VMD), and Sweeping Gas Membrane Distillation (SGMD) [2]

1.3 Aims and Objectives

This current work aimed to enhance and improve the performance of Membrane distillation by:

- Experimental work on Direct Contact Membrane Distillation (DCMD), Vacuum Membrane Distillation (VMD), and Air Gap Membrane Distillation (AGMD) using parametric studies for various parameters, such as inlet feed temperatures, feed concentrations, flow rates, feed-channel depths, etc.
- Examining the performance of Polypropylene (PP), Polyvinylidene fluoride (PVDF) and Polytetrafluoroethylene (PTFE) membranes applied in Air-gap membrane distillation and Vacuum membrane distillation processes

- Studying the seawater desalination performance of Polypropylene and Polyvinylidene fluoride membranes at different flow rates and temperatures using a Direct contact membrane distillation configuration
- Investigating a parametric study at the Kuwait Institute for Scientific Research (KISR) to assess the feasibility of using Direct Contact Membrane Distillation (DCMD), Air Gap Membrane Distillation (AGMD), and Vacuum Membrane Distillation (VMD) processes for desalinating Arabian Gulf Seawater and oilfield-produced water under various operating conditions.

This study examined the impact of increasing hot and cold solution flow channel depths in DCMD, VMD, and AGMD modules developed by the research team. Its findings will lay the groundwork for conducting pilot-scale studies on AGS and oilfield-produced water in the Middle east and globally.

The structure of this current work is divided as follows: Chapter Two deals with experimental and numerical studies that have been investigated in previous studies, showing the comprehensive details of MD system's characteristics and specifying the gaps. The methodology of this current study is presented in Chapter Three, showing the main experimental techniques utilised to represent flow physics, heat and mass characteristics. Chapter Four presents the performance of various parameters on mass and heat transfer using DCMD technology. Chapter Five presents the performance of various parameters on mass and heat transfer using VMD and AGMD systems and compares the results of all systems examined in this current study. Finally, Chapter Six presents the conclusion of this current work and some steps that can be considered for future work. The flow chart for performing the proposed objectives is presented in Figure 1.2.

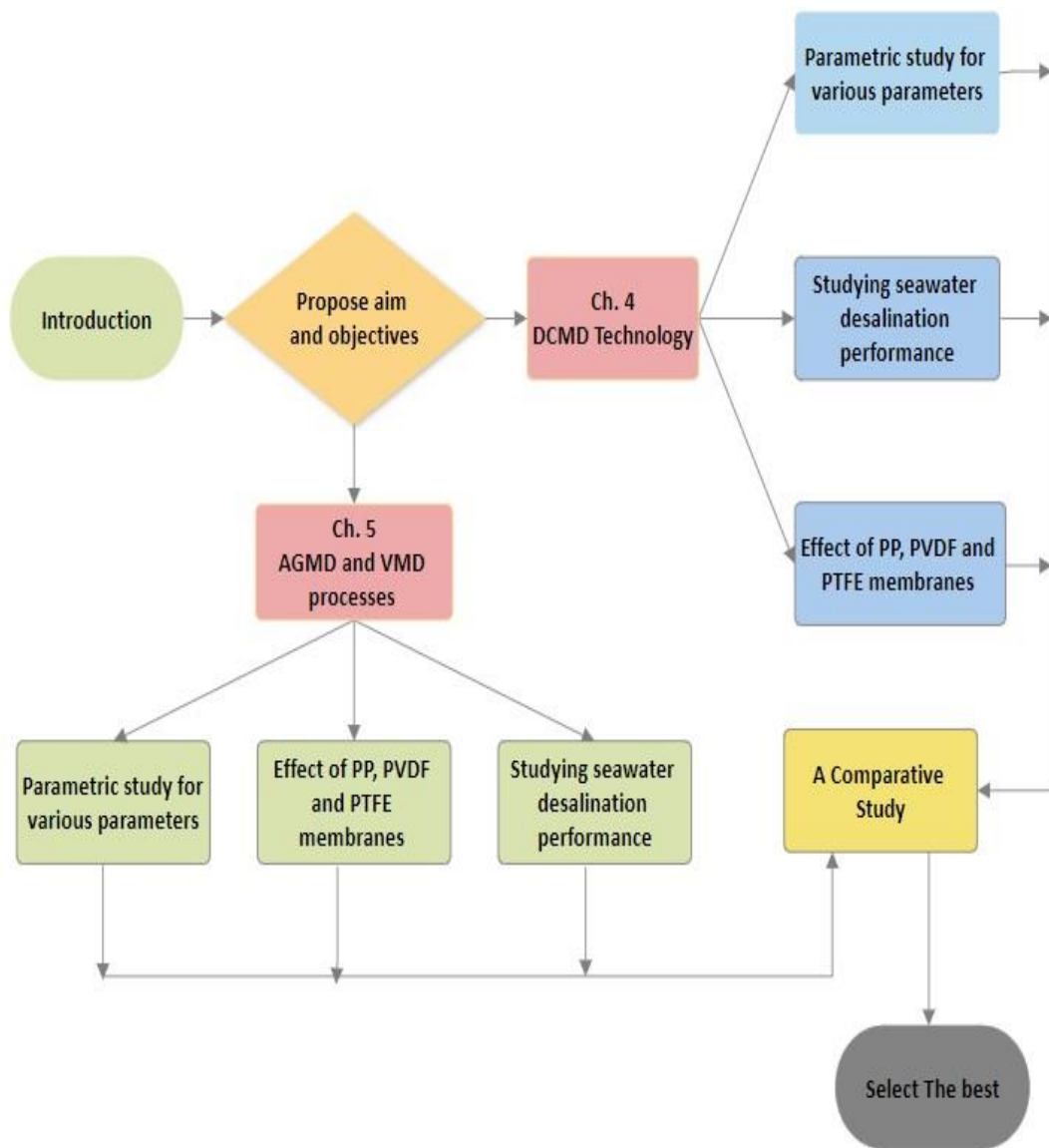


Figure 1.2. Flow Chart for Performing the Proposed Objectives

Chapter 2

Literature Review

2.1 Introduction

Among the various types of desalination technologies available, membrane desalination (MD) can be defined as a desalination process involving a thermally driven membrane based on the vapour–liquid equilibrium (VLE) concept. This type has more advantages than traditional thermal technologies, such as multi-effect distillation (MED) and multi-stage flash (MSF) systems. This is due to several reasons, such as modularity, compactness and smaller energy consumption in most circumstances [3]. Moreover, membrane distillation (MD) requires a lower operating temperature, typically in the range of 303–343 K (30–70°C), and relies on a temperature difference between the feed and permeate sides to drive the process. This leads to lower thermal energy consumption and allows for a modular and compact system design that can effectively reject nearly all non-volatile compounds [4]. Furthermore, MD can treat a wide range of feed type; including hypersaline feed solutions, compared with pressure-driven RO [5]. This technology can be utilised in various industrial and engineering applications, such as wastewater treatment, desalination, textile wastewater treatment and purification of the oil-containing feed stream.

In a typical MD system, the circulating cold permeates and hot feed would generate the vapour pressure difference across both hydrophobic membrane sides owing to the difference in temperature between the hot feed part and the permeate cold part. The vapour generated on the hot feed part passes across the hydrophobic membrane to the cold side. Then, the vapour condenses and generates the distillate. Figure 2.1 shows the typical schematic procedure of the typical MD. The principle of MD involves heating saline feedwater to create a temperature gradient across a hydrophobic membrane, which allows water vapour to evaporate and pass through while blocking liquid water and salts. The vapour then condenses on the cooler side of the membrane, producing purified water. As seen clearly from Figure 2.1, the membrane's pores in MD allow only water vapour molecules from the hot feed to pass through, while the liquid feed is blocked due to the membrane's hydrophobic

nature and low surface energy. Preventing the liquid feed from passing through the membrane is important to keep the membrane pore dry. This requires providing non-polar membrane materials and has low surface energy since water has significant surface tension and is naturally polar [5]. Polar membranes have surface groups with significant differences in electronegativity between the atoms, leading to dipole formation. This means one end of the molecule has a partial positive charge, and the other has a partial negative charge, creating a "polar" character. This polar character allows them to interact strongly with other polar molecules, such as water, making them ideal for processes like reverse osmosis and nanofiltration. Non-polar membranes, on the other hand, have a more even distribution of charge, resulting in a lack of strong interactions with polar molecules like water. This hydrophobic property makes them ideal for processes like membrane distillation.

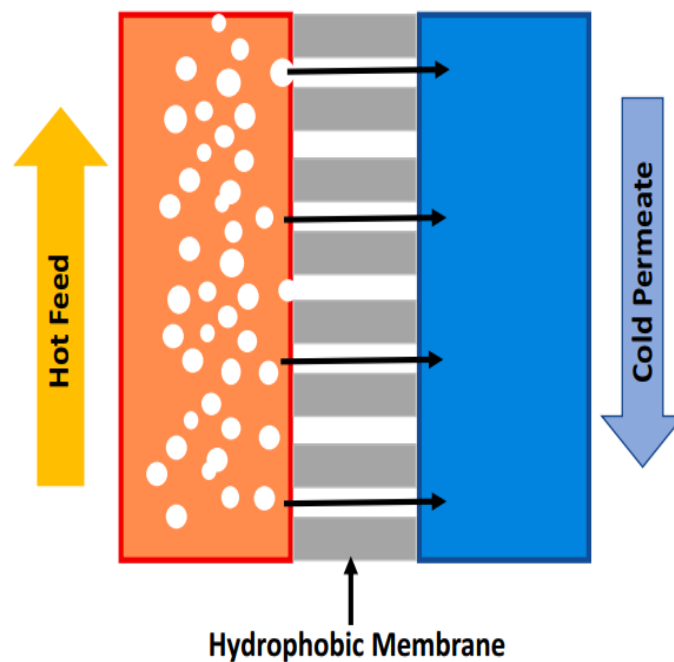


Figure 2.1. Schematic Representation of a Typical MD Process [5]

The current chapter presents the following sections; types of MD, the main technologies of MD design. The chapter also presents the effect of temperature polarization, flow promoters, induction heat and membrane modifications on the thermal performance of the MD. Moreover, the MD characteristics and economics and energy consumption are also discussed.

2.2 Types of MD

Based on the configuration of the MD, the process of water vapour generation, and the methods of collecting/condensing on the cold side, there are four main MD technologies available in the literature: vacuum membrane distillation (VMD), sweeping gas membrane distillation (SGMD), direct contact membrane distillation (DCMD), and air gap membrane distillation (AGMD). All these configurations are shown in Figure 2.2. The function process of each MD configuration is illustrated in Table 2.1, and advantages /disadvantages are also presented [5, 6].

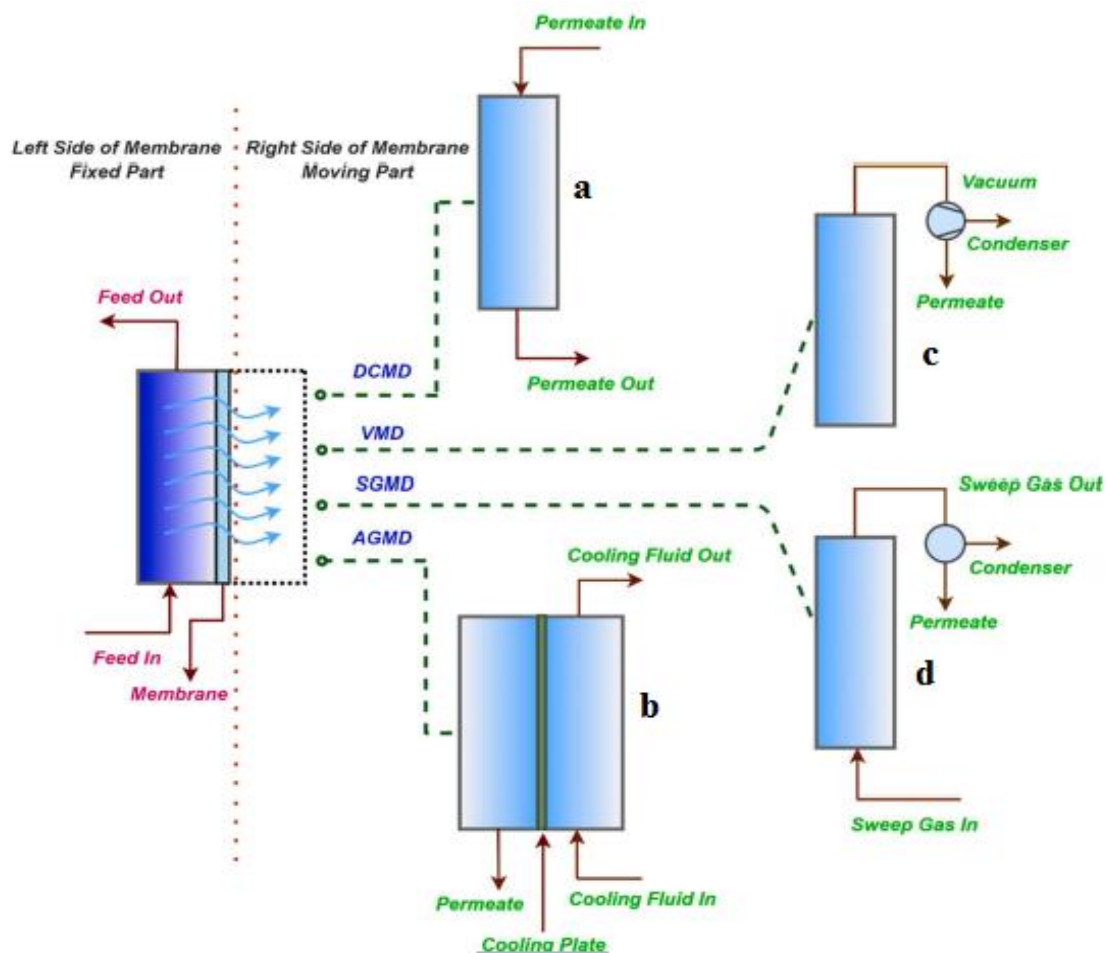


Figure 2.2. Process Flow Schematic Highlighting Differences in Membrane Distillation Configurations, (a) DCMD, (b) AGMD, (c) VMD and (d) SGMD [4]

In the literature, many papers have been presented to compare the performance of the MD configurations considering different variables and various test conditions.

Table 2-1. Functions and Properties of MD Configurations [5, 6]

MD Type	DCMD	AGMD	SGMD	VMD
Process	Cold water is in direct contact with the membrane.	An air gap is inserted between the condensation interface and the membrane.	Sweep gas is inserted and works as a carrier to transport the produced vapour to a condenser.	A vacuum removes the vapours on the permeate section. Then, the vapour is condensed outside the module.
Advantages	<ul style="list-style-type: none"> • Simple design • Different membrane models can be used: flat sheet or hollow fibre. • Two flow types: longitudinal flow and cross-flow • The flux is stable. • The gained output ratio (GOR) is large. 	<ul style="list-style-type: none"> • Low heat loss • High thermal efficiency • Large flux • The permeate section is completely dry. • The fouling tendency is low. 	<ul style="list-style-type: none"> • Sweep gas decreases mass-transfer resistance. • Low thermal polarisation • The permeate section is completely dry. • Conduction heat loss is less. 	<ul style="list-style-type: none"> • The flux is large. • The permeate quality is more stable. • Low thermal polarisation • Conduction heat loss is less.
Disadvantages	<ul style="list-style-type: none"> • Highest conduction heat loss • Lowest thermal efficiency • Largest thermal polarisation • Flux is very sensitive to feed concentration. 	<ul style="list-style-type: none"> • Lower permeate flux • More mass transfer • The design is complex. • The GOR is the smallest. 	<ul style="list-style-type: none"> • A separate condenser is required. • Leakproof gas technology is needed. • The design is complex. • The flux is low. • Difficult heat recovery 	<ul style="list-style-type: none"> • Larger possibility of pore wetting • More fouling • The selectivity of volatile compounds is minuscule. • An external condenser is required. • A vacuum pump is needed.
Applications	<ul style="list-style-type: none"> • Desalination • Aqueous solution concentration 	<ul style="list-style-type: none"> • It can be used widely, especially when there is lower energy availability. 	<ul style="list-style-type: none"> • Azeotropic mixture separation • Wastewater treatment 	<ul style="list-style-type: none"> • Aroma compound recovery • Alcoholic solution treatment.

Ding et al. [7] experimentally investigated a comparison of three separation performances of MD configurations (VMD, DCMD and SGMD) in the case of removal of ammonia from water considering two physical indexes mass transfer coefficient (K_a) and selectivity (β), where selectivity represents the measure of the preferential transport of ammonia. The mass transfer coefficient of the membrane is a function of membrane properties including pore size, overall porosity, thickness, and the mean free path (τ). Results showed that the mass-transfer coefficient was the largest in VMD, moderate in DCMD, and smallest in SGMD. However, the selectivity was the maximum in DCMD, moderate in SGMD and lowest in VMD.

At the same time, the energy requirements in two MD configurations (DCMD and VMD) for a membrane area of 40 cm² have been studied by Criscuoli et al. [8] under different test conditions and flow behaviours. The effects of operating temperatures and stream flow rates on flux, evaporation efficiency, and energy consumption were studied in DCMD, while in VMD, the focus was on analysing the feed flow rate, feed temperature, and the vacuum applied at the permeate side. The feed flow rate varied from 100 to 300 L/h, while the distillate flow rate in DCMD was maintained at 200 L/h. The feed temperature ranged between 40 and 60°C, and the distillate temperature was between 13 and 14°C, whereas, in VMD, the pressures on the permeate side were between 10 and 60 mbar [8]. The results showed that the flow behaviour of the longitudinal flow is very similar to the transversal flow, whereas the cross-flow led to larger fluxes than the longitudinal flow. In terms of the permeate flow ratio, energy consumption and evaporation efficiency, these have been predicted similarly. Moreover, the better performance in terms of the membrane fluxes, evaporation efficiency and energy consumption was marked by VMD. Another research concentrated on the energy efficiency of the DCMD, AGMD and VMD technologies, as investigated by Summers et al. [9], in which they compared the gained output ratio (GOR) of each configuration across the range of membrane module geometries, and operating conditions. The GOR measures the efficiency of the process by comparing the latent heat of evaporation required to produce a unit mass of product water to the amount of energy actually used by the system. A higher GOR indicates that the system is using energy more efficiently, meaning it can produce more water with less energy, which is desirable for both economic and environmental reasons. The results revealed that the GOR was larger in DCMD and

AGMD configurations than in the VMD configuration. The results also indicate that the GOR in the VMD is limited to smaller than 1 (see Figure 2.3).

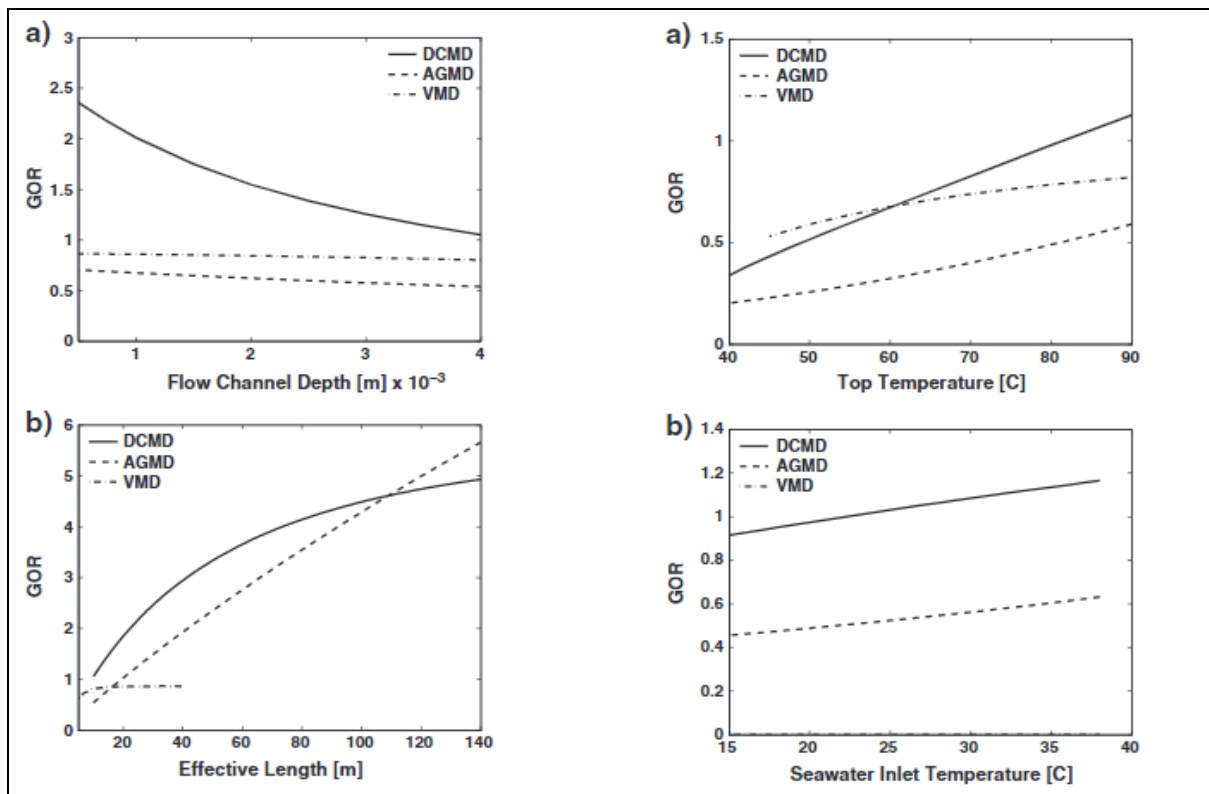


Figure 2.3. Variation of GOR for Different Membrane Distillation Configurations Under Various Test Conditions [9]

More aspects have also been addressed to assess the performance of MD technology, which are the distillate flux and consumption of specific thermal energy of AGMD, VMD, and permeate gap MD (PGMD) as presented by Cipollina et al. [10]. PGMD is a modification of the AGMD module, achieved by closing the distillate output line of the AGMD module and allowing the distillate to fill the air gap, and then exit the module from the top. As per their findings, the largest distillate flux was recorded with PGMD over all examined temperatures, followed by VMD and then AGMD. On the other hand, the largest specific thermal energy consumption was marked by AGMD over all investigated temperatures, followed by VMD and PGMD (see Figure 2.4).

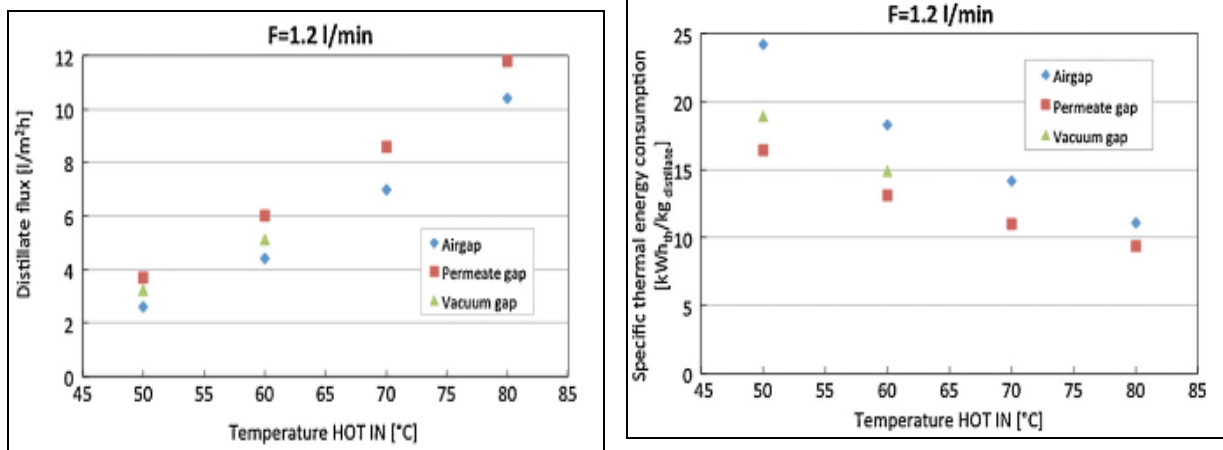


Figure 2.4. Profiles of Distillate Flux and Specific Thermal Energy Consumption in Different MD Configurations [10]

As pointed out previously, the MD technology still experienced a wide range of development in which Swaminathan et al. [11] proposed a new MD arrangement called conductive gap MD (CGMD) and compared it with the PGMD and AGMD. For the new design, three different flow behaviours have also been examined: cross-flow, counter-flow and parallel. The numerical findings indicated that PGMD technology has a GOR larger than AGMD by 20%, whereas the novel CGMD system has a GOR higher than PGMD by two times. Moreover, counter-flow led to the largest energy efficiency, followed by cross-flow and parallel flow.

Among all the previous MD models, the VMD attains a more emerging type due to large permeate flux production under the same temperature gradient, owing to a greater reduction in mass-transfer resistance and moderate energy consumption compared with other MD types. Thus, this type is one of the types that will be considered in the current study. Moreover, the VMD has another advantage over other MD systems: the VMD neglects conduction heat transfer owing to very low vapour pressure, Zhang et al. [12].

2.3 MD Design Techniques

In the design process of MD, four main steps must be considered and taken into account to produce an efficient MD system with effective performance. Thus, the system should be selected and optimised precisely and comprehensively based on the following points: the flow has a uniform distribution, temperature polarisation, flow pressure drops and liquid entry pressure [8]. Apart from the typical VMD design,

various VMD system designs have been proposed in the literature. Shim et al. [13] numerically proposed a multi-VMD system consisting of twelve membrane modules in a one-dimensional model. The idea is to recover the waste heat from the discharge brine. With a feed velocity of 1.0 m/s and a recycle flow ratio of 6.0, water recovery increased to over 48.3% without significantly reducing water production. Additionally, as the recycle flow ratio increased from 0.0 to 6.0, the heat duty decreased from 8.15 MW to 6.98 MW, and the thermal consumption per unit water production remained relatively stable between 2.37 and 2.91 MJ/kg at a recycle flow ratio above 3.0.

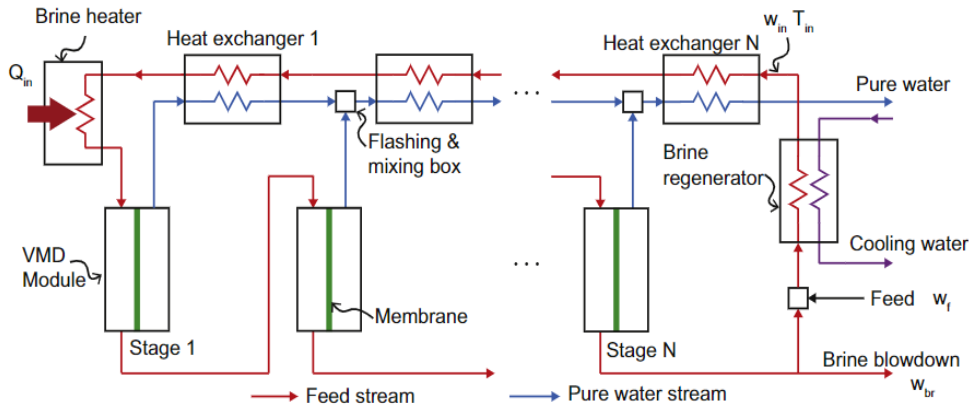
Another new design technique for DCMD technology has been proposed by Izquierdo-Gil [14] based on the constructal theory implementing the Speed-constrained Multi-objective particle swarm optimization (SMPSO) optimisation algorithm to evaluate whether the proposed constructal DCMD design can enhance DCMD performance. SMPSO is an improved particle swarm optimization (PSO) characterized by the use of a strategy to limit the velocity of the particles. The results revealed that the proposed design can lead to better performance under 4.4 kg/m^2 of water mass flux, whereas the typical design can perform better with higher mass fluxes.

The VMD has less energy efficiency than the Multi-Effect Distillation (MED) system due to less effective heat recovery. Thus, introducing a VDM system using a multi-effect technique is important for enhancing heat recovery and energy efficiency. Zhao et al. [15] conducted an experimental investigation using a vacuum-multi-effect-membrane-distillation (V-MEMD) module from Memsys. This compact module employs hydrophobic membranes as a separating medium and makes use of vacuum to enhance membrane distillation process. It was observed that the module's performance and energy efficiency are primarily influenced by the temperatures and flow rates of the heating, cooling, and feed streams. Experimental results show that heating and cooling temperatures significantly impact module flux and energy efficiency, especially under maximum vacuum conditions (e.g., 50 mbar). When the heating temperature is limited, increasing the heating flow rate and optimizing the feed flow rate can enhance the process by increasing the flux. The optimization of the module design shows potential for increasing the GOR from 2.5 to 3.0, which is crucial for the industrialization of membrane distillation technology.

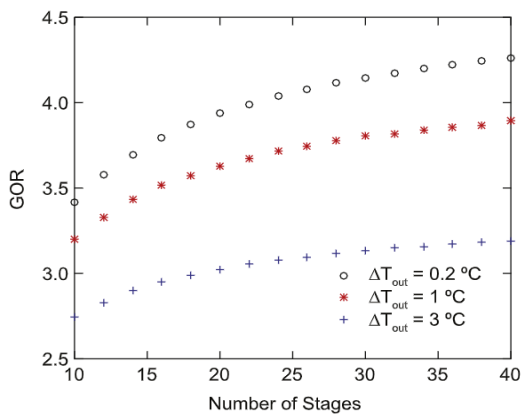
Another contribution has been proposed by Summers et al. [9] to improve the VMD system using multiple stages for up to 20 stages, assuming constant heat exchanger effectiveness. As per their results, the GOR has been reported to be 4 at the top brine temperature of 95 °C.

A new design technique for DCMD technology has been proposed by Khayed et al. [16], using in one casting step the hydrophobic/hydrophilic composite membranes employing the polymer solution method of traditional phase inversion that contains a fluorinated surface modifying macromolecule and hydrophilic host polymer. This work was investigated with a parametric study of various variables. The results showed that the proposed techniques performed better than the commercial ones such as PP, PVDF and PTFE membranes.

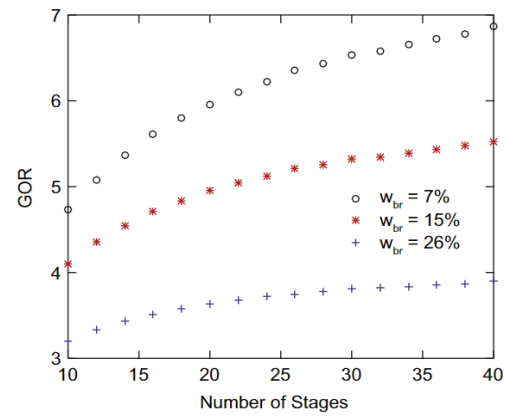
Another technique has been proposed by Chung et al. [17] in which the performance of a multistage vacuum membrane distillation (MSVMD) system, which is thermodynamically similar to MSF, for applications in desalination, brine concentration, and produced water reclamation is studied. The number of stages was varied from 10 to 40. The system's performance was quantified using energy efficiency (GOR), second law efficiency, and specific membrane area. Results show that MSVMD systems can achieve efficiency comparable to conventional MSF systems while requiring reasonable membrane areas across a wide range of feed salinities. Their findings showed that the MSVMD system provided better heat recovery, which gradually increased the GOR from 2.5 to 7. Figure 2.5 shows the flow diagram of MSVMD system and the research results. Feedwater enters the system and is pre-heated sequentially by the condensation energy released from the permeate stream at each stage. It then passes through an external brine heater, which raises the feed temperature to the desired top brine temperature before it enters the first VMD module. After leaving the VMD module, the feed flows into subsequent modules operating at progressively lower pressures. Permeate vapour generated in each module is directed to a flashing and mixing chamber, where it combines with flashed pure water from previous stages before proceeding to the heat exchangers. In steady-state operation, a portion of the brine is recirculated while the remaining brine is rejected as a brine blowdown stream. W_f and W_{br} are feed and brine blowdown salinities, respectively.



(a)



(b)



(c)

Figure 2.5. (a) Flow Diagram of MSVMD System, and (b and c) Effect of Temperature Differences and Brine Salinity on GOR [17]

Another development has been presented by Kim et al. [18] where they developed a solar multi-stage VMD model to be used with various quantities of heat recovery units (HRUs) by implementing the temperature modulating scheme to recover the energy from the permeate vapour to the feed seawater. The number of stages used in a VMD system was 24, with 10 HRUs. The results showed that the water production from the current system was 34% larger than that of a single HRU. Moreover, increasing the HRU from 1 to 10 without using the solar-thermal unit reduced the overall specific energy consumption by 20%. In contrast, when using the solar-thermal unit, the overall specific energy consumption was reduced by 28%–36% less than in the case without the solar-thermal unit.

Another MD design, called a novel dead-end MD (DE-MD), introduced by Mustakeem et al. [19] employed an approach called localized heating, which directly

supplies heat energy to the membrane-liquid interface, ensuring a stable temperature across the membrane. An electric heating coil is used to heat the feedwater close to the membrane-liquid interface. By applying heat to just a thin layer of feedwater at the the membrane-liquid interface, this method reduces temperature polarization (TP), the difference between the membrane surface temperature and the bulk feed temperature. As a result, water vapour flux increases, leading to improved GOR and reduced specific energy consumption compared to conventional bulk feedwater heating methods. The proposed model reduced the specific energy consumption to 57% by increasing the permeate flux and GOR to 45% and $132 \pm 12\%$, respectively, compared with the typical design.

The typical VMD technology has been integrated with solar field technology to collect more thermal energy from sustainable and clean energy, as proposed by Ma et al. [20] as shown in Figure 2.6, to study the process of remote coastal areas or islands. According to their findings, the production rate of domestic drink water over 12 hours reached 8 kg.m^{-2} . The GOR was found to be more than 0.7. This result was without condensation heat recovery. However, by introducing condensation heat recovery, daily water production reached 40 kg.m^{-2} .

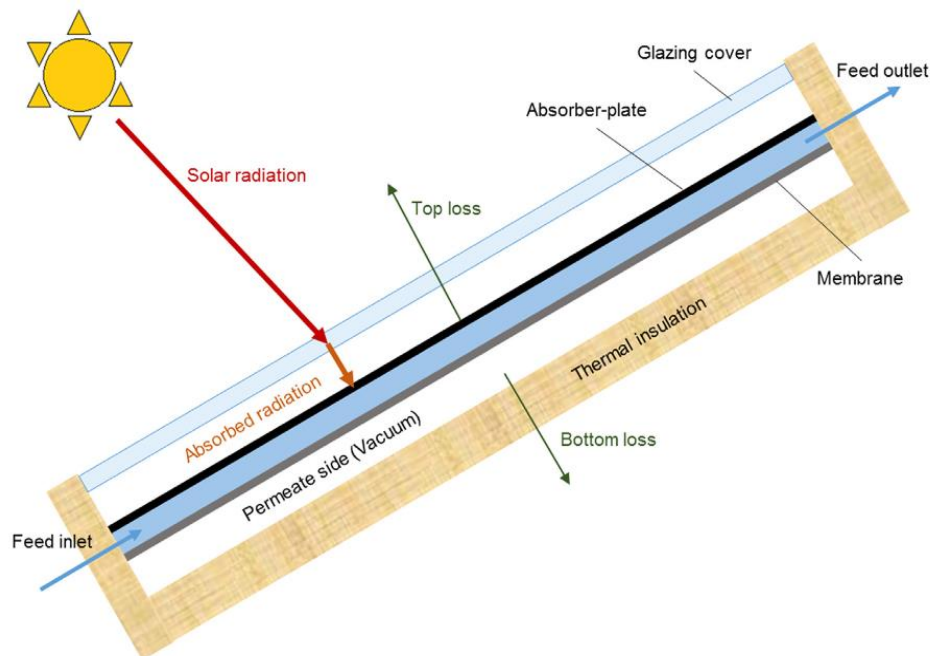


Figure 2.6. Integrated VMD System With the Solar Flat-Plate Collector [20]

Another developed idea has been proposed by Chen et al. [21] to improve the process of liquid desiccant regeneration using a thermodynamic model using a multi-

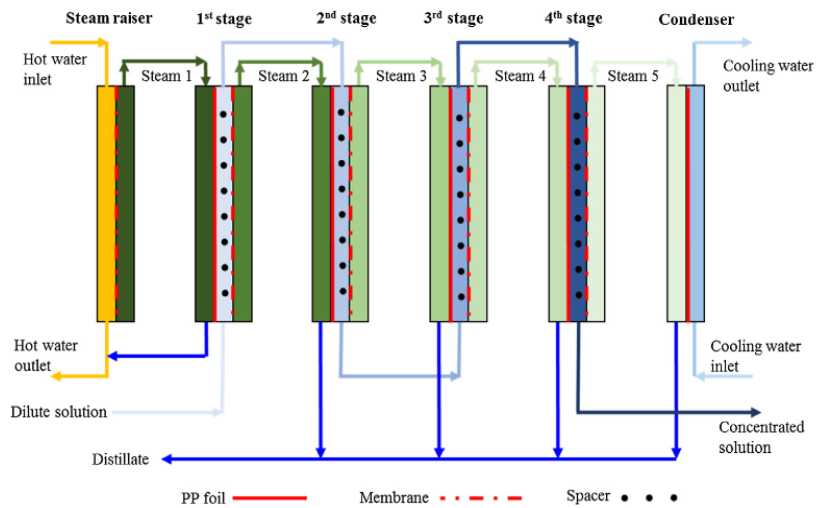
effect VMD system to investigate the process of liquid desiccant regeneration. Several V-MEMD arrangements (4S4L: 4-effect steam 4-effect liquid, 2S4L: 2-effect steam 4-effect liquid and 1S4L: 1-effect steam 4-effect liquid; see Figure 2.7 for more details) have been employed and examined under different operating conditions. The results indicated a significant degradation in the performance of the V-MEMD 4S4L configuration at larger feed concentrations, leading to a decrease in vapour pressure at larger feed concentrations. However, at higher feed concentrations, the 2S4L configuration outperforms the 4S4L and 1S4L configurations. This is because it delivers a higher steam temperature in the final effect, which better sustains evaporation, and it also recovers condensation heat more effectively than the 1S4L configuration.

Krnac et al. [22] explored the feasibility of a DCMD and concentrated photovoltaic (CPV) hybrid system to tackle water scarcity in arid and rural regions. The study results showed a permeate flux of 7.096 L/m²·h, using a PTFE membrane with an area of 0.0491 m², a salinity concentration of 1 ± 0.1%, and a membrane temperature difference of 18.82°C.

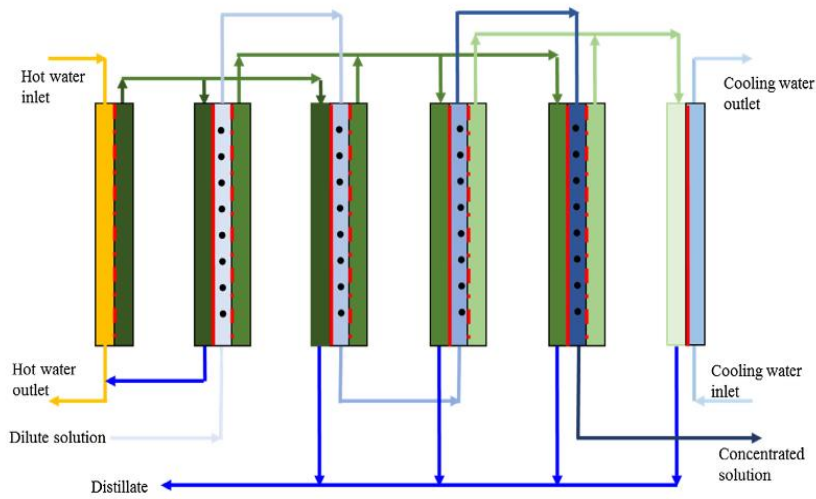
Another contribution of enhancing water production by 50 to 58 % compared to the typical design resulted from a new technique of designing the AGMD by providing a finned surface to improve the freshwater investigated by Bappy et al. [23].

The development of liquid-gap MD instead of Air-gap MD technology has also been addressed by Baek-Gyu Im et al. [24] using a flat sheet with PP as a support layer and PTFE as an active layer. The results showed that the permeate flux produced by the Liquid-gap membrane distillation (LGMD) was significantly affected by the coolant temperature compared with that produced by AGMD technology. Moreover, the increase in the liquid gap decreased the permeate flux produced by LGMD technology exponentially to its smallest value and then increased it asymptotically.

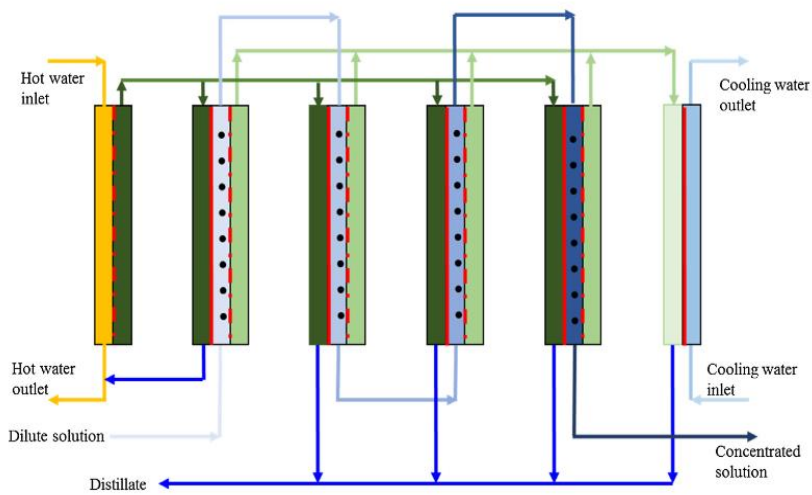
Most previously developed MD systems, DCMD and VMD, use a single stage. In contrast, JungGil Lee et al. [25] modified AGMD technology by adding multi-stages instead of a single stage to enhance its performance. The results revealed that the proposed technology enhanced the GOR by 24.4 times more than that produced by a single stage.



(4S4L)



(2S4L)



(1S4L)

Figure 2.7. Modified V-MEDM Configurations [21]

Previously, only two stage-effect has been presented, while Burhan et al. [26] found that the multi-stage VMD system consumed energy less than the single-effect

VMD system by four times when compared experimentally the performance of single-effect VMD and multi-effect VMD (four stages; see Figure 2.8)

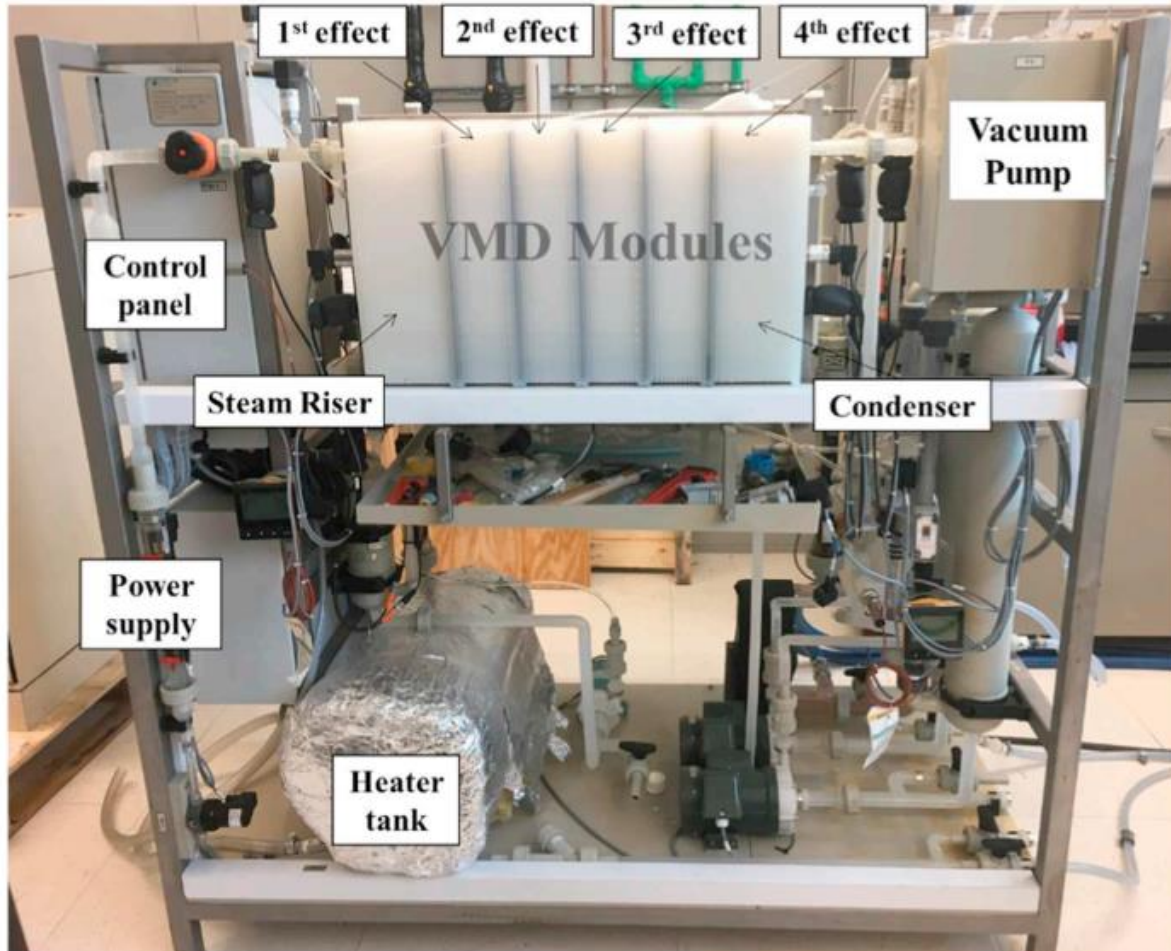


Figure 2.8. Photo of the V-MEMD System [26]

2.4 Temperature Polarisation

Temperature polarisation can be considered the most critical factor in the MD system since this factor represents the process in which the temperature of the membrane interface is different from the bulk feed solution's temperature. The feed-side interface temperature is smaller than the bulk feed solution temperature through the water evaporation procedure at the surface of the membrane since the evaporation latent heat reduces the liquid temperature. This will generate factors affecting an MD system's efficiency and distillate flux. For example, there is an obvious reduction in the driving force when the membrane interface temperature of the water is smaller [27].

To calculate the level of temperature polarisation, the temperature polarisation coefficient (TPC) can be used to evaluate and assess the design of an MD system. This coefficient can be determined using one of the following expressions:

$$TPC = \frac{T_f - T_{fm}}{T_f - T_v} \quad (2.1)$$

The variables (T_f , T_{fm} and T_v) are bulk hot-feed solution temperature on the feed side, membrane surface temperature on the feed side and liquid equilibrium temperature on the permeate side, respectively. The range of TPC is between zero and unity. If the TPC reaches one, this means that the hot-feed solution temperature is much greater than the feed membrane surface temperature, which in turn leads to large restrictions by heat transfer on the membrane system, resulting in a significant temperature polarisation effect. On the other hand, when the hot-feed solution temperature becomes very close to the membrane surface temperature, the TPC approximates zero, and the effect of temperature polarisation becomes meaningless. In such cases, the mass transfer process restricts the MD system [28].

The previous TPC expression was simplified in the VMD system to become only dependent on two variables (surface membrane temperature and hot-feed solution temperature) in the following formula by Chiam and Sarbatly [29].

$$TPC = \frac{T_{fm}}{T_f} \quad (2.2)$$

Martínez-Diez and Vazquez-Gonzalez [30] deduced that the imposed force decreased by 40–65% because of the temperature and vapour pressure change, and this reduction might become even worse with increasing the concentration, decreasing the recirculating rates. A large number of techniques have been proposed in the literature to solve this issue. Most of these techniques can be subdivided into three main categories: membrane modification, flow promoters and self-heated membranes, as presented in Figure 2.9.

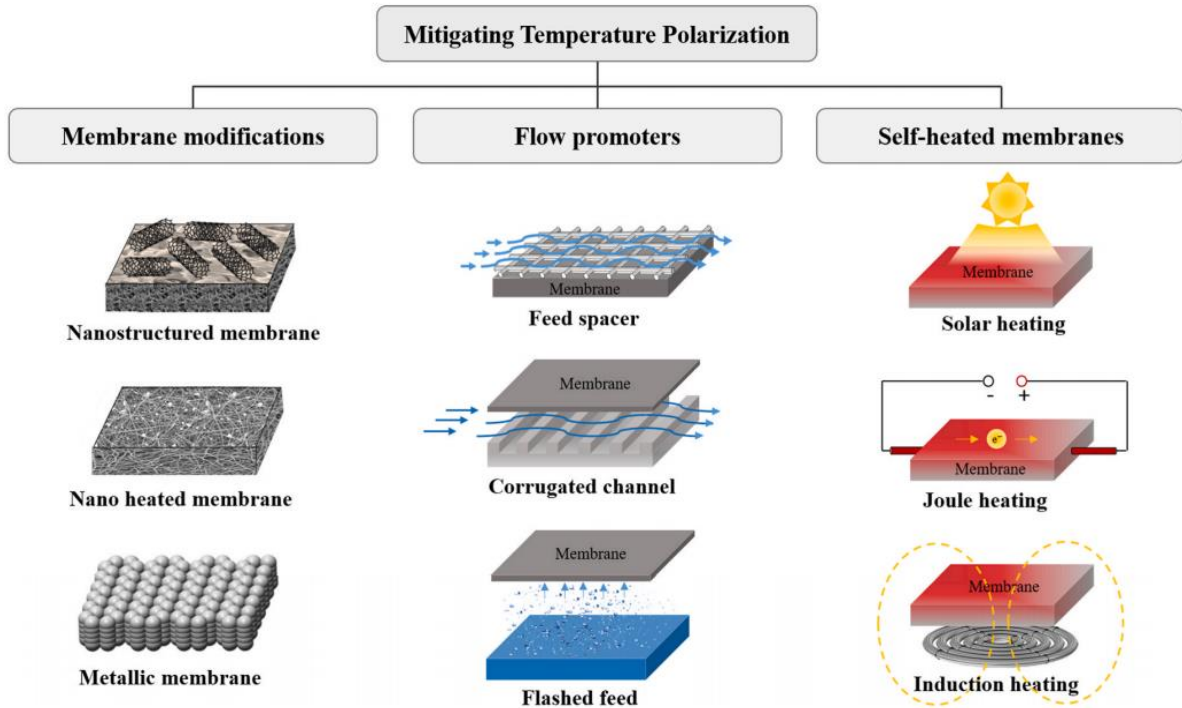


Figure 2.9. Recent Technologies to Overcome Temperature Polarisation in Membrane Distillation [27]

Mericq et al. [31] examined four types of solar energy systems integrated with VMD technology: (a) salinity gradient solar pond (SGSP) connected to VMD, (b) VMD submerged in SGSP, (c) solar collector (SC) connected to VMD and (d) SC connected directly to the VMD as shown in Figure 2.10. The results showed that the TPC reported the maximum value by Model (a) with (0.99), followed by Models (c) and (d) with (0.98), and then 0.81 was recorded by Model (b).

The TPC and concentration polarisation coefficient (CPC) can be significantly affected by changing flow patterns, as deduced by Wu et al. [32] when they studied the effect of flow patterns on the performance of a two-phase VMD system called air-bubbling VMD system. The Reynolds number represents the flow patterns for the two-phase gas and liquid (Re_{tp}). The results showed that both factors (TPC and CPC) have inverse relations with changing the flow patterns and feed inlet temperatures, as shown in Figure 2.11.

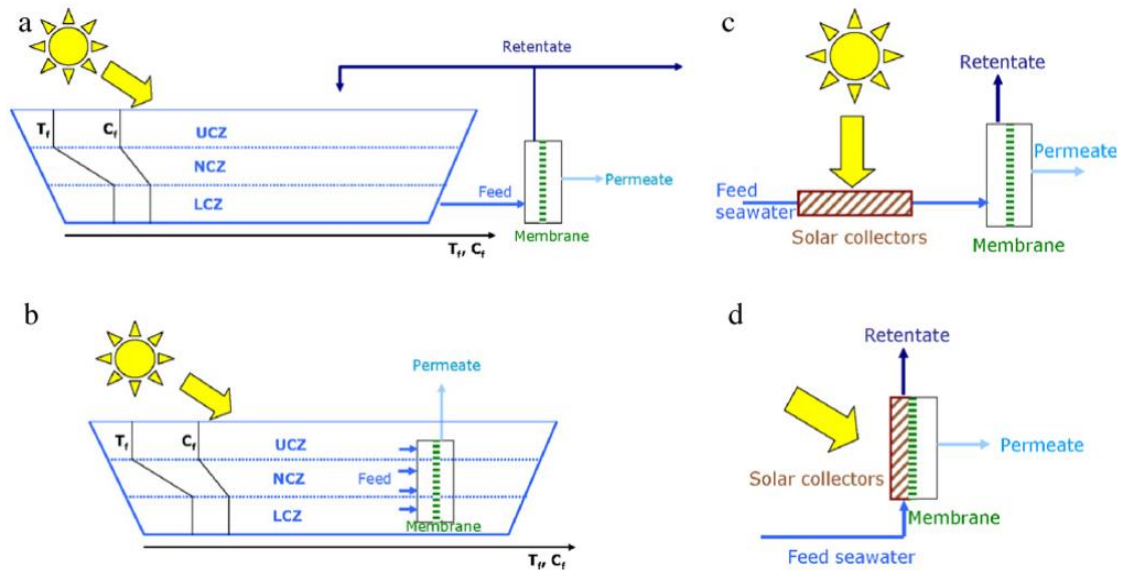


Figure 2.10. Solar Energy Systems Integrated with VMD [31]

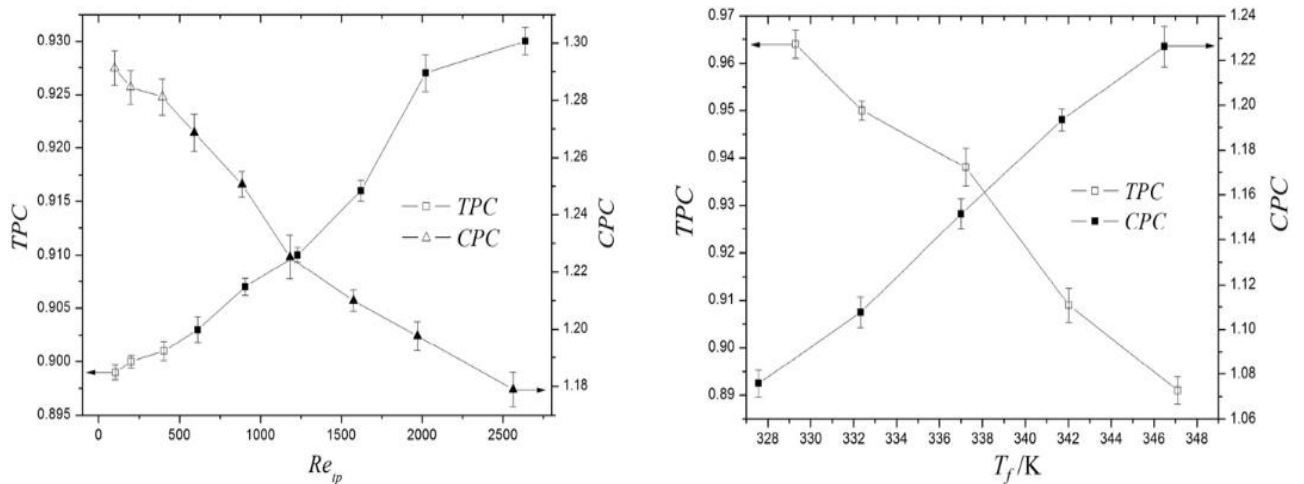


Figure 2.11. Performance of CPC and TPC with Changing Flow Patterns (left) and Feed Inlet Temperature (right) [32]

2.5 Membrane Modification

Another approach has been proposed by Lovineh et al. [33], in which they found that the TPC can affect feed temperature, feed velocity and membrane thickness. More specifically, the TPC decreased with increasing feed temperature, leading to increased specific energy consumption. In contrast, by decreasing the thermal conductivity of the membrane material, the TPC decreased. The polarisation effect decreased even more with the lower thermal conductivity of the membrane

material provided. This led to reduced heat dissipation via the membrane surface. Moreover, the increase in the membrane thickness showed reduced mass flux and increased TPC (see Figure 2.12).

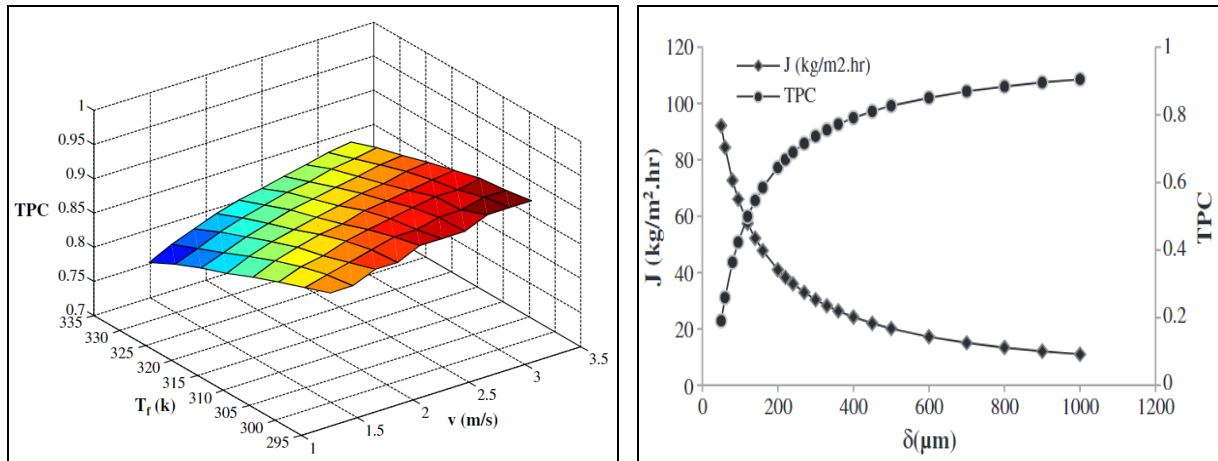


Figure 2.12. Effect of: (a) Feed Temperature and Velocity, and (b) Membrane Thickness on the TPC Performance [33]

Bhadra et al. [34] modified the membrane using detonation nano-diamonds to create a new membrane, which can be described as a member of the nano-carbon category. The new membrane enhanced the water vapour flux in the MD system, reducing the salt by 99.9% by preventing liquid penetration into the membrane pores compared to the conventional membrane.

Efome et al. [35] investigated the effect of super hydrophobic SiO₂ nanoparticles on the polyvinylidene fluoride used in a VMD system. The proposed membrane reported a higher than 99.98% salt rejection, with a permeate flux four times larger than the typical membrane. The usage of a modified membrane by using the carbon nano-tubes immobilization (CNIM-f) on the PTFE membrane under different operating conditions was studied by Bhadra et al. [36]. The proposed modified membrane showed potential for improving the permeate flux by increasing the flow rate and temperature higher than the typical membrane. In contrast, the reduction in salt rejection was higher than the typical membrane with increasing concentration. The images of both membranes are shown in Figure 2.13 from [36].

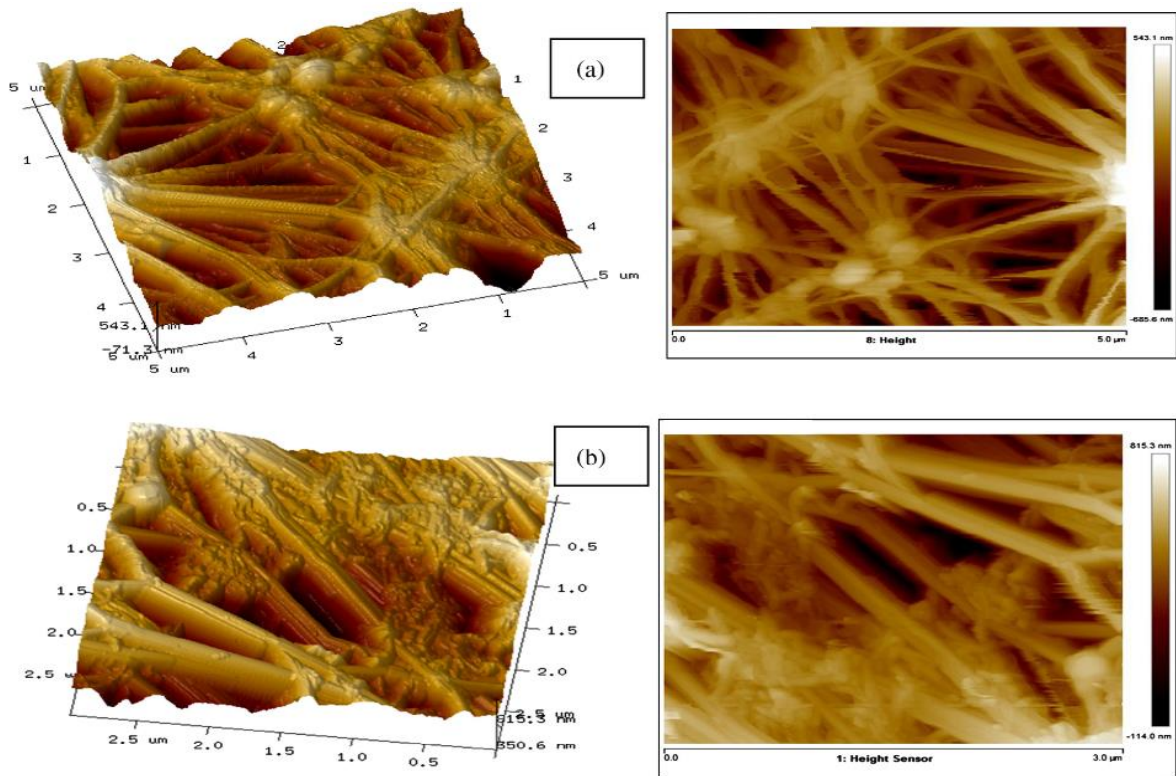


Figure 2.13. Comparison Between (a) Typical Membrane and (b) Modified Membrane [36]

Jafari et al. [37] and Ragnath et al. [38] have proposed further improvements using Graphene quantum dots and Carbon nanotubes immobilised on the membrane surface, respectively. Results showed that the salt was rejected by more than 99.5%, the mass transfer coefficient was increased by 1.8 times greater than that of the unmodified membrane, and the water vapour flux was enhanced by 76% compared with the typical system.

2.6 Flow Promoters

Another technique that can be used to overcome the drawbacks of TP is the use of flow promoters. This technique can be applied through stream turbulence and enhanced flow rates, which leads to improved feed-flow characteristics. However, increasing the flow rate is only sometimes preferred because more energy is required to supply larger flow rates. Moreover, increasing the flow rates causes a higher friction factor, which in turn causes higher shear stress and, finally, can cause damage to the active layer of the membrane. Furthermore, larger flow rates may increase the flow internal pressure higher than the membrane liquid entry pressure

(LEP), reducing membrane selectivity [27]. Therefore, the flow-rate selection should be optimised.

Among several approaches considered in the literature, metallic spacers have been found to develop mixing in the membrane surface vicinity, which in turn leads to a decrease in the thickness of the thermal boundary layer and a reduction in the TP effect by enhancing the heat transfer coefficient. Investigating this approach in the available literature mainly focuses on DCMD. These metallic spacers have been extensively optimised in the literature by Castillo et al. [39], Thomas et al. [40], and Tan et al. [41].

Alsaadi et al. [42] recently proposed another method, the flashed-feed channel, to reduce the TP effect. In this manner, the liquid feed stream is prevented from contacting the surface of the vacuum membrane using a custom-made vacuum module. Figure 2.14 presents the difference between the typical design and the proposed one. They showed that the proposed design provided distillate flux that doubled compared with the typical design under the same flow rate, which is a result of eliminating the TP effect.

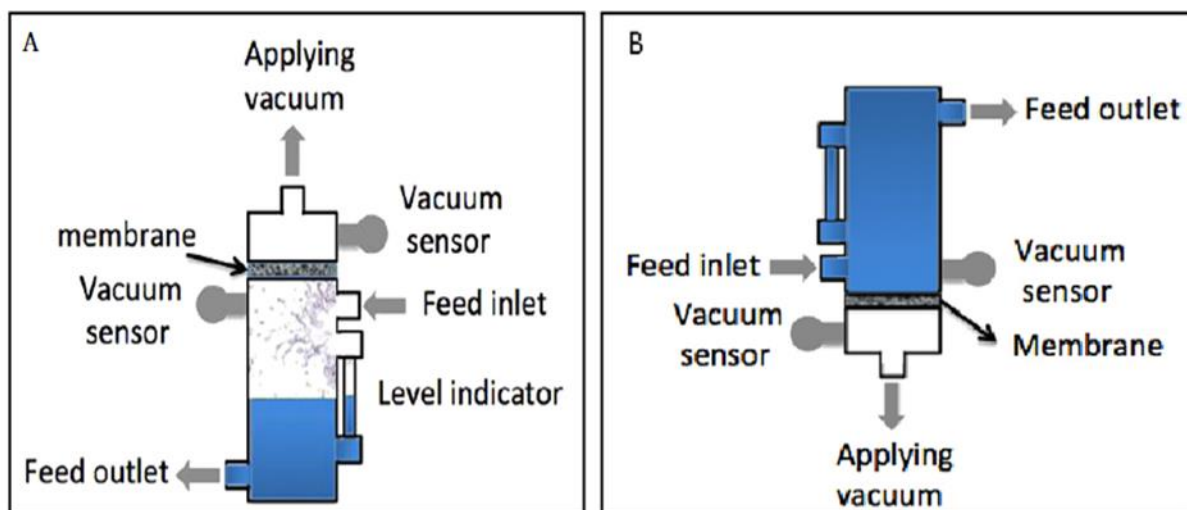


Figure 2.14. Comparison of (A) Custom-made VMD system and (B) Typical VMD Design [42]

Enhancing the flow mixing of the feed flow near the membrane surface is another approach proposed to mitigate the TP effect by creating corrugated feed channels and membranes with different sizes and elevations. This technique showed a potential to be effective in that the distillate flux and energy efficiency increased by 44% and 33%, respectively, compared with the typical DCMD system, as reported by

Mabrouk et al. [43]. Elhenawy et al. [44] recently examined the effects of corrugated feed channel and metallic spacer designs on an AGMD system under different geometries and operating conditions. They showed that the permeate flux provided by the corrugated channel and metallic spacer increased by 50% and 20%, respectively, compared with the typical system. Moreover, the GOR was found to be enhanced by 40% and 10% for both proposed designs.

2.7 Induction Heat

As previously discussed, the MD system provides several advantages compared to other typical systems. However, some aspects are still challenging and need to be resolved, such as high energy consumption, expensive heat management and low permeate flux. Moreover, the membrane system suffers from heat losses due to higher temperature polarisation when the membrane interface temperature is smaller than the feed temperature. This makes obtaining a large amount of the permeate flux for a large salinity feed problematic, according to Anvari et al. [45]. Therefore, some technologies have been investigated and integrated with the VMD system to enhance the heating process on the membrane.

Dudchenko et al. [46] used electrically conducting heater technology integrated with MD to treat saline brine. The results showed that self-heating technology is applicable in the MD system, even though the permeate cost was relatively high. Besides the heating advantage, this technology can also decrease the heat losses caused by the dual layer, increasing the distillate flux [47]. The induction heating process also provided better thermal stability, larger salt rejection and larger flux when the same technique was applied by Roy et al. [48], where a dual hydrophilic-hydrophobic polypropylene membrane was applied in the DCMD system.

Ji et al. [49] introduced a new approach to introducing a heating system in the VMD called the microwave irradiation technique (MWVMD). The results showed that the proposed system can effectively apply uniform heat to the radial direction of the membrane. Moreover, the mass flux increased significantly with increasing feed velocity and temperature compared to the typical VMD system. On the other hand, the mass flux decreased gradually as the vacuum level increased compared with the

typical VMD system, as shown in Figure 2.15. Furthermore, the mechanical properties of the system materials were not affected.

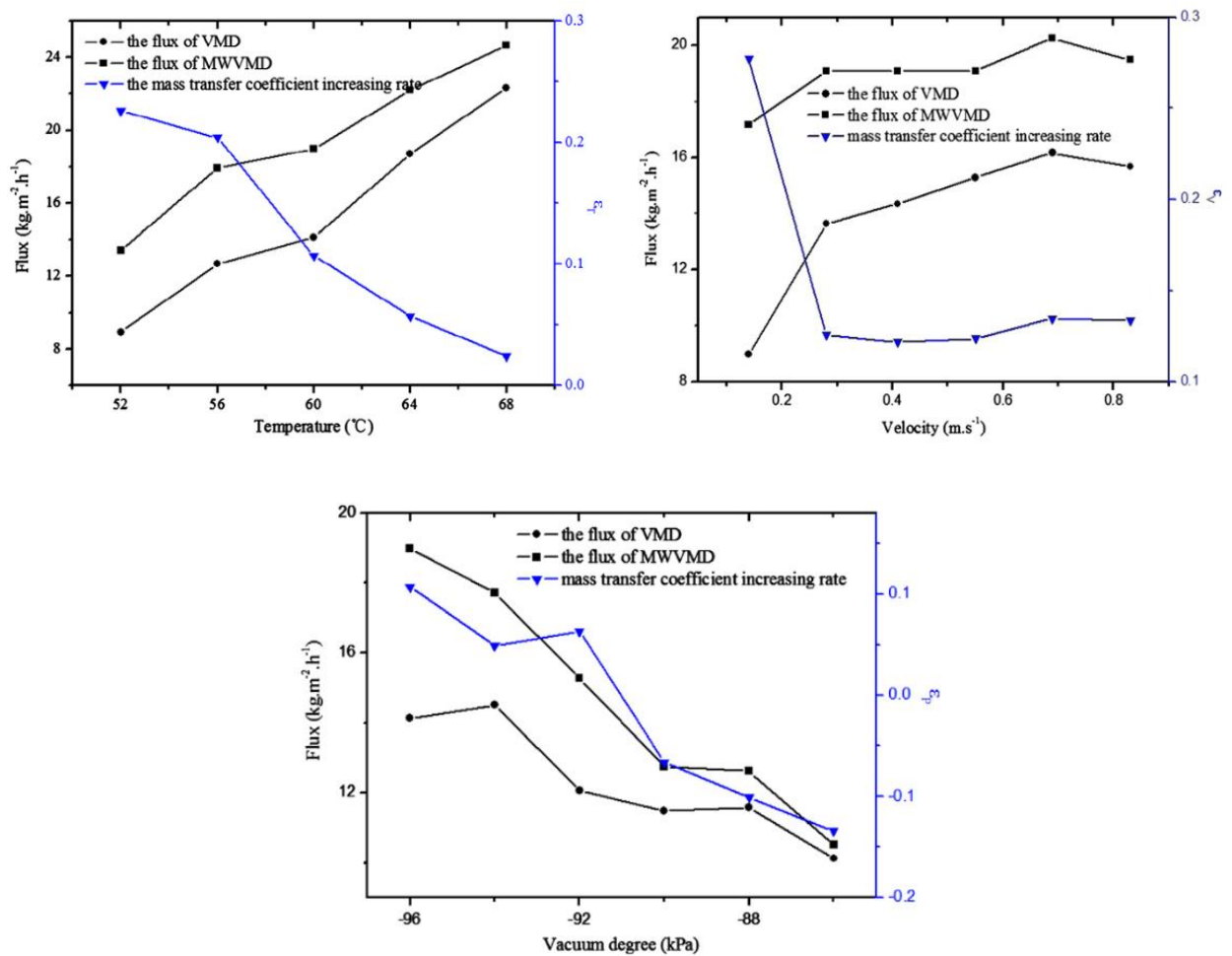


Figure 2.15. Effect of Integrating the Microwave with the VMD System [49]

Another novel design of VMD has been recently proposed by Anvari et al. [45] based on the concept of a self-heating (Induction heating: IH) membrane system enhanced by a large-frequency magnetic field to desalinate a range of saline solutions over a range of operating conditions. The surface membrane was fabricated by spraying nanoparticles called Fe-CNTs. The proposed system has been determined to be different from a typical VMD system in which the optimised permeate flux has been achieved at low flow velocities. The heat transfer process from the system membrane to the surrounding solution by diffusion and convection affected the flux by the residence time in the flow cell. Therefore, the proposed system is more efficient than the typical system in terms of feed stream containing large salinity. Moreover, the permeate flux produced by the proposed system is

larger than that produced by the typical system. In contrast, the specific energy consumption taken by the proposed IH-VMD system is smaller than that consumed by the typical system. Figure 2.16 shows the effect of the proposed system on permeate flux and specific energy consumption compared to a typical VMD system.

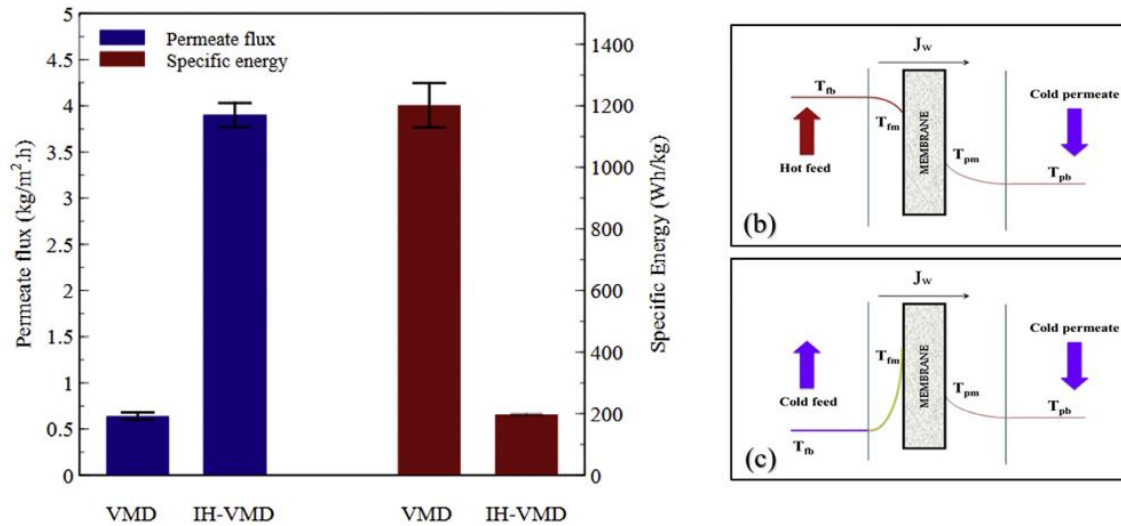


Figure 2.16. Effect of IH-VMD on the Permeate Flux and Specific Energy Consumption Compared with the VMD System [45]

Anvari et al. [50] proposed another novel model that integrates the typical VMD system with the ratio-frequency induction heat (RF-VMD) using the nanofluid called CaSO_4 on the thermally conducting membrane surface. Based on their achievements, the proposed system has enhanced the distillate flux better than the typical VMD system. Moreover, they showed that the distillate flux can be reduced by increasing CaSO_4 concentrations, which can be increased by increasing the Na^+ and Cl^- ions.

Recently, another technique called metallic spacer induction heating was proposed by Tan et al. [51] and integrated with a contact membrane used for water treatment. The metal used is nickel (Ni), which has high thermal conductivity. The results showed that the proposed technology produced a larger flux and energy efficiency than the typical system. The induction heating also allowed the external heating to be applied, without a reduction in energy efficiency. A summary of other heating approaches employed in different MD systems is presented in Table 2.2.

Table 2-2. Summary of Induction Heating Methods and Their Key Achievements in Literature

Reference	Heating Approach	Used Material	Input Heat (W/m ²)	Feed Temp. (K)	MD Type	Flux (kg/m ² .h)
[46]	Joule heating	CNT-PVA	11100	293	MD	7.50
[52]	Solar irradiation	CB-PVA	700	293	NESMD*	0.50
[53]	Solar irradiation	PDA	750	293	DCMD	0.49
[54]	Solar irradiation	Graphene array	1000	298	SVGMD	1.10
[55]	Solar irradiation	cESM-CNT	1000	294	SMD**	1.15
[56]	Solar irradiation	Lens array-CB NPs	700	293	MD	0.33
[57]	Joule heating	NRW	1560	303	VMD	2.00
[58]	Solar irradiation	Ag NPs	23000	303	VMD	25.70
[59]	Solar irradiation	Electrospun Ag NPs	3200	293	VMD	2.50

*NESMD: Nanophotonics-Enabled Solar MD; **SMD: Solar MD

As seen from Table 2-2, the proposed induction heating methods can provide better membrane distillation performance, and these methods are applicable in some MD types and have to be examined in other MDs as well. Moreover, these methods differ in terms of the contribution level in producing flux, specific energy consumption, GOR and energy efficiency. Figure 2.17 shows the contribution levels of most methods in presenting the most-mentioned variables. As can be deduced from Figure 2.17, the largest GOR was provided by the Fe-CNT with the IH-VMD

system proposed by Anvari et al. [27] with the minimum specific energy consumption and leading to the maximum energy efficiency.

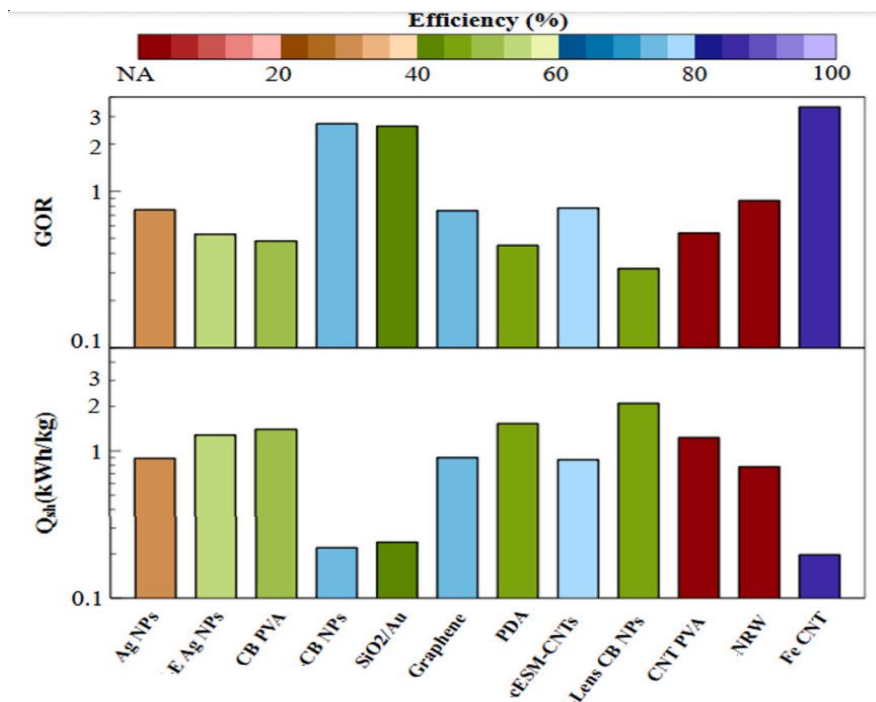


Figure 2.17. Effect of the Induction Heating Methods on the Performance of the MD System [27]

2.8 MD Characteristics

It is widely known that MD performance relies on three main parts: the module's design, membrane properties and operating conditions. In more specific detail, the feed temperature has the largest effect on the transmembrane flux among the examined operating conditions, followed by the flow rate of feed and then the permeated side partial pressure. Naidu et al. [60] performed an experimental study to modify a typical VMD system using vacuum multi-effect MD (V-MEMD) under different test conditions (different flow feed rates and sustainable low feed temperatures). Naidu et al. showed a 64% enhancement in the permeate flux as the feed temperature increased. However, the permeate flux has been reported to decrease by 18–20% when NaCl concentration was increased from one molar (1M) to three molar (3M). Chen et al. [61] studied the effect of a new hollow-fibre membrane in the VMD process called poly(tetrafluoroethylene-co-hexafluoropropylene) (FEP) preparation through the spinning method and compared the achievements with the results of a common hollow membrane PP studied by Li

et al. [62] and another hollow-fibre membrane PVDF used by Wirth and Cabassud [63]. The operation conditions and their results for all three cases are presented in Table 2.3.

Table 2-3. Comparison of Permeate Flux for Different Hollow-Fibre Membranes

Reference	Membrane type	Porosity (%)	Feed solution NaCl (g/L)	Feed Temperature (K)	Vacuum (KPa)	Permeate flux (L/m ² .h)
[61]	FEP	52.8	35	383.0	90	8.4
[62]	PP	50.0	35	333.5	800	3.0
[63]	PVDF	79.0	10	338.0	100	18.1

Deshpande et al. [64] investigated the performance of DCMD technology under two types of design and operating conditions, considering flow Reynolds numbers, the Jacob number, fibre dimensions, and packing (rectangular and staggered arrangements). They found that the rectangular packing with packing angle (δ) 45° and packing fraction (ψ) 0.6 provided the best performance.

Lian et al. [65] numerically studied the effect of different operating conditions on mass and heat transfer in single- and multi-stage VMD technology under cross-flow behaviour. The simulated results indicated that feed temperature and crossflow velocity significantly influence permeate flux across various module packing densities. Increasing the module packing density by 56% led to a 24% decrease in flux at a high operating temperature of 70°C, and over a 50% decrease in flux at a low crossflow velocity of 0.0072 m/s. Moreover, the permeate mass flux is directly affected by increasing the temperature and cross-flow velocity and indirectly influenced by salt concentration and vacuum pressure (see Figure 2.18).

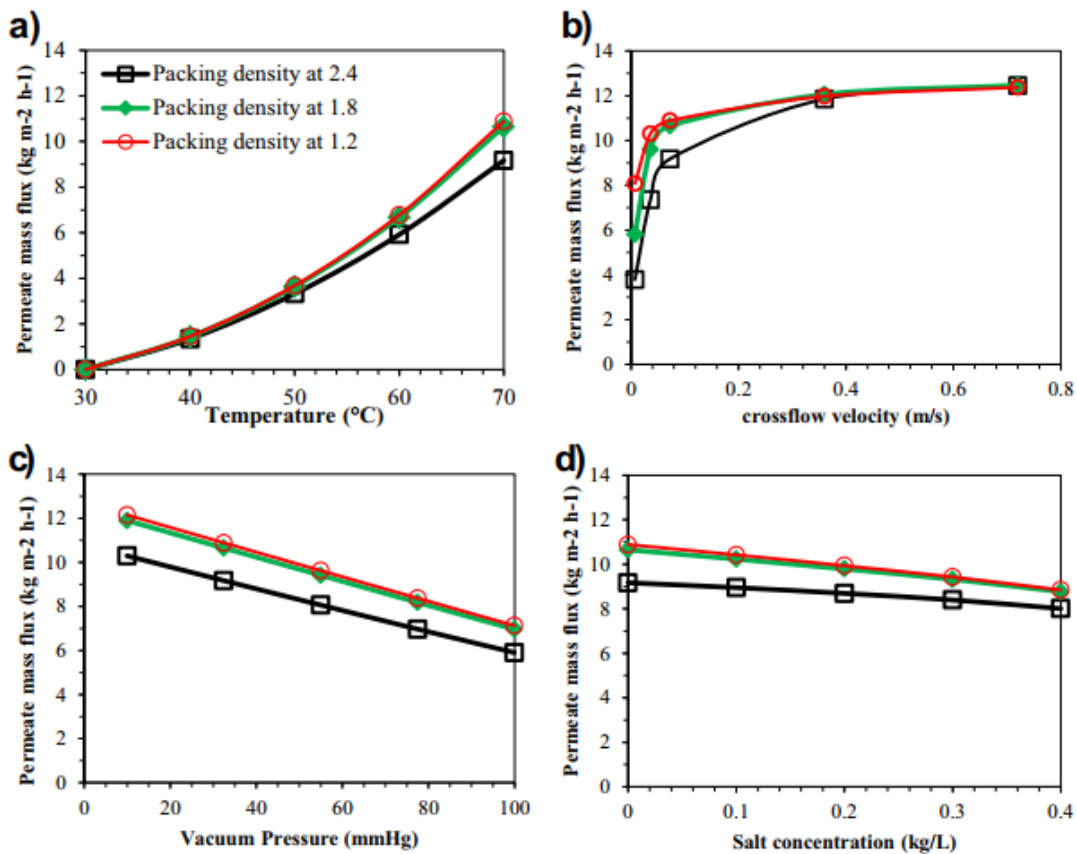


Figure 2.18. Mass Flux Profiles of VMD System Under Different Operating Conditions [65]

The effect of using a channelled coolant plate instead of a flat plate inside the AGMD has been proposed by Bahar. et. al [66]. They revealed that freshwater production improved by 50% compared to the typical flat plate for the same air gap.

Boutikos et al. [67] proposed a theoretical model to optimise the V-MEMD system by studying the design and testing conditions and considering the effect of feed and cold water flow rate, inlet temperature, and saline concentration. Moreover, membrane porosity, pore size and thickness were considered. There are also several effects on water productivity, distillate flux, GOR, recovery ratio and specific energy consumption. The results revealed that increasing the cold-water flow rate, hot water flow rate and hot water inlet temperature gradually enhanced the water productivity, GOR and recovery ratio and reduced the specific thermal energy consumption. On the other hand, increasing the cold-water inlet temperature and membrane thickness decreased water productivity, GOR and recovery ratio and enhanced the specific thermal energy consumption. However, increasing the number

of effects led to enhanced water productivity, GOR and recovery ratio while decreasing the specific thermal energy consumption.

Chen et al. [21] developed a thermodynamic model using a multi-effect VMD system to investigate the process of liquid desiccant regeneration under various operating conditions. They showed that higher hot water temperatures enhanced the regeneration rates and decreased the specific thermal energy consumption since a higher driving force was supplied, leading to better heat recovery and more energy provided to sustain evaporation. Moreover, the regeneration rate and specific thermal energy consumption were observed to be larger with increasing feed-flow rates.

The use of spacer-filled channels instead of typical ones inside the DCMD has been investigated [68]. The results showed that the new technology enhanced the mass flux and heat transfer and, in turn, enhanced the energy utilisation efficiency of the separation.

Burhan et al. [26] deduced that specific energy consumption decreased gradually with increasing hot water temperature and ambient temperature when using a multi-effect VMD system. On the other hand, increasing the hot water temperature enhanced the production rate, whereas increasing the ambient temperature reduced it.

Anvari et al. [45] proposed a VMD system based on the concept of a self-heating (induction heating, IH) membrane system enhanced by a large-frequency magnetic field to desalinate a range of saline solutions over a range of operating conditions. They revealed that permeate flux can be affected by different variables. In more detail, the permeate flux reduces with increasing nanoparticle Fe-CNT layer thickness and at larger flow velocities. On the other hand, the permeate flux increased as the vacuum level and small flow velocities increased. Another interesting point in this study is that increasing the salt concentration increased the permeate flux in the magnetic field VMD system. In contrast, the permeate flux decreased in the typical VMD system, as shown in Figure 2.19.

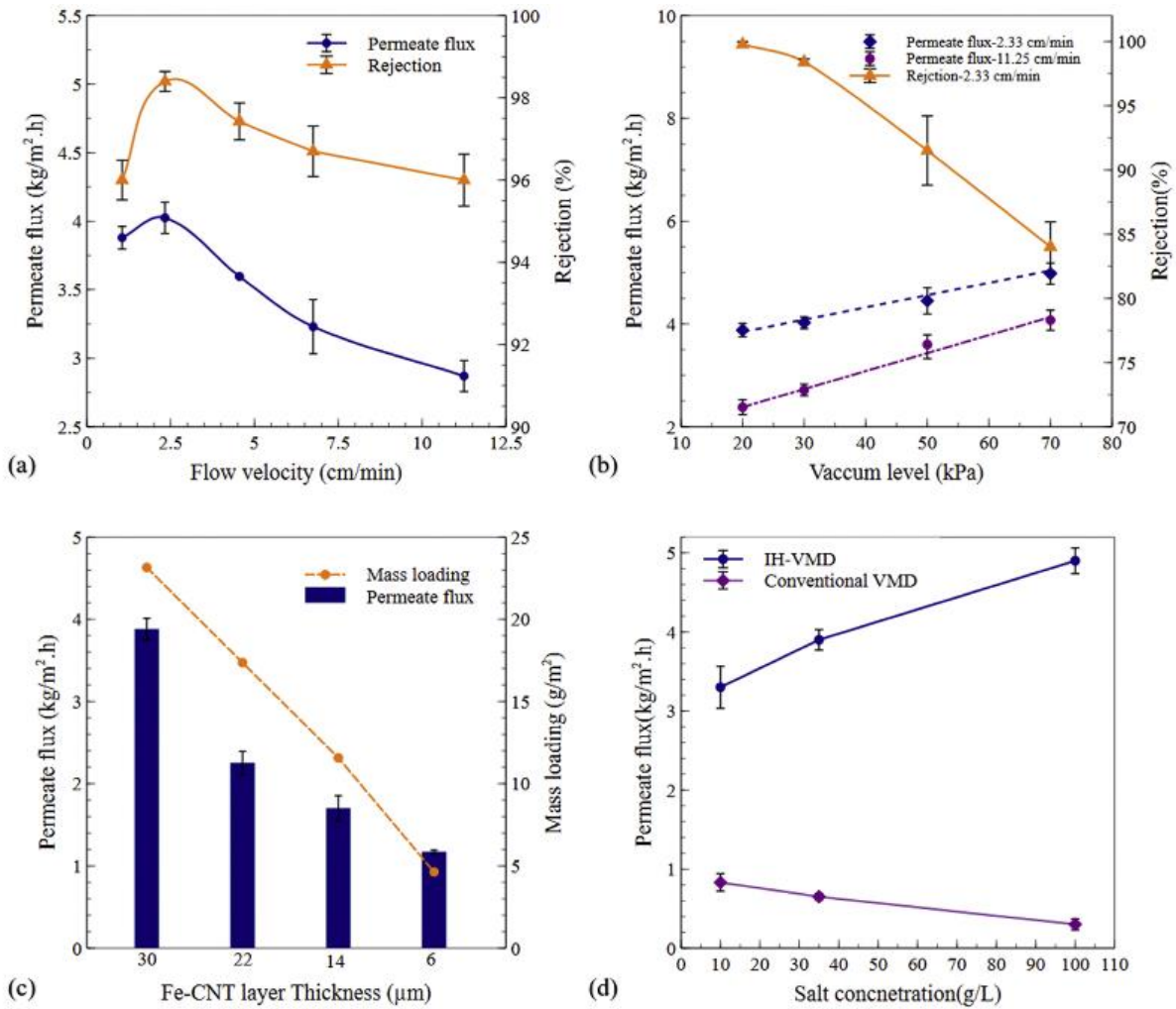


Figure 2.19. Effect of : a) Flow velocity, b) Vacuum level, c) Nanoparticle Layer Thickness, and d) Salt Concentration on Permeate Flux [45]

Chen et al. [69] performed a thermos-economic investigation of a V-MEMD configuration to obtain an optimisation design under different operating test conditions. The results revealed that productivity is directly related to the temperature difference between hot and cooled water. Moreover, increasing the cooling water and seawater flow rates enhances the specific energy consumption, productivity and energy efficiency (see Figure 2.20). They deduced that augmentation in heat and mass transfer can be achieved by increasing the number of membrane frames, which leads to a decrease in energy consumption and boosts freshwater production.

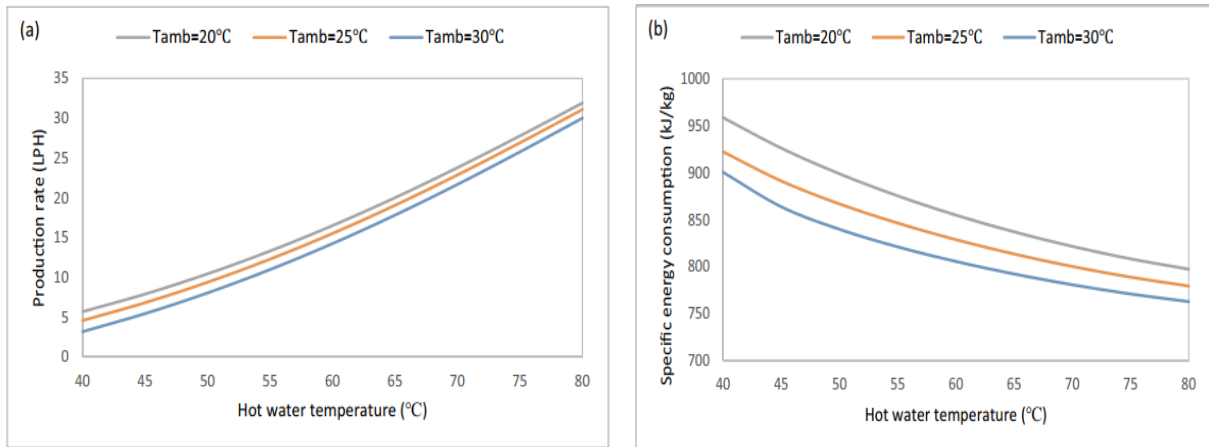


Figure 2.20. Effect of Hot Water Temperature on the Production Rate and Specific Energy Consumption [69]

Omar et al. [70] studied the effect of different VMD configurations ((a) first-stage heating without brine recirculation, (b) first-stage heating with brine recirculation, (c) inter stage heating without brine recirculation and (d) inter stage heating with brine recirculation) under different operating conditions such as a feed temperature, feed-flow rate, vacuum pressure, feed salinity and number of stages on the levelised cost of the water (LCOW). The results showed that increasing the feed temperature and number of stages decreased the LCOW but with different levels based on the configuration used. In contrast, increasing the vacuum pressure increased the LCOW at various levels based on the utilised configuration. However, increasing the feed-flow rate led to a rise in the LCOW in two configurations and a reduction in the LCOW in the others (see Figure 2.21). Furthermore, increasing the feed salinity does not affect the LCOW, but it can be affected by the type of configuration.

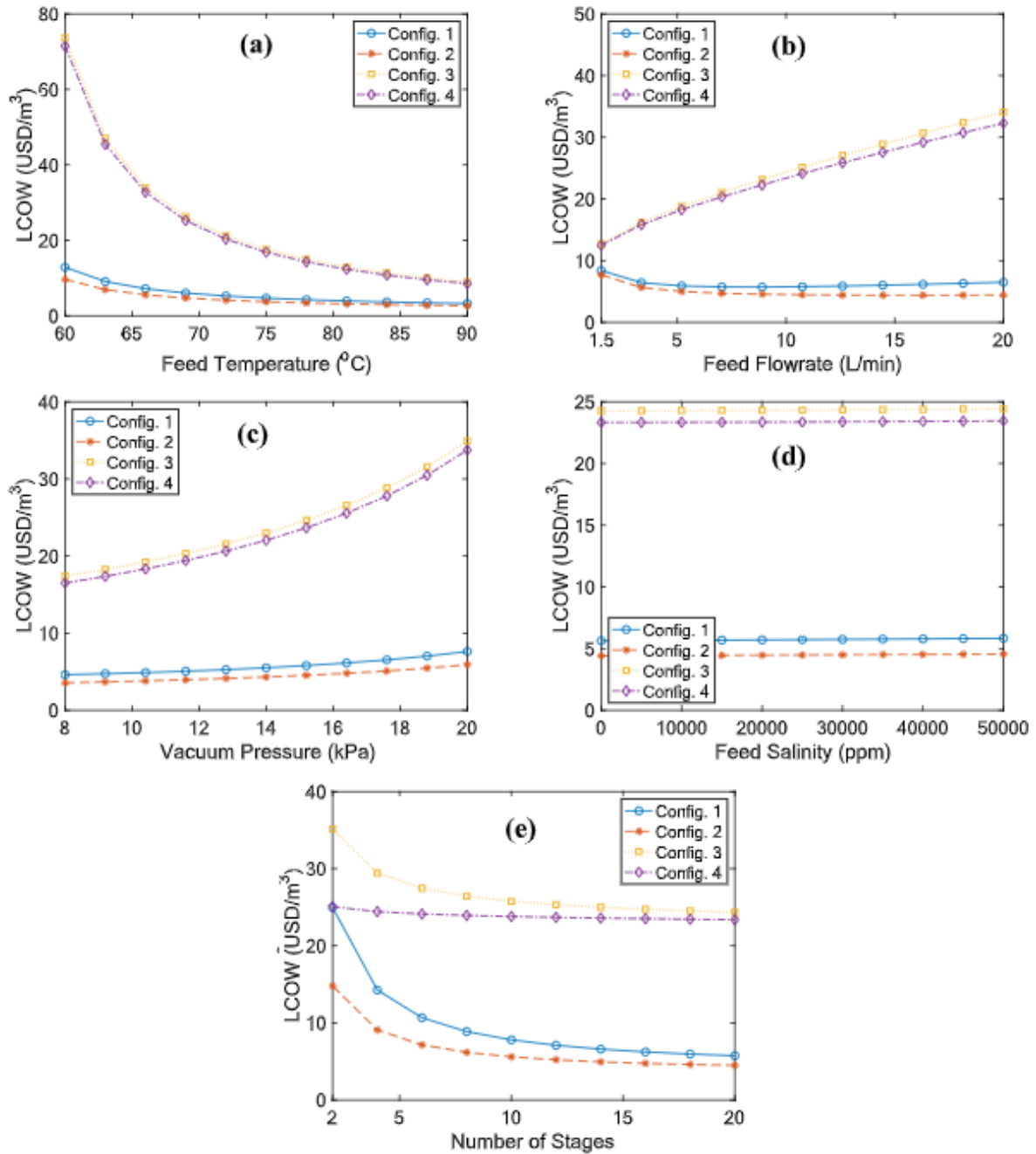


Figure 2.21. Effect of : a) Feed Temperature, b) Feed Flow Rate, c) Vacuum Pressure, d) Feed Salinity, and e) Number of Stages on the LCOW of Different VMD Configurations [70]

2.9 Economics and Energy Consumption in MD

Lee and Kim [71] numerically evaluated the economic and thermal performances of developed multi-stage vacuum membrane distillation (MVMD) technology (with 20 stages) using various arrangements: parallel, series and mix.

MVMD process heats feed stream and passes it through multiple vacuum stages, where reduced boiling points facilitate evaporation through the hydrophobic membrane. The permeate vapour condenses on the other side of each hydrophobic membrane, and the brine is reused in subsequent stages to increase water recovery. In contrast, V-MEMD also heats feedwater and operates under vacuum conditions, but it focuses on energy efficiency by reusing the heat released from vapour condensation in one effect to evaporate more water in the next. This reuse of heat across multiple effects enhances overall energy efficiency. Different cost aspects have been considered to assess the water production cost, including maintenance, capital, operation, and spare costs. The results showed that the mixed MVMD presented the most significant water production, 3.79 m³/day, with a minimum total cost of \$1.16/m³. Moreover, the cost can be reduced to \$0.52/m³ using a waste heat source.

Zhang et al. [72] improved a three-dimensional heat and mass transfer model using the computational fluid dynamics (CFD) technique for a hollow-fibre VMD system using laminar flow conditions to study the effect of different variables on the thermal performance of the VMD system. The results showed that the numerical predictions were in excellent agreement with the experimental results extracted from the literature. The results also showed that the total thermal efficiency was reduced at a large feed velocity owing to the large heat loss. The module length also significantly affected the VMD performance regarding water production, temperature difference and mean flux distributions.

Zhang et al. [73] numerically evaluated the economy and energy consumption in a multi-effect VMD system using a first-stage process and an inter stage heating process over 30 stages using a hollow-fibre module. The highest cost and maximum water production were achieved in the first stage. However, the fourth stage provided the smallest cost with an acceptable level of water production; thus, it was the optimum stage. The fixed and total costs of the four stages were \$0.42/tonne and \$0.59/tonne, respectively, compared to the fixed and total costs of the first stage, which were \$0.78/tonne and \$0.82/tonne, respectively. The results are better than the results concluded by Sarbatly and Chiam [74], in which they assessed the economic efficiency of the VMD system and deduced that the water production cost was \$0.5/m³ for 20,000 m³/d produced from the geothermal energy VMD plant.

A framework for optimising and evaluating energy efficiency for DCMD technology was proposed by Christie et al. [75]. They found that using a heat exchanger at each stage of multi-stage DCMD could enhance MD efficiency and increase GOR. Chen et al. [69] conducted a thermos-economic investigation for a V-MED configuration to obtain an optimisation design under different operating test conditions, considering the desalination cost in the study analysis. The results showed that more than 80% of the final desalination cost is spent on the membrane and energy costs, which gives a prediction that their contribution depends on the variation in the energy price. However, increasing the number of effects of membrane frames causes a reduction in the specific energy consumption, thermal energy price and desalination cost. As can be seen from Figure 2.22 to 2.24, when the system has more numbers of frames, both the production rate and the energy efficiency can be significantly improved due to more heat and mass transfer areas available. However, the specific permeate flux per unit membrane area decreases, meaning more membrane area is required to produce the same amount of freshwater.

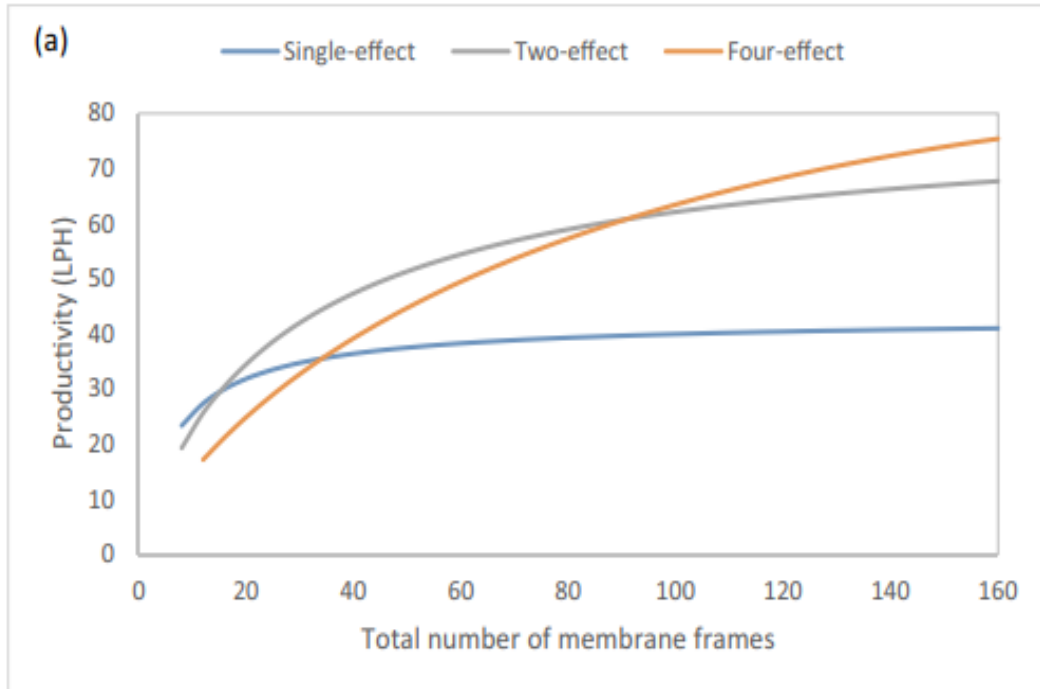


Figure 2.22. Influence of Number of Effects and Membrane Frames on Overall Productivity [69]

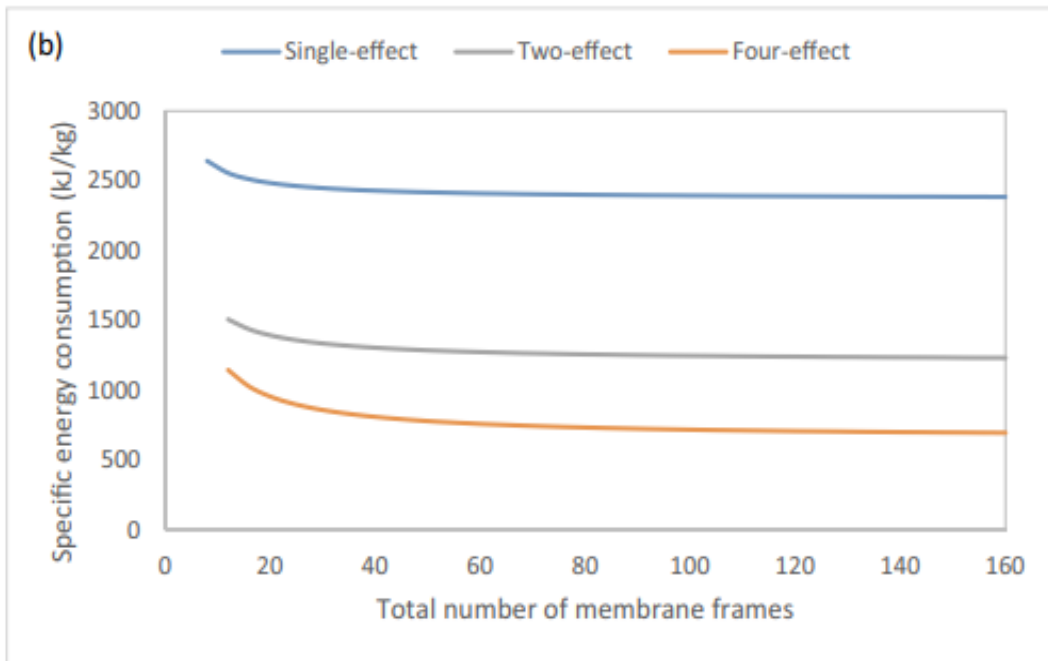


Figure 2.23. Influence of Number of Effects and Membrane Frames on Specific Energy Consumption [69]

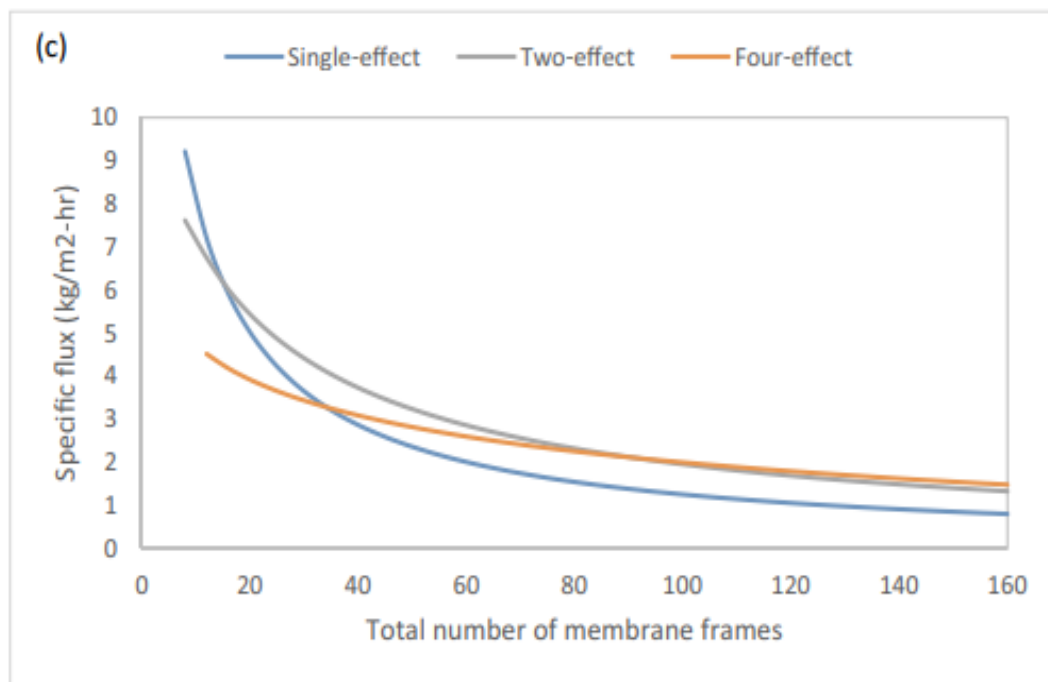


Figure 2.24. Influence of Number of Effects and Membrane Frames on Specific Flux [69]

Criscuoli, A. [76] proposed combining VMD and DCMD technology. They found that the specific thermal energy consumption was reduced to 50%, whereas 100% enhancement was achieved in the GOR ratio and a 69% increase in permeate production compared to typical DCMD technology.

Omar et al. [70] investigated a single-stage VMD system in four different multi-stage arrangements under various operating conditions. These arrangements are (a) first-stage heating without brine recirculation, (b) first-stage heating with brine recirculation, (c) inter-stage heating without brine recirculation and (d) inter-stage heating with brine recirculation. The results showed that the proposed configurations reduced the specific heat consumption by 25–55%. Moreover, a Pareto multi-objective optimisation approach was considered to decide which configuration was the best for specific heat consumption and LCOW. Compared with all considered configurations, an acceptable LCOW range of \$2.27–\$8.30/m³ was provided by the configuration of the first-stage heating with no brine recirculation. The study also compares the four proposed performances and the single-stage VMD system in terms of the total cost spent on every component, as shown in Figure 2.25.

2.10 MD Modelling Techniques

The modelling technique is a very attractive tool that can be utilised to understand the physics aspects, such as heat and mass transfer, and perform an optimum MD design that is the easiest way of changing operating and environmental conditions. All MD types have been extensively studied in many numerical and theoretical investigations. Some of these studies have focused only on one-dimensional models using mass and heat transfer, which are based on energy balance. Other two-dimensional models have been considered, which, based on determining the variable quantities such as velocity, pressure and temperature, are determined along two x-axis and y-axis directions. Moreover, other studies have considered CFD to determine flow properties by solving the Navier–Stokes equations. All these models and techniques have been proposed to predict flow behaviour in a region that experimentation cannot reach and provide more information on all variables in consideration. Moreover, the permeate flux can be easily predicted, and the temperature and concentration polarisation coefficients can be estimated.

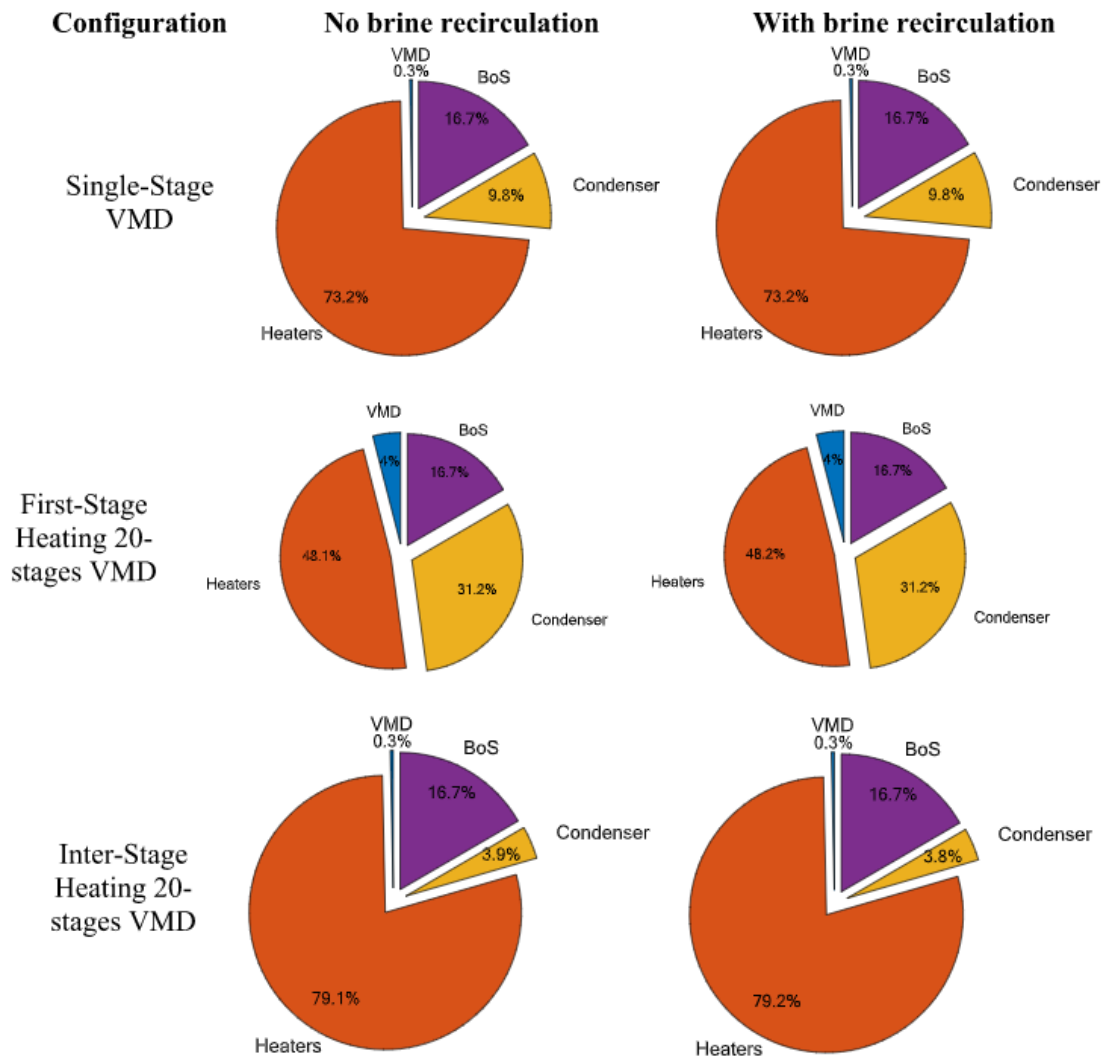


Figure 2.25. Pie Chart Cost Breakdown of Different Multistage VMD Configurations Compared With the Single-Stage VMD System [70]

Shim et al. [13] evaluated the performance of an MVMD system using a one-dimensional mathematical model by predicting water permeate flux and heat and mass-transfer coefficients. Using Aspen Plus, which is process simulation software for modeling, designing, and optimizing chemical processes, the developed model incorporates the equations for mass, momentum, and energy conservation. This model was solved using the finite volume method, and the corresponding flow behaviour was solved using the FORTRAN language. The predicted results agreed with the experimental measurements, as shown in Figure 2.26.

Zuo et al. [77] proposed a two-dimensional model involving all conservation equations (mass, momentum and energy) to represent the flow profiles, such as

temperature and velocity, using a genetic algorithm. The Genetic Algorithm is an advanced numerical method that significantly reduces the number of possible solutions, making it easier to find the optimal design and operating conditions from a manageable set of combinations, rather than from an overwhelming number of possibilities. Moreover, the profile of VMD behaviour is also predicted using a hollow-fibre membrane module. The modelling technique led to easily provisioning an optimised design among different operation variables. The results showed that using the optimised model can enhance water production and decrease water production costs by 38.1% compared with the non-optimised model.

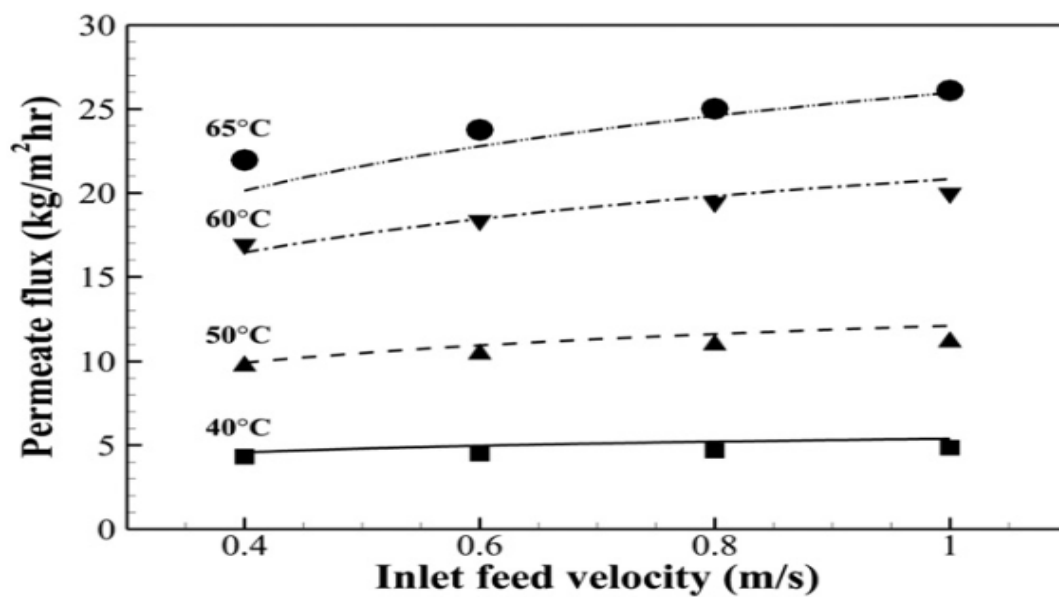


Figure 2.26. Comparison Between the Numerical Finite Volume Results (Lines) Against Experimental Data (Symbol) [13]

Boutikos et al. [67] proposed a theoretical mathematical model based on the energy and mass balances to provide a guideline for the V-MEMD optimum design under different operating conditions. Two case studies were used for the feed channel. Compared with the experimental data, the proposed model showed a significant deviation (2–23%) when using saline water as a feed solution. However, the deviation was reduced to 1.9–11.1% when tap water was used.

The CFD technique has been used by Zhang et al. [73] to simulate the flow behaviour and heat and mass-transfer characteristics in two multi-effect VMD systems in two other models: the inter stage heating process and the first-stage

heating process. Regarding the achievements, the first-stage heating process provided the highest GOR profile. Thus, it was preferred even though the inter stage heating process proposed the highest water recovery.

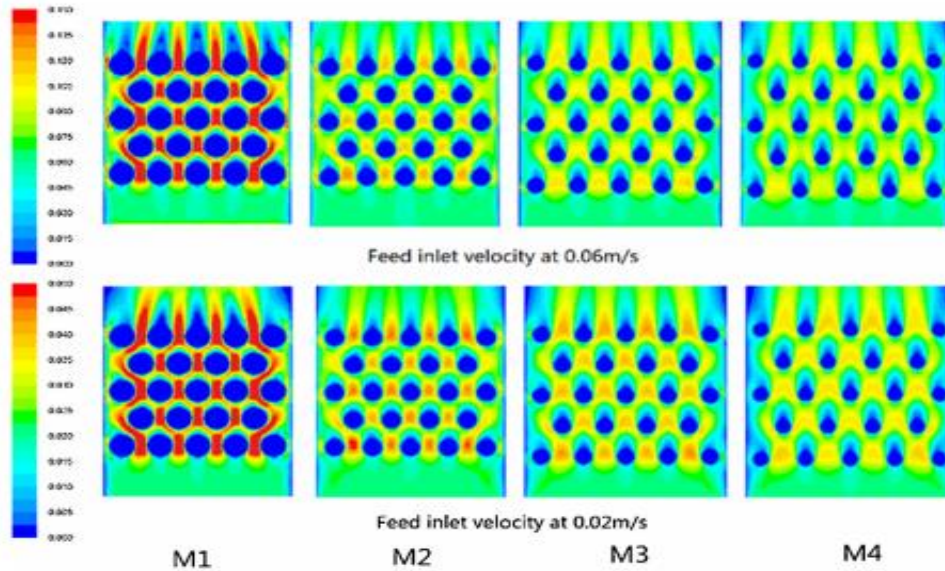
Tang et al. [78] also used a two-dimensional model utilising the finite volume method to solve Navier–Stoke equations using the CFD tool. The flow was a multiphase flow inside the VMD system's porous media to determine the VMD behaviour's permeability. The results showed that the deviation between the experimental data and numerical predictions was not small; thus, more numerical improvements are needed.

Zhang et al. [12] developed a new method for measuring hollow-fibre membrane properties, which can be used for modelling purposes in a VMD system. The method considers gas permeability a function of membrane length, which was extrapolated to zero length. This process provided sufficient information for the membrane materials and was then used for flux modelling. The results showed that the prediction results were very close to the experimental results for a short duration of experimental work (1–2 h).

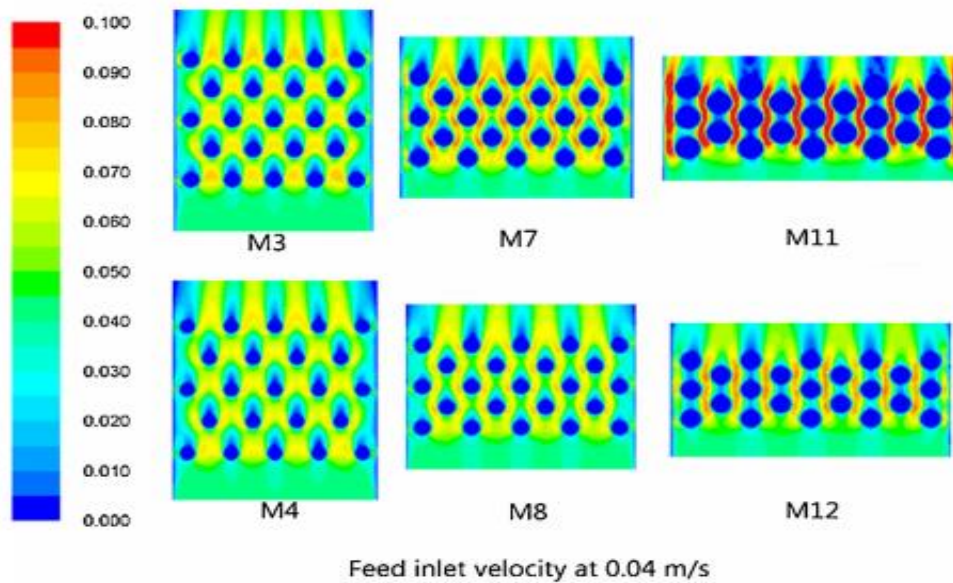
In a three-dimensional study using seven hollow fibre membrane bundles, Lian et al. [65] also used the finite volume technique to simulate a VMD system's heat and mass transfer and cross-flow behaviour. The flux was predicted based on the mass jump method, which is a novel computational approach developed for simultaneous calculation of mass and heat transfer across a membrane, over a temperature range of 303–343 K, cross-velocity in a range of (0.0072–0.72 m/s), and a vacuum pressure range of 10–100 mmHg. The flux predicted by the numerical simulation was found to be different from the experimental one by less than 7%.

Liu et al. [79] used the finite volume method through the CFD tool to study the effect of intersection angle (60–120°) and fibre row space (1.5 d–3.0 d) of fiber configurations in the hollow-fibre VMD system to achieve the optimised design, considering different variables such as permeate flux, heat and mass transfer and the polarisation effect. An accepted agreement between the numerical prediction and the experimental data was obtained. The results were presented using CFD contours in which row space and intersection angles influenced the velocity contours, as shown in Figure 2.27. The fiber configurations are labelled as M1 through M12, where each label represents a specific combination of row space and intersection

angle: M1 to M4 have a 60° angle with row spaces of $1.5d$, $2.0d$, $2.5d$, and $3.0d$, respectively; M5 to M8 have a 90° angle with the same row spaces; and M9 to M12 have a 120° angle with the same row spaces., where d stands for the outside diameter of the fiber. Moreover, the largest permeate flux was achieved by $2.5 d$ row space and an intersection angle of 60° or 90° .



(A)



(B)

Figure 2.27. Effect of (a) Row Spacing ($1.5 D$ to $3.0 D$, M1 to M4) and (b) Intersection Angles (60° to 120°) on Cross-Flow Velocity Magnitude [79]

Anqi et al. [80] studied numerically the performance of a VMD system under different optimised design parameters under laminar and turbulent flow conditions. This study was performed using a three-dimensional transient CFD model and a large eddy simulation turbulence model. The predicted vapour flux was in excellent agreement with the experimental data. They also showed that using a larger inlet temperature and feed rate when inserting the filaments in the feed channel increased more than 50% of the water permeate rate.

Chang et al. [81] numerically studied the effect of batch-submerged VMD systems using the MATLAB tool under different operating test conditions. This system provides a uniform feed temperature with internal heat supplied by the batch-submerged system. The deviation between the experimental data and the numerical predictions was less than 5%. Moreover, the proposed system improved the permeate flux from 5.09 to 9.25 kg/m².h and the GOR from 0.19 to 0.3 when using four hollow fibres compared with the typical VMD system.

2.11 Mathematical Model Formulation

This section describes the mathematical forms that govern heat and mass transfer through the vacuum membrane desalination system and the flow behaviour using the equations and models available in the literature.

2.11.1 Water Mass Flux

The driving force of water flux in vacuum membrane desalination is the difference between the vacuum and feed parts in the water vapour pressure. Therefore, the water flux (J) can be described linearly to the partial pressure gradient and can be calculated based on the following formula by Shim et al. [13]:

$$J = C_V(P_m^F - P_m^V) \quad (2.3)$$

The parameters P_m^F and P_m^V are the membrane surface pressures at the feed and vacuum sides respectively. However, the variable C_V represents the membrane surface coefficient, which can be calculated from the following equation:

$$C_V = 1.064 \frac{r\varepsilon}{\delta\tau} \left(\frac{M_w}{RT}\right)^{0.5} \quad (2.4)$$

The variables $\delta, \tau, \varepsilon$ and r are the membrane thickness, membrane pore tortuosity, porosity and average pore size, respectively. However, the factor R is the universal gas constant, and M_w is the water molecular weight. On the other hand, both Knudsen diffusion and Poiseuille behaviour can take place in the calculation of the membrane surface coefficient, as presented by Chiam and Sarbatly [29], in the following formula:

$$C_v = 1.064 \frac{r\varepsilon}{\delta\tau} \left(\frac{M_w}{RT}\right)^{0.5} + 0.125 \frac{r^2\varepsilon M_w P}{\delta\tau \mu RT} \quad (2.5)$$

Where T and P are the mean vapour temperature and mean vapour pressure in the membrane pores, which can be calculated from the following equations:

$$T = 0.5(T_m^F + T_m^V) \quad (2.6)$$

$$P = 0.5(P_m^F + P_m^V) \quad (2.7)$$

Here, T_m^F and T_m^V are the membrane surface temperatures at the feed and vacuum sides, respectively.

Other investigations, such as by Zhang et al. [72], suggested that mass transfer can be represented by three mechanisms: molecular diffusion, Poiseuille flow and Knudsen diffusion based on the Knudsen number. If the Knudsen number is less than 0.01, then the mass transfer can take place by only Poiseuille flow, and equation (2.5) is used after removing the left part, which represents the Knudsen diffusion part. If the Knudsen number is greater than 0.01 and less than 1, equation (2.5) can be used without removing any part. However, if the Knudsen number is greater than 1, the flow is dominated by the Knudsen diffusion, and equation (2.5) can be used after removing the right part. The Knudsen number (Kn) is defined as follows:

$$Kn = \frac{l}{d} \quad (2.8)$$

Where l represents the transferred gas molecule mean free path and d is the membrane mean pore diameter.

2.11.2 Heat Transfer Coefficient

In the VMD system, the heat transfer coefficient on the vacuum side is minuscule compared with the heat transfer coefficient on the feed side. The heat transfer coefficient on the feed side can be calculated from the following expression:

$$h_F = \frac{Nu k_F}{d_h} \quad (2.9)$$

The variable d_h is the hydraulic diameter of the module measured in metre, k_F represents the feed thermal conductivity measured in W/m K, which is generally speaking to be calculated based on the gas thermal conductivity (k_g), polymer thermal conductivity (k_p) and membrane porosity (ε) from the following expression by Zhang et al. [82]:

$$k_F = \varepsilon k_g + k_p(1 - \varepsilon) \quad (2.10)$$

However, the Nu is the Nusselt number, which has been provided in many correlations in the literature based on the membrane model and Reynolds number (Re) and Prandtl number (Pr). These numbers are given below [33, 70, 83]:

$$Nu = 0.023 Re^{4/5} Pr^{0.3} \quad Re > 10,000 \quad (2.11)$$

$$Nu = 1.86 (Re * Pr * (\frac{D_h}{L}))^{0.38} \quad Re < 2100 \quad (2.12)$$

$$Nu = (0.01089 Re^{1.191} + 27.33) Pr^{1/3} \quad Re < 10,000 \quad (2.13)$$

$$Nu = (0.01724 Re^{1.13} + 28.43) Pr^{1/3} \quad Re > 10,000 \quad (2.14)$$

$$Re = \frac{\rho_F V_F d_h}{\mu_F} \quad (2.15)$$

$$Pr = \frac{C_{pF} \mu_F}{k_F} \quad (2.16)$$

The variables ρ_F , μ_F , C_{pF} and V_F are feed's density, feed's dynamic viscosity, feed's specific heat capacity and feed's velocity respectively.

The heat transferred from the feed side (Q_F) to the vacuum side (Q_m) through the membrane is assumed to be the same and can be calculated as [84]:

$$Q_F = Q_m \quad (2.17)$$

$$Q_F = h_F A(T_F - T_m) \quad (2.18)$$

$$Q_m = AJ\Delta H \frac{d_{lm}}{d_o} \quad (2.19)$$

Here, the variable A represents the heat transfer area, which can be defined as $= \pi L N d_o$, J is the mass flux, d_o is the fibre outer diameter, N is the number of fibres, d_{lm} is the logarithmic mean diameter, and L represents the fibre effective length. The value of heat transfer was taken as the power supplied, which was 2376 W. However, ΔH is the enthalpy of vaporization, which can be calculated based on the mean feed temperature (T_m^F) as, Han et al. [85]:

$$\Delta H = 2024.094 + 1.75231 T_m^F \quad (2.20)$$

2.11.3 Performance Parameters

The GOR can be determined based on the area of membrane A and the enthalpy of vaporisation and supplied power as follows:

$$GOR = \frac{J\Delta H A}{Q_f} \quad (2.21)$$

The specific thermal energy consumption ($STEC$) variable is an important factor that should be considered in MD system calculations, which can be determined from the following formula, Han et al. [85]:

$$STEC = \frac{Q_{in}}{J A} \quad (2.22)$$

2.12 Conclusion

The membrane system significantly affects the production of permeate water. Numerous techniques and various technologies are used in the literature to enhance and improve the overall performance of MD systems using numerical and experimental investigations. As previously discussed, the MD system can be divided into four main categories: vacuum MD (VMD), sweeping gas MD (SGMD), direct contact MD (DCMD), and air gap MD (AGMD).

In this chapter, the numerical and experimental studies that were performed to develop and improve the overall performance of MD systems were reviewed and analysed. Based on the available literature, it can be summarised that parametric

investigations over a wide range of operating conditions (i.e., inlet feed temperatures, feed concentrations, flow rates, channel depths, etc.) have been studied in detail more or less in one or at most in two MD systems. Moreover, the most frequently considered part of the literature is permeate flux. However, in this research, the knowledge gap can be addressed based on several steps: examining the effect of various parameters such as feed temperature, feed concentration, flow rates, and hot and cold channel depths on the overall performance of three types of MD technology configurations, i.e. DCMD, AGMD and VMD.

Moreover, the permeate flux and salt rejection capacities of PP, PVDF, and PTFE membranes was assessed in the AGMD and VMD processes. Furthermore, we studied the seawater desalination performance of PP and PVDF membranes at different flow rates and temperatures using DCMD configuration. Finally, a parametric study was conducted to assess the feasibility of using AGMD and VMD processes for desalinating Arabian Gulf Seawater (AGS) and oilfield-produced water under various operating conditions such as feed temperature and flow rate.

Chapter 3

Methodology

3.1 Introduction

This chapter presents the flow characteristics of MD and experimental procedure. The types of MD membranes considered in the current work are illustrated by showing the main properties of each type. The experimental procedure is detailed, including the preparation of the artificial seawater solution used in the tests. Total Dissolved Solids (TDS) concentration is specified as a key factor, with TDS representing the total amount of dissolved substances, i. e. sodium chloride (NaCl) in the solution. TDS provides an indication of the overall salinity level of the solution, which is critical for simulating different saline concentrations for the experiments. Additionally, the procedure includes measurements of conductivity on both sides of the MD cell for evaluating the concentration of TDS in both the feedwater and the condensate permeate. Temperature sensors measured the temperature of the hot and cold solutions on both sides of the MD cell.

3.2 Experimental Procedure

The experimental procedure used in this current work was performed using a pilot test rig from Convergence Industry B.V., The Netherlands to investigate and examine the thermal and hydraulic performances of various types of MD distillation process arrangements. The experimental rig is managed and integrated with three MD configurations: DCMD, VMD and AGMD models.

The system is composed of a hot side and a cold side, where the temperature difference creates a vapour pressure gradient, enabling water vapour to permeate through the membrane. It is essential for the membrane to remain non-wetted, and a pressure sensor positioned before the cell continuously monitors the pressure drop across the cell over time as a warning indicator. The system is equipped with in-line temperature and conductivity sensors to monitor salinity levels. It can operate in either a once-through mode or with circulation. An optional dosing system is

available to add water, ensuring that the concentration on the feed side remains constant or allowing for dynamic adjustment of salinity. Both the hot and cold sides of the system utilize plastic tubing, and all tubing and connectors are corrosion-resistant, including the flow-through blocks for the sensors. The tubing on both sides is insulated to minimize heat loss. The cold side is cooled by a chiller unit, while the hot side is heated by a heating unit. Both the heater and cooler are controlled and monitored by the system.

In this process, the water-working fluid cannot pass through the membrane. The weight change of the feed tank and permeate tank were measured using weighing balance and used for permeate flux calculation. The permeate flux is calculated using the formula (3.1)

$$J = \frac{\Delta w}{A \cdot \Delta t} \quad (3.1)$$

Δw is the weight change on the permeate side, A is the effective surface area of the porous media (i.e., the area of the membrane that remains in contact with the feed), and Δt is the applied time interval.

In addition to the described system, a flat-sheet membrane module was applied within the DCMD, VMD and AGMD process arrangements. To reduce heat losses, the tubes of the working fluid loops were insulated. The examined experimental rig also has more equipment, such as a plate, frame, and heat exchangers, which are applied to connect to hot or cold-water baths, as presented in Figure 3.1. Figure 3.2 presents the parts of the membrane module that can be customized to different MD configurations.

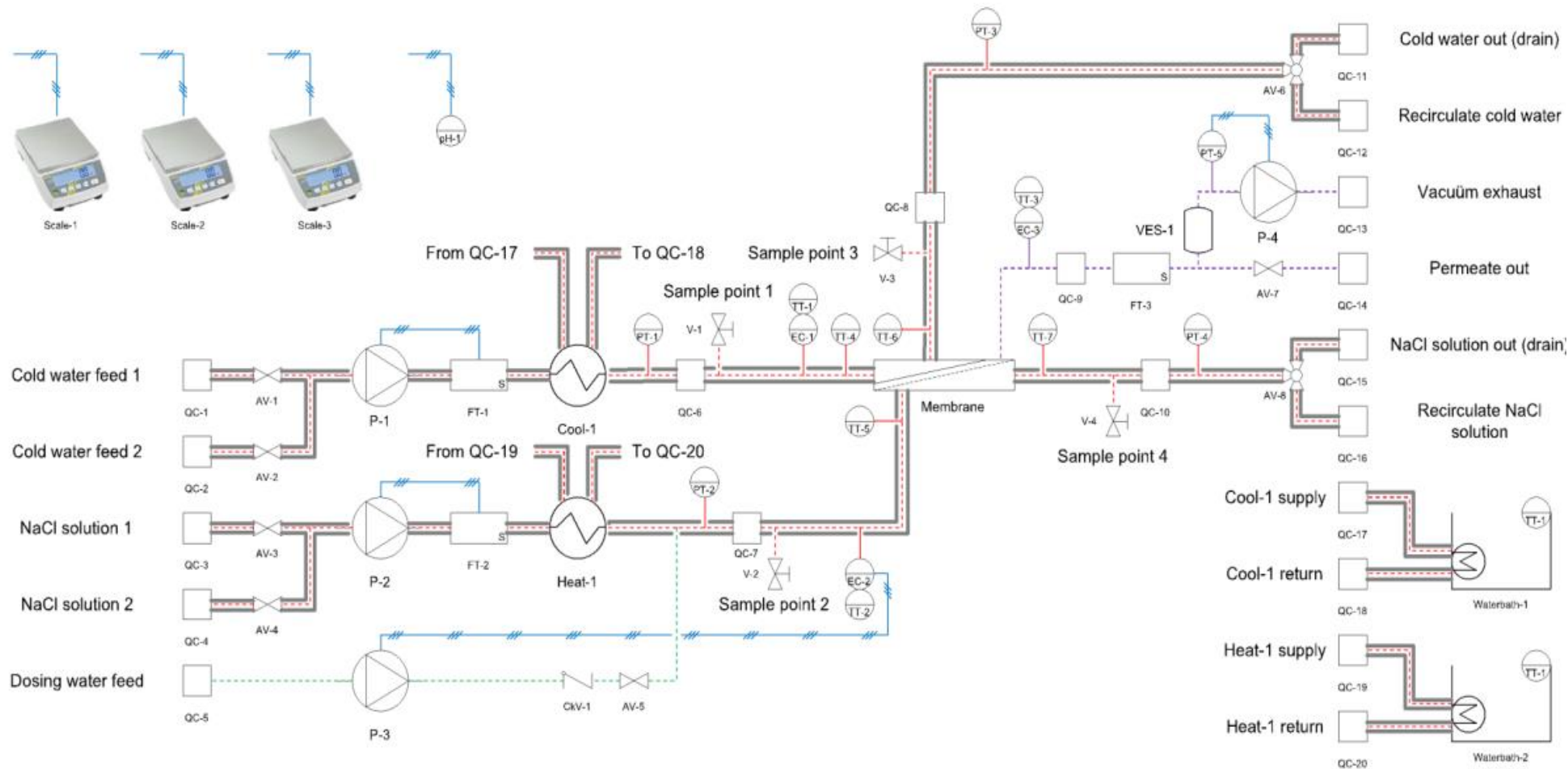
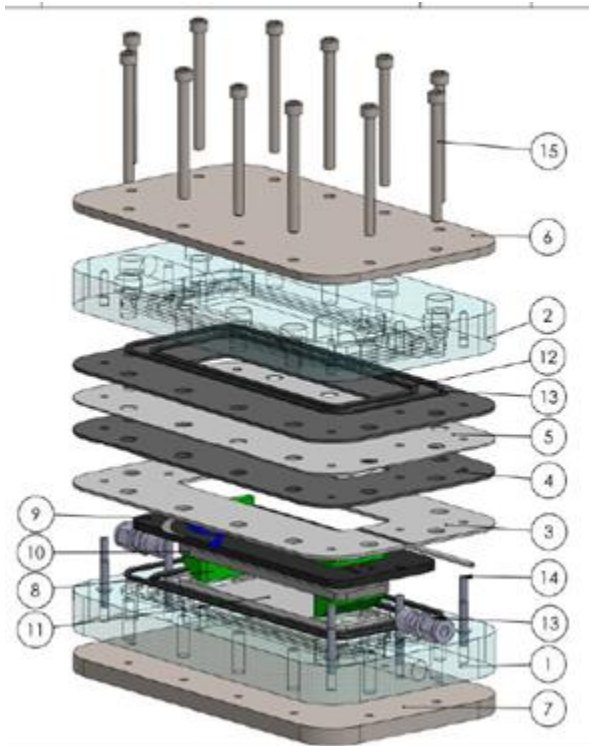


Figure 3.1. Schematic Diagram of the Experimental Rig



1: Membrane cell bottom plate; 2: Membrane cell top plate; 3: Hollow metal plate; 4: Hollow rubber gasket; 5: Condensing plate; 6: Top reinforcement plate; 7: Bottom reinforcement plate; 8: Flow inlet block; 9: membrane cutting template; 10: Porous plate; 11: Non-porous plate; 12 & 13: O-rings; 14: Alignment pin with thread; 15: Bolts
 Figure 3.2. Parts of the MD Membrane Module

Figure 3.3 shows the steps involved in DCMD module assembly from Convergence Industry B.V., The Netherlands. The DCMD membrane module assembly process begins by placing the bottom cell part along with the O-rings (1). Next, a 2mm spacer (2) plate is inserted to compensate for the height of the hollow metal plate (3) that will be added in the following step. The hollow metal plate is then placed on top, creating a new flat surface that allows the O-rings to seal properly. After positioning the hollow metal plate, the membrane (4) is placed on top. Following this, another 2mm spacer plate (6) is added. Finally, the top cell part including the O-rings (5) is placed, and the entire cell is tightened using the bolts (7). Figure 3.4 shows the steps involved in AGMD module assembly from Convergence Industry B.V., The Netherlands. The AGMD module assembly process starts by placing the bottom cell part along with the O-rings (1), which will serve as the channel for cool water flow. Next, the solid metal plate (2) is placed on top of the bottom cell part. This plate will be cooled by the cool water flow, resulting in a

temperature drop on the permeate side of the membrane. After that, a hollow rubber gasket of 2.0mm (3) is placed. Following the gasket, the hollow metal plate (4) with the distillation tube is positioned. This is where the distilled permeate will be collected. Another hollow rubber gasket of 2.0mm (5) is then added, creating an air gap. This air gap can be filled with spacer material to provide support to the membrane. Next, the membrane (6) is placed on top of the assembly. Finally, the top cell part including the O-rings (7) is positioned, allowing the hot feedwater to flow through this section. The entire cell is then tightened using the bolts (8).



Figure 3.3. Components of the DCMD Membrane Module Configuration



Figure 3.4. Components of the AGMD Membrane Module Configuration

3.3 Membrane Characterisation

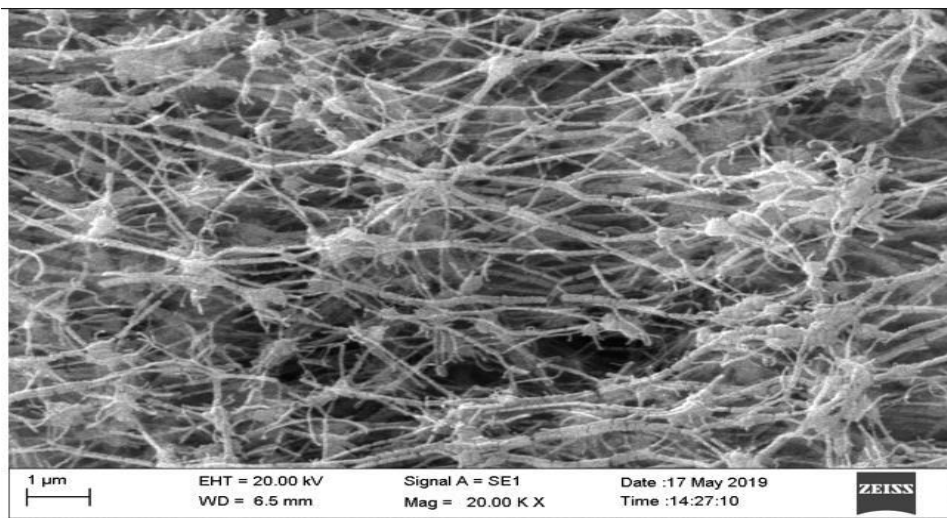
The membranes used in the current work were bought from Sterlitech membrane manufacturers and characterised based on the facilities and equipment at KISR. The main properties of the membrane used in the current study are membrane liquid entry pressure (LEP), water contact angle (WCA), surface roughness and pore size. Using the optical contact angle (CA) measurement and the interface tension meter allows for the determination of the water contact angle (WCA). The contact angle, denoted as θ , indicates how effectively a liquid spreads across a surface. It is geometrically defined as the angle formed at the point where the liquid, gas, and solid phases meet. The balance of forces at this three-phase contact is described by the Young Equation (3.2).

$$\gamma_{SV} = \gamma_{SL} + \gamma_{LV} \cos\theta_Y \quad (3.2)$$

where, γ_{SV} is the surface tension of the liquid, γ_{SL} is the interfacial tension between solid and liquid, and γ_{LV} is the surface tension of the solid i.e. surface free energy, and θ_Y is the Young's contact angle. Water contact angles are the angles formed by a water droplet on a surface. The resulting contact angle is determined by the water's surface tension, the solid's surface energy, and the interfacial tension between the water and the solid. The sessile drop method is the most common way to measure it. A contact angle below 90° indicates a hydrophilic surface, while a contact angle above 90° indicates a hydrophobic surface. However, LEP is used to assess membrane wettability resistance and can be measured using the dead-end filtration approach. Moreover, the evaluation of the pore size is based on the field emission scanning electron microscope (which has the following properties: FESEM, Model EVO MA18) in line with Oxford EDS (X-act) technology. The membrane wall roughness can be distinguished by applying atomic force microscopy (AFM) technology using a trial of 10 nanometres by 10 nanometres. The specifications and main characteristics of the various applied membranes in the current study, i.e. Polypropylene (PP) and Polytetrafluoroethylene (PTFE) are presented in Table 3.1. The membrane surface pictures predicted by the SEM images of the membranes used in the current work are presented in Figure 3.5, whereas the main representation of the surface roughness taken by the AFM images is illustrated in Figure 3.6.

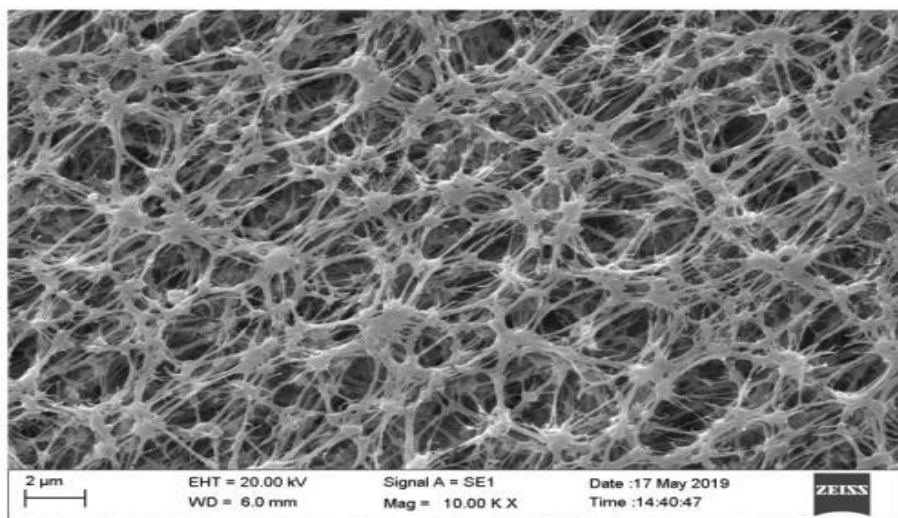
Table 3-1. Characteristics of the Flat-Sheet Membranes

Membrane	Code	Manufacturer	Pore Size (μm)	Membrane Size (mm)	Contact Angle A ($^\circ$)	LEP (bar)
Flat sheet (PP)	PP029025	Sterlitech	0.2	90	108.64	< 0.5
Flat sheet (PTFE)	PTFE023005	Sterlitech	0.2	300 x 300	117.22	< 0.1



PTFE (Sterlitech)

(a) Polytetrafluoroethylene

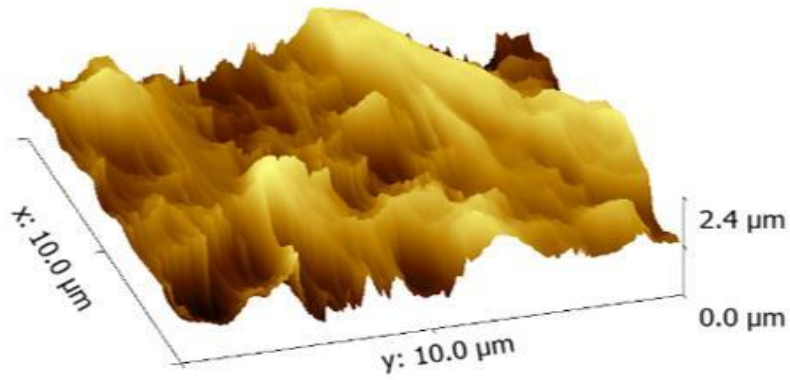


PP membrane

(b) Polypropylene

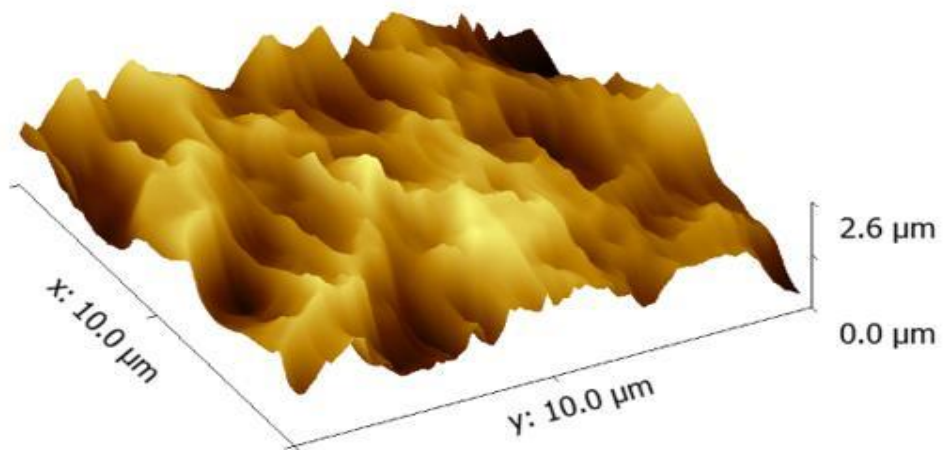
Figure 3.5. Membrane Surface Images Captured by SEM

..



PTFE Membrane (Sterlitech Corporation)

(a) Polytetrafluoroethylene



PP membrane (Sterlitech Corporation)

(b) Polypropylene

Figure 3.6. AFM Image Showing Surface Roughness

3.4 Experimental Technique

Deionized water and sodium chloride (NaCl) solutions with concentrations of up to 26%, prepared using laboratory-grade NaCl from Sigma Aldrich, were utilized. Additionally, Arabian Gulf seawater (AGS) with a total dissolved solids (TDS) concentration of approximately 45,000 ppm, as well as oilfield-produced water, were also used. Measurements of both side conductivities of the MD cells can be used to evaluate the feedwater TDSs and condensate permeate. The feed and permeate are easily controlled by applying four different temperature sensors on each side of the inlet and outlet. In more detail, temperature sensors are used to measure the temperature of the permeate inlet, permeate outlet, feed inlet and feed outlet. The working feed fluid going from the primary source to the MD feed side is performed by employing a proper pump, which can also be used to send the working fluid back to the feeding source, whereas the cold deionised water is supposed to move across the MD cell cold side. Regarding the initial and final weights of both the permeate and feed sources, measuring water permeation can be considered by employing the mass balance approach for measurements every two hours. However, the working water flux J and the salt rejection percentage R can then be determined as follows, as shown in equation (3.1) and (3.3), respectively:

$$J = \frac{\Delta w}{A \cdot \Delta t} \quad (3.1)$$

$$R = \frac{C_f - C_p}{C_f} \quad (3.3)$$

The parameters (Δw , A and Δt) represent the weight change in permeate side, A porous media effective surface area (i.e. area of membrane remains in contact with the feed) and applied time interval, respectively. However, the parameters (C_p and C_f) in the equation (3.3) represents the feed and permeate concentrations respectively.

The DCMD unit comprises a membrane module, heating and cooling systems, pumps, sensors, and tanks for feed and permeate. The process begins with a heated feed stream from an insulated tank, monitored for temperature and flow rate, which is pumped to the membrane module. On the opposite side, a cooled permeate stream is circulated from an insulated tank, also monitored for flow rate

and conductivity to assess permeate quality. The temperature difference across the hydrophobic membrane drives water vapor from the hot feed to the cooler permeate side, where it condenses and is collected. Continuous monitoring of temperature, flow, and conductivity ensures optimal operation, with the amount of permeate measured to evaluate system performance.

In the AGMD module, the heated feed stream from the insulated feed tank is circulated along one side of the hydrophobic membrane. The vapour produced from the hot feed passes through the membrane pores and condenses on a condensation plate, which is separated from the membrane by an air gap. The condensed permeate is then collected. To maintain the necessary temperature of the condensation plate, a cold stream from the insulated cold solution tank is circulated on the opposite side of the module. The change in weight of the permeate tank is used for permeate flux calculation.

In operating the VMD system, a vacuum pump was utilized on the cold side to create a low-pressure environment. This pump was responsible for drawing the permeate vapour through the membrane and into the cold side, where it was condensed. The vacuum pump helped maintain the pressure difference across the membrane, which is the driving force for vapour transport in VMD. The condensed vapor was then collected through a water trap, ensuring that the vapour pressure difference across the membrane remained consistent and that the system operated efficiently. The permeate flux is calculated based on the change in weight of the permeate tank.

Chapter 4

A Performance Feasibility Study of DCMD Systems for Treating Arabian Gulf Seawater and Oilfield-Produced Brine

4.1 Introduction

Seawater desalination technologies have significantly increased the possibility of using seawater as an alternative water source to supply fresh water and relieve many nations' demands for freshwater [86–88]. The demand for potable water has increased steadily over the past two decades due to rising demand from developing villages, towns, municipalities, urban development, commercial operations, agriculture and industry. Consequently, there is a considerable need for the construction and development of seawater desalination plants to meet all nations' fresh water needs, particularly along equatorial lines. The commercial desalination of seawater is typically accomplished through reverse osmosis (RO) membranes, which filter out salt, or through thermal desalination technologies that utilize temperature gradients to drive convective heat and mass transfer [88, 89]. Typically, a thermal procedure involves boiling or evaporating seawater, after which the distillate is collected. Desalination is mainly achieved using conventional energy sources (e.g., oil and gas). The situation is the worst in dry regions, such as the Arabian Gulf Cooperation Council, because practically all freshwater demand is fulfilled by thermal distillation operations that use fossil fuels as their primary energy source [89]. MED and MSF distillation are widely used thermal desalination processes.

Several research investigations are still being conducted to advance MD technology to full-scale industrial and more widespread applications. MD systems currently in use are highly effective. For example, Memstill air gap flat-sheet MD technology under direct contact mode was tested by the Netherlands Organisation for Applied Scientific Research (TNO) [90–91]. The evaluated MD systems delivered high-quality water with salt rejection greater than 99.9%. An MD system integrated with solar energy developed by Fraunhofer for the MEMDIS project was field-tested

in Spain [92]. The MD unit was operated at a feed-water recovery rate of up to 44%, and the membranes achieved a salt rejection of over 99%.

In this chapter, we conducted a parametric study assessing the feasibility of using DCMD for Arabian Gulf seawater (AGS) and oilfield-produced water feed desalination. This study was conducted at the KISR laboratory to assess the DCMD process for desalinating different saline waters under various operating conditions using polypropylene and PVDF membranes. PP and PVDF membranes were chosen for this study because they have excellent properties for direct contact membrane distillation (DCMD). Both materials offer high chemical resistance, thermal stability, and hydrophobicity, making them well-suited for desalination applications [35]. Their hydrophobic nature prevents wetting of the membrane pores, allowing efficient separation of water vapour from saline solutions. Additionally, these membranes have good mechanical strength and durability, which are important for maintaining performance under various operating conditions [35]. Table 4.1 provides an overview of the experiments performed in this study. This chapter presents, for the very first time, the findings of laboratory-scale research carried out in Kuwait to treat AGS, oilfield-produced water and different saline solutions (3.5% to 26% NaCl solutions) utilising DCMD technology. Additionally, this study aimed to investigate the effects of increasing the depths of the hot and cold channels for the feed stream side and permeate stream side, respectively, in a DCMD module developed by the research team. To our knowledge, no study has been reported in the literature on using DCMD with different channel depths for treating AGS and oilfield-produced water as feed streams. This study summarises results in AGS as a precursor to desalination results in oilfield-produced brine substrates, which we believe is novel. In more detail, in the current chapter, the proposed objectives are examined to meet the requirements of the gap specified: performing experimental work on DCMD using parametric study for various parameters: inlet feed temperatures, feed concentrations, flow rates, feed-channel depths, etc. The seawater desalination performance of PP and PVDF membranes at different flow rates and temperatures (45-75°C) using a DCMD configuration was investigated. At temperatures above 75°C, PP and PVDF membranes may undergo structural changes, such as pore collapse and reduced hydrophobicity, which impairs their performance and shortens their lifespan. Therefore, the maximum operating temperature was set at 75 °C for

maintaining membrane stability and effectiveness. The field has been extended using a more industry-applicable membrane than the proposed ones.

Table 4-1. Overview of the Logic of the Experimental Envelop

Parameter		Reasoning
Feed Temperature, °C	45–75	The main reason for studying the effect of temperature on permeate flux is to establish data on how MD performance is affected by the temperature of feed solutions. The 45–75°C temperature range is commonly used in MD research studies because it is within most MD systems' typical operating temperature range. The maximum temperature was set at 75 °C, considering the thermal degradation of the membranes at temperatures above 75 °C.
Flow-rate, L/min	0.6–1.3	This study aims to test the effect of feed flow rate on permeate flux and establish data on how different feed flow rates affect process performance.
Feed Solution Concentration, wt%	Deionised water, 3.5% to 26% NaCl solutions, oilfield-produced water	To test the effect of feed concentration on permeate flux and to establish data to show the feasibility of using MD for feeds with different salt concentrations
Membranes Type	PP and PVDF	To test the performance of different polymeric membranes for AGS desalination and oilfield-produced water

4.2 Materials, Experimental Setup and Procedure

The schematic diagram and photo of the bench-scale MD unit are shown in Figures 4.1 and 4.2, respectively. The bench-scale membrane distillation (MD) unit includes a membrane module, heating and cooling systems, weighing scales, pumps, feed and distillate tanks, temperature and conductivity sensors, and flow

meters. The temperature and conductivity sensors were positioned in the streams leading to the heating and cooling sources.

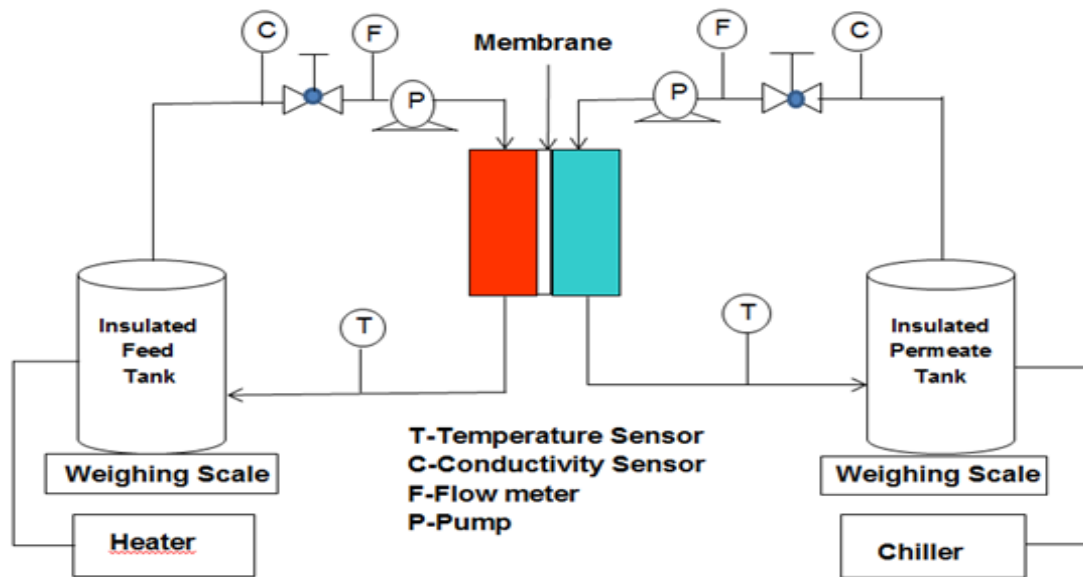


Figure 4.1. Schematic Diagram of the Bench-Scale MD Unit

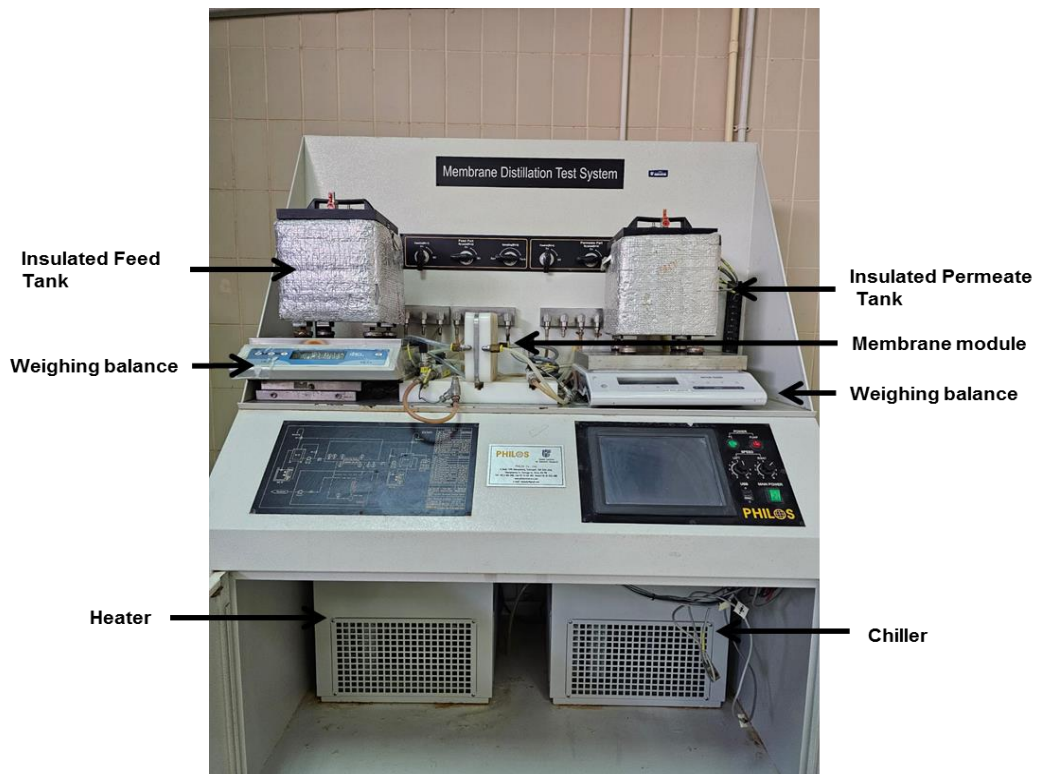


Figure 4.2. Bench-Scale Direct Contact Membrane Distillation (DCMD) Test Unit

The process begins with the feed stream, which is stored in an insulated feed tank. This feed tank is equipped with a heater to maintain the feed solution at the desired temperature. The feed stream is continuously monitored for temperature and flow rate using a temperature sensor and a flow meter, respectively. The heated feed solution is then pumped from the insulated feed tank to the membrane module. On the other side of the membrane module, the permeate stream is circulated from an insulated permeate tank, which is cooled by a chiller to maintain a lower temperature. This cooled side also uses a pump to ensure continuous flow and a flow meter to measure the permeate flow rate. A conductivity sensor monitors the permeate quality by measuring conductivity as well as TDS. The membrane module acts as a barrier between the hot feed stream and the cool permeate stream. The temperature difference across the hydrophobic membrane inside the module drives water vapour from the hot feed side to the cooler permeate side, where it condenses. This vapour flux is facilitated by the difference in temperature, allowing the permeate stream to collect condensed water, which is then stored in the insulated permeate tank. The performance of the system is continuously monitored using various sensors that measure temperature, flow rate, and conductivity. These measurements help maintain optimal operating conditions and improve the system's efficiency. The amount of condensed water, or permeate, is measured using a weighing scale, which helps determine the flux rate and the overall effectiveness of the membrane distillation process.

Flat-sheet membranes with effective areas of 0.0155 m² and 0.003847 m² were used in this study for AGMD and VMD, respectively. The membrane modules were designed and constructed at KISR using Teflon and acrylic materials, as shown in Figures 4.3 and 4.4. The channel depth effect studies were performed using a 0.0155 m² membrane module. Membrane modules with the option of varying channel depths are not commercially available. Accordingly, a new membrane module was designed and developed at KISR to accommodate plates of one mm thickness on the hot and cold-channel sides.

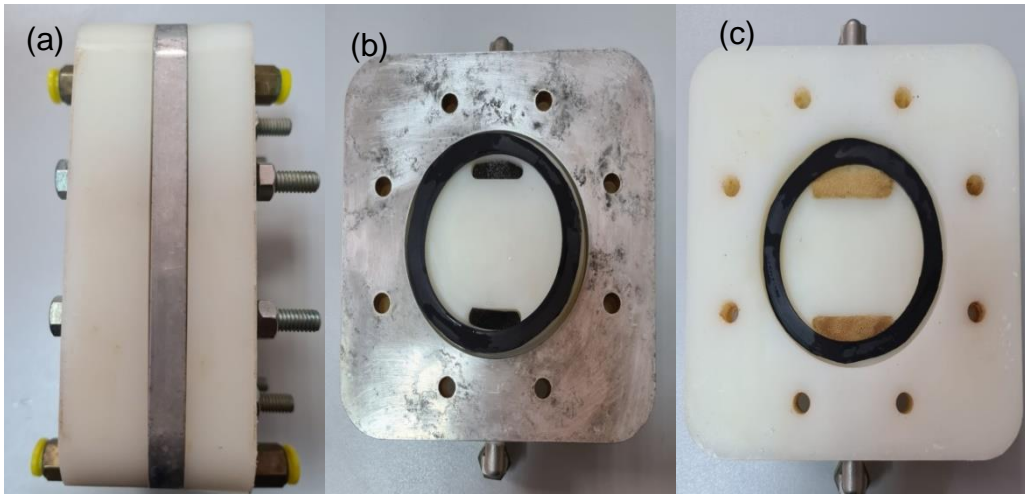


Figure 4.3. (a) Fully Assembled Membrane Module, (b) Feed Section of the Membrane Module, (c) Permeate Section of the Membrane Module

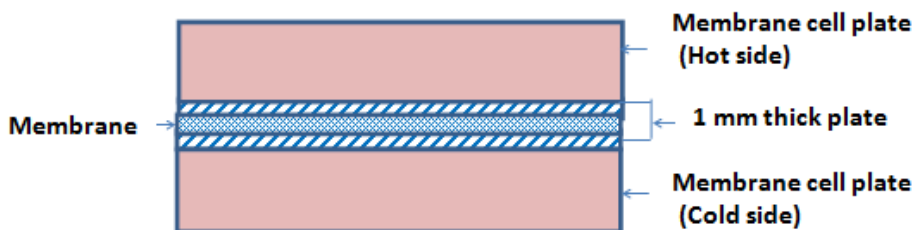
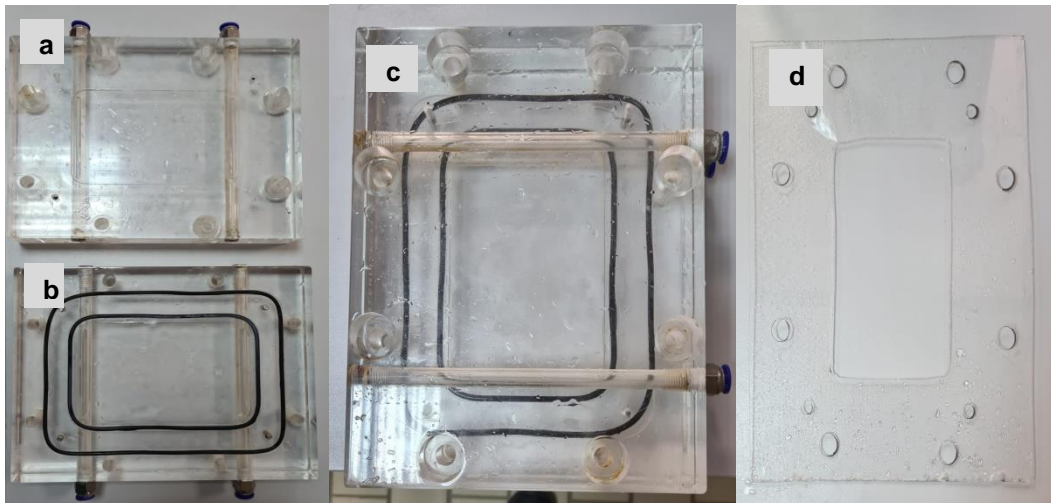


Figure 4.4. DCMD Module Used for Channel Depth Variation Study, (a) and (b) Membrane Cell Plates, (c) Fully Assembled Module, and (d) One mm Thick Plate

Flat-sheet polypropylene (PP) and polyvinylidene fluoride (PVDF) membranes were used in this study. A PVDF membrane (Code: YMJXSP3001, Merck Millipore

Ltd.) with an average pore size of 0.3 μm , a thickness of 150 μm , and a porosity of 60% was used, and the PP membrane (from Celgard 2500) used had an average pore size of 0.064 μm , a thickness of 25 μm , and porosity of 55%. The porosity or the percentage of the membrane's volume occupied by pores or void spaces, of the membranes used in the study was sufficient to ensure high permeability and flux, allowing more water vapour to pass through the membrane effectively. The NaCl used was analytical reagent (AR) grade, with 99.9% purity (Techno Pharmchem, Sodium chloride AR-33127). NaCl solutions were fed at concentrations of 3.5%, 7.0%, 15%, and 26%. The 3.5% NaCl solution is similar to the salinity of seawater, which typically ranges from 3.5% to 4.2% (as in Arabian Gulf seawater). The 7.0% NaCl solution represent more concentrated brine solutions, often found in desalination plants' brine reject streams. A 15% NaCl solution is much more concentrated brine, similar to those found in salt lakes or produced in industrial processes. The 26% NaCl solution is close to the saturation point of NaCl in water at standard conditions, resembling extremely concentrated brine. These concentrations provide a range for testing the membrane's effectiveness in desalinating different levels of saline water. The NaCl solutions were made by dissolving a known amount of NaCl salt in a known amount of deionised water (DI) produced by Millipore's ZRQSV3WW | Direct-Q3 UV Water Purification System. Also, AGS collected from a beach well located at the Desalination Research Plant (DRP) of the KISR in Kuwait was used as feed.

The effectiveness of the DCMD was also studied for desalinating oilfield-produced water collected from Kuwait. Table 4.2 summarises the physiochemical analysis of the AGS used in this study in mg/L. The physiochemical analysis was performed using a DR 5000 Spectrophotometer (Hach, DR 5000) and ion chromatography (Dionex 5000) systems.

A membrane was placed between the hot and cold plates of the DCMD module. The DCMD setup consisted of a hot and cold water loop. The heated feed solution was fed to the hot inlet of the DCMD module and circulated back to the feed tank (see Fig. 4.1). On the cold side of the membrane, deionised water was fed to the cold inlet of the DCMD module and then back to the permeate tank. A circulating bath (Cole Parmer Polystat – Item #EW-12122-02) controlled and maintained the hot- and cold-side temperatures.

Table 4-2. Physiochemical Analysis of Arabian Gulf Seawater (AGS)

Analysis Item	Average Value in mg/L
TDS	43117
Ca ²⁺	817.3
Mg ²⁺	1521.2
Na ⁺	13482
(SO ₄) ²⁻	3440
(HCO ₃) ⁻	142.1
Cl ⁻	23165
K ⁺	331
NO ₃ ⁻	3.78

The flux, i.e. the rate at which water vapour permeates through the membrane from hot feed loop to the cold loop, was calculated by measuring the increase in the weight of the permeate tank over time. A weighing balance (MS32000L/A03, Mettler Toledo) was used to measure changes in the weight of the solutions. After ensuring that the flow rates of the hot feed loop and cold loop, as well as the stream temperatures, had stabilized at the required levels, data logging for each experiment was initiated, and the experimentation was conducted for 90 minutes. Initially, when starting the experiments, the flow and temperature may fluctuate. Therefore, data collection began only once these parameters were stable. Each experiment was conducted in triplicate under consistent test conditions, such as flow rate and temperature. The primary parameter measured was the weight change of the permeate tank (ΔW). The water flux was calculated for each trial and average water flux value was taken for data analysis. The membrane's active surface faced a hot-feed solution. The temperature and conductivity of all streams were measured and recorded manually. Electrical conductivity metres (Thermo Scientific™ Orion™ Star A322 Conductivity Portable Metre) were used to measure electrical conductivity, TDS, salinity and temperature manually. TDS refers to the total concentration of dissolved substances in water, including salts, minerals, and organic matter, whereas, salinity refers to the concentration of salts in water, usually dominated by NaCl. In this study, since the NaCl solution is prepared using deionized water, the TDS and salinity values can be considered equivalent. The membrane's water

vapour flux and salt rejection efficiency were determined using Equations (4.1) and (4.2), respectively. Three trials were conducted for each membrane using similar experimental conditions, and the average permeate flux (water flux) and salt rejection percentage values were reported. As shown in equation (4.1), permeate flux or water flux is the rate at which permeate (the water vapour) passes through the membrane per unit of membrane area. The weight change on the permeate side was measured and converted to volume using the known density of water (the permeate is primarily water, 1 kg = 1 L for pure water). The flux is then calculated by dividing the volume by the membrane area and the duration of the experiment, resulting in units of L/m²h.

$$\text{Water Flux} = \frac{\Delta \text{Weight}}{\text{Water density} \times \text{membrane surface area} \times \Delta \text{time}} \quad (4.1)$$

$$R = \frac{C_f - C_p}{C_f} \quad (4.2)$$

where R is the salt rejection and C_f and C_p are the concentrations of the feed and permeate, respectively. These concentrations were determined via conductivity measurements using a conductivity meter. Conductivity can be used to estimate the concentration of the solution by determining the concentration of sodium chloride that would result in the same conductivity as the sample. Conductivity meters provide the TDS value in mg/L of sodium chloride by comparing the sample's conductivity and temperature to reference data stored in the meter's memory.

4.3 Validation of a DCMD System

In the validation of the DCMD system, various test conditions were assessed, including changes in feed temperature, feed concentration, flow rate on both the hot and cold sides of the MD module, and flow channel depth. The flow rate here refers to the rate at which the hot feed solution and a cold solution is supplied to the feed side and permeates side of the MD membrane module, respectively. The flow rate will have effect on heat transfer and temperature difference across the membrane. The terms "feed-flow rate" and "cold-solution flow rate" in the following sections refers to the flow rate of the solutions in the feed side and permeate side of the module, respectively. This section explores how these conditions impact permeate flux, examining their effects on the efficiency and performance of the DCMD system.

4.3.1 Effect of Feed Temperature

Figure 4.5 shows the influence of feed temperature on permeate flux. The temperature varied from 45–75°C. The cold-side temperature was fixed at 20 °C. The feed used was a 26% NaCl solution. The feed-flow rate and the cold-solution flow rate were fixed at 1.2 L/min. Deionised water was circulated on the cold side of the membrane. As expected, it was observed that the permeate flux increased with the increase in feed temperature. The permeate flux increased to 37.1 L/m²h from 11.6 L/m²h when the temperature was raised from 45 °C to 75 °C.

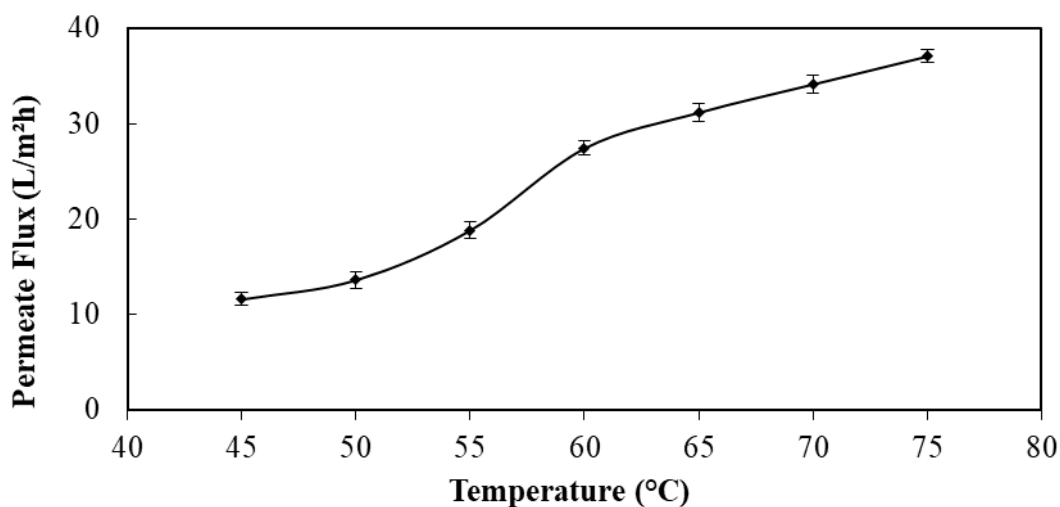


Figure 4.5. Effect of Feed Temperature on the Permeate Flux of Polypropylene Membrane in DCMD

Increasing the temperature will increase the kinetic energy of the liquid molecules, which may overcome the liquid phase intermolecular forces. As a result, evaporation occurs and becomes faster at higher temperatures than lower temperatures. As evaporation increases, the vapour pressure in the feed solution channel also increases, which increases the difference in transmembrane vapour pressure. This increase in transmembrane vapour pressure resulted in high permeate flux with an increase in temperature [93–98]. Table 4.3 shows the permeate flux and salt rejection percentages at different feed temperatures. The permeate flux increased from 18.8 L/m²h at 55°C to 31.2 L/m²h at 65°C, which is an approximate increase of 66%. A further increase of 10°C resulted in only a 19% increase in permeate flux. Although there was a significant increase in flux with

higher temperatures, considering the energy requirement at higher temperatures, the feed temperature for further experiments in this study was set at 65 °C.

Table 4-3. Effect of Temperature on Permeate Flux and Salt Rejection in DCMD

Membrane	Temperature (°C)	Permeate Flux (L/m ² h)	Salt Rejection (%)
PP	45	11.6	99.96
	50	13.6	99.94
	55	18.8	99.97
	60	27.4	99.92
	65	31.2	99.97
	70	34.1	99.96
	75	37.1	99.60

Furthermore, although PP and PVDF membranes can withstand temperatures above 85 °C for short durations, it is generally recommended to maintain a continuous operating temperature around 65 °C to ensure membrane longevity and stable performance. It was observed that feed temperature had less of an effect on the salt rejection property of the membrane. This shows that a high-temperature feed can be used in a DCMD configuration using PP membranes to obtain high water flux with a good salt rejection percentage. Over time, the TDS measurement of the feed solution shows a relatively small reduction in feed concentration (from 26% to 24% salinity) was observed at all tested temperatures, as shown in Table 4-4. This could be due to the flow of water towards the feed side from the cold side loop (deionized water) resulting from the high osmotic pressure difference between the 26% NaCl feed and deionised water. The effect of feed temperature on permeate flux performance is shown in Figure 4.6. As the figure illustrates, the permeate flux remains stable from 20 minutes onwards for most of the tested temperatures. Furthermore, increasing the feeding temperature from 25°C to 70°C results in a noticeable rise in permeate flux. This shows the stability of flux over time and the overall trend of increasing flux with higher temperatures. The figure shows that for feed temperatures between 25°C and 35°C, the flux values are very close because the driving force for the process, likely related to the temperature difference, is not strong enough at these lower temperatures to cause significant changes in flux.

Table 4-4. Salinity of Feed at Different Temperatures Over Time During the Experimentation Period

Time in minutes	Salinity, %						
	75°C	70°C	65°C	60°C	55°C	50°C	45°C
0	26.0	26.0	26.0	26.0	26.0	26.0	26.0
10	25.4	25.3	25.5	25.6	25.6	25.8	25.8
20	25.2	24.8	25.3	25.2	25.0	25.5	25.6
30	24.8	24.5	24.9	24.9	24.8	25.3	25.5
40	24.5	24.4	24.7	24.7	24.5	25.4	25.3
50	24.3	24.3	24.5	24.3	24.4	25.2	25.3
60	24.1	24.1	24.3	24.1	24.4	25.0	25.0
70	24.1	24.2	24.2	24.1	24.4	24.9	24.8
80	24.2	24.2	24.1	24.0	24.2	24.8	24.8
90	24.1	24.2	24.2	24.2	24.3	24.8	24.8

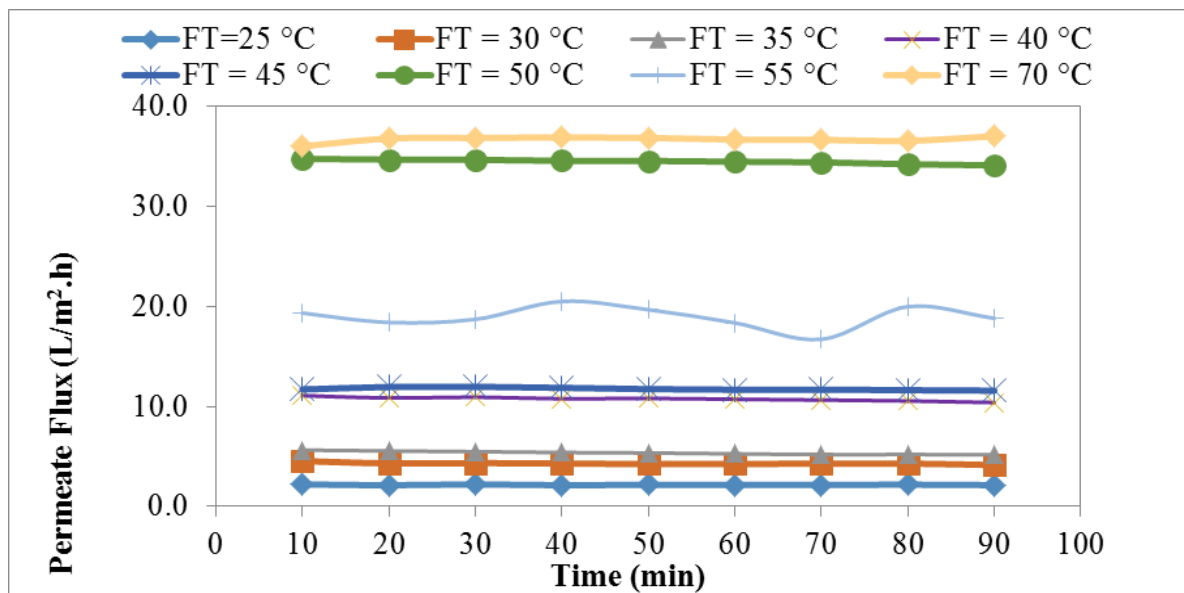


Figure 4.6. Permeate Flux Produced with Time at Different Feed Temperatures

At 40°C and 45°C, there is a noticeable step change in flux, which suggests that at these temperatures, the increased vapour pressure significantly enhances the driving force, leading to a higher flux. The flux at 55°C behaves unusually with fluctuations, possibly due to variations in temperature control during experimentation. Finally, at 50°C and 70°C, the flux is higher and stable because the higher temperature provides a stronger and more consistent driving force for the process, resulting in increased flux.

However, the Nusselt number and TPC as a function of varying feed temperatures are illustrated in Figure 4.7, highlighting the heat transfer performance. TPC can be considered as the measurement of heat exchange is effective between the interfaces and streams with MD. In other words, the larger the TPC, the smaller the heat transfer resistance to/from the channel from/to the interfaces with the MD. Figure 4.7a illustrates that increasing the feed temperature acted at a gradual increase in the TPC. Moreover, the performance of heat transfer through the considered membrane is presented by the Nusselt (Nu) number, which represents the convection heat transfer to the conduction heat transfer. It is well known that enhancing the Nu number depends on two non-dimensionless numbers: the Reynolds number and the Prandtl number.

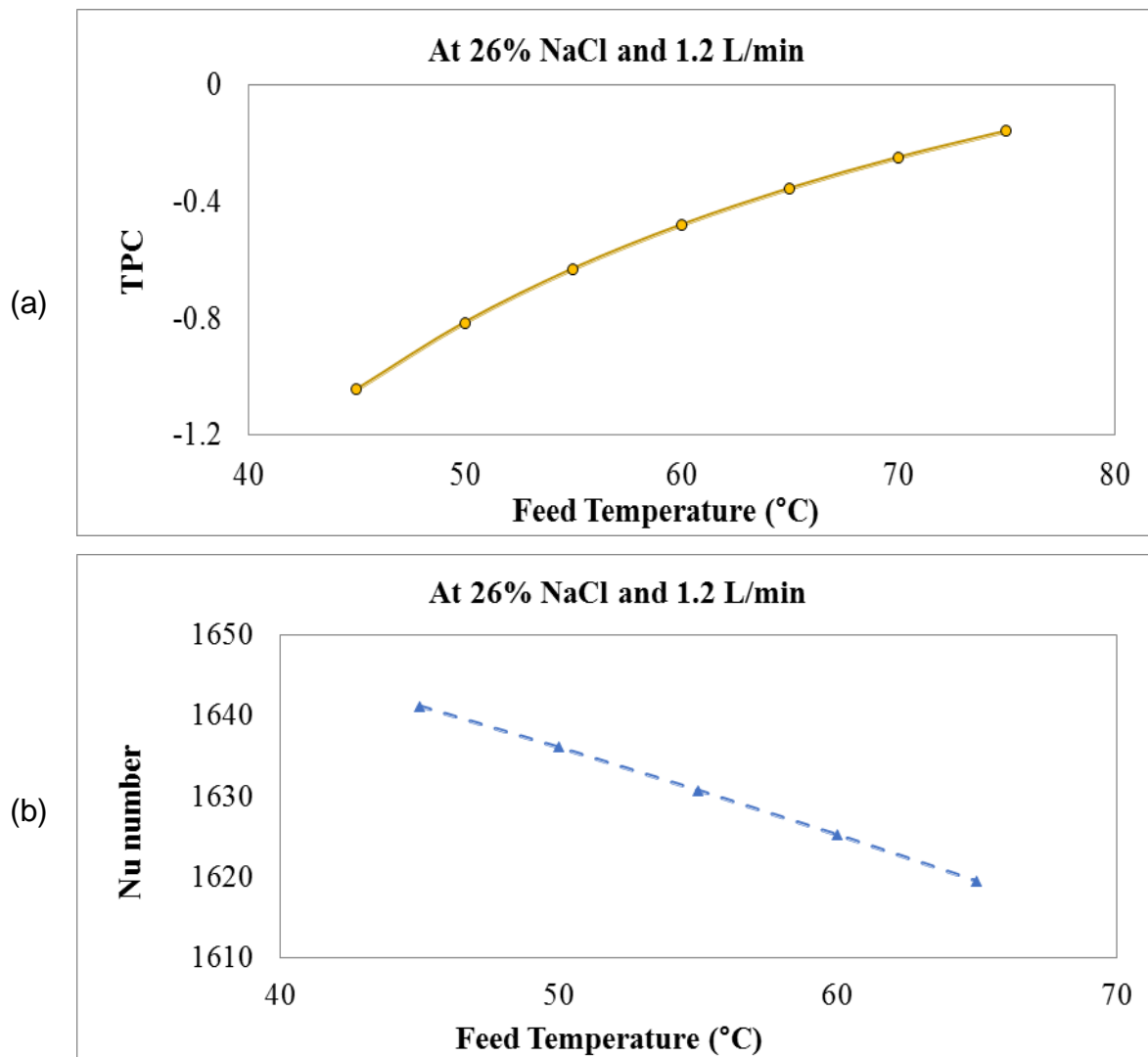


Figure 4.7. Effect of Feed Temperature on (a) TPC and (b) the Nusselt Number in DCMD

However, since the 1.2 L/min flow rate is only considered in Figure 4.7b, the Prandtl number can only be changed to influence the Nu number. The change in feed temperature acted to change the thermal properties. However, the Prandtl number decreased gradually as the feed temperature increased. Thus, the lower the feed temperature, the higher the Nu number at the same feed-flow rate.

Regarding energy performance, the Gain Output Ratio (GOR) is another critical parameter to consider when evaluating the thermal desalination process. It represents the ratio of latent heat associated with the produced water vapour to the input heat, presented in Figure 4.8a. In other words, the GOR indicates the useful energy employed to produce the permeate. As can be seen, increasing the feed temperature acted at a gradual increase in the GOR. This may be due to the partial pressure difference, which led to a vapour flux. The vapour flux is directly proportional to the GOR as represented by the equation (4.3)

$$\text{GOR} = J_m \Delta H A / Q_{in} \quad (4.3)$$

where J_m is the vapour flux, ΔH is the Latent heat of vaporization, A is the surface area and Q_{in} is the heat input. In equation 4.3, J_m reflects the amount of vapour produced per unit area. An increase in vapour flux, due to a higher partial pressure difference, leads to more efficient utilization of input heat energy, which in turn enhances the GOR. Higher feed temperatures generally improve GOR by reducing the energy required for desalination, thereby increasing process efficiency. However, the benefits of higher feed temperatures must be balanced against potential operational challenges, such as scaling and material degradation. On the other hand, the performance of specific thermal energy consumption (STEC) over a range of inlet feed temperatures is presented in Figure 4.8b. STEC is an important metric used in thermal desalination processes, to evaluate the amount of thermal energy required to produce a unit mass of freshwater, as shown in equation (4.4). It is typically measured in units like kJ/kg or MJ/m³ or kWh/m³, which reflect the energy efficiency of the desalination process.

$$\text{STEC} = \text{Total Thermal Energy Input} / \text{Permeate output} \quad (4.4)$$

It can be deduced that the performance of the GOR is inversely related to that of the STEC. A higher GOR indicates better performance and efficiency, typically achieved at higher feed temperatures. This means that as GOR increases, the

system uses its energy more effectively, producing more freshwater per unit of energy consumed, while STEC decreases, indicating less energy is required per unit of water produced. STEC tends to decrease with increasing inlet feed temperatures, as higher temperatures reduce the amount of energy needed to bring the feedwater to the required operating conditions.

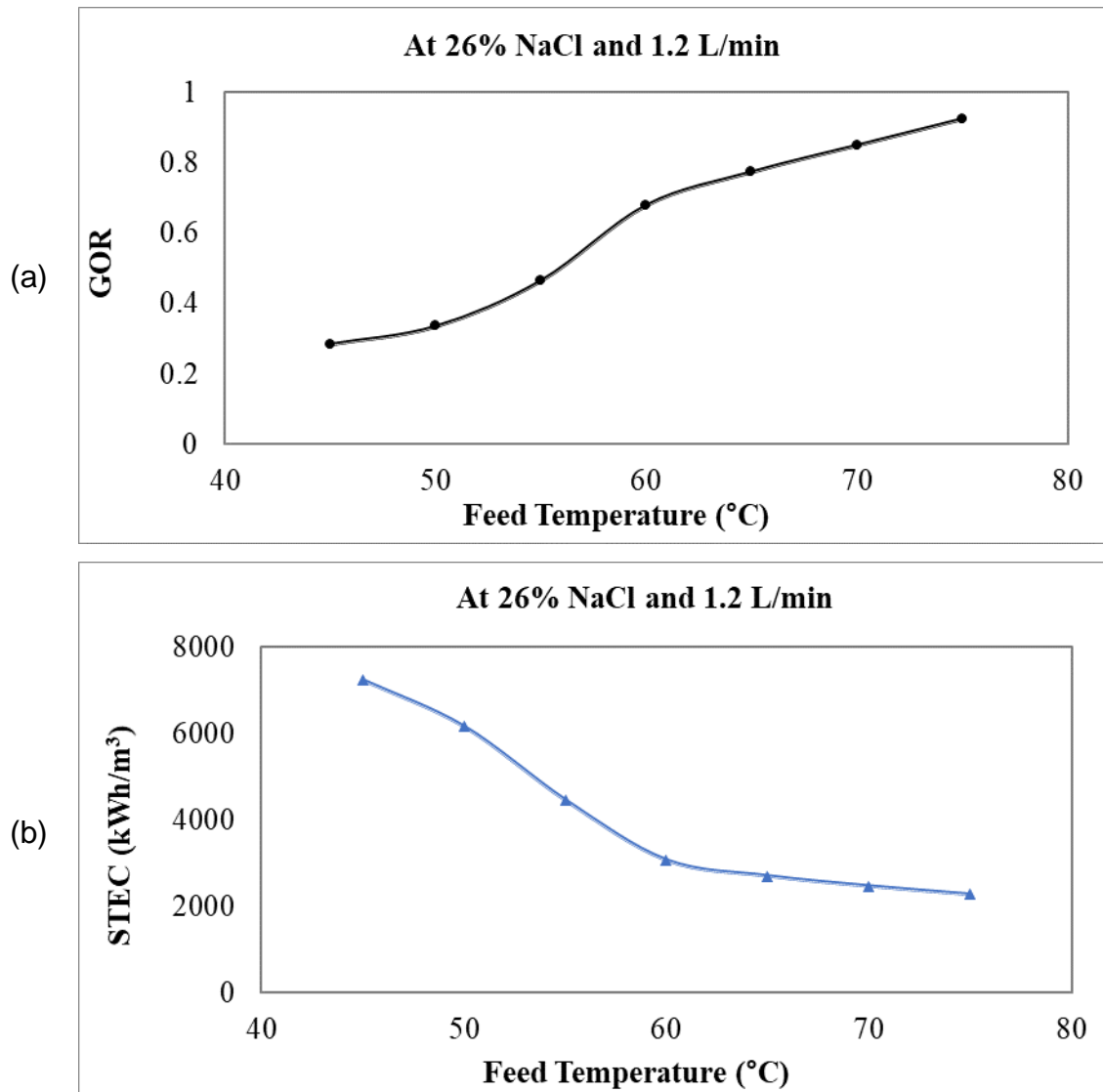


Figure 4.8. Effect of Feed Temperature on (a) GOR and (b) STEC in DCMD

4.3.2 Effect of Feed Concentration

Figure 4.9 shows the effect of feed concentration on the permeate flux. The tests were conducted using deionised water and a NaCl solution at 3.5%, 7.0%, 15% and 26% concentrations, respectively, as feed. The flow rate at the feed and cold-solution channels was 0.9 L/min. Polypropylene was used as the membrane. The feed-side and coolant-side temperatures were 65°C and 5°C, respectively. Deionised

water circulated on the coolant side of the module (as shown in the schematic in Fig. 4.1). From Figures 4.9 and 4.10, it has been validated that increasing the concentration of the feed results in a decrease in permeate flux. According to the results shown in Fig. 4.9, there was a 50% reduction in the permeate flux produced when the concentration of NaCl in the feed solution was elevated from 0–26%. This reduction might be due to the accumulation of salt molecules on the membrane surface, which can cause a hindrance to vapour transportation through the membrane. However, this requires further investigation in future to fully understand the underlying reasons.

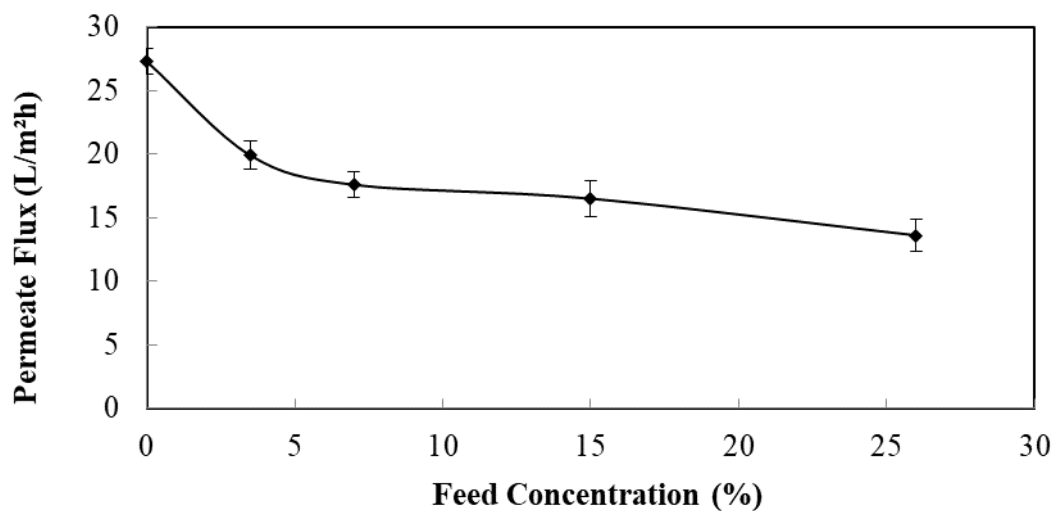


Figure 4.9. Effect of Feed Concentration on the Permeate Flux of Polypropylene Membrane in DCMD

Furthermore, due to temperature polarisation, the feed-side membrane surface might have been colder than the bulk feed, as heat was transported from the bulk feed via the boundary layer to the membrane surface. The slight increase in flux over time shown in Figure 4.10 might be due to the system reaching a more stable operating condition or slight temperature increases, which could enhance vapour pressure slightly. However, long-term performance requires further study in future.

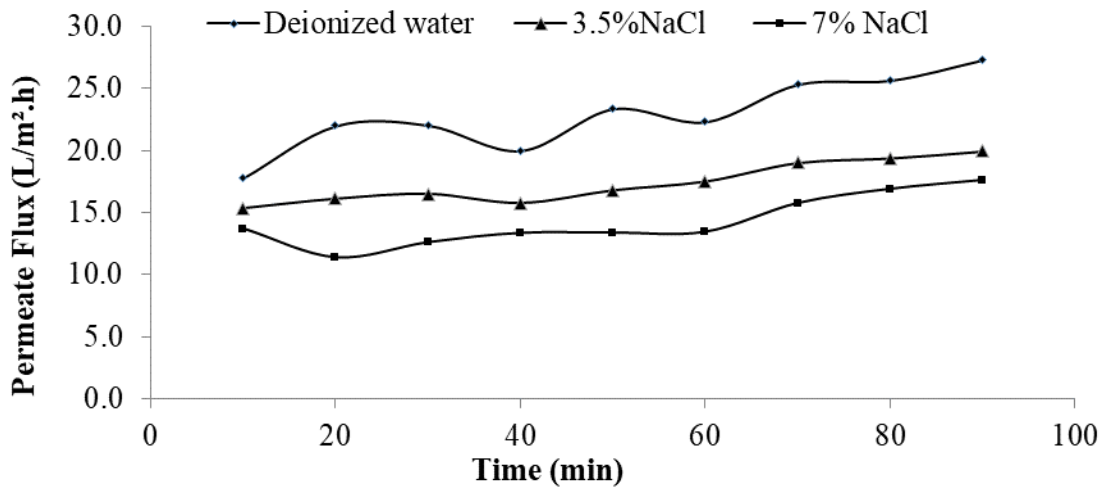


Figure 4.10. Permeate Flux at Different Feed Concentrations and Uniformity of Permeate Flux Over Desalination Time

Further observation showed that as the feed concentration increased, the time required to achieve the same permeate flux also increased. For example, after 10 minutes of operation using deionised water as the feed, a permeate flux of 17.8 L/m².h was obtained (see Table 4.5). When the feed concentration was increased to 3.5% NaCl, it took almost one hour (between 50 and 60 minutes) to get the same permeate flux of approximately 17 L/m² h.

Table 4-5. Permeate Flux at Different Feed Concentrations Over Time

Time (min.)	Water Flux, L/m ² .h		
	Deionised Water	3.5% NaCl	7% NaCl
0	0.0	0.0	0.0
10	17.8	15.3	13.7
20	22.0	11.3	11.4
30	22.1	12.0	12.6
40	20.0	15.8	13.3
50	23.4	16.8	13.4
60	22.3	18.0	13.4
70	25.3	18.9	15.8
80	25.7	19.4	16.9
90	27.3	19.9	17.6

However, obtaining the same flux ($16.9 \text{ L/m}^2 \text{ h}$) took nearly an hour and a half (between 80 and 90 minutes) when the feed concentration was increased to 7% NaCl. This trend is important and shows the sensitivity of the permeate-to-feed concentration. This trend indicates that any increase in feed concentration requires more energy and time to create the required vapour pressure for permeate flux to occur. This could be mainly due to the strong hydrogen bonding formed between NaCl and water molecules at higher feed concentrations.

Figure 4.11 shows the effect of the feed concentration on salt rejection. When the feed solution concentration was raised, the conductivity of the permeate rose slightly, but there was also a slight drop amounting to rejected salt. The high concentration of NaCl in the feed solution might have lowered the LEP, which caused a small rise in the permeate TDS.

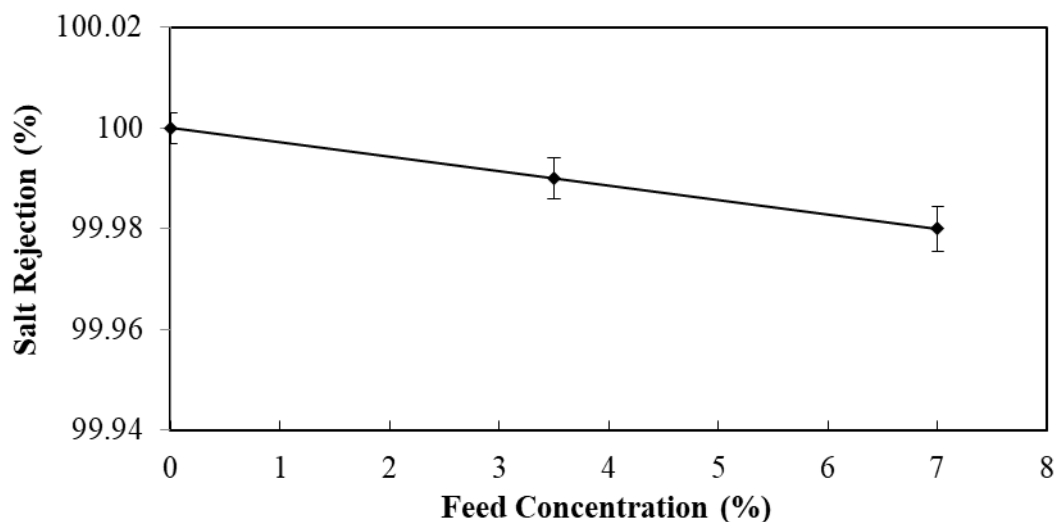


Figure 4.11. Effect of Feed Concentration on the Salt Rejection of Polypropylene Membrane in DCMD

However, regarding heat transfer performance, the Nusselt number and TPC with changing feed concentrations are presented in Figure 4.12. TPC can be considered as the measurement of heat exchange is effective between the interfaces and streams with MD. Figure 4.12a shows a gradual decrease in TPC with increasing feed concentration. Figure 4.12b shows how the Nu number increases gradually as the feed concentration of NaCl increases from 0–26% at a constant feed rate of 0.9 L/min and an inlet feed temperature of $65 \text{ }^\circ\text{C}$.

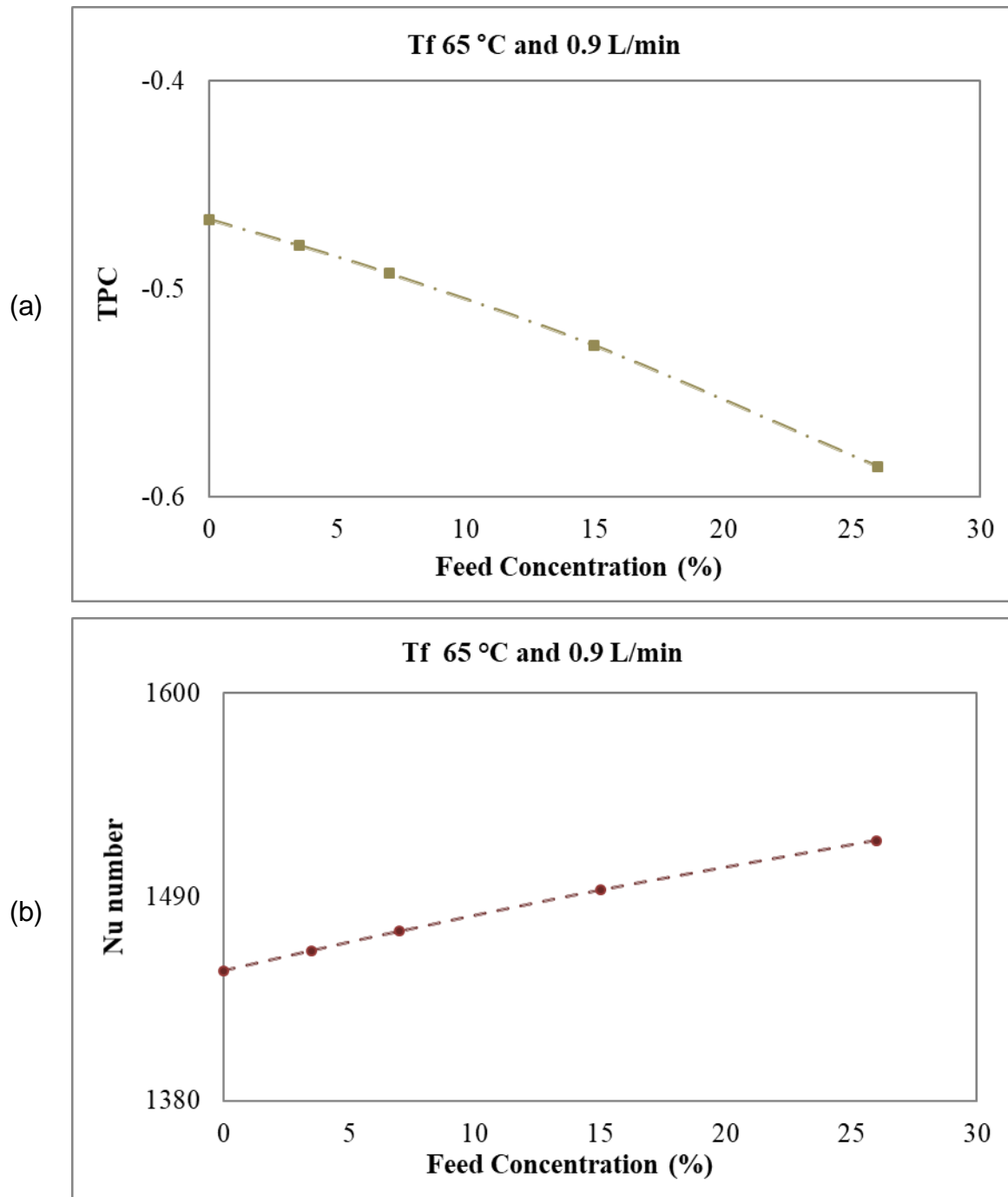


Figure 4.12. Effect of Feed Concentration on (a) TPC and (b) the Nusselt Number in DCMD

This is expected since the Nu number, as stated earlier, is influenced only by Reynolds Number (Re) and Prandtl number (Pr). Nu number is often expressed as, $Nu = f(Pr, Re)$. The Nusselt number represents the ratio of convective heat transfer to conductive heat transfer in a fluid flow. However, changing feed concentration means changing the fluid's thermal properties: density, dynamic viscosity, specific

heat capacity and thermal conductivity. As the concentration of solutes in the solution increases (i.e. feed concentration increases), the thermal conductivity of the solution decreases, which in turn reduces the conductive heat transfer. This is because conductive heat transfer relies on the thermal conductivity of the medium through which heat is being conducted. When the thermal conductivity decreases due to higher solute concentration, the ability of the solution to conduct heat also diminishes. Since Nu is inversely proportional to conductive heat transfer, decrease in conductive heat transfer will increase Nu . In other words, higher feed concentrations may lead to higher Prandtl numbers, impacting the heat transfer performance of the process, and resulting in a higher Nu number.

Regarding energy performance, the GOR with changing the feed concentrations is another critical parameter that can be considered to evaluate the thermal desalination process, which represents the ratio of latent heat associated with produced water vapour to input heat, which is calculated according to the equation 4.1 and presented in Figure 4.13a. In other words, the GOR indicates the amount of energy used to produce the permeate. As can be seen, increasing the feed concentrations resulted in a gradual decrease in the GOR. This may be due to the higher permeate flux produced with a smaller concentration, directly proportional to the GOR. On the other hand, the performance of STEC over a range of inlet feed concentrations is calculated according to the equation 4.4 and is presented in Figure 4.13b. It can be deduced that a higher GOR means higher performance produced by the flow at the considered higher feed temperature. This not only resulted in a higher GOR but also led to minimising the thermal energy requirements. Moreover, fouling or stuck salt on the surface of the membrane can lead to reduced flux production. The presented data show that the higher feed concentration and the smaller GOR provide the higher STEC.

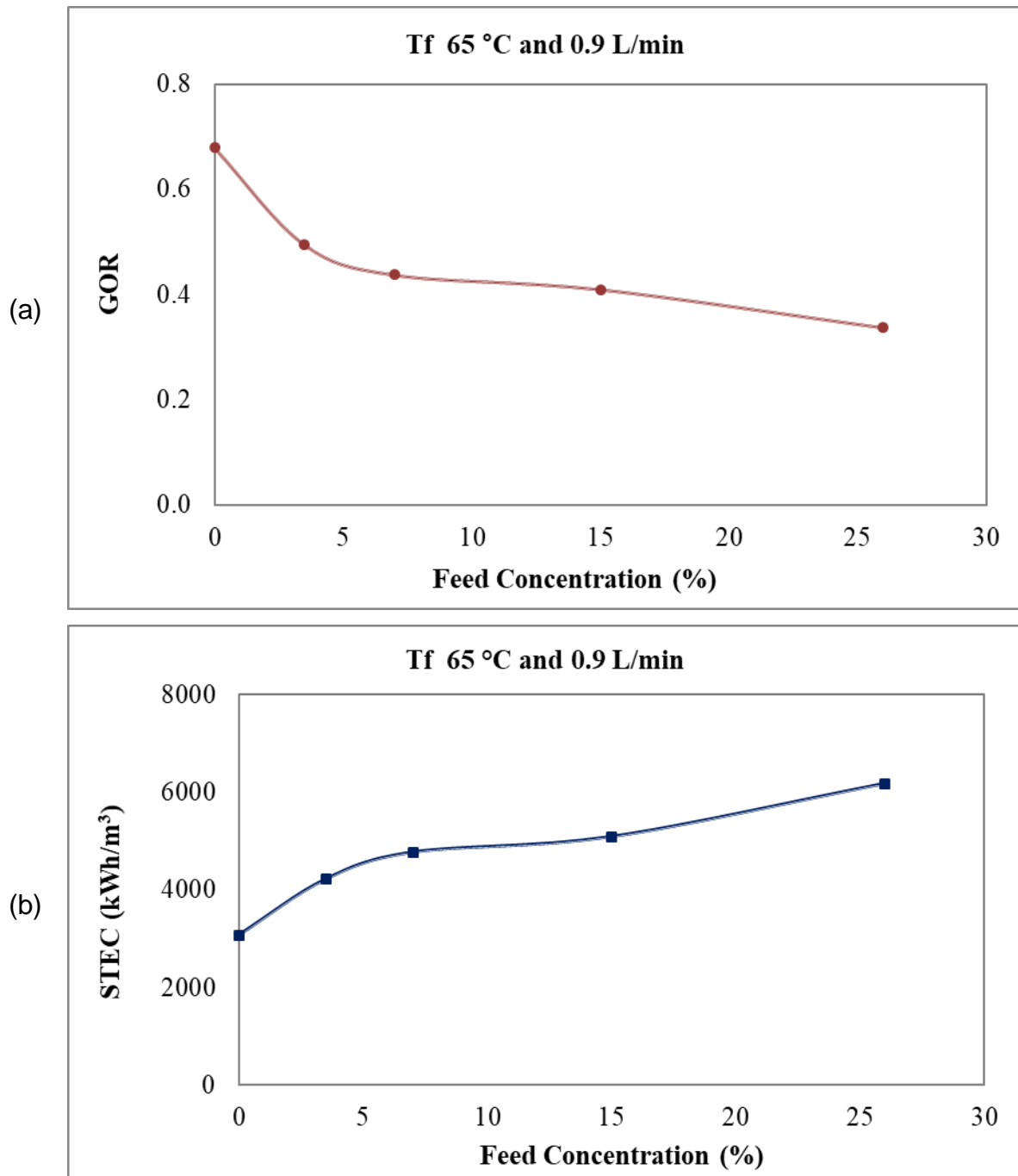


Figure 4.13. Effect of Feed Concentration on (a) GOR and (b) STEC in DCMD

4.3.3 Effect of Flow Rate

Figure 4.14 shows the effect of the flow rate on permeate flux. The tests used 7.0 wt% NaCl solution as feed and deionised water as a coolant medium. The temperatures of the feed and coolant sides were 65 °C and 5°C, respectively. The flow rate of the feed and cold-solution channels varied from 0.6L/min to 1.3L/min. The experiment was conducted using a polypropylene membrane. As shown in Figures 4.14 and 4.15, an increase in water flux in conjunction with an increase in

the flow rate was observed. The temperature gradient was reduced between the membrane surface and the solutions (i.e., feed and coolant). This increased vapour pressure, enhancing mass transfer in the membrane region [93, 99–101]. The positive effects of turbulence on permeate flux have encouraged researchers to develop turbulence promoters for MD and membrane filtration processes [102, 103]. Another factor to consider is the residence time of fluid in a channel. The residence time is the duration of the fluid's stay in the channel while moving from the inlet port to the output port. The fluid residence time in the channel is longer at low flow rates, but at higher flow rates, the fluid residence time is shorter. Therefore, greater heat transfer between the membrane and the medium may occur at lower flow rates, thus reducing the vaporisation impact. At increased flow rates, the heat transfer rate decreases, thus accelerating the vaporisation process. To our knowledge, this effect of residence time on vapour pressure and permeate flux in MD has not yet been studied, making it a potential area of interest for future research. In this current study, the impact of flow rate on salt rejection was negligible (see Figure 4.16).

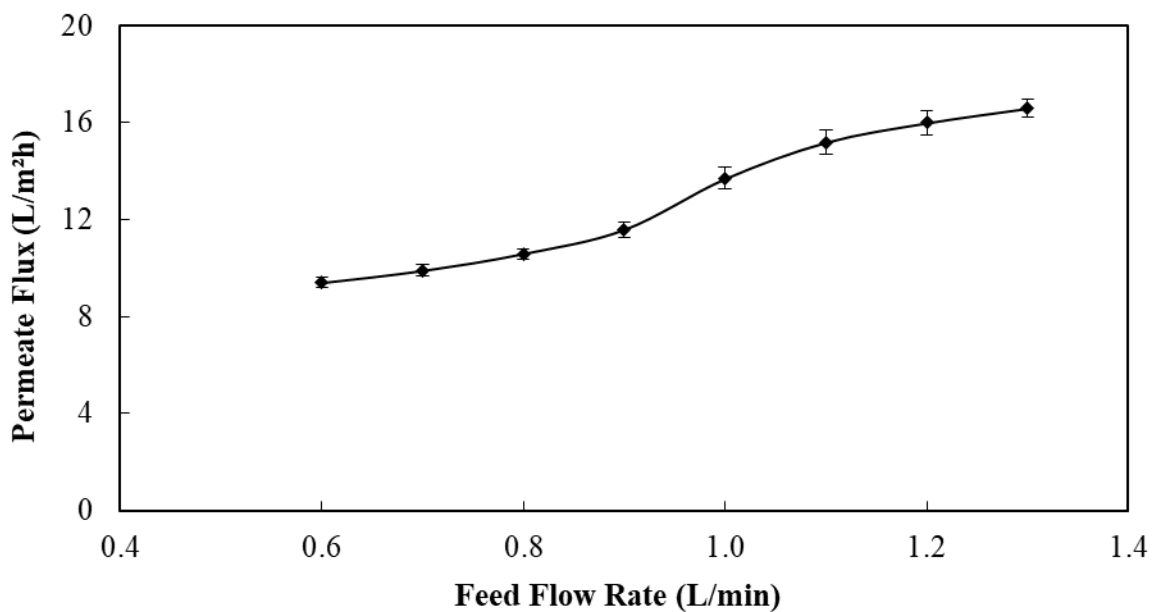


Figure 4.14. Effect of Feed Flow Rate on the Permeate Flux of Polypropylene Membrane in DCMD

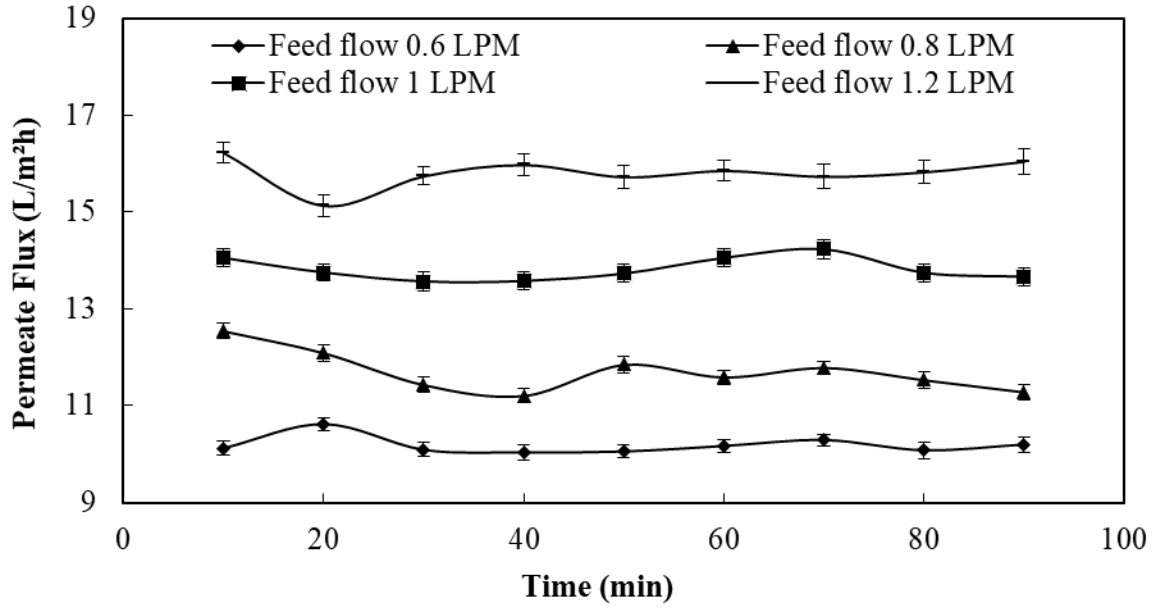


Figure 4.15. Permeate Flux at Different Feed-Flow Rates and Comparative Consistency Over Desalination Time in DCMD

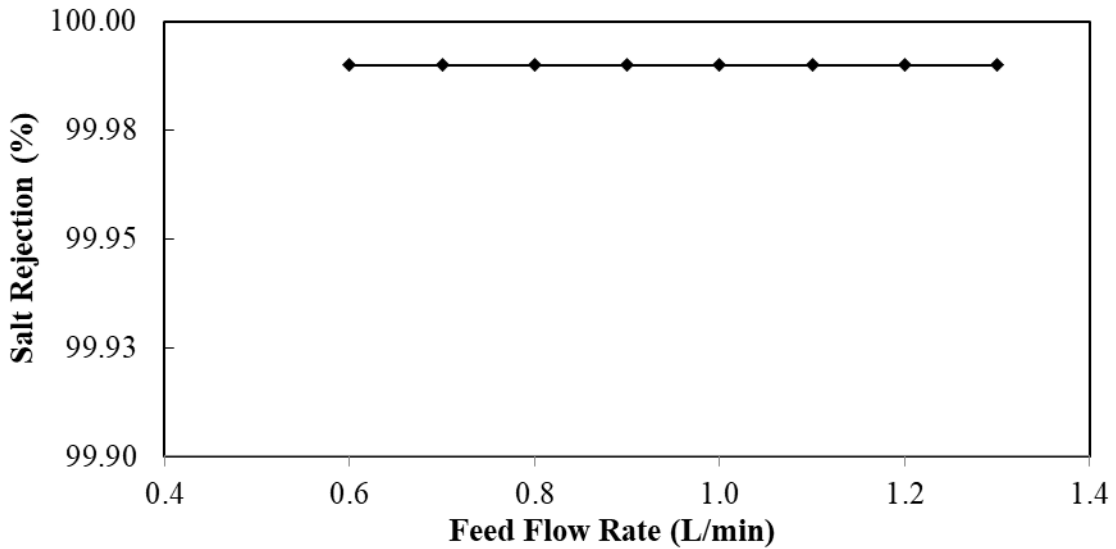


Figure 4.16. Effect of Flow Rate on the Salt Rejection of Polypropylene Membrane in DCMD

Figure 4.17 shows the impact of varying inlet flow rates on heat transfer performance, specifically the Nusselt number (Nu) and Total Power Consumption (TPC). Figure 4.17a indicates that increasing feed flow rates leads to a gradual rise in TPC. The Nusselt number, which reflects the ratio of convective to conductive heat transfer through the membrane, is influenced by two non-dimensional numbers:

the Reynolds number (Re) and the Prandtl number (Pr). As shown in Figure 4.17b, with the feed temperature kept constant, changes in the Reynolds number, due to varying feed flow rates, affect the Nusselt number. Increased feed flow rates enhance inertia forces and flux rates, resulting in a higher Nusselt number. Conversely, lower feed flow rates lead to a smaller Nusselt number, given the same feed temperature and concentration.

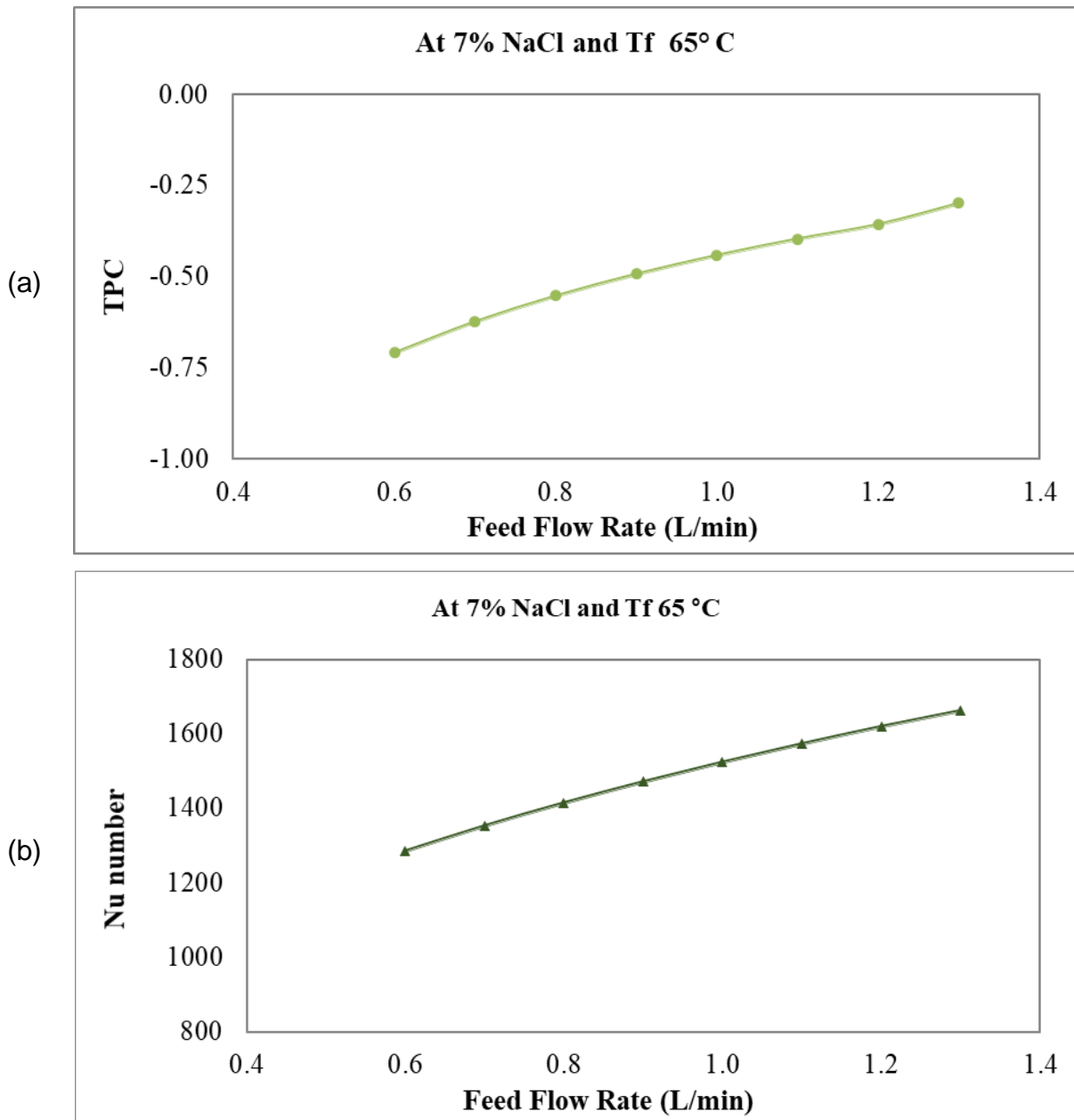


Figure 4.17. Effect of Feed Flow Rate on (a) TPC and (b) the Nusselt Number in DCMD

The GOR at a range of flow rates is calculated according to the equation (4.1) and is presented in Figure 4.18a. As can be seen, increasing the feed-flow rate acted at a gradual increase in the GOR. This indicates that increasing the flow rates led to an increase in the permeate flux produced. On the other hand, the performance of STEC over a range of inlet feed-flow rates is calculated according to the equation (4.4) and is presented in Figure 4.18b. It can be deduced that a higher GOR means higher performance produced by the flow at the considered higher feed temperature. This not only resulted in a higher GOR but also led to minimising the thermal energy requirements.

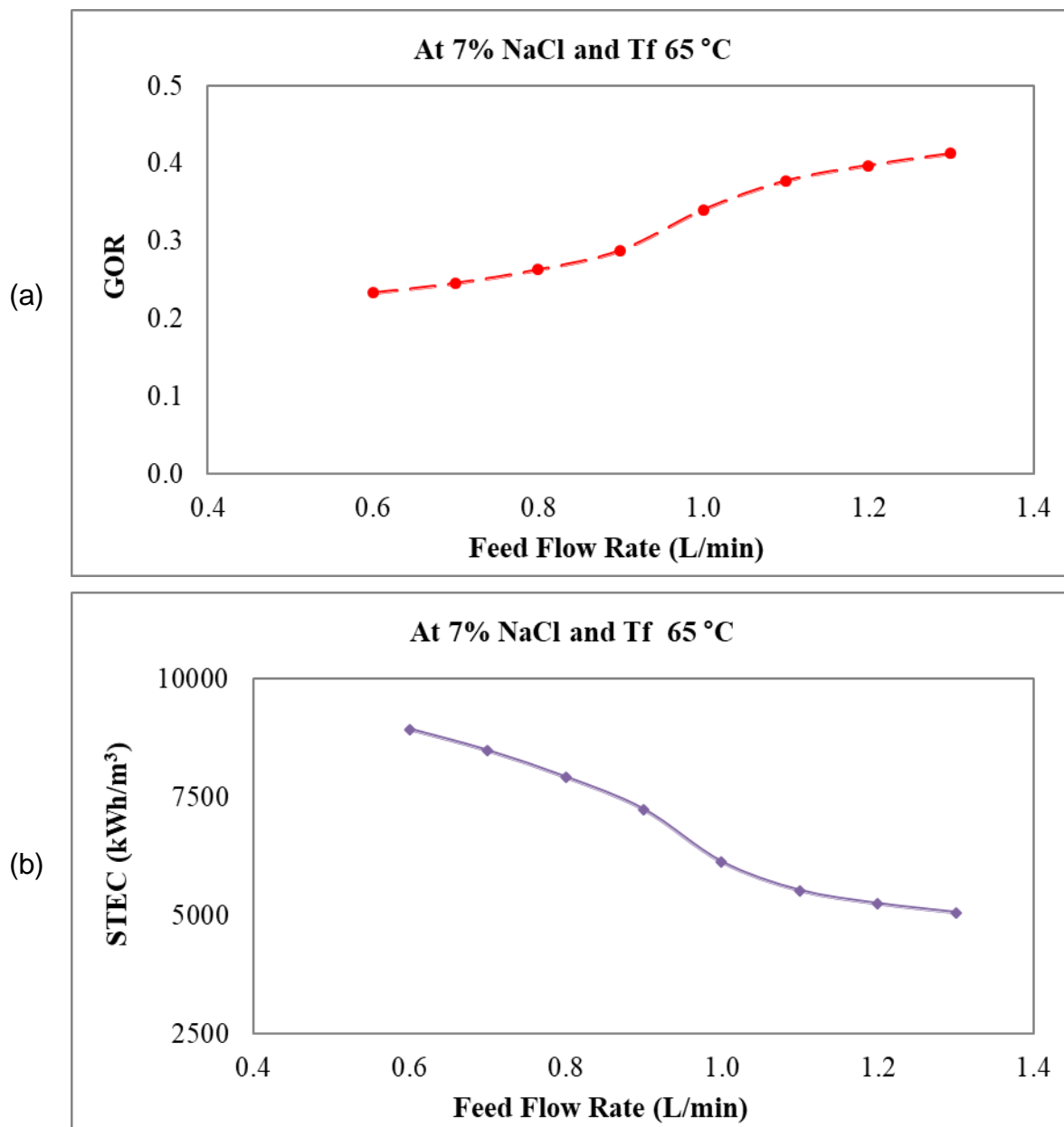


Figure 4.18. Effect of Feed Flow Rate on (a) GOR and (b) STEC in DCMD

4.3.4 Effect of Channel Depth on Permeate Flux

The effect of hot and cold solution flow channel depth on permeate flux is also investigated. Tests were conducted with a NaCl solution containing 7.0% by weight as the feed and deionised water as the cooling medium. The temperature of the feed side was 65 °C, and the temperature of the coolant side was 5 °C. The feed and cold-solution channels maintained a flow rate of 1.3L/min. The experiment was carried out using a PP membrane.

The flow channel depth refers to the distance between the membrane surface and the inner surface of the membrane cell plate, which determines the space through which the hot and cold solutions flow. A larger channel depth allows a greater volume of fluid to pass through, while a smaller channel depth restricts the flow to a smaller volume. For instance, if the channel depth on the hot side of the membrane is increased, more feed solution will flow on that side (the hot side of the membrane). Similarly, increasing the channel depth on the cold side will allow a greater volume of the cooling solution to flow through.

The channel volume (the space where the solution contacts the inner surface of the membrane cell plate and the membrane) can be adjusted by inserting plates with openings that are similar to those in the membrane cell. These plates act as spacers, either increasing or decreasing the space between the membrane and the cell wall, thereby controlling the amount of fluid flow. By adjusting the number of plates (adding more plates if a greater channel depth is required), the flow channel depth can be customized.

As shown in Figure 4.4, one mm thick plates were inserted between the membrane and the membrane cell plates on both the hot and cold sides to increase the channel depth. The number of plates used depended on the desired channel depth; for example, to achieve a 4 mm flow channel depth, four 1 mm thick plates were inserted. This was done to increase the volume and flow of the solutions on both sides of the membrane. In the literature, there is still a knowledge gap in investigating the effect of channel depth on the performance of MD technology. In the initial set of studies, the depth of the flow channel on the hot side of the membrane module was varied from 1 mm to 8 mm, while the depth on the cold side was kept constant at 2 mm. Further experiments were conducted by varying the depth of the flow channel on the cold side while maintaining a constant depth of 2

mm on the hot side. While conducting the experiments, the flow channel depth at one side was kept constant while the flow channel depth on the other side was varied. By keeping the flow channel depth on one side constant, it was easy to observe how the flow channel depth changes on the other side impact permeate flux, without the added complexity of simultaneous changes on both sides. This approach helps in understanding the specific influence of channel depth on the permeate flux. Figure 4.19 shows the effect of flow channel depth (hot and cold flow channels) upon permeate flux.

As shown in Figure 4.19, although the reduction in permeate flux with an increase in channel depth was minimal at a low flow channel depth, the reduction in flux was much higher at greater channel depths. Figure 4.19 reveals that when the cold-channel depth was increased to 10 mm from 4 mm, the flux was reduced from 7.8 to 7.2 L/m².h. The likely reason for this reduction in permeate flux is that increasing the cold channel depth reduces the velocity of the fluid flow on the cold side of the membrane. Lower flow velocity leads to decreased turbulence, which in turn reduces the convective heat transfer rate. As a result, there is less efficient cooling on the cold side, which can lower the overall driving force for the process, thereby reducing the permeate flux.

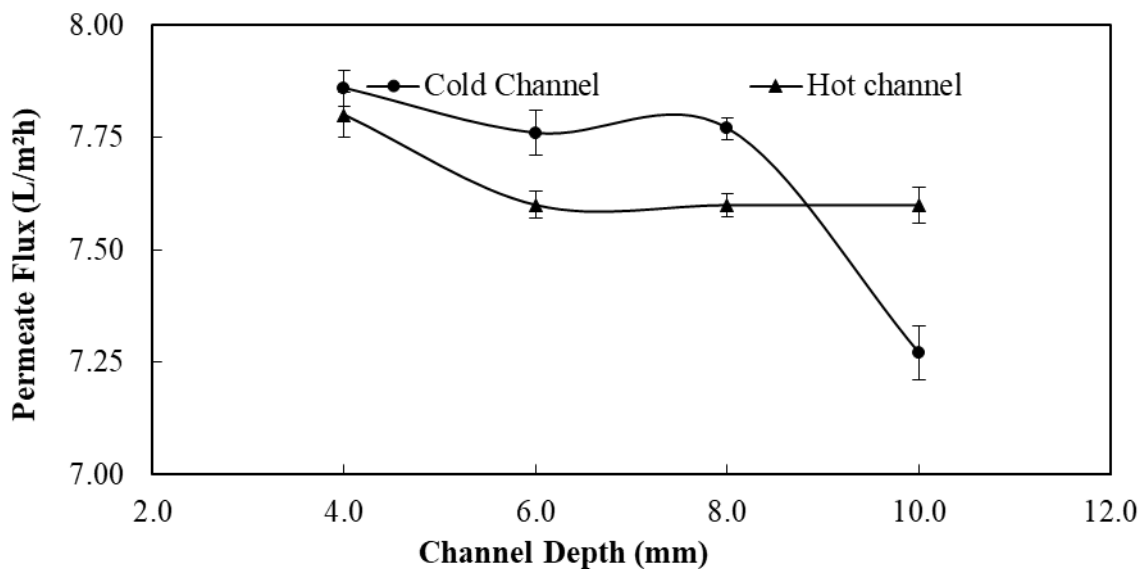


Figure 4.19. Permeate Flux at Different Flow Channel Depths Showing Improved Flux at Lower Depths

The flux values were most affected by variations in cold-channel depth rather than hot-channel depth variation. The effect of gap width on flux was less sensitive at lower gap depths due to the thermos-physical characteristics of water and the effects of natural convection within the gap. Heat and mass flow across the channel depth were affected minimally at a lower channel depth. This impact can vary depending on the medium in the channel, such as the air or sand [104–105].

Figure 4.20 shows the permeate flux values at different flow rates and temperatures while maintaining the hot-channel depth at 8 mm and the cold-channel depth at 2 mm. It is evident from Figure 4.20 that the permeate flux at higher channel depths can be increased by increasing the flow and temperature. At a hot-channel depth of 8 mm and a cold-channel depth of 2 mm, the flux increased to 8.9 L/m².h from 7.6 L/m².h upon increasing the flow to 2 L/min. Furthermore, upon raising the temperature from 65 °C to 85 °C, the flux increased by almost 56%, from 8.9 L/m².h to 13.9 L/m².h. Higher temperatures on the hot side enhance the driving force for mass transfer due to increased vapour pressure, which results in higher flux.

The effect of natural convection on flux can be inferred from Figure 4.20, where increased permeate flux is observed at higher hot-side temperatures. At higher temperatures, the buoyancy-driven natural convection is likely more significant. This convection can enhance the mass transfer on the hot side, thereby increasing the permeate flux. The figure shows that with increasing temperature (from 65°C to 80°C) and maintaining a higher flow rate (2 L/min), the permeate flux continues to rise, suggesting that natural convection effects are contributing to this increase. As the feed temperature rises, the difference in temperature between the hot feed and the cooler side of the system becomes larger. This temperature difference creates stronger natural convection currents within the gap. When the feed temperature is higher while keeping the coolant temperature constant, these convection currents become more intense. The stronger convection enhances the movement of heat and mass through the gap, which increases the rate of vaporization and, consequently, the permeate flux. In other words, higher feed temperatures lead to more effective natural convection, which improves the efficiency of the process and results in a greater permeate flux. In summary, the figure demonstrates that both increasing the flow rate and raising the hot side

temperature can enhance permeate flux, with higher temperatures likely promoting greater natural convection, further contributing to increased flux.

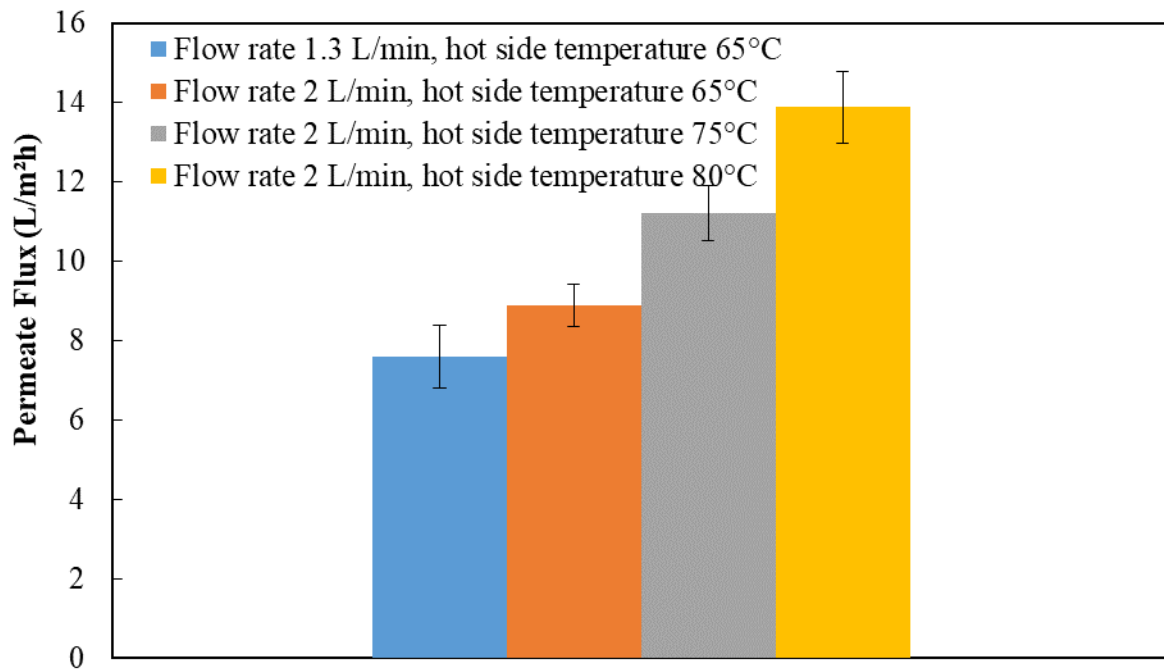


Figure 4.20. Permeate Flux at Different Flow Rates and Temperatures (Hot-side Depth of 8 mm and Cold-side Depth of 2 mm)

However, changing flow channel depth increased the STEC gradually, reaching the maximum value at 6 mm and no further increase beyond this value for the hot channel, as shown in Figure 4.21a. On the other hand, the STEC recorded a gradual increase with increasing channel depth, reaching the maximum value at a channel depth of 10 mm for the cold channel. This behaviour is expected to be achieved since these profiles are the same as those of the flux produced, as shown in Figure 4.19. However, no significant difference was observed between the performance of GOR (gained output ratio) produced by the hot and cold channels, except for the larger channel depth, as observed in Figure 4.21b.

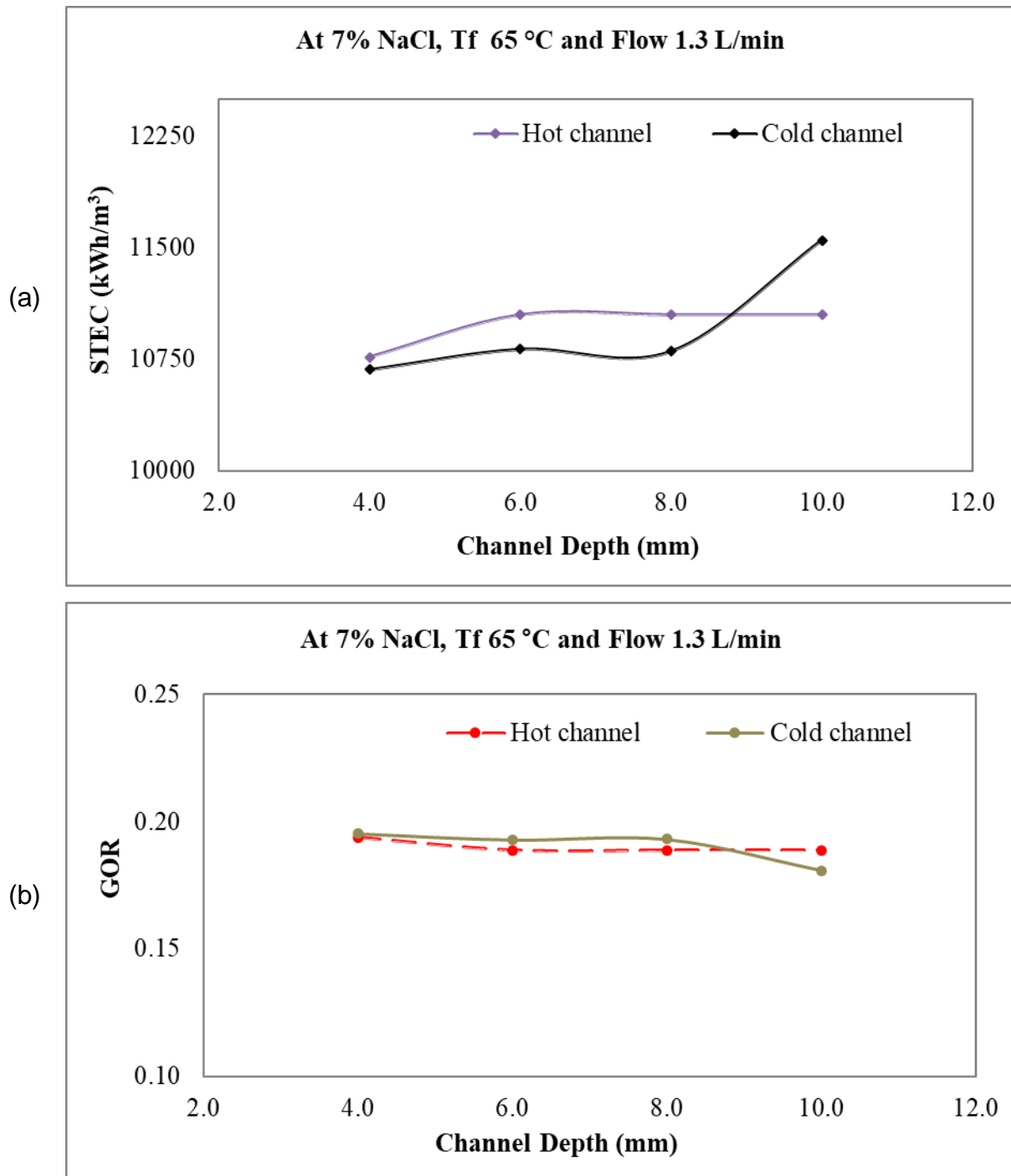


Figure 4.21. Effect of Channel Depths on (a) GOR and (b) STEC in DCMD

However, changing the channel depth does not affect the heat transfer performance since both the Re and Pr numbers are constants, and the flow rate has been set at 1.3 L/min with a fixed inlet temperature of 65 °C. This is evident in Figure 4.22 for both considered parameters: Nu number and TPC.

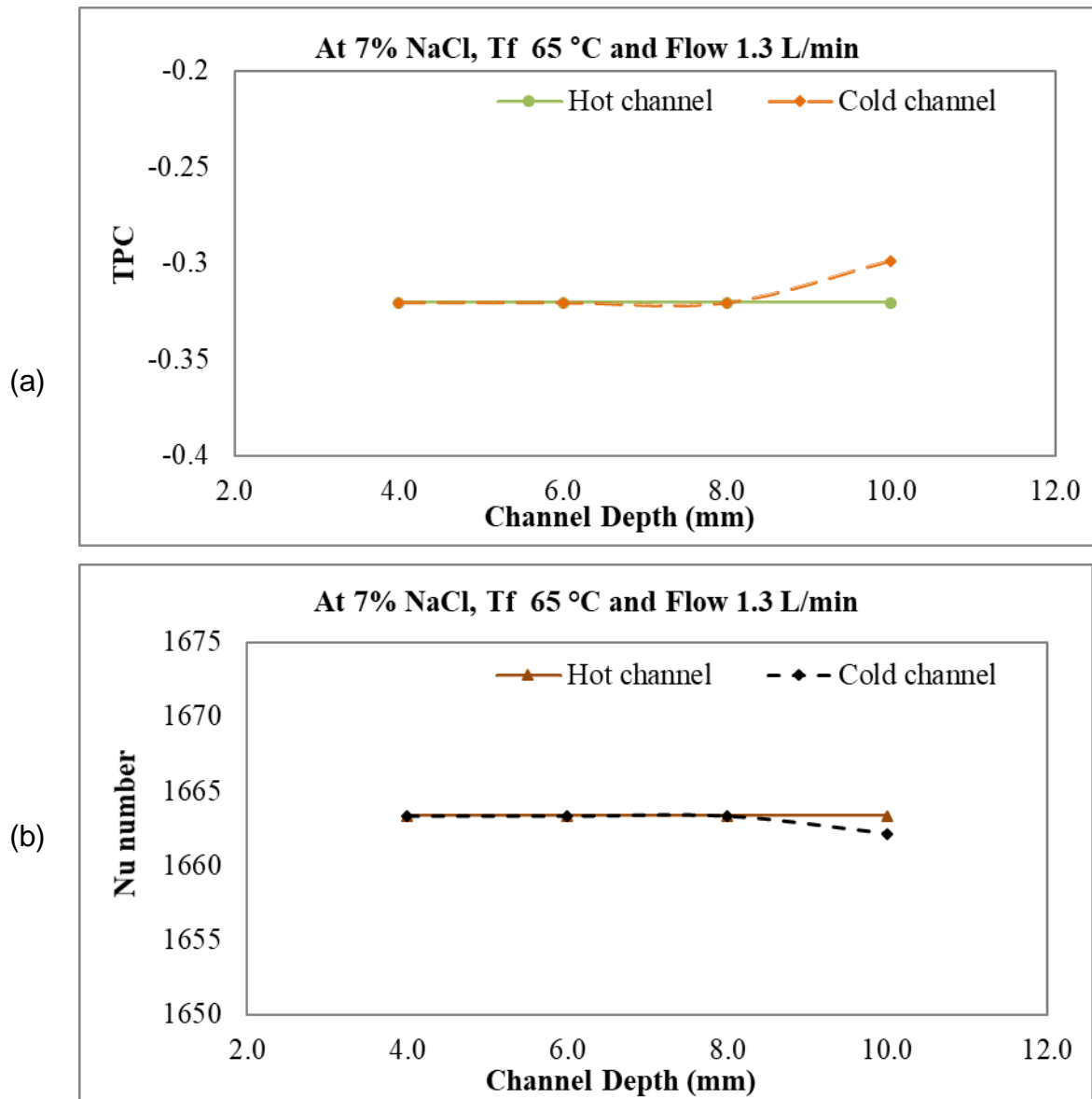


Figure 4.22. Effect of Channel Depths on (a) TPC and (b) Nusselt Number in DCMD

4.4 An Oilfield-Produced Water Desalination Performance Study Using the DCMD Process

It is well known that MD is effective for treating various streams of water such as seawater and brackish water, industrial waste water from textile, pharmaceutical, chemical industries, food and beverage industry effluents, shale gas produced water, etc. [4, 106–115]. It has recently been utilised to filtrate the oil-containing feed stream [116, 117]. The viability of employing DCMD for oilfield produced water desalination is examined. Oilfield-produced water collected from an oil field was utilised as feed without pre-treatment. The cooling medium utilised was deionised

water. The temperature of the feed side was 80 °C and 85 °C. The temperature of the coolant side was 5 °C. The feed and cold-solution channels maintained a flow rate of 2 L/min. The experiments on flow channel depth variation (discussed in the previous sections) showed that highest permeate flux was obtained with hot-channel depth 8 mm and the cold-channel depth 2 mm. Accordingly, the aforementioned channel depths were used for oilfield-produced water experiments also. The experiment was conducted using a polypropylene membrane. The experimental results in Figure 4.23 show the permeate flux as a function of time. It was observed that DCMD is highly efficient in desalinating oilfield-produced water. The permeate flux in this experiment was 11.5 L/m².h and 12.5 L/m².h at 80 °C and 85 °C, respectively. The stable permeate flux indicates that the fouling resistance of the membrane was good. However, there is good scope for future work, as long-term performance and potential challenges over extended operation periods require further study.

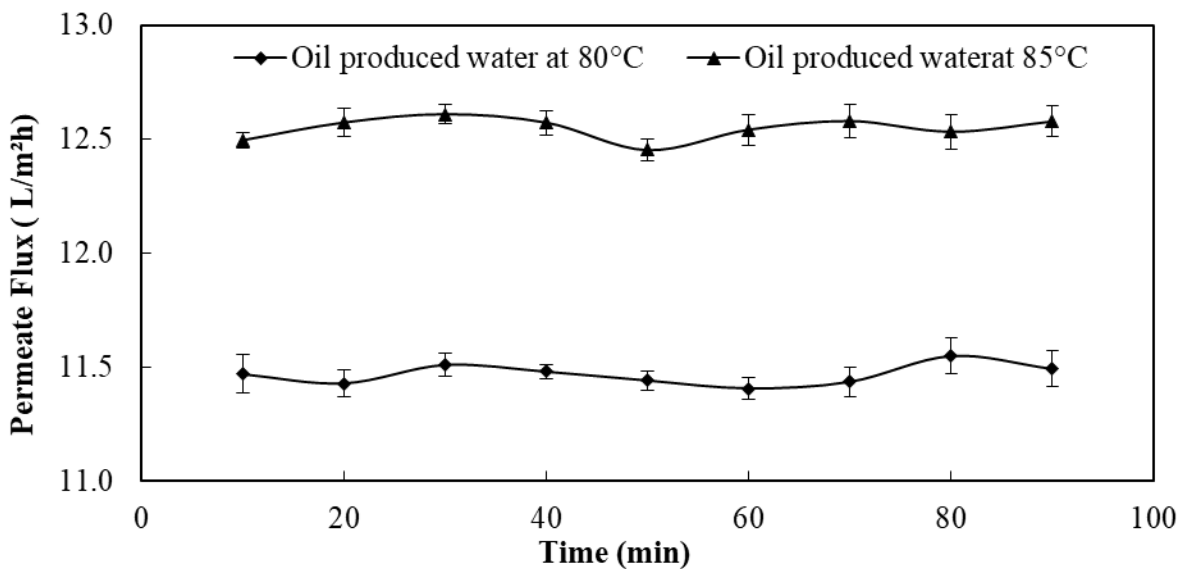


Figure 4.23. Permeate Flux at Different Temperatures Using Oilfield-Produced Water in DCMD

Studies have reported slight fouling of the membrane in the long run. In such a scenario, washing the membrane with deionised water effectively cleans the membrane and restores the permeate flux [117]. Furthermore, the salt rejection was almost 100% (viz. 99.98–99.99%) at both temperatures and maintained the same rejection percentage throughout this current study, as shown in Figure 4.24. The

results demonstrate the massive potential of DCMD to treat hypersaline oilfield-produced water with a salt rejection of more than 99.9% overall.

The observed stable, reliable salt rejection parameters were attributed to the membranes' resistance to wetting over the testing period. This means that the membrane effectively maintains its hydrophobic properties ensuring that only water vapour permeates through the membrane, while liquid water and salts are kept out. The selected membranes were hydrophobic and demonstrated only the transport of water vapours through the membrane pores.

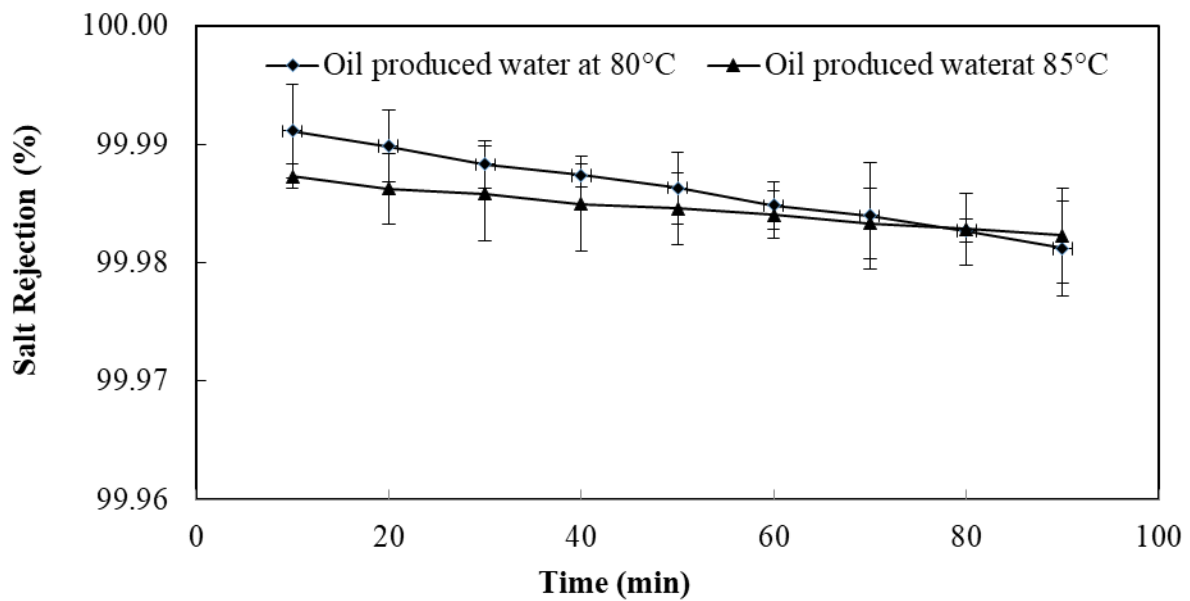


Figure 4.24. Salt Rejection Percentage at Different Temperatures Using Oilfield-Produced Water in DCMD

Table 4.6 shows the analytical results, i.e. the chemical and physical analysis of major composition and characteristics, of the feedwater sample and permeate collected after the DCMD process. It has been observed that when DCMD is used for treating oil-produced water, it demonstrates several key advantages in contaminant removal. The data indicates that DCMD is an effective and promising method for significantly reducing TDS, suspended solids, oil, and organic content. Its capability to handle high salinity and complex contaminants makes it particularly well-suited for oil and gas industry applications, where water reuse or discharge quality must comply with stringent environmental regulations.

Table 4-6. Physicochemical Analysis of Oilfield-Produced Water and Permeate Water

Parameter	Unit	Feedwater	Permeate water
TDS	mg/L	168000	413
Total suspended solid (TSS)	mg/L	95	< 2
Chloride	mg/L	99,420	223
Sodium	mg/L	44,417	88
Calcium	mg/L	12,247	21
Magnesium	mg/L	2,029	9
Potassium	mg/L	1,836	8
Strontium	mg/L	345	3
Oil and Grease	mg/L	71.8	< 0.75
Total organic carbon (TOC)	mg/L	9.5	2.4
Turbidity	NTU	64	0.9

4.5 Seawater Desalination Performance of PP and PVDF Membranes at Different Flow Rates and Temperatures Using the DCMD Configuration

This study investigated the desalination performance of flat-sheet PP and PVDF membranes using the AGS feed collected from the DRP in Kuwait. The feed temperature was 65°C, and the cold-side temperature was kept at 5°C. The flow rate of hot and cold-side water varied from 0.6–0.9 L/m. Experiments were conducted for both membranes at different flow rates, and the results are summarised in Table 4.6. Table 4.6 shows that the water flux increased with an increase in the flow rate for the PP and PVDF membranes. The highest water flux for PP and PVDF membranes was 13.2 L/m²h and 17.8 L/m²h, respectively, when AGS was used as the feed solution.

PP membranes achieved higher salt rejection compared to PVDF membranes; whereas PVDF membranes showed a higher water flux than PP membranes (see Table 4.7). PP is a non-polar, semi-crystalline thermoplastic polymer. PP membranes are generally more hydrophobic than PVDF membranes. The hydrophobic nature of PP membranes enhances their ability to reject salts and

other non-volatile solutes because it prevents water and dissolved salts from wetting the membrane pores. In MD, this characteristic is crucial for maintaining the vapour–liquid interface at the pore entrance, which is essential for effective salt rejection. Furthermore, PP membranes generally have a lower surface energy compared to PVDF membranes. Lower surface energy means a reduced tendency for foulants to adhere to the membrane surface. Reduced fouling can help maintain high salt rejection rates because fouling can cause wetting of the membrane pores and compromise salt rejection efficiency. PP membranes are suitable for applications requiring reasonable water flux and high salt rejection. In contrast, PVDF membranes can be used in applications where salt rejection is not a major concern.

Table 4-7. Water Flux and Salt Rejection Percentages of PP and PVDF Membranes at Different Flow Rates Using AGS Feed

Membrane	Flow Rate, L/h	Water Flux, L/m ² h	Salt Rejection, %
PP	0.6	11.7	99.98
	0.9	13.2	99.98
PVDF	0.6	12.5	78.83
	0.9	17.8	75.89

4.6 Conclusion

This chapter described the results of investigating the feasibility of the DCMD process for desalinating different saline waters (3.5% to 26% NaCl solutions), including AGS and oilfield-produced water, under various operating conditions such as feed temperature, flow rate, and feed concentration. Additionally, tests were conducted by varying the channel depth of the DCMD module to assess its impact on MD performance. The membranes used were Polypropylene and Poly vinylidene fluoride.

The feed temperature ranged from 45 °C to 75 °C. The permeate flux increased to 37.1 L/m²h from 11.6 L/m²h when the temperature was raised from 45 °C to 75 °C as mentioned in Table 4-3. It was observed that increments in feed-water temperatures increase transmembrane vapour pressure and result in a high permeate flux. Additionally, at higher temperatures, the viscosity of a feed solution decreases, which can lead to an improvement in hydrodynamic conditions and result

in a higher flux. Overall, temperatures ranging from 45–75 °C are commonly used in MD research studies because they are within the typical operating temperature range for most MD systems and allow for high permeate flux while minimising the risk of thermal degradation. At temperatures below 45 °C, the vapour pressure of a feed solution may not be high enough to provide a sufficient driving force for mass transfer, resulting in low permeate flux. Temperatures above 75°C increase the risk of thermal degradation of polymeric membranes and heat-sensitive feed solutions, resulting in decreased membrane performance and flux with time. Moreover, increasing the feed temperature resulted in a gradual increase in the GOR. This may be due to the partial pressure difference, which in turn leads to a larger mass flux that is directly proportional to the gained output ratio, whereas the performance of Gained Output Ratio (GOR) is the opposite performance of STEC; thus, the higher GOR means higher performance produced by the flow at the considered higher feed temperature.

NaCl solutions at concentrations of 3.5–26%, deionised water, oilfield-produced water and AGS were used as the feed at different stages of this study. The increase in feed concentration resulted in reduction of permeate flux. As shown in Figure 4.9, there was a 50% reduction in permeate flow when the NaCl concentration in the feed solution was increased from 0% to 26%. Upon an increase in NaCl feed concentration, the hydrogen bonding between the NaCl and water molecules might increase, and hence, more energy is required to vaporise the feed solution. This shows that more time and energy might be needed to produce permeate flux when the feed concentration is increased. However, increasing the feed concentrations resulted in a gradual decrease in the GOR. This may be due to the higher permeate flux produced at smaller concentrations, directly proportional to the GOR. This not only resulted in a higher GOR but also led to minimising the thermal energy requirements. This result occurred when we used a smaller concentration of feed. The amount of time needed to produce the same permeate flux was also increased when the feed concentration was increased.

The study on the effect of flow rate on permeate flux showed that the flux increased with an increase in the flow rate. This might be due to turbulence and the reduction of temperature and concentration polarisation effects. Additionally, at lower flow rates, greater heat transfers between the membrane and the feed medium can

occur, which may reduce the vaporization effect. Conversely, at higher flow rates, the heat transfer rate between the membrane and the feed decreases, leading to faster vaporization and resulting in a higher permeate flux. Also, increasing the feed-flow rate resulted in a gradual increase in the GOR. This suggests that higher flow rates resulted in an increase in the permeate flux generated. On the other hand, the performance of STEC with increasing feed-flow rates showed a gradual decrease.

The effect of a direct contact membrane distillation system on different hot-feed and cold-solution channel depths was also studied using a DCMD module developed by the research team. It was also shown that the deeper channel depths (hot and cold) are suitable for higher permeate flux. However, higher flow rates and temperatures are required to obtain a higher permeate flux upon increasing the hot-channel depth. Moreover, changing flow channel depth increased the STEC gradually, reaching the maximum value at 6 mm and no further increase beyond this value for the hot channel. In contrast, the STEC recorded a gradual increase with increasing channel depth, reaching the maximum value at a channel depth of 10 mm for the cold channel.

The experimental results showed that DCMD was highly efficient in desalinating oilfield-produced water obtained from Kuwait. This is consistent with the results reported in studies that used effluent water from other parts of the world. The permeate flux was 11.5 L/m²h. and 12.5 L/m²h at 80 °C and 85 °C, respectively. The results indicate the enormous potential of the DCMD to treat hypersaline oilfield-produced water, with an overall rejection of salts above 99.9%.

The comparison of PP and PVDF membrane performance for AGS desalination revealed that PP membranes had a higher salt rejection rate but lower water flux. In comparison, PVDF membranes had a lower salt rejection rate but higher water flux. This observation is important because it suggests that PP membranes may be more suitable than PVDF membranes for seawater desalination, leading to more energy-efficient and cost-effective desalination. PP membranes are ideal for situations where a balance of water flow and salt removal is necessary. In contrast, PVDF membranes are suitable for applications where salt removal is not a primary concern.

This study successfully established and generated reference data on DCMD technology for desalinating different saline waters at the laboratory-scale level under

realistic operating conditions. Specifically, it used actual AGS (considerably higher salinity than most other seawaters) and oilfield-produced water as feed. Overall, the results are promising, and we recommend conducting further laboratory- and pilot-scale studies using other MD technologies, such as VMD, AGMD and SGMD, to desalinate AGS and oilfield-produced water.

Chapter 5

A Comparative Study of Air-Gap and Vacuum-Driven Membrane Distillation Modules for Seawater Desalination and Oilfield- produced water treatment

5.1 Introduction

The most significant advantage of the MD process over conventional desalination methods is its lower energy consumption due to the process requiring low-grade energy associated with evaporation at ambient pressure [66, 118]. A simulation study by Baghbanzadeh et al. [119] on zero thermal input membrane distillation (ZTIMD) showed that ZTIMD is more economically effective than existing seawater desalination technologies and can produce pure water at a significantly lower cost of \$0.28/m³ with a specific energy consumption of 0.45 kWh/m³. The ZTIMD process requires no external thermal input, as the enthalpy of the surface seawater is used to generate the necessary thermal energy, and the bottom seawater serves as the heat sink. However, the ZTIMD process faces three major challenges: (1) the low working temperature of 30°C or less provides a small driving force for membrane distillation, potentially increasing membrane costs due to the requirement of more membranes; (2) the small water recovery rate necessitates large amount of feed and associated pre-treatment costs (15–20 times more than conventional desalination processes); and (3) the need to pump bottom seawater over long distances to the plant site as a coolant increases both capital and operational costs [119]. Utilizing low-grade waste heat from industrial and power plants offers an alternative approach to ZTIMD, making the MD process more viable for various applications. The waste heat from steam ejectors blow down, boiler blow down, dump condenser, flue gas chambers, etc., can be used for the MD process [120, 121].

The operating conditions and membrane properties significantly impact MD process performance. The main factors affecting the MD process's performance are feed temperature, feed concentration, the feed and coolant flow rates, permeate temperature, temperature difference and mean temperature and vapour pressure difference [2, 123, 124]. The temperature of the feed- and permeate-side mediums

significantly impacts permeate flux. The Antoine equation (Equation 5.1) states that vapour pressure increases exponentially with temperature.

$$\log_{10}(P) = A - [B / (T + C)] \quad (5.1)$$

where P is the calculated vapour pressure in bar (on an absolute scale) and T is the temperature in Kelvin, A, B and C are Antoine coefficients specific to the substance.

In all MD configurations, the permeate flux increases exponentially with increasing feed temperature [123]. If the feed input temperature remains constant, increasing the coolant temperature reduces transmembrane vapour pressure and lowers permeate flux [123, 125]. Similarly, if the temperature of the coolant is held constant, an increase in the temperature of the feed results in a rise in the transmembrane vapour pressure, leading to an increase in the permeate flux [2, 124]. According to the Antoine equation, increasing temperature causes a greater change in vapour pressure because diffusivity and temperature have a direct relationship [125, 126].

As the feed temperature rises, so does the mass-transfer coefficient across the membrane. Furthermore, as the feed temperature increases, temperature polarisation decreases [2]. In conclusion, the coolant-side temperature and distillate flux have an inverse relationship; a greater vapour pressure difference at low temperatures results in higher distillate fluxes. As a result, the highest flux can be obtained at the highest and lowest feed and permeate temperatures, respectively [127]. Feed concentration also influences permeate flux. The vapour pressure drops as the feed concentration (i.e. NaCl) is increased, resulting in a low permeate flux. Furthermore, as the influence of concentration polarisation increases with an increase in feed concentration, the mass-transfer coefficient of the boundary layer at the feed side decreases. Additionally, as the surface membrane temperature declines due to concentration polarization, the heat transfer coefficient of the boundary layer also decreases [2, 123]. These results in reduced permeate flux with non-volatile feed solutions [2,128, 129]. In the case of feed solutions containing volatile components, such as alcohols, the effect of increasing feed concentration on permeate flux is determined by the volatile component's thermodynamic properties and its interaction with water [2]. An increase in volatile component concentration may result in a greater permeate flux as vapour pressure rises.

Another parameter that affects MD flux is the flow rate of the feed and cold sides. As the feed-flow rate increases, the heat transfer coefficient on the feed side of the membrane module increases and reduces the effects of temperature and concentration polarisation. Accordingly, higher distillate fluxes are obtained at higher feed-flow rates [2,124,125]. Furthermore, research has shown that a counter-current flow arrangement has more heat- and mass-transfer efficiency than a co-current flow system [127]. With DCMD and SGMD systems, an increase in the cold stream flow rate on the permeate side of the membrane module enhances heat transfer on the permeate side of the module and minimises the temperature and concentration polarisation effect. As the heat transfer coefficient on the permeate side grows, the temperature at the membrane surface approaches the bulk permeate-side temperature; thus, the driving force and permeate flow increase [2, 123]. However, due to the dominant effect of the air gap in the case of AGMD, the effect of the permeate-side flow rate on permeate flux is almost negligible [125, 130]. In brief, the increase in permeate flow rate has a significant impact on DCMD and SGMD due to the direct contact between the cold stream and the membrane, but it has a negligible effect on AGMD because of the air gap's insulating effect. In some cases, the non-condensable gases present in the feed also evolve with vapour upon heating. These gases may block the membrane pores and cause mass-transfer resistance. As a result, the permeate flux declines [131]. Degassing feed and cold-side solutions lower the partial pressure difference and reduce the resistance to molecular diffusion into the pores [131, 132].

Another factor to be considered in MD is temperature polarization. The thermal boundary layer forms at the membrane surface due to temperature differences between the membrane surface and the bulk solutions, leading to temperature polarization. This temperature polarisation feature reduces the effectiveness of mass transportation [115].

Membrane thickness, membrane porosity, membrane pore size, pore-size distribution, pore tortuosity, membrane surface chemistry, etc., are some of the other parameters that can affect the performance of the MD process [2]. The hydrophobic nature of the membrane, in general, prevents the solution from penetrating the pores, resulting in a vapour–liquid interface at each pore entrance. In the MD process, microfiltration membranes made of hydrophobic polymers, such as

polypropylene (PP), polytetrafluoroethylene (PTFE), and polyvinylidene fluoride (PVDF), are used. PTFE and PVDF have surface energies of 9.1 and 30.3 kN/m, respectively. They also have thermal conductivities as low as 0.22- 0.45 Wm⁻¹K⁻¹ and good chemical stability at MD operating temperatures. Their pore sizes are typically in the range of 0.2-1.0 μm, with thicknesses ranging from 0.06–0.25 mm [82]. Larger pore-size membranes can produce a greater permeate volume. However, as the pore size increases, the LEP decreases. If the feed pressure exceeds the LEP, liquids may be able to enter the pores. This causes the membrane to become wet [133]. To avoid wetting membrane pores, pore size should be kept as small as possible, which contradicts the requirement for higher MD permeability. For each MD application, an optimum value must be determined based on the type of feed solution to be treated [2]. Because of the availability of a large evaporation area, membranes with high porosity can achieve a higher permeate flux. In terms of energy efficiency, higher porosities reduce conductive heat transfer through the membrane solid material because the heat transfer coefficient of the air/gas is lower than that of the polymer. The typical membrane porosity in MD configurations ranges between 60% and 85% [132, 134]. Membrane tortuosity is defined as the average length of the pore channels in relation to the thickness of the membrane. High tortuosity values result in a lower permeate flux [2].

The chapter four focused on various aspects related to the experimental work on DCMD through a parametric study involving different parameters such as inlet feed temperatures, feed concentrations, flow rates, and feed-channel depths. It also examined the feasibility of desalinating oilfield produced water using the DCMD process. Furthermore, it investigated the seawater desalination performance of PP and PVDF membranes at different flow rates within a DCMD configuration. This means that the previous chapter only concentrated on the performance of DCMD technology.

However, in the current chapter, this research presents a parametric study conducted at the KISR to assess the feasibility of using AGMD and VMD processes for desalinating AGS and oilfield-produced water under various operating conditions as shown in Table 5-1. The study utilised PP, PVDF, and PTFE membranes and, for the first time, investigated the effects of air gap depths and vacuum space on the AGMD and VMD modules developed at KISR. This study is the first to report on

using different vacuum spaces in a VMD process and provide valuable insights into treating different saline solutions (AGS and oilfield-produced water) using AGMD and VMD technology. After assessing the results in the current chapter, the MD technologies are compared and evaluated to propose the best candidate. The current chapter has been published.

Table 5-1. Experimental Framework and Methodology

Parameter		Reasoning
Feed Temperature, °C	65–85	The study investigated how AGMD and VMD systems respond to different feed solution temperatures, with a 65–85 °C temperature range commonly used in MD research. The maximum temperature tested was 85 °C to avoid thermal degradation of the membranes, which can occur at higher temperatures.
Flow-rate, L/min	1.3–2.0	The experiment aimed to study the impact of varying feed-flow rates on the performance of AGMD and VMD processes by measuring the resulting permeate flux. The goal was to establish data that provided insights into how the feed-flow rate affects the performance of the two processes.
Feed Solution Concentration, wt%	3.5% to 26% NaCl solutions, oilfield-produced water, Arabian Gulf Seawater	To investigate the impact of varying feed concentrations on the permeate flux and to assess the viability of employing MD for feeds with varying levels of salt concentration, including oilfield-produced water and actual seawater
Membranes	Polypropylene, Polyvinylidene fluoride and Polytetrafluoroethylene	To test the performance of different polymeric membranes for desalination of both AGS and oilfield-produced water in the AGMD and VMD configurations

5.2 Materials and Methods

5.2.1 Experimental Setup and Procedure

The bench scale MD unit, as shown in Figure 4.2, can accommodate different MD configuration cells for testing. This study used flat-sheet membranes with effective areas of 0.0155 m² and 0.003847 m² for both AGMD and VMD. The membrane modules, showed in Figure 5.1 and 5.2, were designed and built at KISR using Teflon and acrylic materials. The channel depth effect experiments were conducted on a 0.0155 m² membrane module. Currently, there are no commercially accessible membrane modules that offer the capability to adjust the depth of their channels. As a result, a new membrane module was designed and developed at the KISR to accommodate different plates of one mm thickness on the hot- and cold-channel sides. Figure 5.1 and 5.2 show schematic representations and images of the VMD and AGMD cells, respectively.

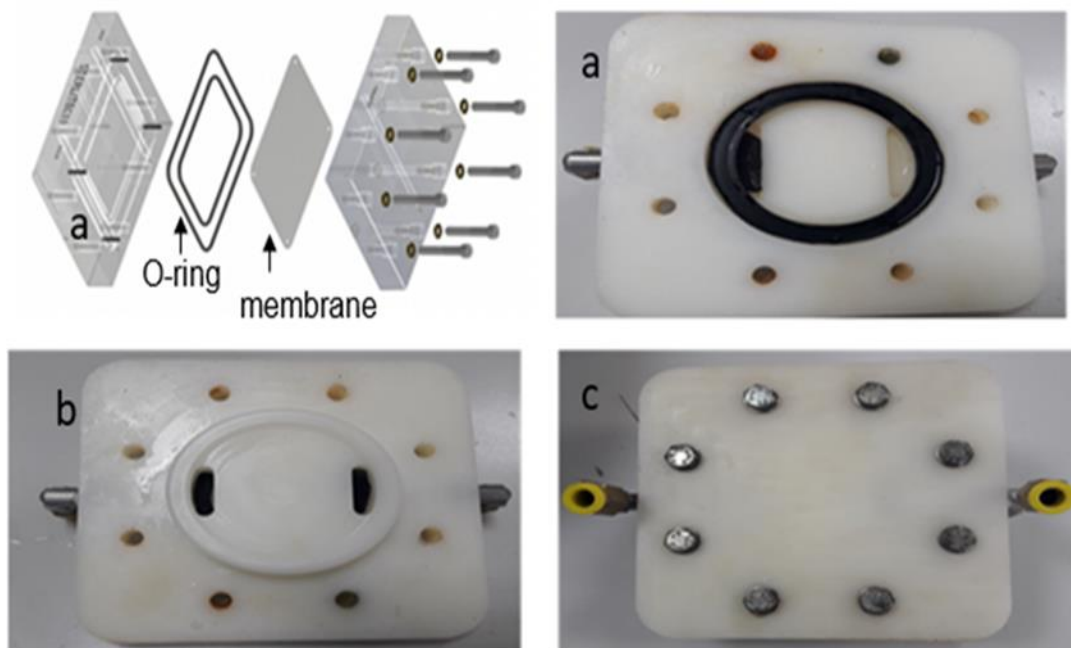


Figure 5.1. Schematic Representation and Photos of the VMD Membrane Module (a) Feed Side Shell, (b) Vacuum Side Shell, (c) Assembled VMD Module

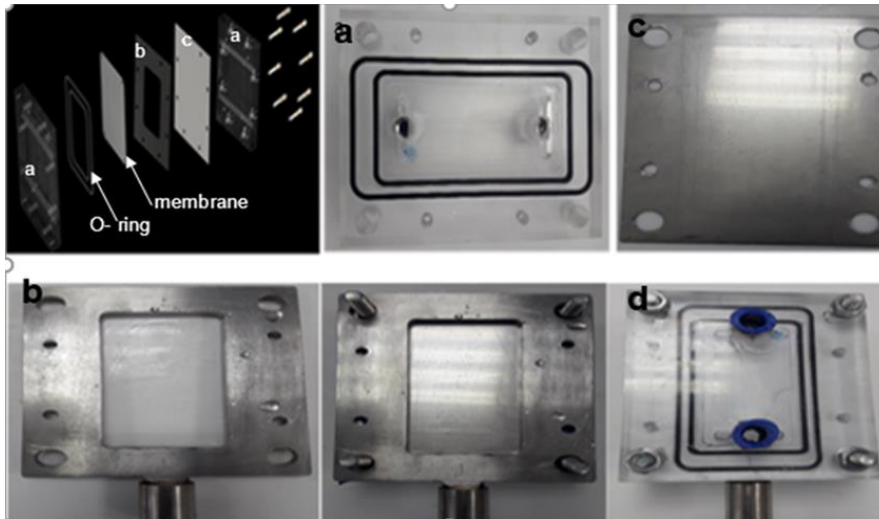


Figure 5.2. Schematic Representation and Photos of the AGMD Membrane Module, (a) Membrane Module Shell Plate, (b) Plate to Introduce Air Gap, (c) Condensation Plate, (d) Assembled AGMD Module

Figure 5.3 and 5.4 show schematic representations of AGMD and VMD processes, respectively [135]. Figure 5.5 and 5.6 shows the schematic diagram of AGMD and VMD setup, respectively.

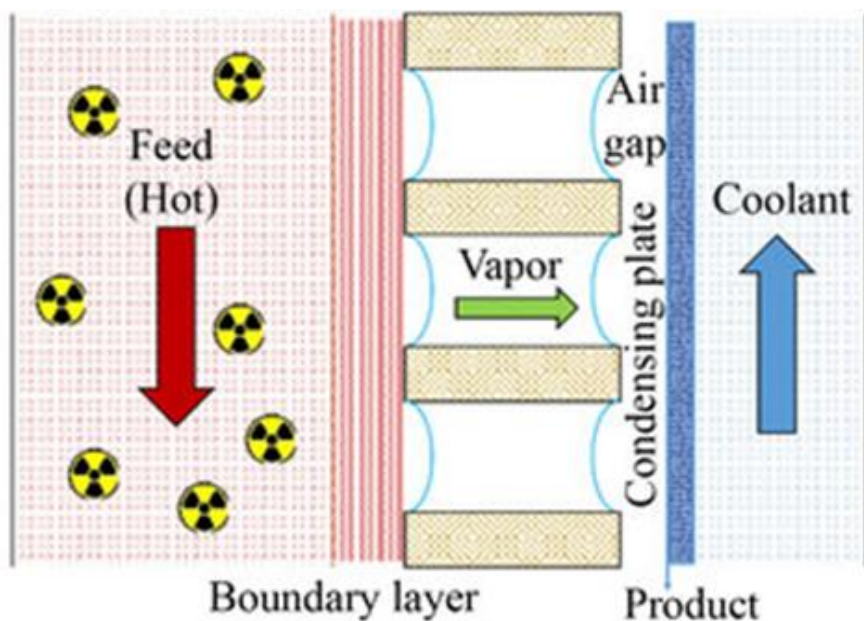


Figure 5.3. Schematic Representation of the AGMD Process [135]

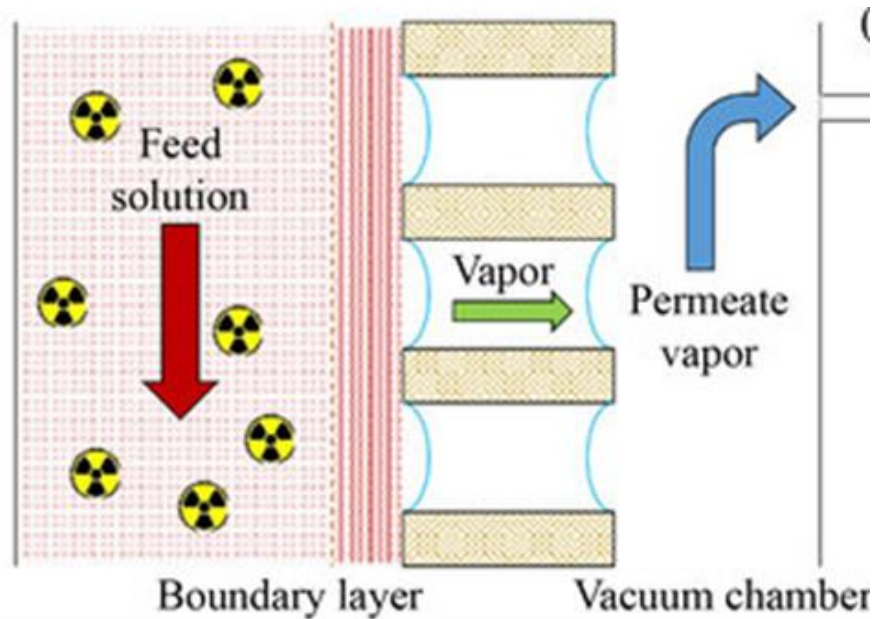


Figure 5.4. Schematic Representation of the VMD Process [135]

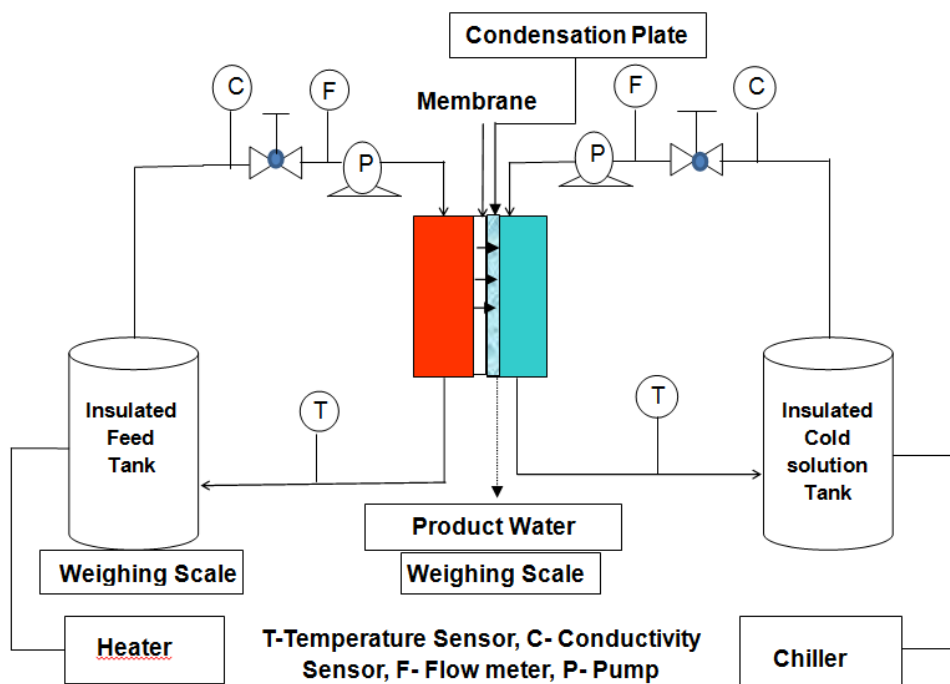


Figure 5.5. Schematic Diagram of AGMD Setup

In the AGMD process as shown in Figure 5.5, the hot feed solution is stored in an insulated feed tank on the left side of the diagram. The solution is heated using a heater to the desired temperature. A pump (P) then circulates this heated feed solution into the membrane module, with the flow rate being monitored by a flow meter (F). The feed temperature is constantly measured using a temperature sensor

(T) to ensure optimal operating conditions. As the hot feed enters the membrane module, it evaporates, with water vapour passing through the membrane and air gap. On the cold side (right side), the insulated cold solution tank contains a chilled solution maintained by a chiller, which keeps the temperature around 5°C. This cooling solution is circulated through the system by another pump (P), with the flow rate monitored by the flow meter (F). The cold solution ensures that the water vapor condenses on the surface of the condensation plate, producing purified water. The collected product water is then measured by a weighing scale.

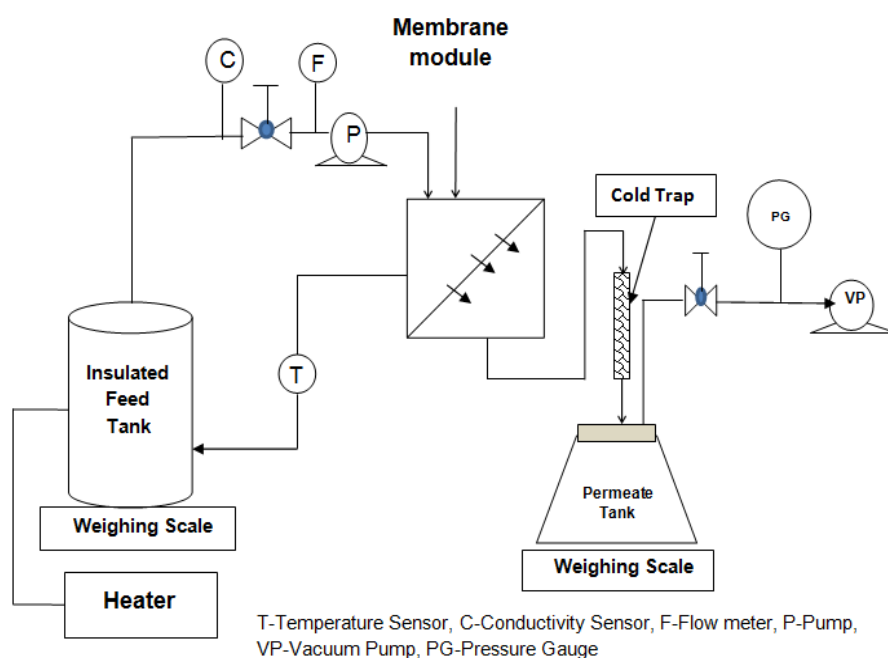


Figure 5.6. Schematic Diagram of VMD Setup

Figure 5.6 illustrates the VMD process, where the hot feed solution, stored in an insulated feed tank and heated by a heater, is pumped through the membrane module. A vacuum pump (VP) is applied to the permeate side of the membrane to create a low-pressure environment, pulling the vapour through the membrane pores. The vapor is then collected in the cold trap and condensed, while the pressure gauge (PG) monitors the vacuum level. The collected permeate is stored in the permeate tank, and the overall system performance is monitored using temperature sensors (T), flow meters (F), and conductivity sensors (C).

Flat-sheet PP, PVDF and PTFE membranes were used in this study. Merck Millipore Ltd. supplied the PVDF (YMJXSP3001) membrane, and Celgard 2500

supplied the PP membrane. The PTFE (PTFE023005) membranes were procured from the Sterlitech Corporation. The NaCl used was AR grade, with a purity of 99.9%. (Techno Pharmchem, Sodium chloride AR – 33127). NaCl solutions with concentrations of 3.5%, 7.0%, 15%, and 26% were used as feed solutions. The NaCl solutions were prepared by dissolving a known amount of NaCl salt in a known amount of deionised water (DI) produced by Millipore’s ZRQSV3WW | Direct-Q3 UV Water Purification System. Furthermore, AGS collected from a beach well at the KISR’s DRP in Kuwait was used as feed. The effectiveness of AGMD and VMD was also investigated for oilfield-produced water collected from Kuwait. The physiochemical analysis of the AGS used in this study is summarised in Table 5.2. The physiochemical analysis was carried out using a DR 5000 Spectrophotometer (Hach, DR 5000) and an ion chromatography system (Dionex 5000). The experimental tests were carried out using flat-sheet membranes with effective areas of 0.0155 m² and 0.003847 m² for both AGMD and VMD.

Table 5-2. Chemical Analysis of Arabian Gulf Seawater

Parameter	Average Value in mg/L
TDS	43415
Ca ²⁺	798.5
Mg ²⁺	1510.5
Na ⁺	13397
(SO ₄) ²⁻	3257
(HCO ₃) ⁻	138.7
Cl ⁻	24101
K ⁺	297
NO ³⁻	3.57

Each experiment ran for 90 minutes after the system stabilised. The experiments were conducted three times, and the average value was used for the analysis. The membrane-active surface was directed towards the warm feed solution in the AGMD and VMD experiments. Electrical conductivity, TDS, salinity and temperature were manually measured with the help of electrical conductivity metres (Thermo Scientific™ Orion™ Star A322 Conductivity Portable Meter).

5.3 Results and Discussions

5.3.1 Influence of Feed Temperature

The effects of feed temperature on permeate flux in the AGMD configuration is illustrated in Figure 5.7. Figure 5.8 shows the influence of feed temperature on vapour flux in the VMD configuration. The test temperature varied from 70°C to 85°C in the AGMD experimentation. The temperature on the cold side was maintained at 5 °C. The feed used was a 7% NaCl solution. Both the flow rate of the feed and the flow rate of the coolant solution were maintained at 1.3 L/min. Deionised water was circulated on the cold side to keep the condensing plate at the required temperature.

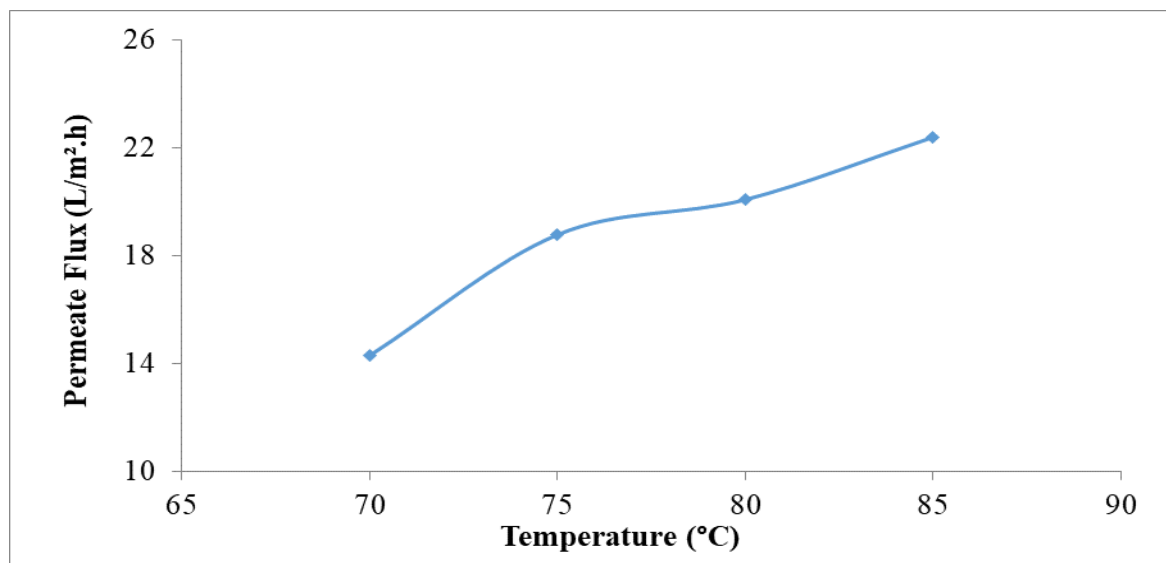


Figure 5.7. Effect of Feed Temperature on Permeate Flux in AGMD

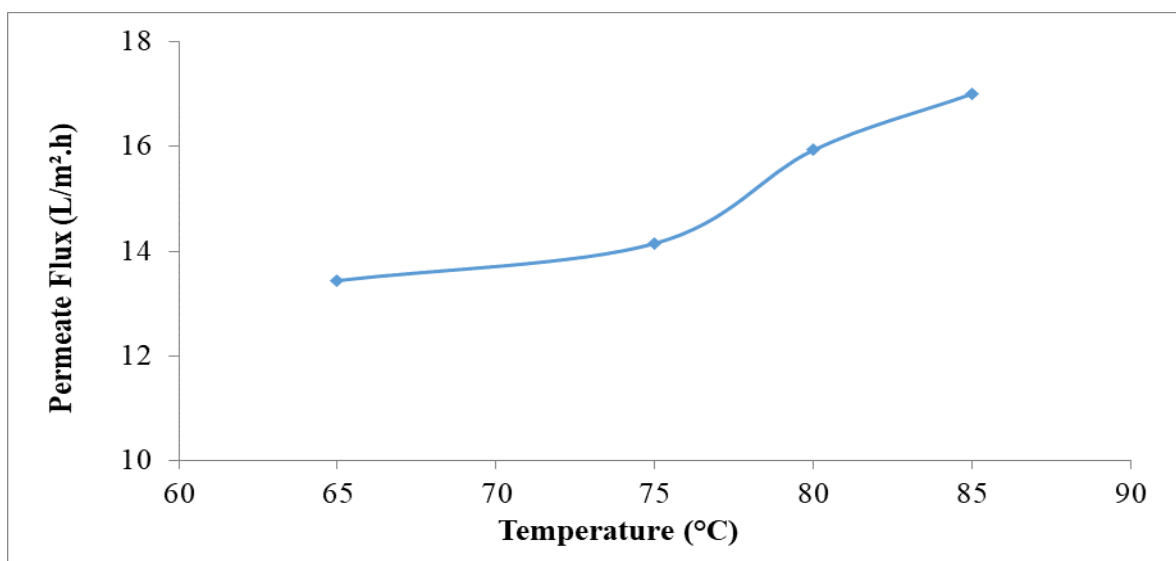


Figure 5.8. Effect of Feed Temperature on Permeate Flux in VMD

In the VMD experimentation, the feed temperatures were 65 °C, 75 °C, 80 °C and 85 °C. The feed used was a 7% NaCl solution. The vacuum pressure was kept at 100 kPa. The feed-flow rate was 1.3 L/min. In the AGMD experimentation, when the temperature was increased from 70 °C to 85 °C, the permeate flux surged from 14.3 to 22.4 L/m²h (i.e., an increase of 56.64%). In the VMD experimentation, an increase in temperature from 65 °C to 85 °C resulted in an increase in the permeate flux from 13.4 to 17.0 L/m²h (i.e., an increase of about 26.87%). A temperature increase increased the permeate flux in the AGMD and VMD configurations. This can be explained by the Antoine equation (5.1), which shows that at lower feed temperatures, the change in vapour pressure with temperature is relatively minor. However, as the feed temperature rises, the impact on vapour pressure becomes more significant, thereby increasing the permeate flux [136]. A slight increase in temperature can lead to a significant rise in vapour pressure and, as a result, an increase in the system's flux in proportion to that rise in vapour pressure. When the temperature difference between the two sides of the membrane is raised, the diffusion coefficient is positively affected, resulting in an increased vapour flux [137, 138]. Also, the temperature polarisation will decrease as the feed temperature increases [139, 140]. Since there is a direct correlation between temperature and diffusivity, the mass-transfer coefficient improves when working at higher temperatures [141].

Figure 5.9 compares permeate flux at feed temperatures in different AGMD and VMD configurations. It was observed that the permeate flux of AGMD increased more rapidly with temperature than VMD, which could be due to the enhanced driving force resulting from the temperature difference between the feed and coolant streams in AGMD. Feed temperature was observed to have a lesser effect on the salt rejection percentage in the AGMD and VMD configurations. This demonstrates that AGMD and VMD configurations using PP membranes can use high-temperature feeds to achieve high water flux while maintaining a good salt rejection percentage. In both configurations, the percentage of salt rejected was greater than 99.95%.

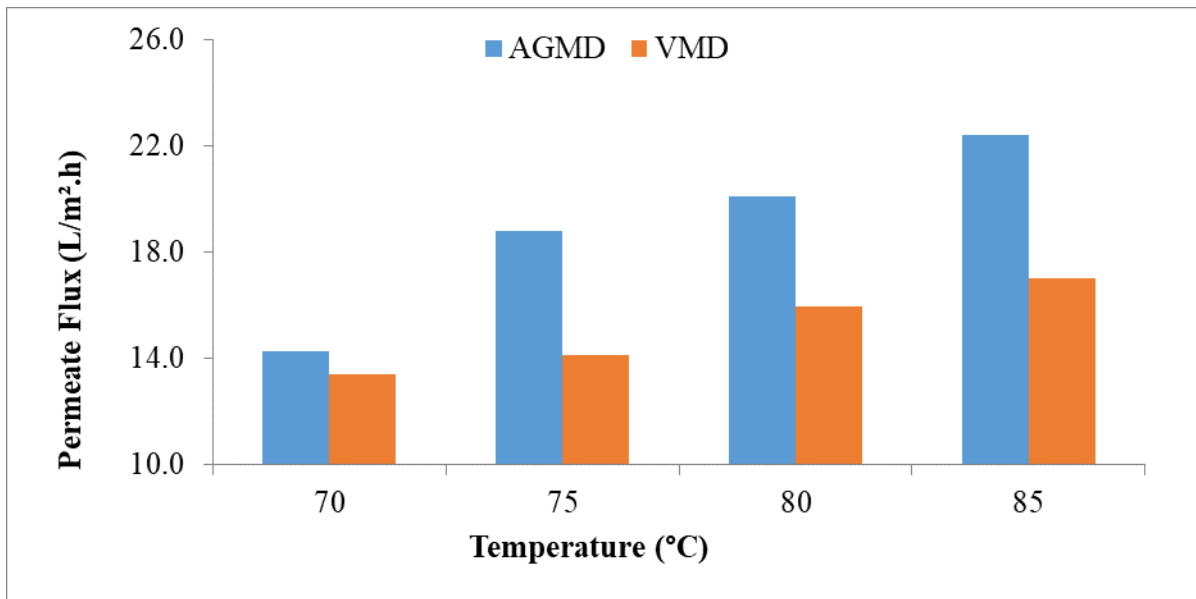


Figure 5.9. Comparison of Permeate Flux at Different Feed Temperatures in AGMD and VMD Configurations

Regarding heat transfer performance, the Nusselt numbers for both systems with changing feed temperatures are presented in Figure 5.10. The heat transfer performance through the membrane is characterized by the Nusselt (Nu) number, which represents the ratio of convective heat transfer to conductive heat transfer.

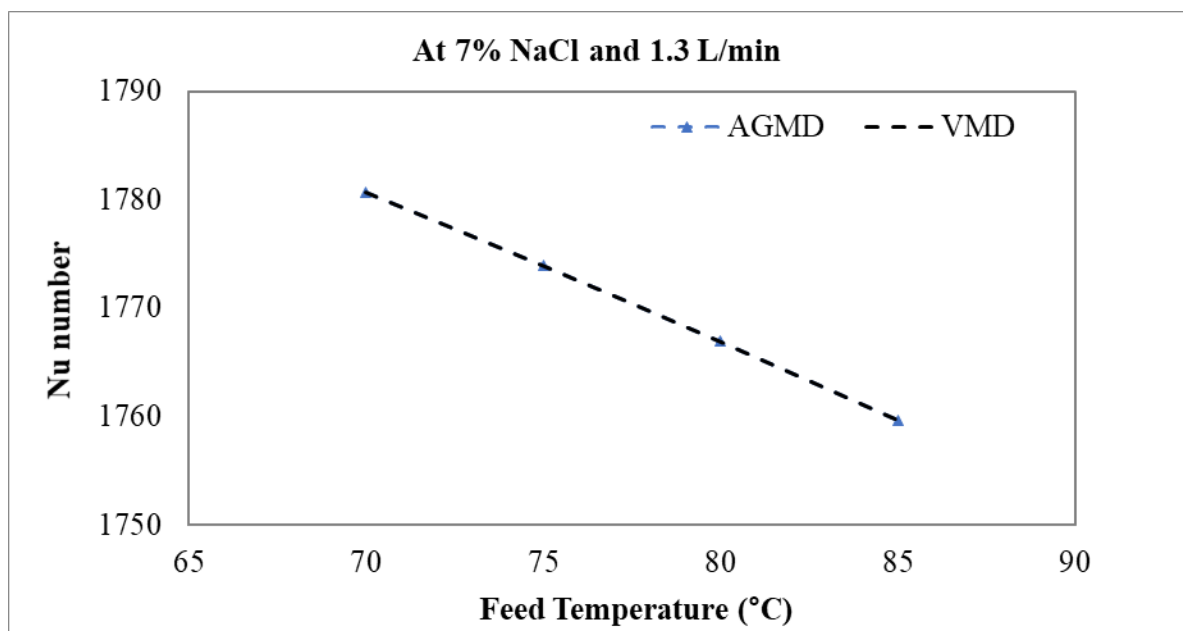


Figure 5.10. Effect of Feed Temperature on Nusselt Number in AGMD and VMD

It is well established that improving the Nu number depends on two dimensionless numbers: the Reynolds number and the Prandtl number. Since the

1.3 L/min flow rate is only considered in Figure 5.10, the Prandtl number is the only factor that can be adjusted to affect the Nu number. As the feed temperature changes, it alters the thermal properties, leading to a gradual decrease in the Prandtl number with increasing feed temperature. Consequently, at the same feed flow rate, a lower feed temperature results in a higher Nu number.

The GOR for the AGMD and VMD systems is presented in Figure 5.11. Increasing the feed temperature gradually increased the GOR for the AGMD and VMD systems. This may be due to the partial pressure difference, which led to a larger mass flux directly proportional to the gained output ratio. On the other hand, the performance of specific thermal energy consumption (STEC) over a range of inlet feed temperatures is presented in Figure 5.12. It can be deduced that the performance of GOR is the opposite of STEC; thus, a higher GOR means higher performance is produced by the flow at the higher feed temperature. This not only resulted in a higher GOR but also led to minimising the thermal energy requirements. Moreover, both systems recorded an increase in the GOR with increasing the feed temperature but with different contributions, in which the performance of GOR recorded by the AGMD was larger than that produced by VMD. The performance of STEC recorded by both MD systems also presents different contributions of increase, as presented in Figure 5.12.

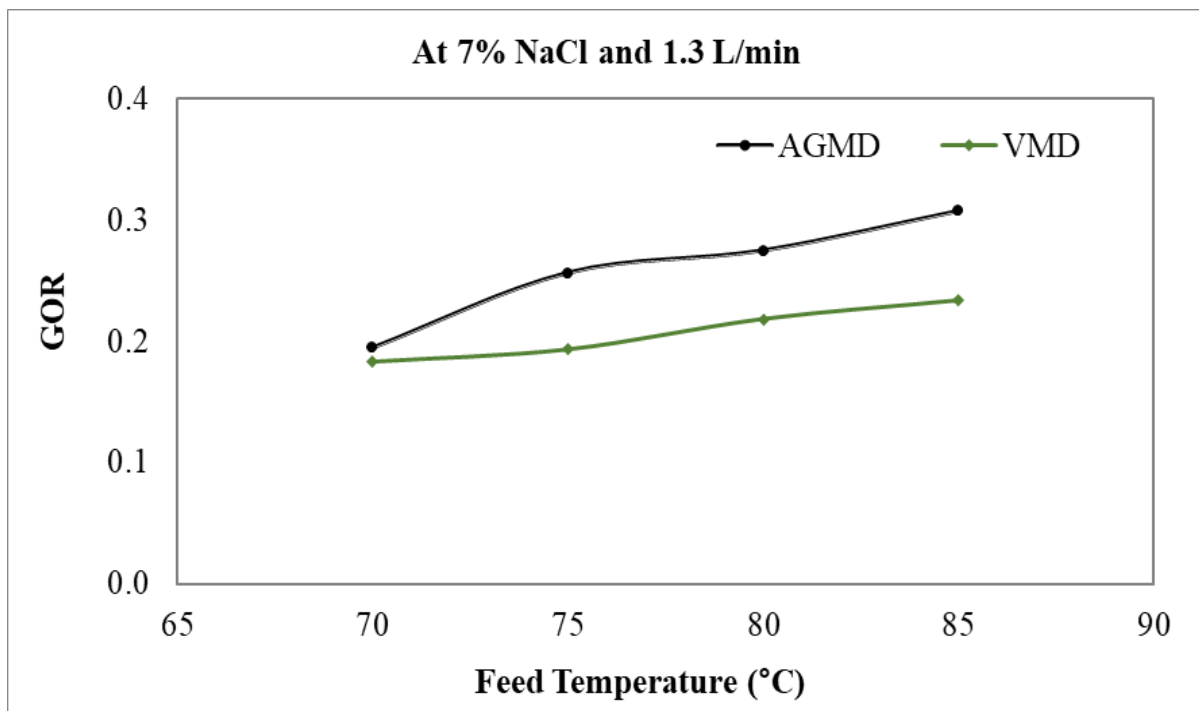


Figure 5.11. Effect of Feed Temperature on GOR in AGMD and VMD

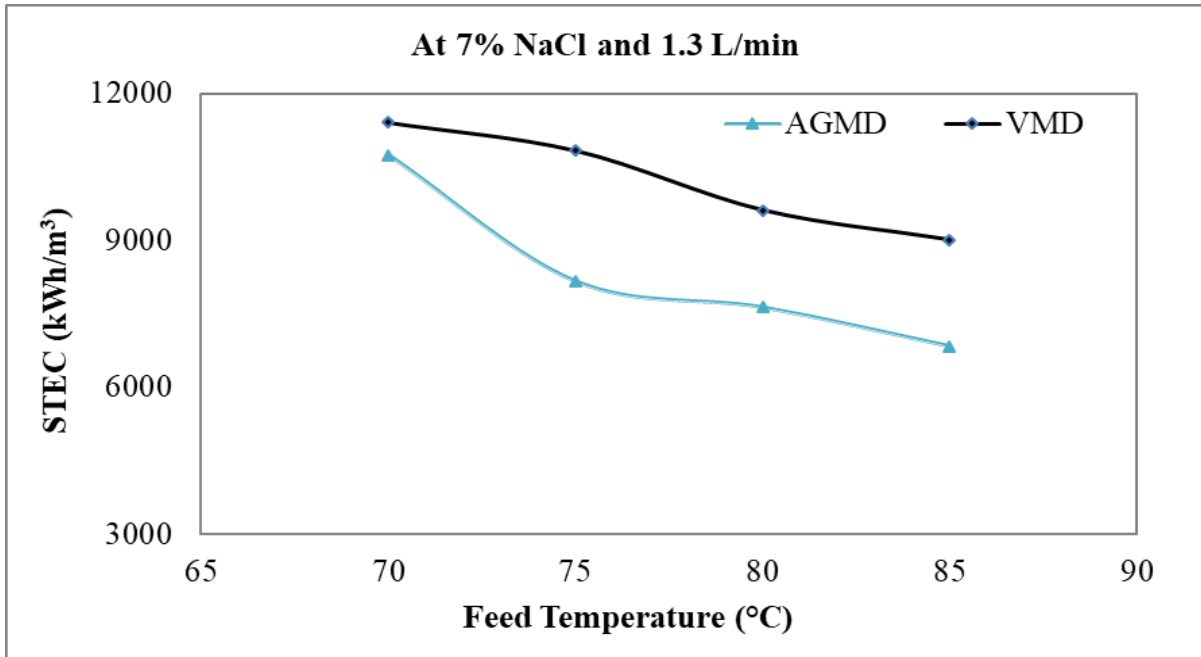


Figure 5.12. Effect of Feed Temperature on STEC in AGMD and VMD

5.3.2 Influence of Solute Concentration on Feed

Figure 5.13 illustrates the impact of the feed concentration on permeate flux in an AGMD configuration. The feed was a NaCl solution with concentrations of 3.5%, 7.0%, 15%, and 26%. AGS obtained from the DRP beach well was also utilised as feed. At the feed solution and coolant medium, the flow rate was 2L/min. The utilised membrane was polypropylene. The temperatures on the feed and coolant sides were 85°C and 5°C, respectively. On the coolant side of the AGMD module, deionised water was circulating. This study found that the permeate flux varied with feed concentration, with values of 26.35 L/m².h, 21.77 L/m².h, 19.53 L/m².h, and 13.69 L/m².h observed for feed concentrations of 3.5%, 7%, 15%, and 26% NaCl, respectively.

Figure 5.14 shows how feed concentration affects permeate flux in a VMD configuration. NaCl concentrations of 3.5%, 7.0%, 15%, and 26% were used in the feed. The flow rate of the feed solution was 2 L/min. A PP membrane was used in the experiment. The feed-side temperature was 85 °C. The vacuum pressure was maintained at 100 kPa. For the VMD configuration, this study observed that the permeate flux decreased with increasing feed concentration, with values of 21.14 L/m².h, 20.33 L/m².h, 19.41 L/m².h and 18.64 L/m².h obtained for feed concentrations of 3.5%, 7%, 15%, and 26% NaCl, respectively.

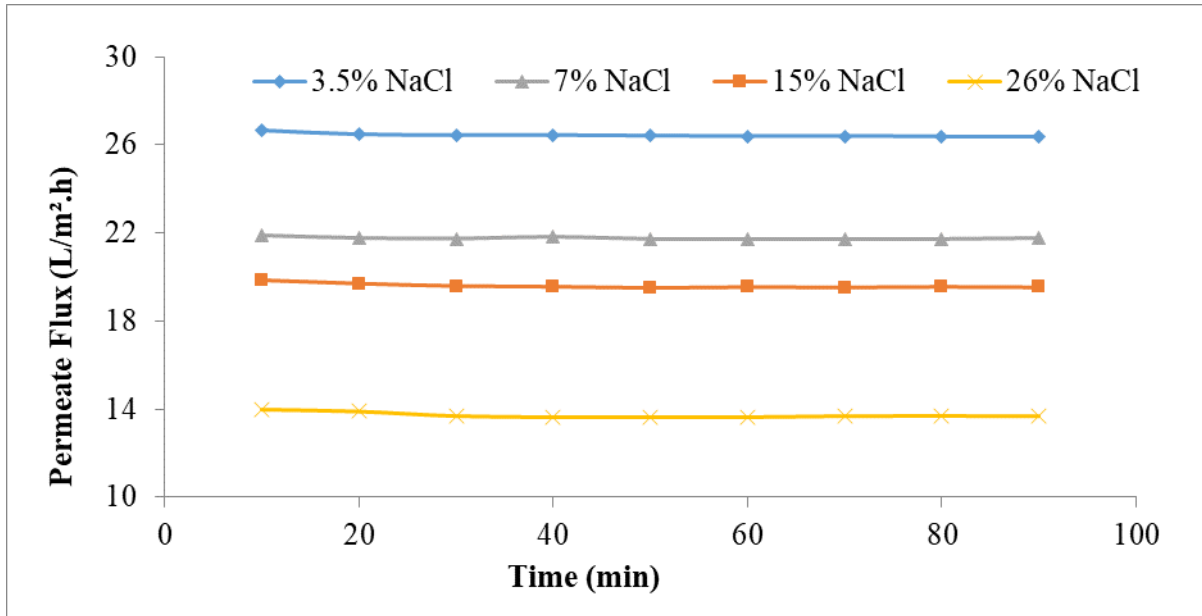


Figure 5.13. Permeate Flux Over Time at Different Feed Concentrations in AGMD

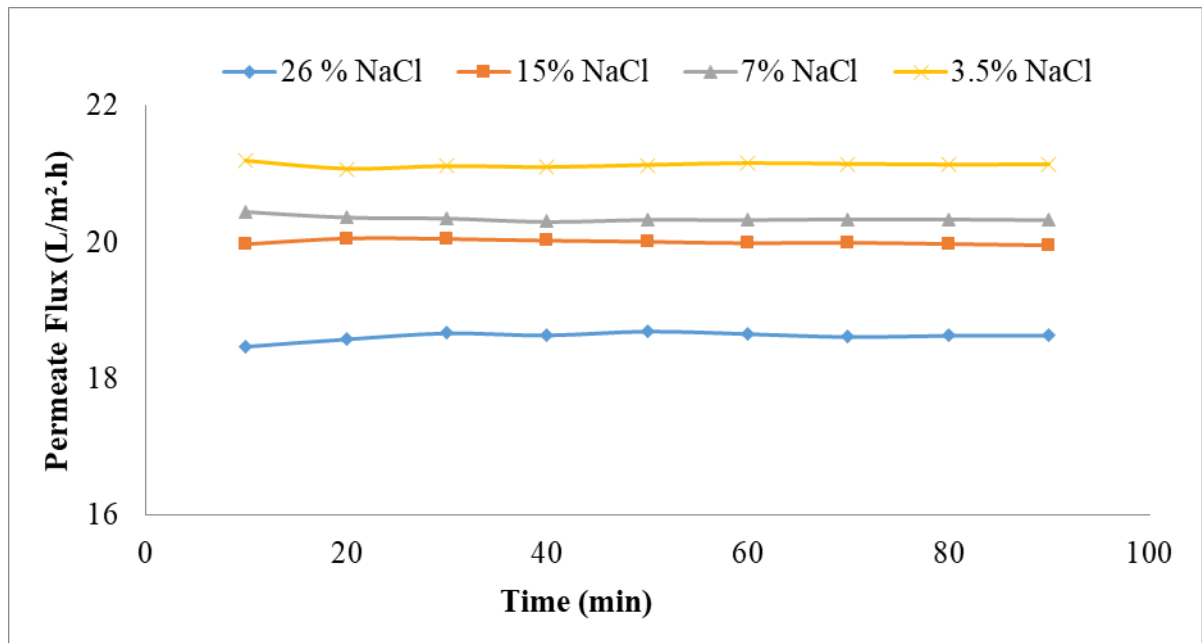


Figure 5.14. Permeate Flux Over Time at Different Feed Concentrations in VMD

Figure 5.15 compares the permeate flux in the AGMD and VMD configurations at different feed concentrations. Flux decreased with increasing feed concentration in both the AGMD and VMD configurations. This observation supports the findings reported in other publications [137,142,143].

As the NaCl feed concentration increased from 3.5% to 7%, 15%, and 26%, the AGMD configuration experienced reductions in permeate flux by 17%, 26%, and

48%, respectively. However, compared to the aforementioned AGMD configuration study results in this chapter, the reduction in flux with increased feed concentration was slightly lower in the VMD configuration. When the NaCl feed concentration was raised from 3.5% to 7%, 15%, and 26%, the permeate flux in the VMD configuration decreased by 5%, 10%, and 15%, respectively. Figure 5.15 shows that AGMD outperformed VMD at lower feed concentrations, while VMD performed well at higher feed concentrations. At higher feed concentrations, there is a chance of fouling, and pores become blocked by solute molecules. Due to the vacuum application, fouling and pore blocking might have reduced and resulted in a higher flux at higher concentrations in the VMD.

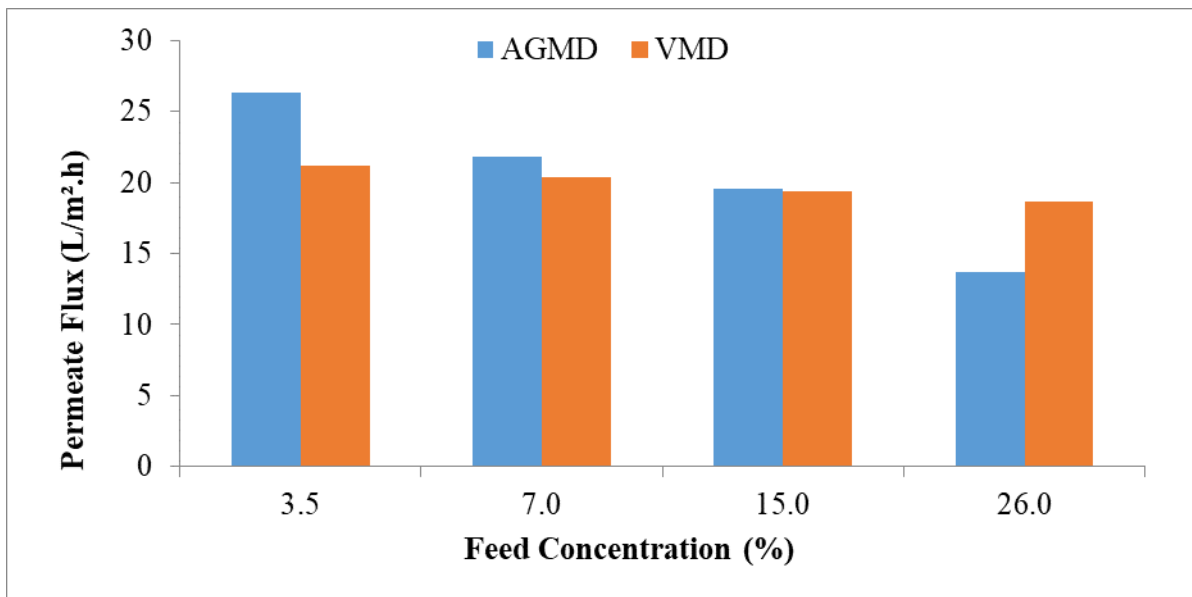


Figure 5.15. Comparison of Permeate Flux at Various Feed Concentrations in AGMD and VMD

The decrease in permeate flux with increase in feed concentration was observed with all the three MD configurations, i.e. DCMD, AGMD and VMD, as shown in Figures 4.10, 5.13 and 5.14, respectively. The decrease in flux with increasing feed concentrations could be caused by reduced water vapour pressure and rising temperature polarisation [137,142,143]. Another possible explanation for the decrease in flux is a decline in water activity as the concentration increases. Furthermore, the mass-transfer coefficient of the boundary layer at the feed side decreases due to high-concentration polarisation. Moreover, as the surface membrane temperature drops, so does the heat transfer coefficient at the boundary

layer. All of these factors reduce vapour pressure, which, in turn, reduces flux [144]. However, in contrast to other membrane desalination technologies, such as RO, where high feed salinity negatively impacts system performance, the effect of feed concentration on permeate flux in all MD configurations is less significant.

The salt rejection percentage by AGMD and VMD configurations was less affected by feed concentration. This showed that AGMD and VMD configurations are appropriate for applications with relatively high feed concentrations. The amount of salt rejected in both configurations exceeded 99.5%.

Regarding heat transfer performance, the Nusselt numbers with changing the feed concentrations are presented in Figure 5.16. Figure 5.16 shows how the Nu number increases gradually as the feed concentration of NaCl increases from 0% to 26% at a constant feed rate of 2 L/min and an inlet feed temperature of 85 °C. The reason behind the increase in Nu number with feed concentration is described in section 4.3.2.

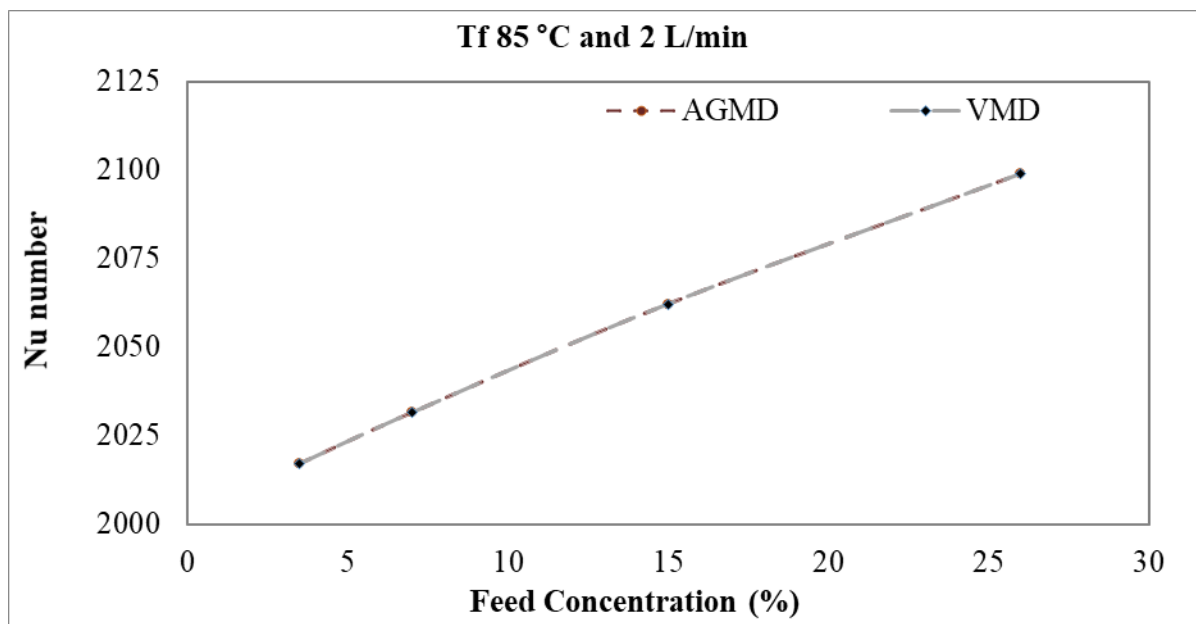


Figure 5.16. Effect of Feed Concentration on Nusselt Number in AGMD and VMD

In terms of energy performance, the GOR with changing the feed concentrations is presented in Figure 5.17. It is observed that increasing the feed concentrations led to a gradual decrease in the GOR, and is likely due to the higher permeate flux generated at lower concentrations, which is directly proportional to the GOR. However, while the GOR decreased in both MD systems (AGMD and VMD) as the feed concentration increased, the rate of reduction was different. This could be

due to the MD design, in which the AGMD system recorded a sharp reduction in the GOR through all loading of feed concentration, whereas the VMD system recorded a gradual reduction.

However, Figure 5.18 presents the performance of STEC over a range of inlet feed concentrations. A higher GOR means higher performance the flow produces at the considered higher feed temperature. Additionally, fouling or salt accumulation on the membrane surface can result in decreased flux production. The data presented indicate that higher feed concentrations and smaller GOR values lead to increased STEC.

When comparing the effect of increasing solution concentration on the GOR and STEC in DCMD, AGMD and VMD systems, the results showed that at a concentration of 26%, the order of GOR was DCMD (0.34) > VMD (0.26) > AGMD (0.188). In contrast, the order of STEC was AGMD (11197 kWh/m³) > VMD (8225 kWh/m³) > DCMD (6173 kWh/m³).

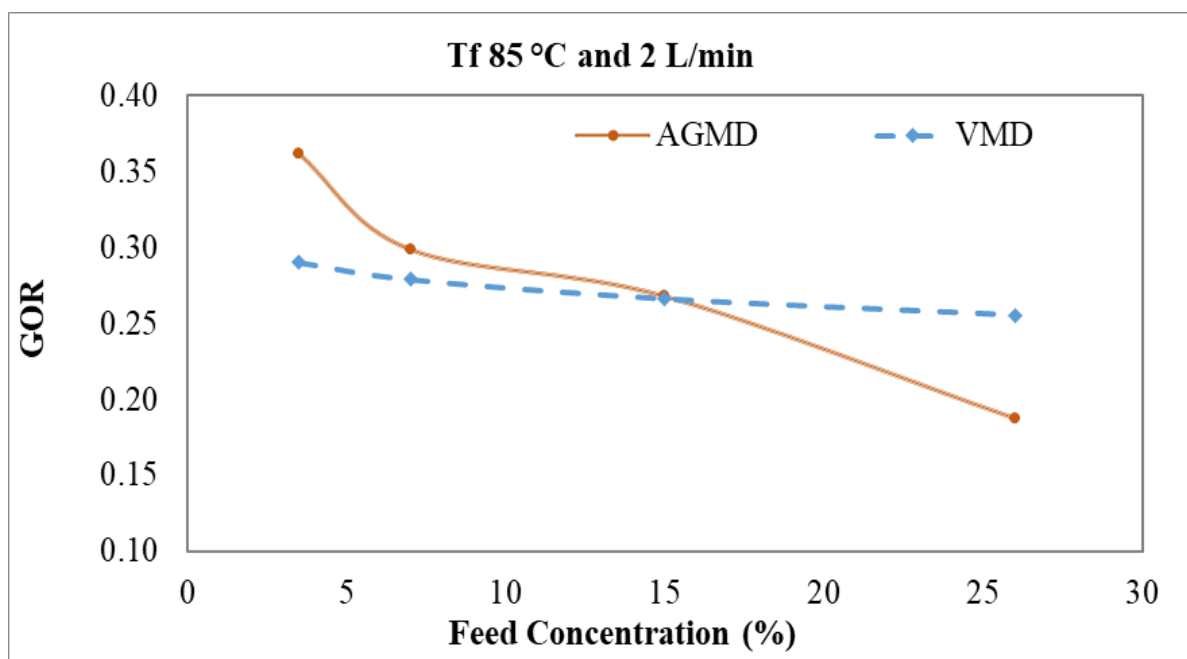


Figure 5.17. Effect of Feed Concentration on GOR in AGMD and VMD

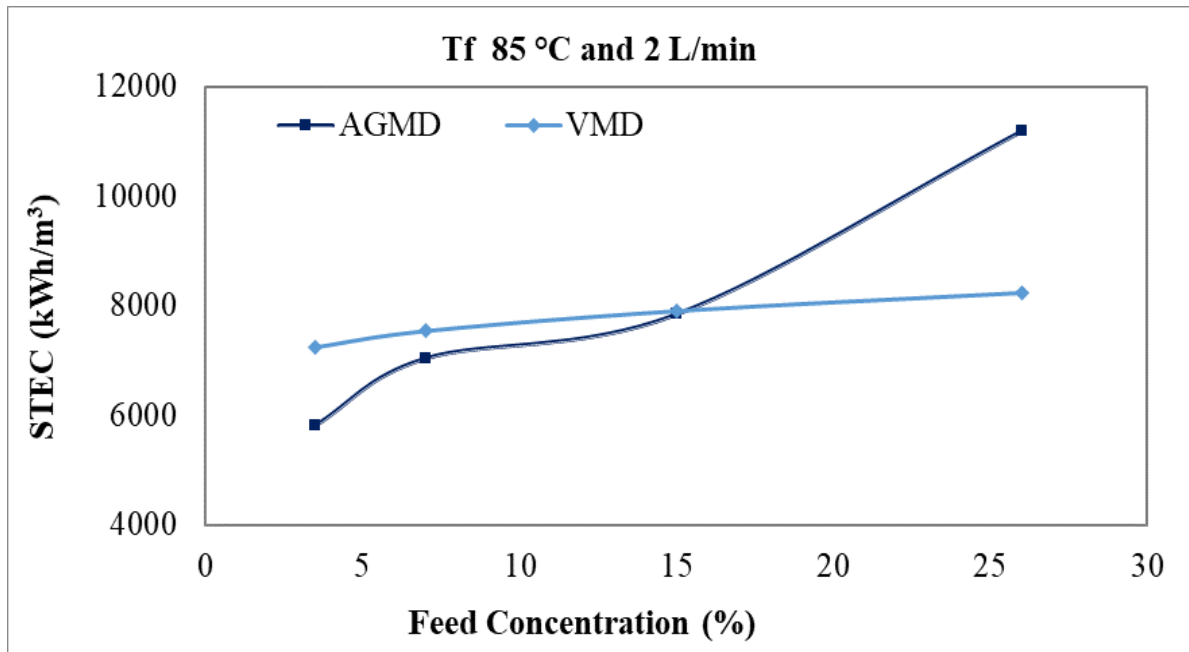


Figure 5.18. Effect of Feed Concentration on STEC in AGMD and VMD

5.3.3 Influence of Feed Flow Rate on Permeate Flux

The influence of the feed flow rate on permeate flux under conditions of constant feed temperature and constant coolant temperature using a polypropylene membrane is investigated. The impact of feed flow on the vapour permeate flux in AGMD configuration is depicted in Figure 5.19, while Figure 5.20 illustrates the effect of feed flow on vapour permeate flux in the VMD setup. The tests were conducted using a 7% NaCl solution as the feed. The temperatures of the feed and coolant sides were 85 °C and 5 °C, respectively. The feed flow rate varied from 1.3 to 2.0 litres per minute. The vacuum pressure was kept constant at 100 kPa in the VMD configuration. As presented in Figures 5.19 and 5.20, permeate flux increased as the flow rate increased.

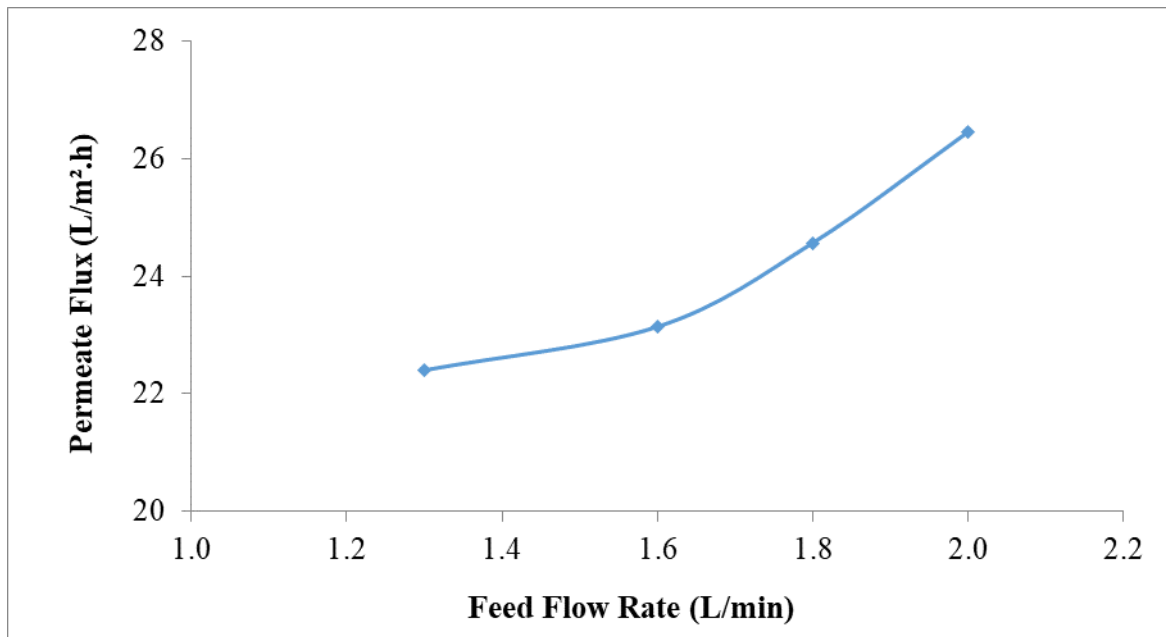


Figure 5.19. Effect of Feed Flow Rate on Permeate Flux in AGMD

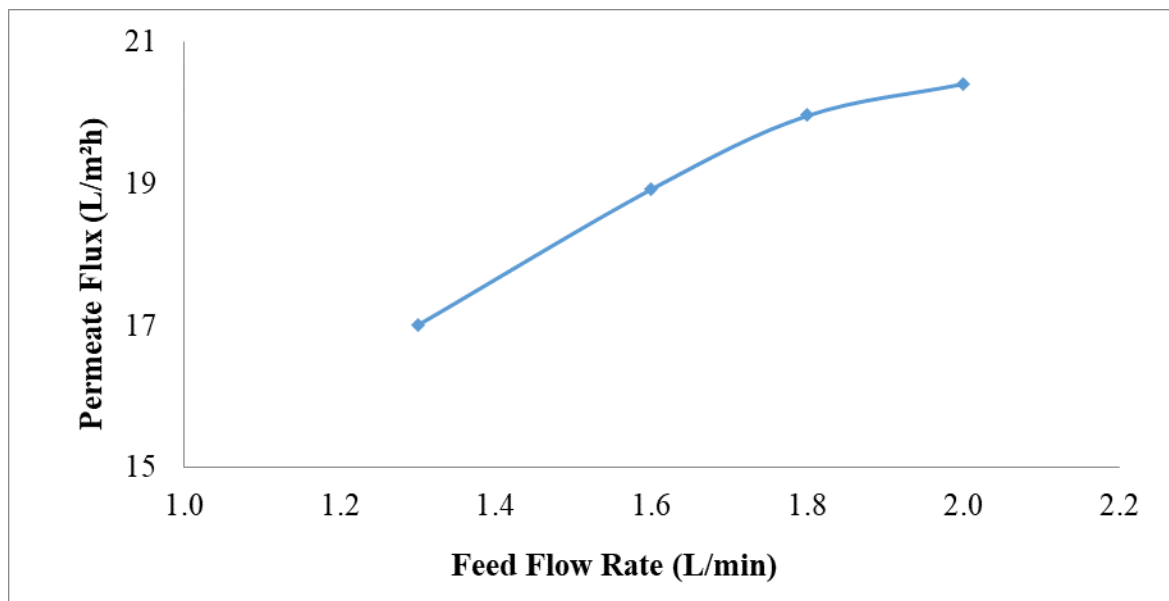


Figure 5.20. Effect of Feed Flow Rate on Permeate Flux in VMD

Figures 4.14, 5.19, and 5.20 illustrate similar trends across different types of membrane distillation processes: DCMD, AGMD, and VMD, respectively. Increasing the flow rate enhances water flux by reducing the temperature gradient between the membrane surface and the solutions, which boosts vapour pressure and mass transfer. This effect is consistent across the different types of membrane distillation, with turbulence promoting permeate flux. Furthermore, fluid residence time in a channel decreases with higher flow rates, leading to less effective heat transfer and

accelerated vaporization. Studies have suggested that a higher flow velocity improves flux by reducing temperature and concentration polarisation in feed and coolant channels through improved mixing [145,146]. Srisurichan et al. [141] reported that operating with a high feed flow rate reduces boundary layer resistance and increases the heat transfer coefficient, leading to a higher flux. According to Chen et al. [145] increasing the volumetric flow rate increases fluid velocity, improving the convective heat transfer coefficient and reducing the temperature polarisation effect. This reduction in the temperature polarisation effect enhances the permeate flux. For the specific conditions in this study, increasing the flow velocity from 1.3 litres per minute to 2.0 litres per minute (i.e., 1.5-fold increases) led to a 1.2-fold increase in flux in the AGMD and VMD configurations. In the AGMD configuration, a rise of 18.1% (i.e., from 22.39 L/min.to 26.45 L/min) in the permeate flux was seen when the feed flow rate increased from 1.3 to 2.0 litres per minute, whereas the permeate flux increase rate was 19.9% (i.e., from 17.02 L/min.to 20.41 L/min) in the VMD configuration. In the AGMD and VMD configurations, the salt rejection percentage was close to 99.9% and was largely unaffected by the feed flow rate.

Figure 5.21 compares the permeate flux in the AGMD and VMD configurations at different feed flow rates. In AGMD, the flux increased from 22.4 to 26.4 L/m²h, which is approximately a 1.2-fold increase. In VMD, the flux increased from 17 to 20 L/m²h, which is approximately a 1.2-fold increase as well. This means that the rate of increase in permeate flux with flow rate was indeed nearly the same for both configurations. The permeate flux was not highly sensitive to an increase in flow rate, which may be because the main resistance of AGMD and VMD is located in the gap on the coolant side of the configurations, and there is less temperature polarisation effect compared to other MD configurations, such as DCMD.

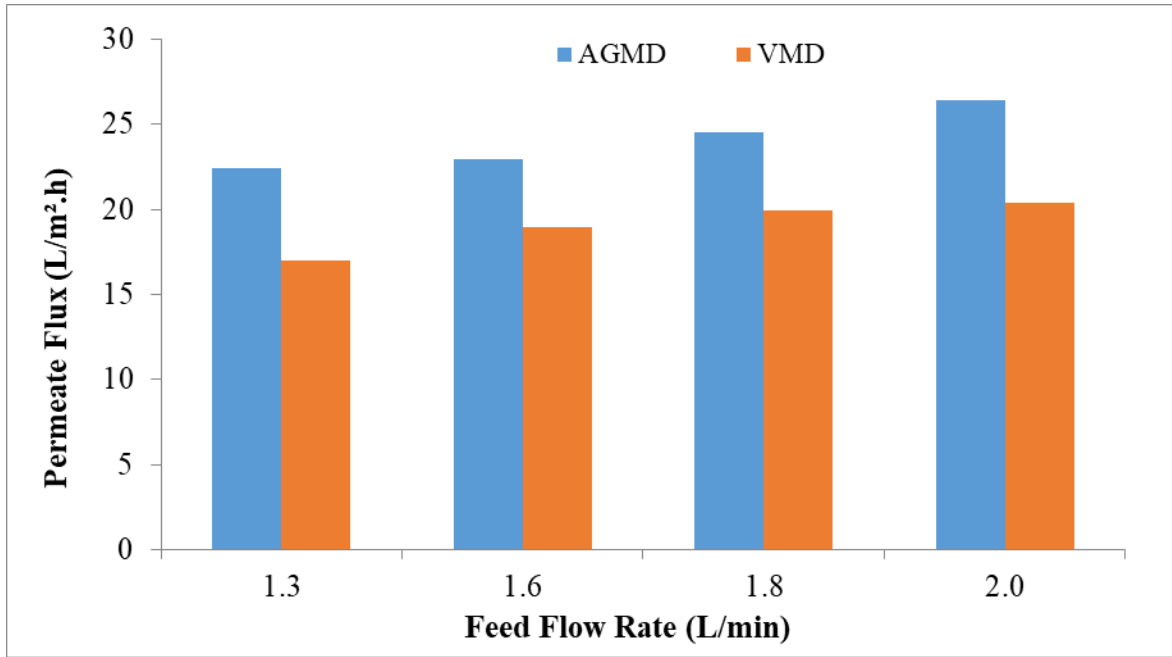


Figure 5.21. Comparison of Permeate Flux at Various Feed Flow Rates in AGMD and VMD

Regarding heat transfer performance, the Nusselt number with changing flow rate is presented in Figure 5.22 for both systems VMD and AGMD at 7% NaCl concentration and 85 °C inlet feed temperature.

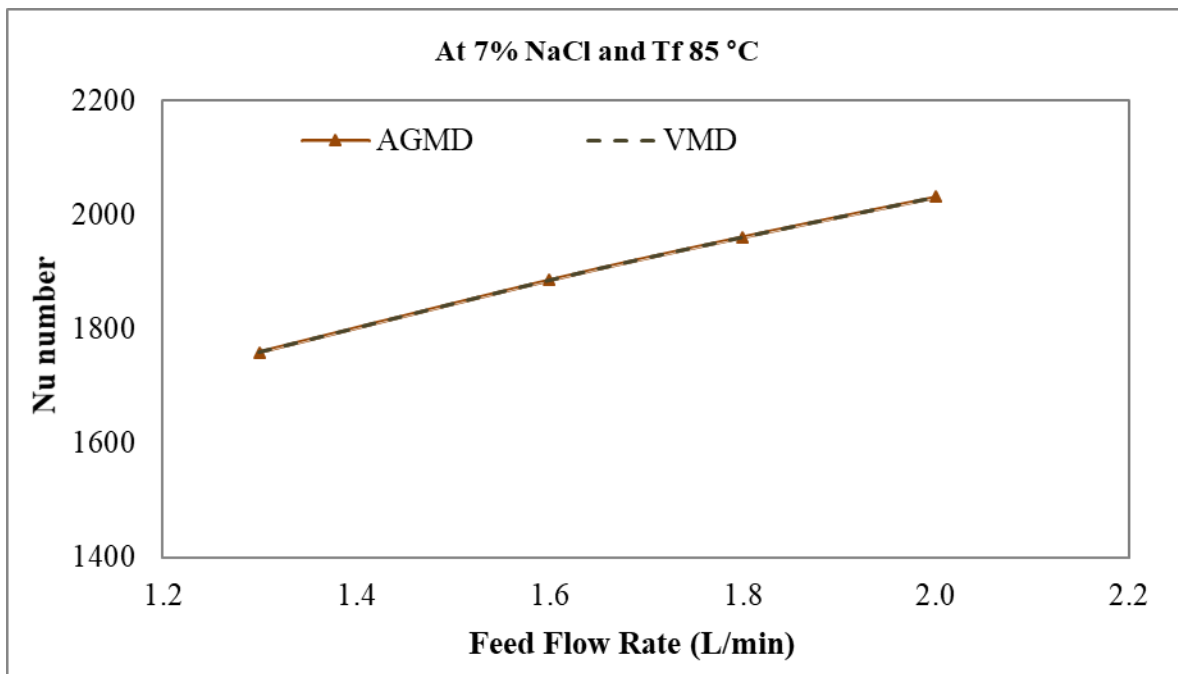


Figure 5.22. Effect of Feed Flow Rate on Nusselt Number in AGMD and VMD

The Nusselt (Nu) number, which measures convection relative to conduction heat transfer through the membrane, is influenced by the Reynolds and Prandtl numbers. In Figure 5.22, with a constant inlet feed temperature, only the Reynolds number affects the Nu number. As the feed-flow rate increases, the inertia forces changes, leading to faster flow. Therefore, at the same feed inlet temperature and concentration, a lower feed-flow rate results in a smaller Nu number.

The GOR of the considered flow at a range of flow rates is presented in Figure 5.23. As can be seen, increasing the feed-flow rate acted at a gradual increase in the GOR. This indicates that as the flow rates increased, the permeate flux also increased accordingly. However, the performance of both MD systems is different in terms of the enhancement level in which the AGMD system recorded the larger increase in the value of GOR compared with that recorded by the VMD system. On the other hand, the performance of STEC over a range of inlet feed-flow rates is presented in Figure 5.24. It can be deduced that a higher GOR means higher performance produced by the flow at the considered higher feed temperature. This not only resulted in a higher GOR but also led to minimising the thermal energy requirements. Moreover, the STEC's reduction level differs from each system, in which the AGMD recorded a larger reduction than the VMD system.

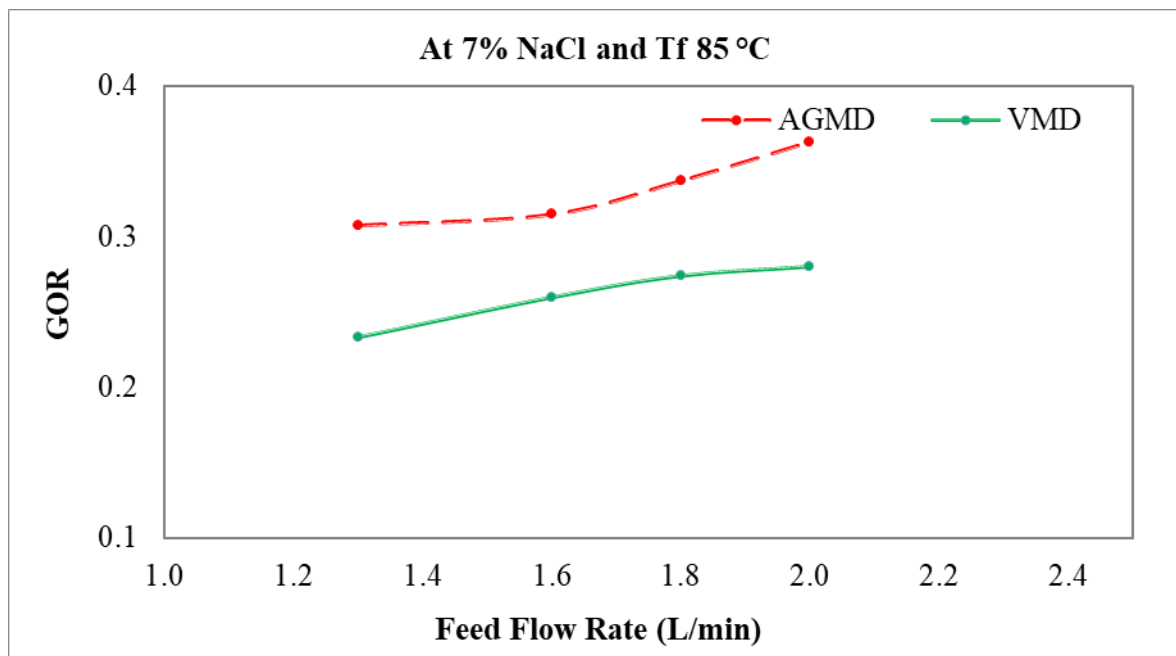


Figure 5.23. Effect of Feed Flow Rate on GOR in AGMD and VMD

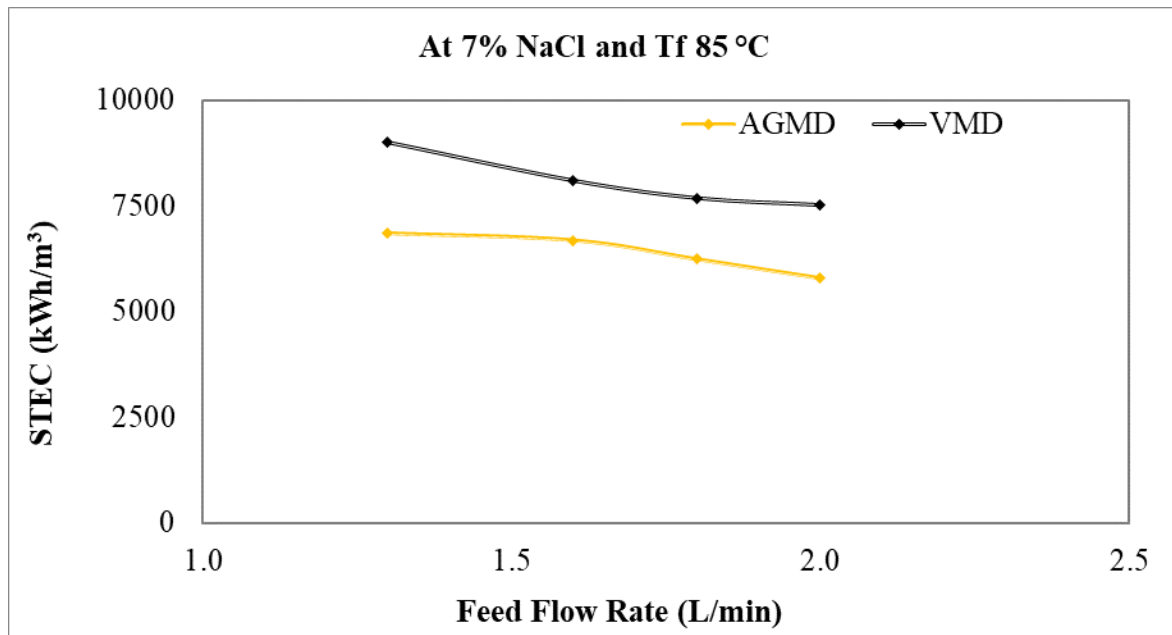


Figure 5.24. Effect of Feed Flow Rate on STEC in AGMD and VMD

5.3.4 Influence of Air Gap Depth and Vacuum Space on Permeate Flux

In the AGMD configuration, the initial set of experiments was carried out by varying the air gap depth (i.e., from 2–8 mm) while maintaining the hot-channel depth constant at 2 mm. Plates of one mm thickness were added to obtain the desired air gap between the membrane and the condensing plate. The next stage of AGMD experimentation includes experiments at a constant air gap (8 mm) and different feed-channel depths (2–8 mm). In the VMD configuration, in the initial phase of experimentation, the depth of the vacuum space varied from 2 mm to 8 mm by adjusting the number of plates added between the membrane and the cold trap while keeping the depth of the feed channel constant at 2 mm.

The next stage of the VMD experimentation was performed at a constant vacuum space depth (8 mm) but with varying depths of the feed channel from 1 mm to 8 mm. In both configurations, the membrane tested was a polypropylene membrane. The feed solution was a 7% NaCl solution at 85 °C, and the coolant used in the AGMD configuration was deionised water at 5 °C, both flowing at a rate of 2 L/min. Figure 5.25 shows the relationship between permeate flux and air gap depth in the AGMD configuration. It was observed that the percentage of permeate flux decrease was 16% when the air gap depth was increased to 8 mm from 2 mm. Figure 5.26 shows the relationship between permeate flux and hot-channel depth in

the AGMD configuration. It was observed that the percentage of permeate flux decrease was 34.6% when the hot-channel depth was increased to 8 mm from 1 mm.

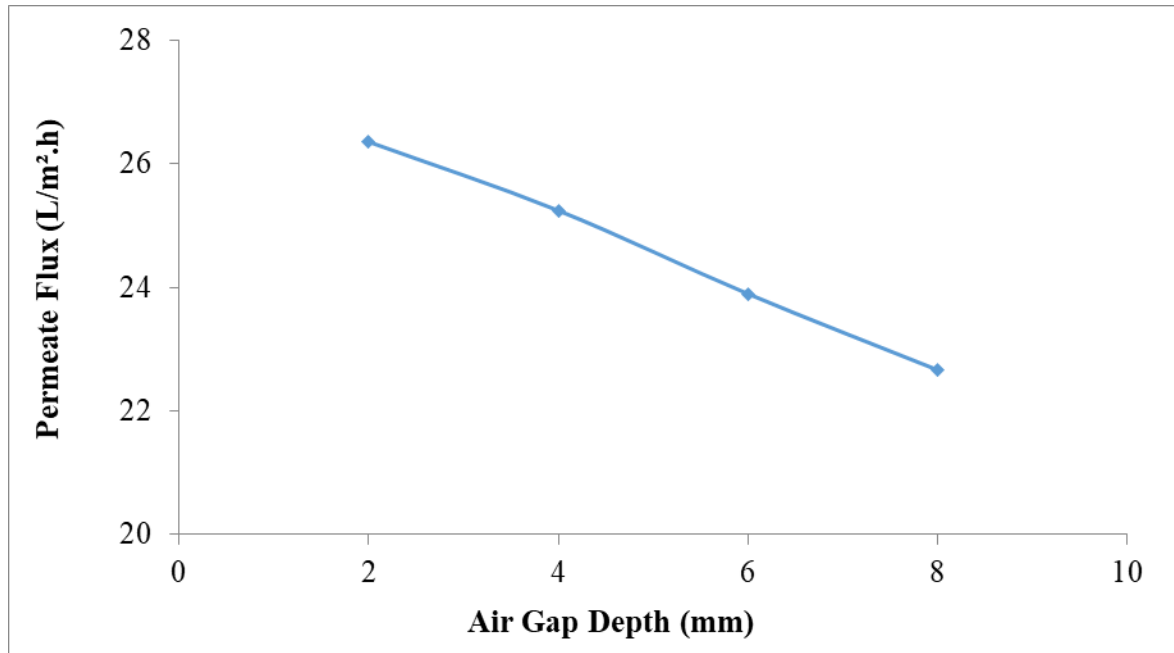


Figure 5.25. Effect of Air Gap Depth on Permeate Flux in AGMD Configuration at Constant Hot-Channel Depth

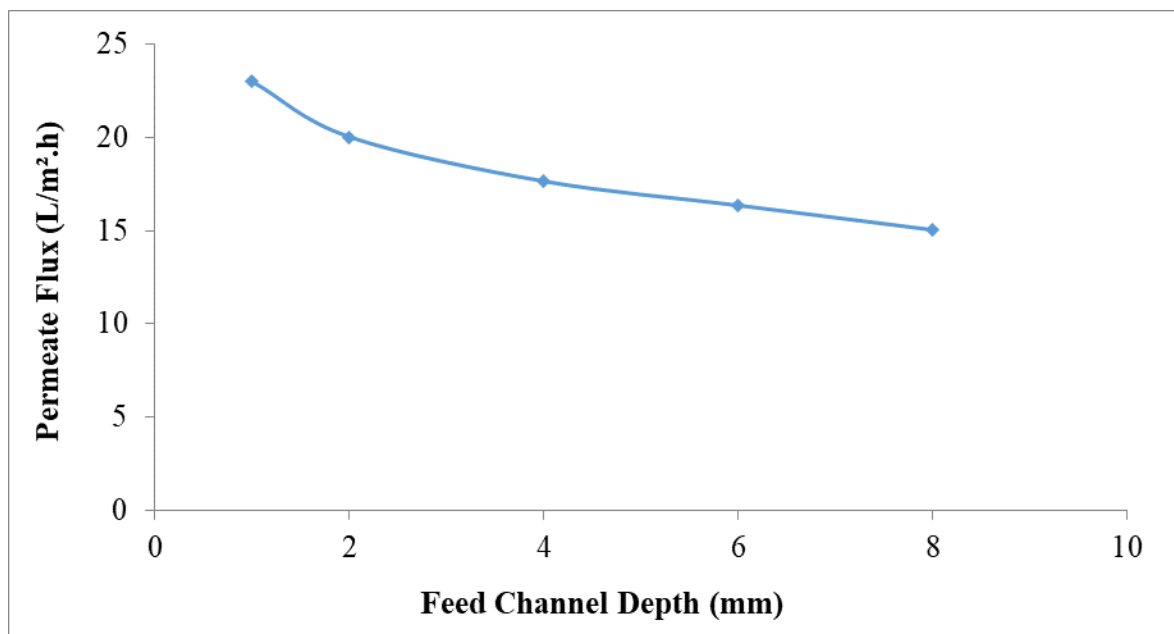


Figure 5.26. Effect of Feed-Channel Depth on Permeate Flux in AGMD Configuration at Constant Cold-Channel Depth

Banat and Simandl [130] found that reducing the width of the gap leads to a rise in the temperature gradient and, as a result, an increase in the permeate flux. Reducing channel depth may lead to a higher concentration of thermal energy within a smaller space. Accordingly, the temperature distribution will be almost uniform within the space. Upon increasing the gap width, there may be a non-uniform temperature distribution within the space. The temperature gradient between the feed and cold channels might have been higher at lower channel depths, which could have produced more flux.

Figure 5.27 shows the VMD configuration's relationship between permeate flux and vacuum space. It was observed that the percentage of permeate flux increase was 28% when the vacuum space depth was increased to 8 mm from 2 mm. Figure 5.28 shows the VMD configuration's relationship between permeate flux and hot-channel depth. It was observed that the percentage of permeate flux increase was 15.5% when the hot-channel depth was increased to 8 mm from 2 mm. Increasing the hot channel depth allows for a larger volume of hot feed solution, which increases the surface area for heat exchange and better maintains the temperature difference across the membrane. This larger temperature gradient promotes more efficient vaporization, leading to a 15.5% increase in permeate flux. It can be observed that the AGMD and VMD systems' responses to channel depth and variation studies were different.

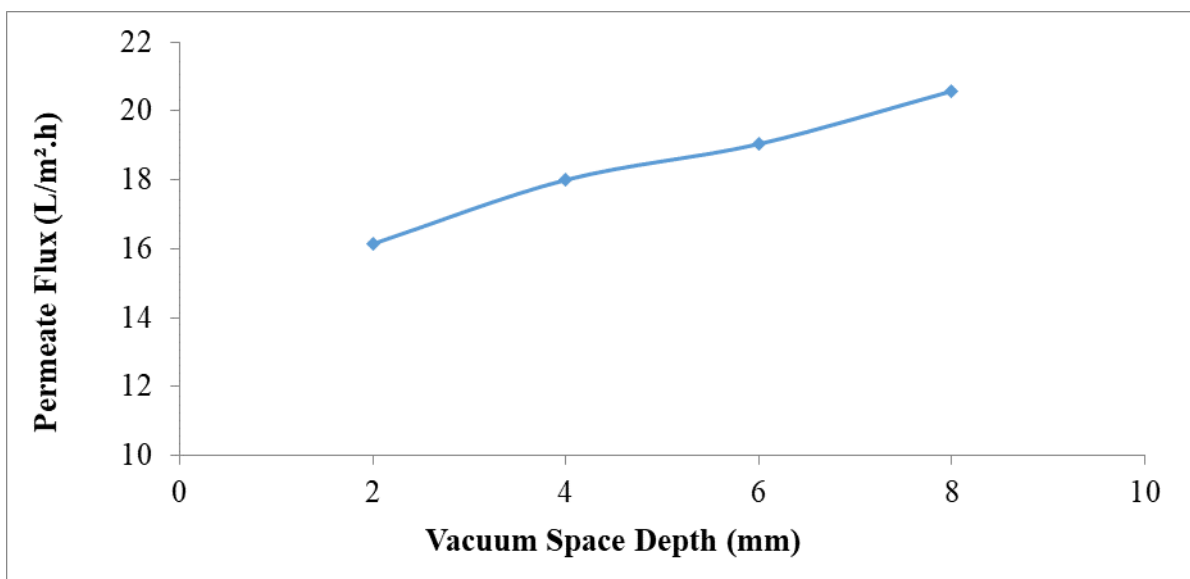


Figure 5.27. Effect of Vacuum Space Depth on Permeate Flux in VMD Configuration at Constant Feed-Channel Depth

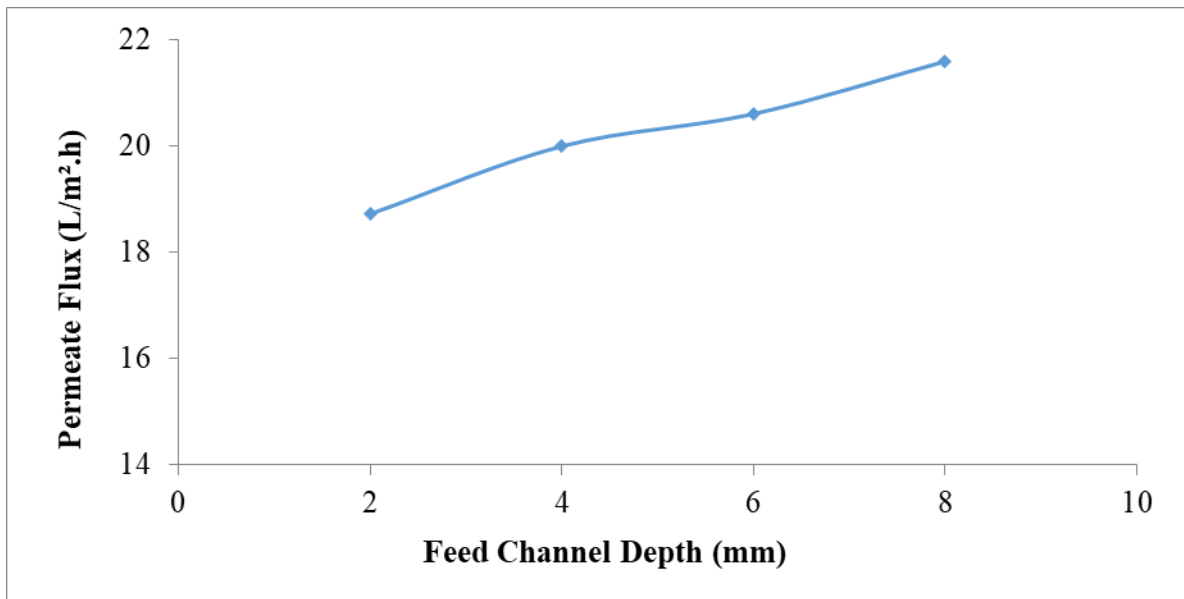


Figure 5.28. Effect of Feed-Channel Depth on Permeate Flux in VMD Configuration at Constant Vacuum Space

In the AGMD configuration, permeate flux decreased with an increase in feed channel and air gap depths, whereas an increase in permeate flux with feed channel and vacuum space depths was observed in the VMD experiments. In the VMD configuration, increasing the vacuum space depth enhances permeate flux because the increased vacuum creates a larger pressure gradient across the membrane, which drives more vapour through the membrane. As a result, increasing the vacuum space depth from 2 mm to 8 mm leads to a 28% increase in permeate flux. Increasing the vacuum space led to increased permeate flux, with a nonlinear relationship between the two. Specifically, when the vacuum space was increased four times, the resulting increase in flux was only 1.3 times. This nonlinear relationship could be due to several factors, including limitations in mass transfer or heat transfer across the membrane surface, saturation of the driving force for mass transfer, or potential changes in the properties of the membrane or feed solution at high vacuum levels.

The observed higher flux at lower air gaps in AGMD suggests that smaller air gaps are preferable in AGMD configurations. However, since increasing the vacuum space significantly enhances permeate flux in VMD, larger vacuum space can be considered more beneficial in VMD configurations. The higher flux at lower gaps in the AGMD could be attributed to the reduced effects of the heat and mass-transfer mechanisms at smaller gaps. At smaller gaps, there is less distance for heat and

mass transfer to occur, leading to a potential decrease in temperature polarisation and concentration polarisation effects. This could result in higher flux rates. However, it is important to note that the specific mechanisms underlying this behaviour may vary depending on the experimental setup and conditions, and further studies are needed to understand the observed behaviour fully.

Changing the channel depth changed the performance of the produced flux in both cases. In more detail, increasing the channel depth in the AGMD system increased the resistance of producing water flux. This resistance refers to the fact that a deeper channel can reduce the efficiency of the heat and mass transfer processes that are crucial for generating water flux. Thus, the STEC increased gradually, reaching the maximum value at 8 mm for cold and hot channels, as shown in Figure 5.29a. On the other hand, the performance of AGMD reflects the opposite behaviour with the GOR parameter in which the GOR has decreased gradually with increasing channel depth, reaching the minimum value at the maximum channel depth for both hot and cold channels, as presented in Figure 5.29b. However, a significant difference was observed between the performance of STEC and GOR produced by the hot and cold channels. In this system, it is well known that increasing the channel depth decreases the produced water flux and that more energy can be consumed, thus leading to an increase in specific energy consumption. Increasing energy consumption leads to increased energy losses; thus, a smaller amount of permeate flux can be gained. Therefore, the GOR decreased as the channel depth increased.

Compared to the AGMD system, the performance of the VMD system behaved in the opposite direction, as increasing the channel depth acted at producing a higher amount of produced flux since increasing the channel depth in this system does not form a resistance to prevent the water flux from becoming condensate; thus, more production of flux has been supplied. In this system, conductive heat loss through the membrane is neglected. Moreover, in the VMD system, the permeate part is under vacuum conditions, which prevents boundary layer deformation on this part. Therefore, a significant gain in the heat ratio is achieved by increasing the channel depth, and a significant reduction in energy consumption is presented by increasing the channel depth, as presented in Figure 5.30.

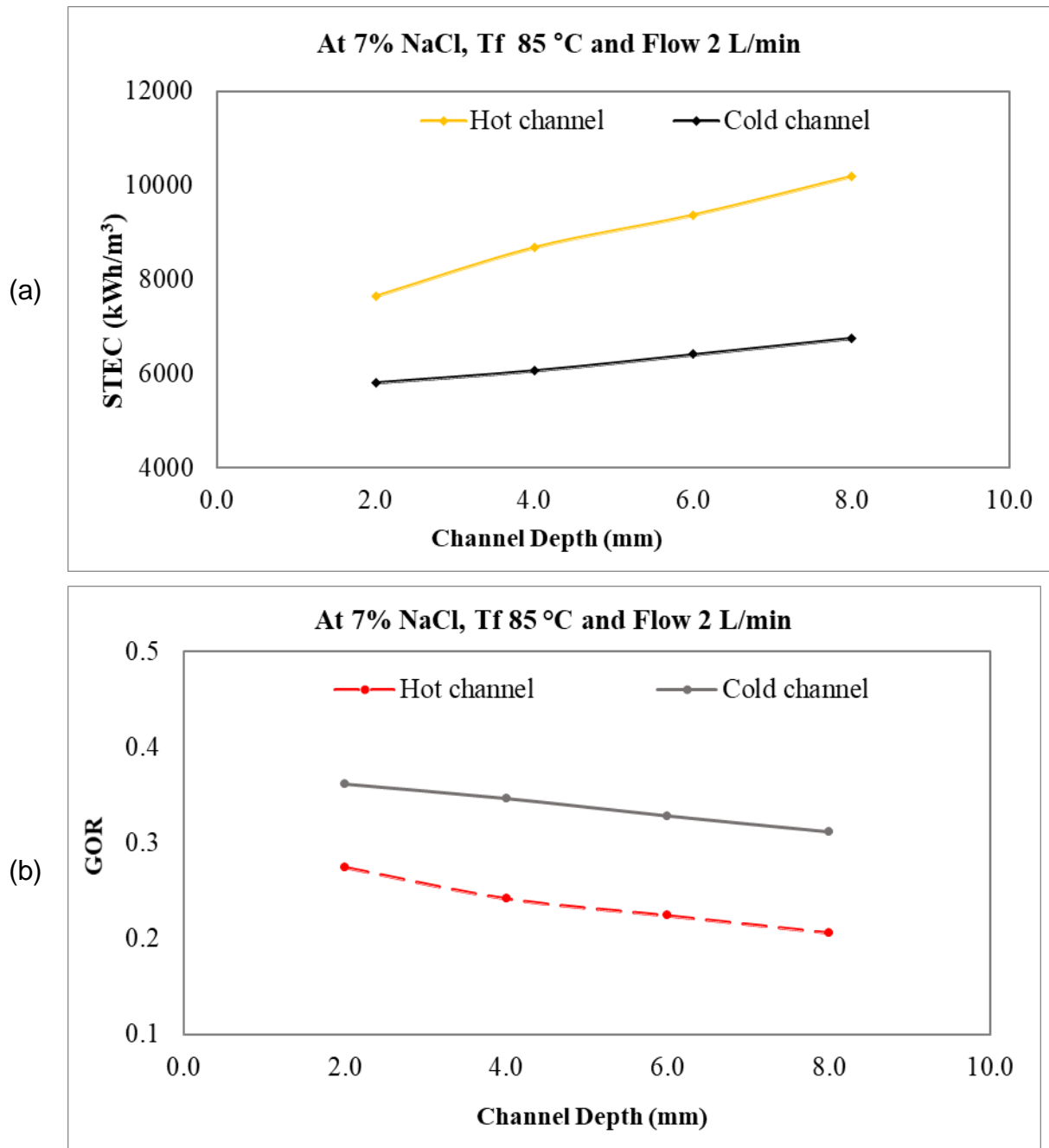


Figure 5.29. Effect of Channel Depth on (a) STEC and (b) GOR in AGMD

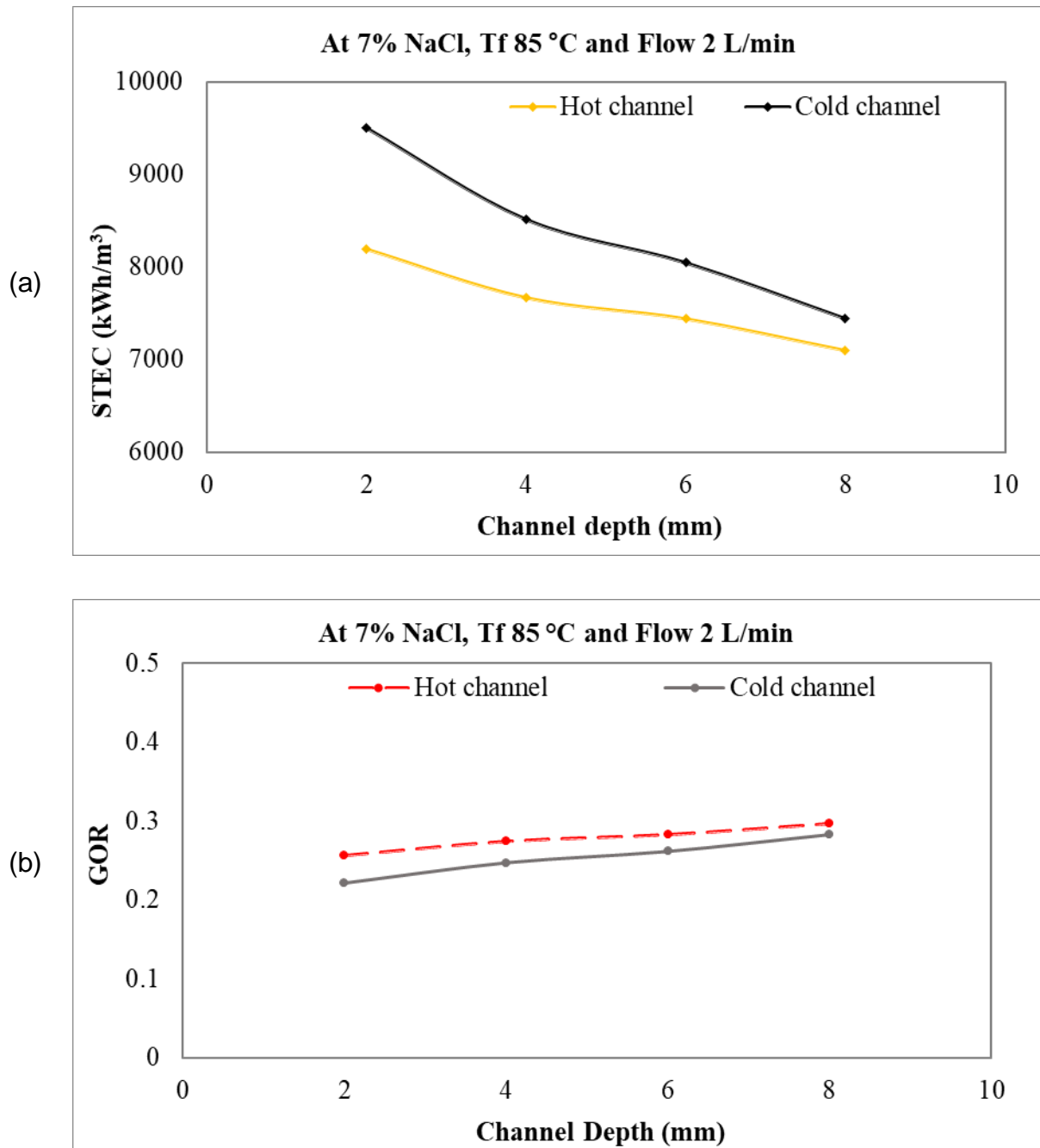


Figure 5.30. Effect of Channel Depth on (a) STEC and (b) GOR in VMD

5.3.5 Performance of AGMD and VMD Processes for Treating Oilfield-produced Water and AGS

The feasibility of using AGMD and VMD to treat oilfield-produced water using water directly as feed without pre-treatment is also investigated. In the AGMD process, deionised water was used as the cooling medium, with a feed temperature of 85 °C. The VMD experimentation was conducted at 80 °C and 85 °C feed temperatures. The cooling side temperature was 5 °C for the AGMD and VMD

processes. The feed and cooling solution channels were operated at a flow rate of 2 L/min. The AGMD experimentation was carried out with an air gap depth of 8 mm, while the VMD experimentation was conducted with a vacuum space of 8 mm. The experiment was performed using a polypropylene membrane. The permeate flux obtained was 15 L/m².h in the AGMD experiment at 85°C. Figure 5.31 shows the permeate flux obtained from VMD experimentation using oilfield-produced water as feed at 80 °C and 85 °C. It was observed that there is an increase in permeate flux with temperature. The permeate flux was 23 L/m².h and 21.35 L/m².h at 85 °C and 80 °C, respectively. The experiment's results show that AGMD and VMD processes were highly efficient in treating oilfield-produced water. Figure 5.32 shows the permeate flux obtained from the AGMD and VMD experiments using AGS obtained from beach wells and feed at 85 °C. Based on the experimental results shown in Figure 5.32, VMD exhibited a higher permeate flux of 18 L/m²h compared to AGMD's permeate flux of 15.1 L/m²h, indicating that VMD is a more effective process for treating AGS obtained from a beach well at 85°C. Therefore, these findings suggest that VMD may be a preferable process for seawater desalination compared to AGMD.

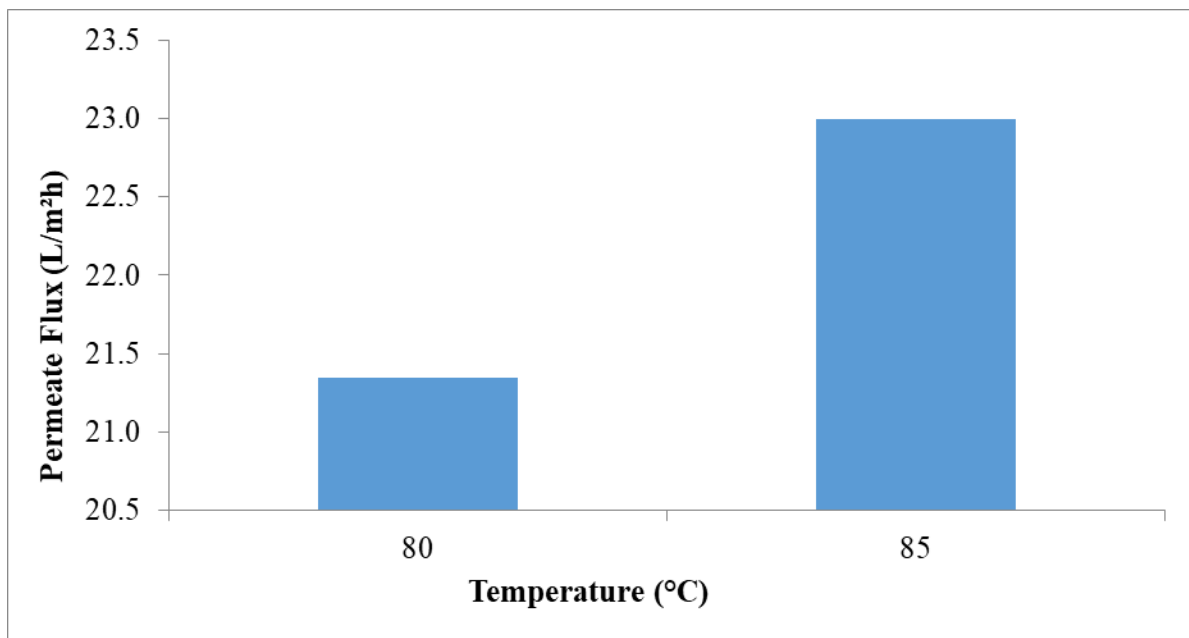


Figure 5.31. Permeate Flux in VMD Experimentation Using Oilfield-Produced Water as Feed at 80°C and 85°C

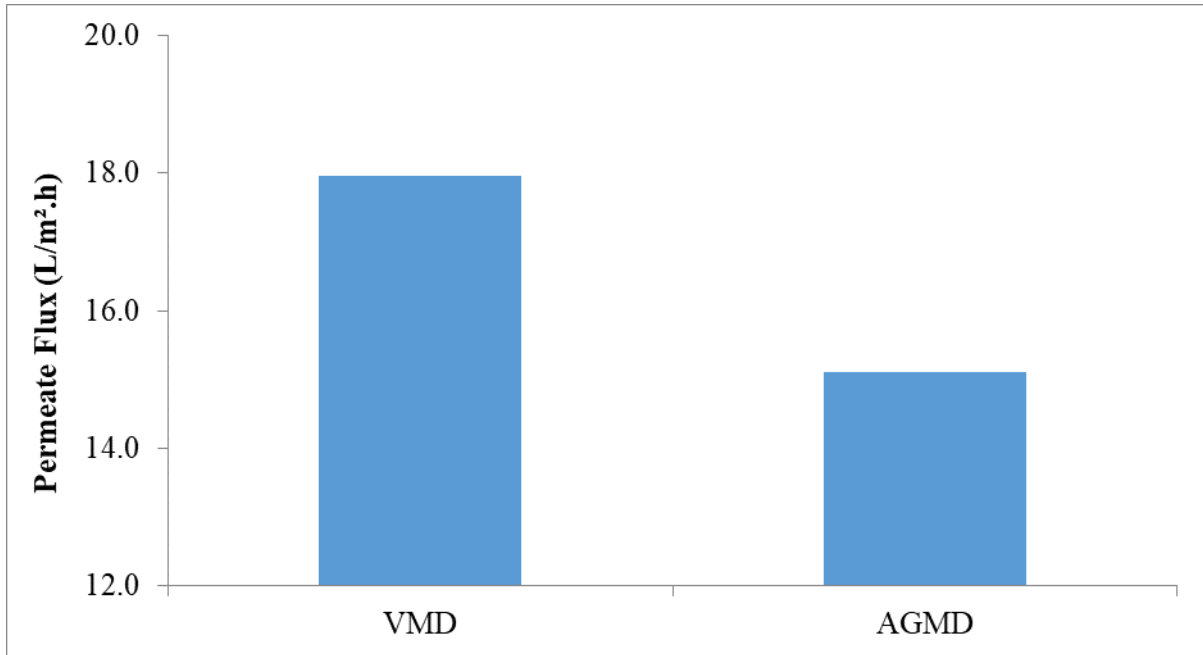


Figure 5.32. Permeate Flux from VMD and AGMD Experiments Using AGS from Beach Well as Feed at 85°C

Table 5-3 shows the chemical and physical analysis of major composition and characteristics, of the feedwater sample and permeate collected after the AGMD and VMD experiments using oilfield produced water.

Table 5-3. Chemical and Physical Analysis of Oilfield-Produced Water and Permeate Water from AGMD and VMD

Parameter	Unit	FeedWater	VMD Permeate Water	AGMD Permeate Water
TDS	mg/L	168000	17	364
Total suspended solid (TSS)	mg/L	95	< 2	2
Chloride	mg/L	99420	12	214
Oil and Grease	mg/L	71.8	< 0.75	< 0.75
TOC	mg/L	9.5	3.4	3.4
Turbidity	NTU	64	0.5	1.3

The chemical analysis comparison of permeate water using the DCMD, AGMD and VMD configurations, as shown in table 4-5 and 5-3, respectively shows that VMD process appears to be comparatively more effective at removing TDS and

chloride from the oil-produced water. On the other hand, DCMD performs better in reducing TOC compared to AGMD and VMD processes. Furthermore, VMD achieves the lowest turbidity, indicating it might be the best choice for producing the clearest permeate. The permeate TDS values show that salt rejection was almost 99.9% all the three MD processes. In summary, VMD provides the slightly better overall performance in removing dissolved solids, chloride, and turbidity, but DCMD might be preferable for applications sensitive to organic contamination due to its lower TOC levels. However, further studies are required to study the long-term performance of AGMD and VMD processes for treating oilfield-produced water.

5.3.6 Performance of PP, PVDF and PTFE Membranes in the AGMD and VMD Process

The effectiveness of flat-sheet membranes made of PP, PVDF and PTFE was examined in the AGMD and VMD processes using a 7% NaCl solution as the feed. The tests were performed at feed temperatures of 80 °C and 85 °C, with a cooling side temperature of 5 °C. In the AGMD process, deionised water was utilised as the cooling medium. The water flux and salt rejection percentages of the PP, PVDF and PTFE membranes using VMD configuration are summarised in Table 5.4.

Table 5-4. Water Flux and Salt Rejection Performance of PP, PVDF, and PTFE Membranes in VMD

Membrane	Temperature, °C	Water Flux, L/m ² h	Salt Rejection, %
PP	80	18.1	99.97
	85	20.3	99.98
PVDF	80	104.2	99.97
	85	112.1	99.97
PTFE	80	11.5	99.97
	85	13.3	99.97

The water flux increased with an increase in temperature for the Polypropylene (PP), Polyvinylidene fluoride (PVDF) and Polytetrafluoroethylene (PTFE) membranes in VMD configuration. The order of fluxes observed in the VMD configuration is Polyvinylidene fluoride (PVDF) > Polypropylene (PP) > Polytetrafluoroethylene (PTFE). The PTFE membranes showed an increase of

16.1% in flux with an increase in temperature from 80 °C to 85 °C. The flux increased by 14.2% and 7.6% for the PP and PVDF membranes, respectively. The results showed that the tested membranes achieved 99.97% salt rejections. Table 5.5 shows the performance behaviour of the PP, PVDF and PTFE membranes in the AGMD configuration.

Membrane	Temperature, °C	Water Flux, L/m ² h	Salt Rejection, %
PP	80	18.6	99.97
	85	21.8	99.97
PVDF	80	16.3	99.97
	85	18.0	99.97
PTFE	80	10.3	99.97
	85	12.4	99.97

The order of fluxes observed in the AGMD configuration is Polypropylene (PP) > Polyvinylidene fluoride (PVDF) > Polytetrafluoroethylene (PTFE). The PP membranes showed an increase of 17.2% in flux with an increase in temperature from 80 °C to 85 °C, whereas, the flux increased by 10.4% and 20.4% for the PVDF and PTFE membranes, respectively.

5.4 Conclusion

This study assessed the viability of using AGMD and VMD processes to desalinate NaCl solutions of different concentrations (3.5%, 7%, 15% and 26%), AGS and oilfield-produced water, under varying operating conditions using PP, PVDF, and PTFE membranes. It also investigated the effect of feed temperature, feed concentration, feed flow rate, air gap, and vacuum space depth on permeate flux in AGMD and VMD configurations.

This study investigated the effect of temperature on the permeate flux in two different MD configurations, AGMD and VMD, using a 7% NaCl solution as a feed. In the AGMD experiments, the test temperature varied from 70 °C to 85 °C, while the temperature on the cold side was always maintained at 5 °C. When the temperature was increased from 70 °C to 85 °C, the permeate flux surged from 14.3 L/m²h to

22.4 L/m²h, an increase of 56.64%. In the VMD experiments, feed temperatures varied from 65 °C to 85 °C. An increase in temperature from 65 °C to 85 °C resulted in an increase in the permeate flux from 13.4 to 17.0 L/m²h, an increase of about 26.87%. The findings showed that temperature increase increased the permeate flux in the AGMD and VMD configurations. The Antoine equation explains that this can be attributed to the significant rise in vapour pressure with increasing temperature. An increase in the temperature difference between the two sides of the membrane also positively affected the diffusion coefficient, resulting in increased vapour flux while decreasing temperature polarisation. These results suggest that higher temperatures can improve MD processes' mass-transfer coefficients.

In this study, the impact of feed concentration on permeate flux in the AGMD and VMD configurations was also investigated using NaCl solutions with concentrations of 3.5%, 7%, 15% and 26%. As the NaCl feed concentration increased from 3.5% to 7%, 15%, and 26%, the AGMD configuration saw a reduction in permeate flux by 17%, 26%, and 48%, respectively. In comparison, the VMD configuration experienced a slightly smaller reduction in flux with the same increases in feed concentration. Specifically, when the NaCl concentration was raised from 3.5% to 7%, 15%, and 26%, the permeate flux in the VMD configuration decreased by 5%, 10%, and 15%, respectively. This study found that permeate flux decreased with increasing feed concentration in both the AGMD and VMD configurations. The reduction in permeate flux was higher in the AGMD configurations than in the VMD configurations. The decrease in flux with increasing feed concentration was due to reduced water vapour pressure, increasing temperature polarisation and a decline in water activity. However, the increase in feed concentration had a smaller impact on the salt rejection percentage, suggesting that both AGMD and VMD configurations are well-suited for applications involving relatively high feed concentrations. The results suggest that AGMD outperforms VMD at lower feed concentrations while VMD performs well at higher feed concentrations. The amount of salt rejection exceeded 99.5% in both configurations. Based on these findings, it is recommended to consider the effect of feed concentration on permeate flux when designing and operating AGMD and VMD configurations for desalination applications.

Increasing the feed concentrations led to a gradual decrease in the GOR for both AGMD and VMD systems, with AGMD experiencing a sharper decline

compared to VMD. This trend is likely due to the higher permeate flux achieved at lower concentrations, which directly impacts the GOR. The difference in reduction levels between the two systems suggests that AGMD is more sensitive to changes in feed concentration, resulting in a more pronounced drop in efficiency as concentration increases, whereas VMD shows a more gradual decline in GOR under similar conditions. Consequently, VMD may be more resilient to efficiency losses at higher feed concentrations compared to AGMD. The performance of STEC recorded by both MD systems also presents different contributions of increase. On the other hand, the data showed that the higher feed concentration and the smaller GOR provide the higher STEC.

The influence of feed flow rate on permeate flux using a PP membrane was also investigated under constant feed and coolant temperatures using AGMD and VMD configurations. The tests were conducted using 7.0 wt% NaCl solution as feed, with the temperatures of the feed and coolant sides at 85 °C and 5 °C, respectively. In AGMD, the flux increased from 22.4 to 26.4 L/m²h, and in VMD, it increased from 17 to 20 L/m²h. Both systems showed a similar rate of increase in permeate flux with flow rate, approximately a 1.2-fold increase, indicating that the effect of flow rate on flux was nearly identical for both configurations. The salt rejection percentage was close to 99.9% and was largely unaffected by the feed flow rate. AGMD outperformed VMD at all feed flow rates, and the increase in permeate flux with flow rate was almost the same for both configurations. Permeate flux was not very sensitive to the increase in flow rate. This may be due to the main resistance of AGMD and VMD located in the gap on the coolant side of the configurations, resulting in a lower temperature polarisation effect than the DCMD configurations. Based on these findings, operating at higher flow rates is recommended to improve flux by reducing temperature and concentration polarisation, which will enhance mixing and reduce boundary layer resistance.

The change in feed flow rate changed the inertia force and resulted in faster flow as the flow rate increased. Thus, the lower the feed-flow rate, the smaller the Nu number at the same feed inlet temperature and feed concentration.

Increasing the feed flow rate resulted in a gradual rise in the GOR, indicating that higher flow rates led to an increase in permeate flux in both MD systems. However, the level of improvement varied between the two systems, with AGMD

showing a more significant increase in GOR compared to VMD. This difference in performance can likely be attributed to the distinct design characteristics of the two systems. AGMD benefits from a more effective heat recovery mechanism due to the presence of an air gap, which allows for the recovery and reuse of latent heat from the condensing vapour. As feed flow rates increase, this heat recovery becomes more efficient, leading to a larger boost in GOR. On the other hand, VMD relies on vacuum-driven mass transfer across the membrane and does not benefit from similar heat recovery. Consequently, the GOR improvement in VMD is more dependent on mass transfer efficiency, which results in a less pronounced increase in GOR compared to AGMD. Moreover, the STEC's reduction level differs from each system in which the AGMD recorded a larger STEC reduction than the VMD system.

The experimental results showed that the AGMD and VMD systems responded differently to variations in channel depths. In the AGMD configuration, the permeate flux decreased with an increase in feed channel and air gap depths, while in the VMD configuration, an increase in permeate flux was observed with an increase in feed channel and vacuum space depths. It was observed that increasing the cold-channel air gap depth from 2 mm to 8 mm resulted in a 16% decrease in permeate flux. Similarly, Figure 5.22 shows that increasing the hot-channel depth from 1 mm to 8 mm led to a 34.6% decrease in permeate flux. This reduction in flux with larger gap widths may be due to a non-uniform temperature distribution within the channel. At smaller channel depths, the temperature gradient between the feed and cold channels is likely higher, which could have resulted in higher permeate flux. However, the specific mechanisms underlying this behaviour may vary depending on the experimental setup and conditions, and further studies are needed to understand the observed behaviour fully. Overall, the experimental results suggest that the AGMD and VMD configurations can be optimised by carefully selecting the feed channel, air gap depths, and vacuum space, leading to higher flux rates and improved separation efficiency.

This study investigated the use of AGMD and VMD for treating oilfield-produced water and AGS. The experiments were carried out without pre-treatment. A polypropylene membrane was used in the experiments. The permeate flux obtained from treating oilfield-produced water was 15 L/m².h in AGMD at 85 °C, and in VMD, the permeate flux increased with a flux of 23 L/m².h at 85 °C. VMD

demonstrated higher permeate flux (18 L/m²h) compared to AGMD (15.1 L/m²h), making it a more effective process for treating AGS from a beach well at 85°C. Analytical results from oilfield-produced water treatment, shown in Tables 4-5 and 5-3, indicated that VMD slightly outperformed AGMD in removing dissolved solids and chloride, with both processes achieving nearly 99.9% salt rejection. However, DCMD was more effective in reducing TOC levels, making it a better choice for applications where minimizing organic contamination is crucial. Overall, VMD offers slightly better performance in terms of removing dissolved solids, chloride, and turbidity, while DCMD is more proficient in reducing TOC, indicating that VMD may be a preferable process for treating oilfield-produced water when compared to AGMD. Salt rejection was almost 99.9% in both AGMD and VMD, with VMD performing slightly better than AGMD in treating oilfield-produced water. However, further studies are recommended to investigate the long-term performance of AGMD and VMD processes for treating oilfield-produced water.

The performance of PTFE membranes, along with PP and PVDF membranes, was examined in AGMD and VMD processes using a 7% NaCl solution as the feed. The tests were conducted at feed temperatures of 80°C and 85°C, with a cooling side temperature of 5°C. In the AGMD process, deionized water was used as the cooling medium. In the VMD configuration, the water flux increased with temperature for all membranes, following the order Polyvinylidene fluoride (PVDF) > Polypropylene (PP) > Polytetrafluoroethylene (PTFE). Specifically, PTFE membranes showed a 16.1% increase in flux when the temperature was raised from 80°C to 85°C, while PP and PVDF membranes saw increases of 14.2% and 7.6%, respectively. All tested membranes achieved a high salt rejection rate of 99.97%. In the AGMD configuration, the order of flux performance differed: Polypropylene (PP) > Polyvinylidene fluoride (PVDF) > Polytetrafluoroethylene (PTFE). The PP membranes showed a 17.2% increase in flux with the temperature increase, while PVDF and PTFE membranes exhibited increases of 10.4% and 20.4%, respectively. In brief, both AGMD and VMD processes demonstrated that water flux increases with temperature across all membrane types, though the order of performance varies between configurations. VMD favoured PVDF membranes for higher flux, while AGMD favoured PP membranes. PTFE membranes showed consistent

improvements in flux across both processes. All membranes achieved excellent salt rejection, confirming their effectiveness for desalination.

Overall, the study generated promising results by establishing reference data on AGMD and VMD technologies for desalinating different saline waters at the laboratory scale under realistic operating conditions, including the actual AGS and oilfield-produced water, which has a considerably higher salinity than other seawaters. However, further laboratory- and pilot-scale studies are recommended to investigate the long-term performance of AGMD and VMD processes.

Chapter 6

Conclusion and Future Research

6.1 Conclusion

This work investigated the performance of three different types of membrane distillation technology: vacuum MD (VMD), direct contact MD (DCMD), and air gap MD (AGMD), using experimental approaches.

The feasibility of the DCMD process for desalinating different saline waters, AGS and oilfield-produced water under various operating conditions using polypropylene and PVDF membranes was investigated at the laboratory scale. Experiments were conducted to determine the effect of feed temperature, flow rate, and feed concentration on permeate flux.

The feed temperature was varied within the range of 45°C to 75°C. During these tests, with a constant cold-side temperature maintained at 20°C, a 26% NaCl feed solution, and a flow rate of 1.2 L/min, the permeate flux demonstrated a marked increase. As the feed temperature rose from 45°C to 75°C, the permeate flux improved substantially, rising from 11.6 L/m²h to 37.1 L/m²h. This indicates that increasing the feed temperature significantly enhances the permeate flux, highlighting the strong influence of thermal conditions on the system's performance. It was observed that increments in feedwater temperatures increase transmembrane vapour pressure and result in high permeate flux. Additionally, at higher temperatures, the viscosity of the feed solution decreases, which can improve hydrodynamic conditions and result in a higher flux. At temperatures below 45 °C, the vapour pressure of the feed solution may not be high enough to provide a sufficient driving force for mass transfer, resulting in low permeate flux. Temperatures above 75 °C increase the risk of thermal degradation of polymeric membranes as they may undergo structural changes, such as pore collapse and reduced hydrophobicity, which impairs their performance and shortens their lifespan. Moreover, increasing the feed temperature resulted in a gradual increase in the GOR. This may be due to the partial pressure difference, which in turn led to a larger mass flux that is directly proportional to the gained output ratio, whereas the performance of GOR is the opposite performance of STEC; thus, a higher GOR

means higher performance produced by the flow at the considered higher feed temperature.

NaCl solutions at concentrations of 3.5–26%, deionised water, oilfield-produced water and AGS were used as feed at different stages of this study. The increment in feedwater concentration caused a decrease in the permeate flux. It was shown that there was a reduction of 50% amounting to permeate flow that was produced when the concentration of NaCl in the feed solution was elevated from 0% to 26%. Upon an increase in NaCl feed concentration, hydrogen bonding between the NaCl and water molecules might increase; hence, more energy is required to vaporise the feed solution. This shows that more time and energy might be needed to produce permeate flux when the feed concentration is increased. However, increasing the feed concentrations gradually decreased the GOR (gained output ratio). This may be due to the higher permeate flux produced at smaller concentrations, directly proportional to the GOR.

The water flux increased with an increase in the flow rate due to turbulence, which reduced the effects of temperature and concentration polarisation. Additionally, greater heat transfers between the membrane and the medium may occur at lower flow rates and reduce the vaporisation impact. At increased flow rates, the heat transfer rate between the membrane and medium will decrease, accelerating the vaporisation process, which results in higher permeate flux. Also, increasing the feed-flow rate acted at a gradual increase in the GOR. This indicates that increasing the flow rates led to an increase in the permeate flux produced. On the other hand, the performance of STEC with increasing feed-flow rates showed a gradual decrease.

The performance of the direct contact membrane distillation system on different hot-feed and cold-solution channel depths was also studied using a DCMD module developed by the research team. The flux reduction was much greater at bigger cold-channel depths. It was observed that lower channel depths (both hot and cold) are suitable for higher permeate flux. Moreover, changing the flow channel depth increased the STEC, gradually reaching the maximum value at 6 mm and no further increase beyond this value for the hot channel. In contrast, the STEC recorded a gradual increase with the increase in cold channel depth, reaching the maximum value at a channel depth of 10 mm.

It was shown that higher flow rates and temperatures are required to obtain a higher permeate flux upon increasing the hot-channel depths. Experimental results show that DCMD was highly efficient in desalinating oilfield-produced water obtained from Kuwait. The permeate flux was 11.5 L/m².h and 12.5 L/m².h at 80 °C and 85 °C, respectively. The results indicate the enormous potential of DCMD to treat hypersaline oilfield-produced water with an overall rejection of salts above 99.9%.

The comparison of PP and PVDF membrane performance for AGS desalination revealed that PP membranes had a higher salt rejection rate but lower water flux, While PVDF membranes had a lower salt rejection rate but higher water flux. This observation is important because it suggests that PP membranes may be more suitable than PVDF membranes for seawater desalination, leading to more energy-efficient and cost-effective desalination. PP membranes are ideal for situations where a balance of water flow and salt removal is necessary. In contrast, PVDF membranes are suitable for applications where salt removal is not a primary concern.

This study successfully established and generated reference data on DCMD technology for desalinating different saline waters at the laboratory-scale level under realistic operating conditions and, more specifically, using actual AGS (which has a considerably higher salinity than other seawaters) and oilfield-produced water as a feed.

This study also aimed to assess the viability of using AGMD and VMD processes to desalinate different types of saline water, including AGS and oilfield-produced water, under varying operating conditions, using membranes made from polypropylene, polyvinylidene fluoride and polytetrafluoroethylene. This study investigated the effect of feed temperature, feed concentration, feed flow rate, air gap and vacuum space depth upon permeate flux in AGMD and VMD configurations. This study investigated the effect of temperature on the permeate flux in two different MD configurations, AGMD and VMD, using a 7% NaCl solution as feed. In the AGMD experiments, the test temperature varied from 70-85 °C, while the temperature on the cold side was always maintained at 5 °C. When the temperature was increased from 70 °C to 85 °C, the permeate flux surged from 14.3–22.4 L/m²h, an increase of 56.64%. In the VMD experiments, feed temperatures varied from 65 °C to 85 °C. An increase in temperature from 65 °C to 85 °C resulted in an increase

in the permeate flux from 13.4 to 17.0 L/m²h, an increase of about 26.87%. The findings showed that an increase in temperature resulted in an increase in permeate flux for both configurations.

Moreover, both systems recorded increased GOR (gained output ratio) with increasing the feed temperature but with different contributions. The performance of GOR recorded by the AGMD is larger than that produced by VMD. The performance of the STEC value recorded by both MD systems also presents different contributions of decrease while increasing feed temperature.

In this study, the impact of feed concentration on vapour permeate flux in AGMD and VMD configurations was also investigated using NaCl solutions with concentrations of 3.5%, 7%, 15% and 26%. This study found that the vapour permeate flux decreased with increase in NaCl feed concentration in both the AGMD and VMD configurations. The reduction in vapour permeate flux was higher in AGMD configurations than in VMD configurations. The decrease in vapour flux with increasing feed concentration was due to reduced water vapour pressure, increasing temperature polarisation and a decline in water activity. However, feed concentration affected the salt rejection percentage less, indicating that both AGMD and VMD configurations are suitable for applications with relatively high feed concentrations. The results suggest that AGMD outperforms VMD at lower feed concentrations while VMD performs well at higher feed concentrations. The amount of salt rejection exceeded 99.5% in both configurations. Based on these findings, it is recommended to consider the effect of feed concentration on permeate flux when designing and operating AGMD and VMD configurations for desalination applications.

However, increasing the feed concentrations decreased the GOR in both MD systems but with different reduction levels. This could be due to the MD design, in which the AGMD system recorded a sharp decrease in the GOR (gained output ratio) through all loading of feed concentration, whereas the VMD system recorded a gradual reduction. On the other hand, the data showed that the higher feed concentration and the smaller GOR provide the higher STEC (specific thermal energy consumption).

The influence of feed flow rate on permeate flux using a polypropylene membrane was also investigated under constant feed and coolant temperatures using AGMD and VMD configurations. The tests were conducted using 7.0% NaCl

solution as feed, with the temperature of feed and coolant sides at 85 °C and 5 °C, respectively. In both AGMD and VMD, the flux increased by approximately 1.2-fold (from 22.4 to 26.4 L/m²h in AGMD and from 17 to 20 L/m²h in VMD), indicating a similar rate of increase in permeate flux with flow rate for both configurations. The salt rejection percentage was close to 99.9% and was largely unaffected by the feed flow rate. AGMD outperformed VMD at all feed flow rates, and the increase in permeate flux with flow rate was almost the same for both configurations. The permeate flux was not highly sensitive to the increase in flow rate. This may be due to the main resistance of AGMD and VMD being located in the gap on the coolant side of the configurations, resulting in a lower temperature polarisation effect than DCMD configurations. Based on these findings, it is recommended that higher flow rates be operated to improve flux by reducing temperature and concentration polarisation, improving mixing, and reducing boundary layer resistance.

The change in feed-flow rate changed the inertia force and resulted in faster flow. Thus, the lower the feed-flow rate, the smaller the Nu number at the same feed inlet temperature and feed concentration. However, the performance of the two MD systems differed in terms of GOR enhancement, with the AGMD system showing a larger increase in GOR compared to the VMD system. This may be due to the nature of the system design. Moreover, the STEC's reduction level differs from each system in which the AGMD recorded a larger STEC reduction than the VMD system.

The experimental results indicated that AGMD and VMD systems exhibited different responses to variations in channel depths. In the AGMD configuration, permeate flux decreased as feed channel and air gap depths increased, while in the VMD configuration, permeate flux increased with greater feed channel and vacuum space depths. Specifically, increasing the cold-channel air gap depth from 2 mm to 8 mm in AGMD resulted in a 16% decrease in flux, and increasing the hot-channel depth from 1 mm to 8 mm led to a 34.6% decrease. This reduction in flux with larger gap widths may be due to a less uniform temperature distribution, where smaller channel depths maintain a higher temperature gradient, promoting greater flux. However, the specific mechanisms underlying this behaviour may vary depending on the experimental setup and conditions, and further studies are needed to understand the observed behaviour fully. Overall, the experimental findings indicate that optimizing the AGMD and VMD configurations can be achieved by carefully adjusting

the feed channel, air gap depth, and vacuum space. These adjustments can result in higher permeate flux and enhanced separation efficiency.

This study investigated the use of AGMD and VMD for treating oilfield-produced water and AGS. The experimental results for both oilfield-produced water and AGS from beach well demonstrated that both AGMD and VMD are effective processes for water treatment, achieving good permeate flux rates. AGMD produced a vapour permeate flux of 15 L/m².h for oilfield-produced water at 85°C, while VMD achieved higher fluxes of 23 L/m².h at 85°C and 21.35 L/m².h at 80°C. For AGS from beach well at 85°C, VMD recorded a flux of 18 L/m².h, compared to 15.1 L/m².h for AGMD. While VMD showed slightly higher efficiency in both cases, AGMD also performed well, proving its suitability for these applications. Both processes are viable options for water treatment, though VMD may be more advantageous in terms of permeate flux, especially at higher temperatures. The salt rejection was almost 99.9% in both AGMD and VMD, with VMD performing slightly better than AGMD in treating oilfield-produced water. However, further studies are required to investigate the long-term performance of the AGMD and VMD processes for treating oilfield-produced water.

Experiments were conducted to compare the effectiveness of flat-sheet membranes made of PP, PVDF and PTFE in AGMD and VMD processes using a 7% NaCl solution as the feed. The results showed that the tested membranes achieved salt rejections as high as 99.97%, and the order of fluxes observed in the VMD configuration was Polyvinylidene Fluoride (PVDF) > Polypropylene (PP) > Polytetrafluoroethylene (PTFE). PTFE membranes showed an increase of 16.1% in flux with the rise in temperature, while the increases were 14.2% and 7.6% for the PP and PVDF membranes, respectively. In the AGMD configuration, the order of fluxes observed was Polypropylene (PP) > Polyvinylidene Fluoride (PVDF) > Polytetrafluoroethylene (PTFE).

Overall, the study generated promising results by establishing reference data on AGMD and VMD technologies for desalinating different saline waters at the laboratory scale under realistic operating conditions, including the actual AGS and oilfield-produced water, which has a considerably higher salinity than other seawaters. However, further laboratory- and pilot-scale studies are recommended to investigate the long-term performance of the AGMD and VMD processes.

6.2 Future Research

MD technology has many advantages in engineering and industrial applications. This technology is essential because it is helpful in people's lives, such as drinking water. However, improving this technology has resulted in many enhancements to reach the optimum and most efficient uses. However, there is still a large volume of ideas and techniques that can be applied to enhance the efficiency of this technology experimentally and numerically.

The following ideas and techniques can be applied in future research work to enhance the efficiency of MD technology:

- 1- Integrating all types of MD technology with the parabolic trough collector can be applied to use solar energy as a sustainable, renewable source to provide the required power.
- 2- Perform numerical simulations to investigate parametric studies to reach an optimum MD design using all types of MD systems over a wide range of parameters: feed concentrations, feed temperatures, flow rates, etc.
- 3- The available literature has a limited volume of high-concentration solutions in heat- and mass-transfer modes. Thus, the influence of high-concentration feeds should be investigated using all types of MD technology.
- 4- More investigations are required to experimentally and numerically examine the effect of operating conditions on energy consumption on all types of MD technologies.
- 5- Further research studies are recommended to explore the optimal combination of membrane configurations with different materials to enhance the performance of membrane distillation processes.
- 6- The performance of MD technology verifies the requirement for investigating MD hardware, such as large-porosity hydrophobic membranes with a proper thickness, which are supposed to provide low-heat conductive polymers, leading to decreased waste energy.
- 7- MD technology requires selecting the most efficient materials and operative conditions for accurately modelling scale-up and scale-down.
- 8- Investigate the water treatment plant's production cost to evaluate MD technology's potential.

- 9- More studies are required to composite polyethylene (PE) with other materials to obtain a higher level of water flux in all types of MD technologies.
- 10- Study the long-term effects of temperature polarisation at feed temperatures of 80°C and 85°C and its influence on permeate flux stability.
- 11- Explore the influence of fluid residence time in the feed and cold side channel, particularly at low and high flow rates, on heat transfer and vaporisation, to better understand its effect on vapour pressure and permeate flux in MD systems.
- 12- Examine the long-term performance of DCMD for oilfield-produced water desalination at feed temperatures of 80°C and 85°C, with specific focus on membrane fouling resistance and extended operation periods.

References

1. Woldemariam, D.M., Kullab, A. and Martin, A.R., 2017. District heat-driven water purification via membrane distillation: New possibilities for applications in pharmaceutical industries. *Industrial & Engineering Chemistry Research*, 56(9), pp.2540-2548.
2. Parani, S. and Oluwafemi, O.S., 2021. Membrane distillation: recent configurations, membrane surface engineering, and applications. *Membranes*, 11(12), p.934.
3. Amy, G., Ghaffour, N., Li, Z., Francis, L., Linares, R.V., Missimer, T. and Lattemann, S., 2017. Membrane-based seawater desalination: Present and future prospects. *Desalination*, 401, pp.16-21.
4. Kalla, S., 2021. Use of membrane distillation for oily wastewater treatment—a review. *Journal of Environmental Chemical Engineering*, 9(1), p.104641.
5. Ahmed, F.E., Lalia, B.S., Hashaikeh, R. and Hilal, N., 2020. Alternative heating techniques in membrane distillation: A review. *Desalination*, 496, p.114713.
6. Abu-Zeid, M.A.E.R., Zhang, Y., Dong, H., Zhang, L., Chen, H.L. and Hou, L., 2015. A comprehensive review of vacuum membrane distillation technique. *Desalination*, 356, pp.1-14.
7. Ding, Z., Liu, L., Li, Z., Ma, R. and Yang, Z., 2006. Experimental study of ammonia removal from water by membrane distillation (MD): The comparison of three configurations. *Journal of membrane Science*, 286(1-2), pp.93-103.
8. Criscuoli, A., Carnevale, M.C. and Drioli, E., 2008. Evaluation of energy requirements in membrane distillation. *Chemical Engineering and Processing: Process Intensification*, 47(7), pp.1098-1105.
9. Summers, E.K. and Arafat, H.A., 2012. Energy efficiency comparison of single-stage membrane distillation (MD) desalination cycles in different configurations. *Desalination*, 290, pp.54-66.
10. Cipollina, A., Di Sparti, M.G., Tamburini, A. and Micale, G., 2012. Development of a membrane distillation module for solar energy seawater desalination. *Chemical engineering research and design*, 90(12), pp.2101-2121.

11. Swaminathan, J., Chung, H.W., Warsinger, D.M., AlMarzooqi, F.A. and Arafat, H.A., 2016. Energy efficiency of permeate gap and novel conductive gap membrane distillation. *Journal of Membrane Science*, 502, pp.171-178.
12. Zhang, J., Duke, M., Hoang, M., Xie, Z., Groth, A., Tun, C. and Gray, S., 2013. Modelling of vacuum membrane distillation. *Journal of membrane science*, 434, pp.1-9.
13. Shim, S.M., Lee, J.G. and Kim, W.S., 2014. Performance simulation of a multi-VMD desalination process including the recycle flow. *Desalination*, 338, pp.39-48.
14. Izquierdo-Gil, M.A., Garcia-Payo, M.C. and Fernández-Pineda, C., 1999. Air gap membrane distillation of sucrose aqueous solutions. *Journal of membrane science*, 155(2), pp.291-307.
15. Zhao, K., Heinzl, W., Wenzel, M., Büttner, S., Bollen, F., Lange, G., Heinzl, S. and Sarda, N., 2013. Experimental study of the memsys vacuum-multi-effect-membrane-distillation (V-MEMD) module. *Desalination*, 323, pp.150-160.
16. Khayet, M., Matsuura, T., Mengual, J.I. and Qtaishat, M., 2006. Design of novel direct contact membrane distillation membranes. *Desalination*, 192(1-3), pp.105-111.
17. Chung, H.W., Swaminathan, J. and Warsinger, D.M., 2016. Multistage vacuum membrane distillation (MSVMD) systems for high salinity applications. *Journal of Membrane Science*, 497, pp.128-141.
18. Kim, Y.D., Thu, K. and Choi, S.H., 2015. Solar-assisted multi-stage vacuum membrane distillation system with heat recovery unit. *Desalination*, 367, pp.161-171.
19. Mustakeem, M., Qamar, A., Alpatova, A. and Ghaffour, N., 2021. Dead-end membrane distillation with localized interfacial heating for sustainable and energy-efficient desalination. *Water Research*, 189, p.116584.
20. Ma, Q., Ahmadi, A. and Cabassud, C., 2018. Direct integration of a vacuum membrane distillation module within a solar collector for small-scale units adapted to seawater desalination in remote places: Design, modeling & evaluation of a flat-plate equipment. *Journal of Membrane Science*, 564, pp.617-633.

21. Chen, Q., Ja, M.K., Li, Y. and Chua, K.J., 2018. Thermodynamic optimization of a vacuum multi-effect membrane distillation system for liquid desiccant regeneration. *Applied energy*, 230, pp.960-973.
22. Krnac, A., Araiz, M., Rana, S., Velardo, J. and Date, A., 2019. Investigation of direct contact membrane distillation coupling with a concentrated photovoltaic solar system. *Energy Procedia*, 160, pp.246-252.
23. Bappy, M.J.P., Bahar, R., Ibrahim, S. and Ariff, T.F., 2017. Enhanced freshwater production using finned-plate air gap membrane distillation (AGMD). In *MATEC Web of Conferences* (Vol. 103, p. 06014). EDP Sciences.
24. Im, B.G., Lee, J.G., Kim, Y.D. and Kim, W.S., 2018. Theoretical modeling and simulation of AGMD and LGMD desalination processes using a composite membrane. *Journal of Membrane Science*, 565, pp.14-24.
25. Lee, J., Alsaadi, A.S. and Ghaffour, N., 2019. Multi-stage air gap membrane distillation reversal for hot impaired quality water treatment: concept and simulation study. *Desalination*, 450, pp.1-11.
26. Burhan, M., Shahzad, M.W., Ybyraiymkul, D., Oh, S.J., Ghaffour, N. and Ng, K.C., 2019. Performance investigation of MEMSYS vacuum membrane distillation system in single effect and multi-effect mode. *Sustainable Energy Technologies and Assessments*, 34, pp.9-15.
27. Anvari, A., Yancheshme, A.A., Kekre, K.M. and Ronen, A., 2020. State-of-the-art methods for overcoming temperature polarization in membrane distillation process: A review. *Journal of membrane science*, 616, p.118413.
28. Bandini, S., Gostoli, C. and Sarti, G.C., 1992. Separation efficiency in vacuum membrane distillation. *Journal of membrane Science*, 73(2-3), pp.217-229.
29. Chiam, C.K. and Sarbatly, R., 2013. Vacuum membrane distillation processes for aqueous solution treatment—A review. *Chemical Engineering and Processing: Process Intensification*, 74, pp.27-54.
30. Martínez-Díez, L. and Vazquez-Gonzalez, M.I., 1999. Temperature and concentration polarization in membrane distillation of aqueous salt solutions. *Journal of membrane science*, 156(2), pp.265-273.
31. Mericq, J.P., Laborie, S. and Cabassud, C., 2011. Evaluation of systems coupling vacuum membrane distillation and solar energy for seawater desalination. *Chemical Engineering Journal*, 166(2), pp.596-606.

32. Wu, C., Li, Z., Zhang, J., Jia, Y., Gao, Q. and Lu, X., 2015. Study on the heat and mass transfer in air-bubbling enhanced vacuum membrane distillation. *Desalination*, 373, pp.16-26.
33. Lovineh, S.G., Asghari, M. and Rajaei, B., 2013. Numerical simulation and theoretical study on simultaneous effects of operating parameters in vacuum membrane distillation. *Desalination*, 314, pp.59-66.
34. Bhadra, M., Roy, S. and Mitra, S., 2014. Nanodiamond immobilized membranes for enhanced desalination via membrane distillation. *Desalination*, 341, pp.115-119.
35. Efome, J.E., Baghbanzadeh, M., Rana, D., Matsuura, T. and Lan, C.Q., 2015. Effects of superhydrophobic SiO₂ nanoparticles on the performance of PVDF flat sheet membranes for vacuum membrane distillation. *Desalination*, 373, pp.47-57.
36. Bhadra, M., Roy, S. and Mitra, S., 2016. Flux enhancement in direct contact membrane distillation by implementing carbon nanotube immobilized PTFE membrane. *Separation and Purification Technology*, 161, pp.136-143.
37. Jafari, A., Kebria, M.R.S., Rahimpour, A. and Bakeri, G., 2018. Graphene quantum dots modified polyvinylidene fluoride (PVDF) nanofibrous membranes with enhanced performance for air Gap membrane distillation. *Chemical Engineering and Processing-Process Intensification*, 126, pp.222-231.
38. Rangunath, S., Roy, S. and Mitra, S., 2018. Carbon nanotube immobilized membrane with controlled nanotube incorporation via phase inversion polymerization for membrane distillation based desalination. *Separation and Purification Technology*, 194, pp.249-255.
39. Castillo, E.H.C., Thomas, N., Al-Ketan, O., Rowshan, R., Al-Rub, R.K.A., Nghiem, L.D., Vigneswaran, S., Arafat, H.A. and Naidu, G., 2019. 3D printed spacers for organic fouling mitigation in membrane distillation. *Journal of Membrane Science*, 581, pp.331-343.
40. Thomas, N., Sreedhar, N., Al-Ketan, O., Rowshan, R., Al-Rub, R.K.A. and Arafat, H., 2018. 3D printed triply periodic minimal surfaces as spacers for enhanced heat and mass transfer in membrane distillation. *Desalination*, 443, pp.256-271.

41. Tan, Y.Z., Ang, E.H. and Chew, J.W., 2019. Metallic spacers to enhance membrane distillation. *Journal of Membrane Science*, 572, pp.171-183.
42. Alsaadi, A.S., Alpatova, A., Lee, J.G., Francis, L. and Ghaffour, N., 2018. Flashed-feed VMD configuration as a novel method for eliminating temperature polarization effect and enhancing water vapor flux. *Journal of Membrane Science*, 563, pp.175-182.
43. Mabrouk, A., Elhenawy, Y. and Moustafa, G., 2016. Experimental evaluation of corrugated feed channel of direct contact membrane distillation. *J. Membr. Sci. Technol*, 6(2).
44. Elhenawy, Y., Elminshawy, N.A., Bassyouni, M., Alanezi, A.A. and Drioli, E., 2020. Experimental and theoretical investigation of a new air gap membrane distillation module with a corrugated feed channel. *Journal of Membrane Science*, 594, p.117461.
45. Anvari, A., Kekre, K.M., Yancheshme, A.A., Yao, Y. and Ronen, A., 2019. Membrane distillation of high salinity water by induction heated thermally conducting membranes. *Journal of Membrane Science*, 589, p.117253.
46. Dudchenko, A.V., Chen, C., Cardenas, A., Rolf, J. and Jassby, D., 2017. Frequency-dependent stability of CNT Joule heaters in ionizable media and desalination processes. *Nature nanotechnology*, 12(6), pp.557-563.
47. Qtaishat, M., Khayet, M. and Matsuura, T., 2009. Novel porous composite hydrophobic/hydrophilic polysulfone membranes for desalination by direct contact membrane distillation. *Journal of Membrane science*, 341(1-2), pp.139-148.
48. Roy, S., Bhadra, M. and Mitra, S., 2014. Enhanced desalination via functionalized carbon nanotube immobilized membrane in direct contact membrane distillation. *Separation and Purification Technology*, 136, pp.58-65.
49. Ji, Z., Wang, J., Hou, D., Yin, Z. and Luan, Z., 2013. Effect of microwave irradiation on vacuum membrane distillation. *Journal of membrane science*, 429, pp.473-479.
50. Anvari, A., Kekre, K.M. and Ronen, A., 2020. Scaling mitigation in radio-frequency induction heated membrane distillation. *Journal of membrane science*, 600, p.117859.

51. Tan, Y.Z., Chandrakant, S.P., Ang, J.S.T., Wang, H. and Chew, J.W., 2020. Localized induction heating of metallic spacers for energy-efficient membrane distillation. *Journal of Membrane Science*, 606, p.118150.
52. Dongare, P.D., Alabastri, A., Pedersen, S., Zodrow, K.R., Hogan, N.J., Neumann, O., Wu, J., Wang, T., Deshmukh, A., Elimelech, M. and Li, Q., 2017. Nanophotonics-enabled solar membrane distillation for off-grid water purification. *Proceedings of the National Academy of Sciences*, 114(27), pp.6936-6941.
53. Wu, X., Jiang, Q., Ghim, D., Singamaneni, S. and Jun, Y.S., 2018. Localized heating with a photothermal polydopamine coating facilitates a novel membrane distillation process. *Journal of Materials Chemistry A*, 6(39), pp.18799-18807.
54. Gong, B., Yang, H., Wu, S., Xiong, G., Yan, J., Cen, K., Bo, Z. and Ostrikov, K., 2019. Graphene array-based anti-fouling solar vapour gap membrane distillation with high energy efficiency. *Nano-Micro Letters*, 11, pp.1-14.
55. Han, X., Wang, W., Zuo, K., Chen, L., Yuan, L., Liang, J., Li, Q., Ajayan, P.M., Zhao, Y. and Lou, J., 2019. Bio-derived ultrathin membrane for solar driven water purification. *Nano Energy*, 60, pp.567-575.
56. Dongare, P.D., Alabastri, A., Neumann, O., Nordlander, P. and Halas, N.J., 2019. Solar thermal desalination as a nonlinear optical process. *Proceedings of the National Academy of Sciences*, 116(27), pp.13182-13187.
57. Song, L., Huang, Q., Huang, Y., Bi, R. and Xiao, C., 2019. An electro-thermal braid-reinforced PVDF hollow fiber membrane for vacuum membrane distillation. *Journal of Membrane Science*, 591, p.117359.
58. Politano, A., Di Profio, G., Fontananova, E., Sanna, V., Cupolillo, A. and Curcio, E., 2019. Overcoming temperature polarization in membrane distillation by thermoplasmonic effects activated by Ag nanofillers in polymeric membranes. *Desalination*, 451, pp.192-199.
59. Ye, H., Li, X., Deng, L., Li, P., Zhang, T., Wang, X. and Hsiao, B.S., 2019. Silver nanoparticle-enabled photothermal nanofibrous membrane for light-driven membrane distillation. *Industrial & Engineering Chemistry Research*, 58(8), pp.3269-3281.

60. Naidu, G., Choi, Y., Jeong, S., Hwang, T.M. and Vigneswaran, S., 2014. Experiments and modeling of a vacuum membrane distillation for high saline water. *Journal of Industrial and Engineering Chemistry*, 20(4), pp.2174-2183.
61. Chen, K., Xiao, C., Huang, Q., Liu, H., Liu, H., Wu, Y. and Liu, Z., 2015. Study on vacuum membrane distillation (VMD) using FEP hollow fiber membrane. *Desalination*, 375, pp.24-32.
62. Li, J.M., Xu, Z.K., Liu, Z.M., Yuan, W.F., Xiang, H., Wang, S.Y. and Xu, Y.Y., 2003. Microporous polypropylene and polyethylene hollow fiber membranes. Part 3. Experimental studies on membrane distillation for desalination. *Desalination*, 155(2), pp.153-156.
63. Wirth, D. and Cabassud, C., 2002. Water desalination using membrane distillation: comparison between inside/out and outside/in permeation. *Desalination*, 147(1-3), pp.139-145.
64. Deshpande, J., Nithyanandam, K. and Pitchumani, R., 2017. Analysis and design of direct contact membrane distillation. *Journal of Membrane Science*, 523, pp.301-316.
65. Lian, B., Wang, Y., Le-Clech, P., Chen, V. and Leslie, G., 2016. A numerical approach to module design for crossflow vacuum membrane distillation systems. *Journal of Membrane Science*, 510, pp.489-496.
66. Bahar, R., Hawlader, M.N.A. and Ariff, T.F., 2015. Channeled coolant plate: A new method to enhance freshwater production from an air gap membrane distillation (AGMD) desalination unit. *Desalination*, 359, pp.71-81.
67. Boutikos, P., Mohamed, E.S., Mathioulakis, E. and Belessiotis, V., 2017. A theoretical approach of a vacuum multi-effect membrane distillation system. *Desalination*, 422, pp.25-41.
68. Chang, H., Hsu, J.A., Chang, C.L. and Ho, C.D., 2015. CFD study of heat transfer enhanced membrane distillation using spacer-filled channels. *Energy Procedia*, 75, pp.3213-3219.
69. Chen, Q., Muhammad, B., Akhtar, F.H., Ybyraiymkul, D., Muhammad, W.S., Li, Y. and Ng, K.C., 2020. Thermo-economic analysis and optimization of a vacuum multi-effect membrane distillation system. *Desalination*, 483, p.114413.
70. Omar, A., Nashed, A., Li, Q. and Taylor, R.A., 2021. Experimental and numerical evaluation of the energy requirement of multi-stage vacuum

- membrane distillation designs. *Separation and Purification Technology*, 257, p.117303.
71. Lee, J.G. and Kim, W.S., 2014. Numerical study on multi-stage vacuum membrane distillation with economic evaluation. *Desalination*, 339, pp.54-67.
 72. Zhang, Y., Peng, Y., Ji, S. and Wang, S., 2016. Numerical simulation of 3D hollow-fiber vacuum membrane distillation by computational fluid dynamics. *Chemical Engineering Science*, 152, pp.172-185.
 73. Zhang YongGang, Z.Y., Peng YueLian, P.Y., Ji ShuLan, J.S., Qi JiaWei, Q.J. and Wang ShaoBin, W.S., 2017. Numerical modeling and economic evaluation of two multi-effect vacuum membrane distillation (ME-VMD) processes.
 74. Sarbatly, R. and Chiam, C.K., 2013. Evaluation of geothermal energy in desalination by vacuum membrane distillation. *Applied Energy*, 112, pp.737-746.
 75. Christie, K.S., Horseman, T. and Lin, S., 2020. Energy efficiency of membrane distillation: Simplified analysis, heat recovery, and the use of waste-heat. *Environment international*, 138, p.105588.
 76. Criscuoli, A., 2021. Thermal performance of integrated direct contact and vacuum membrane distillation units. *Energies*, 14(21), p.7405.
 77. Zuo, G., Guan, G. and Wang, R., 2014. Numerical modeling and optimization of vacuum membrane distillation module for low-cost water production. *Desalination*, 339, pp.1-9.
 78. Tang, N., Zhang, H. and Wang, W., 2011. Computational fluid dynamics numerical simulation of vacuum membrane distillation for aqueous NaCl solution. *Desalination*, 274(1-3), pp.120-129.
 79. Liu, J., Wang, Q., Han, L. and Li, B., 2017. Simulation of heat and mass transfer with cross-flow hollow fiber vacuum membrane distillation: The influence of fiber arrangement. *Chemical Engineering Research and Design*, 119, pp.12-22.
 80. Anqi, A.E., Usta, M., Krysko, R., Lee, J.G., Ghaffour, N. and Oztekin, A., 2020. Numerical study of desalination by vacuum membrane distillation—Transient three-dimensional analysis. *Journal of Membrane Science*, 596, p.117609.
 81. Chang, Y.S., Ooi, B.S., Ahmad, A.L., Leo, C.P. and Lau, W.J., 2020. Numerical study on performance and efficiency of batch submerged vacuum membrane

- distillation for desalination. *Chemical Engineering Research and Design*, 163, pp.217-229.
82. Zhang, J., Dow, N., Duke, M., Ostarcevic, E. and Gray, S., 2010. Identification of material and physical features of membrane distillation membranes for high performance desalination. *Journal of membrane science*, 349(1-2), pp.295-303.
 83. Dudchenko, A.V., Hardikar, M., Anand, A., Xin, R., Wang, R., Gopu, C. and Mauter, M.S., 2022. Guidance on nusselt number correlation selection in membrane distillation. *ACS ES&T Engineering*, 2(8), pp.1425-1434.
 84. Lawson, K.W. and Lloyd, D.R., 1997. Membrane distillation. *Journal of membrane Science*, 124(1), pp.1-25.
 85. Han, X., Wang, W., Zuo, K., Chen, L., Yuan, L., Liang, J., Li, Q., Ajayan, P.M., Zhao, Y. and Lou, J., 2019. Bio-derived ultrathin membrane for solar driven water purification. *Nano Energy*, 60, pp.567-575.
 86. BAHAR, R., 2010. Conversion of saline water to fresh water using air gap membrane distillation (AGMD).
 87. Fadhil, S., Alsalhy, Q.F., Makki, H.F., Ruby-Figueroa, R., Marino, T., Criscuoli, A., Macedonio, F., Giorno, L., Drioli, E. and Figoli, A., 2019. Seawater desalination using PVDF-HFP membrane in DCMD process: Assessment of operating condition by response surface method. *Chemical Engineering Communications*, 206(2), pp.237-246.
 88. Greenlee, L.F., Lawler, D.F., Freeman, B.D., Marrot, B. and Moulin, P., 2009. Reverse osmosis desalination: water sources, technology, and today's challenges. *Water research*, 43(9), pp.2317-2348.
 89. Ghaffour, N., 2009. The challenge of capacity-building strategies and perspectives for desalination for sustainable water use in MENA. *Desalination and Water Treatment*, 5(1-3), pp.48-53.
 90. Tarnacki, K., Meneses, M., Melin, T., Van Medevoort, J. and Jansen, A., 2012. Environmental assessment of desalination processes: Reverse osmosis and Memstill®. *Desalination*, 296, pp.69-80.
 91. Hanemaaijer, J.H., van Medevoort, J., Jansen, A.E., Dotremont, C., van Sonsbeek, E., Yuan, T. and De Ryck, L., 2006. Memstill membrane distillation-a future desalination technology. *Desalination*, 199(1-3), pp.175-176.

92. Raluy, R.G., Schwantes, R., Subiela, V.J., Peñate, B., Melián, G. and Betancort, J.R., 2012. Operational experience of a solar membrane distillation demonstration plant in Pozo Izquierdo-Gran Canaria Island (Spain). *Desalination*, 290, pp.1-13.
93. Ameen, N.A.M., Ibrahim, S.S., Alsalhy, Q.F. and Figoli, A., 2020. Highly saline water desalination using direct contact membrane distillation (DCMD): experimental and simulation study. *Water*, 12(6), p.1575.
94. Eziyi, I., Krothapalli, A., Osorio, J.D., Ordonez, J.C. and Vargas, J.V.C., 2013, August. Effects of salinity and feed temperature on permeate flux of an air gap membrane distillation unit for sea water desalination. In *2013 1st IEEE Conference on Technologies for Sustainability (SusTech)* (pp. 142-145). IEEE.
95. Alklaibi, A.M. and Lior, N., 2005. Membrane-distillation desalination: status and potential. *Desalination*, 171(2), pp.111-131.
96. El-Bourawi, M.S., Ding, Z., Ma, R. and Khayet, M., 2006. A framework for better understanding membrane distillation separation process. *Journal of membrane science*, 285(1-2), pp.4-29.
97. Liu, C. and Martin, A., 2005. Membrane Distillation and Applications for Water Purification in Thermal Cogeneration-A Prestudy.
98. Walton, J., Lu, H., Turner, C., Solis, S. and Hein, H., 2004. Solar and waste heat desalination by membrane distillation. *Desalination and water purification research and development program report*, 81, p.20.
99. Pal, P. and Manna, A.K., 2010. Removal of arsenic from contaminated groundwater by solar-driven membrane distillation using three different commercial membranes. *water research*, 44(19), pp.5750-5760.
100. Garcia-Payo, M.C., Izquierdo-Gil, M.A. and Fernández-Pineda, C., 2000. Air gap membrane distillation of aqueous alcohol solutions. *Journal of Membrane Science*, 169(1), pp.61-80.
101. Chen, L. and Wu, B., 2021. Research progress in computational fluid dynamics simulations of membrane distillation processes: a review. *Membranes*, 11(7), p.513.
102. Chang, H., Ho, C.D., Chen, Y.H., Chen, L., Hsu, T.H., Lim, J.W., Chiou, C.P. and Lin, P.H., 2021. Enhancing the Permeate Flux of Direct Contact Membrane

- distillation modules with inserting 3D printing turbulence promoters. *Membranes*, 11(4), p.266.
103. Jiang, B., Hu, B., Yang, N., Zhang, L., Sun, Y. and Xiao, X., 2021. Study of turbulence promoters in prolonging membrane life. *Membranes*, 11(4), p.268.
104. Ismail, M., Fotowat, S. and Fartaj, A., 2014. Effect of channel size on heat transfer and pressure drop in thin slabs minichannel heat exchanger. *International Journal of Mechanical Engineering and Mechatronics*, 2(1), pp.33-42.
105. Alawad, S.M. and Khalifa, A.E., 2019. Analysis of water gap membrane distillation process for water desalination. *Desalination*, 470, p.114088.
106. Salmanli, O.M., Yuksekdog, A. and Koyuncu, I., 2022. Boron removal by using vacuum assisted air gap membrane distillation (VAGMD). *Environmental Technology & Innovation*, 26, p.102395.
107. Guan, Z., Lv, J., Bai, P. and Guo, X., 2016. Boron removal from aqueous solutions by adsorption—A review. *Desalination*, 383, pp.29-37.
108. Martin, A. and Dahl, O., 2020. Techno-economic system analysis of membrane distillation process for treatment of chemical mechanical planarization wastewater in nano-electronics industries. *Separation and Purification Technology*, 248, p.117013.
109. Li, M., Li, K., Wang, L. and Zhang, X., 2020. Feasibility of concentrating textile wastewater using a hybrid forward osmosis-membrane distillation (FO-MD) process: Performance and economic evaluation. *Water Research*, 172, p.115488.
110. Yang, G., Zhang, J., Peng, M., Du, E., Wang, Y., Shan, G., Ling, L., Ding, H., Gray, S. and Xie, Z., 2021. A mini review on antiwetting studies in membrane distillation for textile wastewater treatment. *Processes*, 9(2), p.243.
111. Dow, N., García, J.V., Niadoo, L., Milne, N., Zhang, J., Gray, S. and Duke, M., 2017. Demonstration of membrane distillation on textile waste water: assessment of long term performance, membrane cleaning and waste heat integration. *Environmental Science: Water Research & Technology*, 3(3), pp.433-449.
112. Yadav, A., Yadav, P., Labhasetwar, P.K. and Shahi, V.K., 2021. CNT functionalized ZIF-8 impregnated poly (vinylidene fluoride-co-

- hexafluoropropylene) mixed matrix membranes for antibiotics removal from pharmaceutical industry wastewater by vacuum membrane distillation. *Journal of Environmental Chemical Engineering*, 9(6), p.106560.
113. Munirasu, S., Haija, M.A. and Banat, F., 2016. Use of membrane technology for oil field and refinery produced water treatment—A review. *Process safety and environmental protection*, 100, pp.183-202.
114. Kim, J., Kwon, H., Lee, S., Lee, S. and Hong, S., 2017. Membrane distillation (MD) integrated with crystallization (MDC) for shale gas produced water (SGPW) treatment. *Desalination*, 403, pp.172-178.
115. Alkhudhiri, A., Darwish, N. and Hilal, N., 2013. Produced water treatment: application of air gap membrane distillation. *Desalination*, 309, pp.46-51.
116. Kalla, S., 2021. Use of membrane distillation for oily wastewater treatment—a review. *Journal of Environmental Chemical Engineering*, 9(1), p.104641.
117. Al-Salmi, M., Laqbaqbi, M., Al-Obaidani, S., Al-Maamari, R.S., Khayet, M. and Al-Abri, M., 2020. Application of membrane distillation for the treatment of oil field produced water. *Desalination*, 494, p.114678.
118. Liu, C. and Martin, A., 2005. Membrane Distillation and Applications for Water Purification in Thermal Cogeneration-A Prestudy.
119. M. Baghbanzadeh, D. Rana, C. Q. Lan and T. Matsuura, Zero thermal input membrane distillation, a zero-waste and sustainable solution for freshwater shortage, *Applied Energy*, 187 (2017), 910–928.
120. González, D., Amigo, J. and Suárez, F., 2017. Membrane distillation: Perspectives for sustainable and improved desalination. *Renewable and Sustainable Energy Reviews*, 80, pp.238-259.
121. Adham, S., Hussain, A., Matar, J.M., Does, R. and Janson, A., 2013. Application of membrane distillation for desalting brines from thermal desalination plants. *Desalination*, 314, pp.101-108.
122. Alkhudhiri, A., Darwish, N. and Hilal, N., 2012. Membrane distillation: A comprehensive review. *Desalination*, 287, pp.2-18.
123. Kiss, A.A. and Kattan Read, O.M., 2018. An industrial perspective on membrane distillation processes. *Journal of Chemical Technology & Biotechnology*, 93(8), pp.2047-2055.

124. Walton, J., Lu, H., Turner, C., Solis, S. and Hein, H., 2004. Solar and waste heat desalination by membrane distillation. *Desalination and water purification research and development program report*, 81, p.20.
125. Alklaibi, A.M. and Lior, N., 2007. Comparative study of direct-contact and air-gap membrane distillation processes. *Industrial & engineering chemistry research*, 46(2), pp.584-590.
126. Liu, C. and Martin, A., 2005. Membrane Distillation and Applications for Water Purification in Thermal Cogeneration-A Prestudy.
127. Manawi, Y.M., Khraisheh, M., Fard, A.K., Benyahia, F. and Adham, S., 2014. Effect of operational parameters on distillate flux in direct contact membrane distillation (DCMD): Comparison between experimental and model predicted performance. *Desalination*, 336, pp.110-120.
128. Khayet, M., 2011. Membranes and theoretical modeling of membrane distillation: A review. *Advances in colloid and interface science*, 164(1-2), pp.56-88.
129. Khayet, M., Mengual, J.I. and Matsuura, T., 2005. Porous hydrophobic/hydrophilic composite membranes: application in desalination using direct contact membrane distillation. *Journal of Membrane Science*, 252(1-2), pp.101-113.
130. Banat, F.A. and Simandl, J., 1994. Theoretical and experimental study in membrane distillation. *Desalination*, 95(1), pp.39-52.
131. Martinez, L. and Florido-Diaz, F.J., 2001. Theoretical and experimental studies on desalination using membrane distillation. *Desalination*, 139(1-3), pp.373-379.
132. Alklaibi, A.M. and Lior, N., 2005. Membrane-distillation desalination: status and potential. *Desalination*, 171(2), pp.111-131.
133. Chernyshov, M.N., Meindersma, G.W. and de Haan, A.B., 2003. Modelling temperature and salt concentration distribution in membrane distillation feed channel. *Desalination*, 157(1-3), pp.315-324.
134. El-Bourawi, M.S., Ding, Z., Ma, R. and Khayet, M., 2006. A framework for better understanding membrane distillation separation process. *Journal of membrane science*, 285(1-2), pp.4-29.

135. Wang, J. and Zhuang, S., 2019. Removal of cesium ions from aqueous solutions using various separation technologies. *Reviews in Environmental Science and Bio/Technology*, 18, pp.231-269.
136. Souhaimi, M.K., Khayet, M. and Matsuura, T., 2011. Membrane distillation: principles and applications.
137. Qtaishat, M., Matsuura, T., Kruczek, B. and Khayet, M., 2008. Heat and mass transfer analysis in direct contact membrane distillation. *Desalination*, 219(1-3), pp.272-292.
138. Gunko, S., Verbych, S., Bryk, M. and Hilal, N., 2006. Concentration of apple juice using direct contact membrane distillation. *Desalination*, 190(1-3), pp.117-124.
139. Phattaranawik, J., Jiraratananon, R. and Fane, A.G., 2003. Heat transport and membrane distillation coefficients in direct contact membrane distillation. *Journal of membrane science*, 212(1-2), pp.177-193.
140. Matheswaran, M., Kwon, T.O., Kim, J.W. and Moon, I.S., 2007. Factors affecting flux and water separation performance in air gap membrane distillation. *Journal of Industrial and Engineering Chemistry*, 13(6), pp.965-970.
141. Srisurichan, S., Jiraratananon, R. and Fane, A.G., 2006. Mass transfer mechanisms and transport resistances in direct contact membrane distillation process. *Journal of membrane science*, 277(1-2), pp.186-194.
142. Martínez-Díez, L. and Vazquez-Gonzalez, M.I., 1999. Temperature and concentration polarization in membrane distillation of aqueous salt solutions. *Journal of membrane science*, 156(2), pp.265-273.
143. Martinez, L., 2004. Comparison of membrane distillation performance using different feeds. *Desalination*, 168, pp.359-365.
144. Lawson, K.W. and Lloyd, D.R., 1997. Membrane distillation. *Journal of membrane Science*, 124(1), pp.1-25.
145. Chen, T.C., Ho, C.D. and Yeh, H.M., 2009. Theoretical modeling and experimental analysis of direct contact membrane distillation. *Journal of Membrane Science*, 330(1-2), pp.279-287.
146. Keshavarzzadeh, A.H., 2020. Design and bio-inspired optimization of direct contact membrane distillation for desalination based on constructal law. *Scientific Reports*, 10(1), p.16790.